Spatial organisation of ecologically-relevant high order flow properties and implications for river habitat assessment

Giuditta Trinci

A thesis submitted for the degree of Doctor of Philosophy,

School of Geography, Queen Mary University of London

2017

I, Giuditta Trinci, confirm that the research included within this thesis is my own work or that where it has been carried out in collaboration with, or supported by others, that this is duly acknowledged below and my contribution indicated. Previously published material is also acknowledged below.

I attest that I have exercised reasonable care to ensure that the work is original, and does not to the best of my knowledge break any UK law, infringe any third party's copyright or other Intellectual Property Right, or contain any confidential material.

I accept that the College has the right to use plagiarism detection software to check the electronic version of the thesis.

I confirm that this thesis has not been previously submitted for the award of a degree by this or any other university.

Signature:

Date: 6th March 2017

Erasmus Mundus
Joint Doctorate Programme

SMART - Science for MAnagement of Rivers and their Tidal systems

PhD in river science

Research for this thesis was conducted within the framework of SMART (Science for MAnagement of Rivers and their Tidal systems), which is an Erasmus Mundus Joint Doctoral Programme (EMJD).

EMJDs aim to foster cooperation between higher education institutions and academic staff in Europe and third countries with a view to creating centres of excellence and providing a highly skilled 21st century workforce enabled to lead social, cultural and economic developments. All EMJDs involve mandatory mobility between the universities in the consortia and lead to the award of recognised joint, double or multiple degrees.

The SMART programme represents a collaboration among The University of Trento, Queen Mary University of London, and Frei University Berlin. Each doctoral student within the SMART programme has conformed to the following during their 3 years of study:

(i) Supervision by a minimum of two supervisors in two institutions (their primary and secondary institutions).

(ii) Study for a minimum period of 6 months at their secondary institution.

(iii) Successful completion of a minimum of 30 ecus of taught courses.

(iv) Collaboration with an associate partner to develop a particular component / application of their research that is of mutual interest.

(v) Submission of a thesis within 3 years of commencing the programme.

Abstract

The turbulent properties of flow in rivers are of fundamental importance to aquatic organisms yet are rarely quantified during routine river habitat assessment surveys or the design of restoration schemes due to their complex nature. This thesis uses a detailed review of the literature to highlight the various ways in which plants and animals modify the flow field, how this can deliver beneficial effects; and how turbulence can also generate threats to growth and survival. The thesis then presents the results from detailed field assessments of turbulence properties undertaken on low, intermediate and high gradient rivers to advance scientific understanding of the hydrodynamics of rivers and inform effective habitat assessment and restoration. A reach-scale comparison across sites reveals spatial variations in the relationships between turbulent parameters, emphasising the need for direct measurement of turbulence properties, while a geomorphic unit scale assessment suggests that variations in turbulence at the scale of individual roughness elements, and/or within the same broad groupings of geomorphic units (e.g. different types of pools) can have an important influence on hydraulic habitat. The importance of small-scale flow obstructions is further emphasised through analysis of the temporal dynamics of turbulence properties with changes in flow stage and vegetation growth. The highest magnitude temporal changes in turbulence properties were associated with individual boulders and vegetation patches respectively, indicating flow intensification around these sub-geomorphic unit scale features. Experimental research combining flow measurement with underwater videography reveals that more sophisticated turbulence parameters provide a better explanation of fish behaviour and habitat use under field conditions, further supporting direct measurement of turbulent properties where possible. The new insights into interactions between geomorphology, hydraulics and aquatic organisms generated by this work offer opportunities for refining habitat assessment and restoration design protocols to better integrate the important role of turbulence in generating suitable physical habitat for aquatic organisms.

Acknowledgements

First, I would like to express my sincere gratitude to my supervisors Dr. Gemma Harvey and Dr. Alex Henshaw from Queen Mary University of London, Dr. Walter Bertoldi, from the University of Trento, and Dr. Franz Holker, from IGB- Berlin, for their assistance, enthusiasm and continuous support through this thesis. My heartfelt gratitude goes to Gemma and Alex for being there, having faith in my abilities, encourage and guide me at all stages of this thesis. Without their guidance and help, this thesis would not have been possible.

I have been surrounded by great colleagues within the school of Geography (QMUL), the Mechanical and Environment Engineering Department (Trento) and the IGB institute (Berlin) that have provided an enriching environment and valuable help throughout this project. In particular, I would like to thank the SMART doctorates (past and present) and staff who have been personally and academically supportive and helpful during my complex mobility. Thanks to all of them I have always felt at home during my periods in London, Trento and Berlin. Special thanks go to Umesh Sing, Navid Maroof, Maria Vasilyeva, Tesfaye Terekegn, Vittoria Scorpio, Marco Redolfi, Ines Di Dato, Mirko Mucciarelli, Martino Salvaro, Michael Plebani and Marcello Trinci for their invaluable assistance and precious time during my fieldworks. I must also acknowledge Lorenzo Forti (Hydraulics Lab, Trento) for the design and build of the very functional and stable support for the Acoustic Doppler Velocimeter that I used during my surveys. I must also acknowledge Ed Oliver (QMUL) for producing the final version of two figures used in this thesis, and for the review in the Wiley review journal WIREs Water.

The present research was possible thanks to the SMART (Science for the MAnagement of Rivers and their Tidal systems) Joint Doctorate Erasmus Mundus programme funded by the European Union. This programme has provided an extraordinary opportunity for interdisciplinary learning and research in river science, for building contacts and creating new ideas.

Special thanks to Alejandra and Martina for their great support, help in the editing and layout assistance of the manuscript.

To my family and closest friends your support and cheering with positive thinking have given me the strength and perseverance to walk through this path.

I would also like to personally thank M. who inspires me with rich conversations, constantly supporting me in many different ways, with endless patience and encouragement.

Finally, I dedicate this thesis to my grandmas, Leonetta and Liliana, for teaching me about natural wildlife in the Tuscany hills, and for encouraging me to set ambitious goals during my life. Without them I would not be who I have become today.

Table of Contents

List of Figures

List of Tables

1.1 The research context

A sound understanding of the interactions between fluvial processes and aquatic organisms (animals and plants) is crucial for sustainable river management and restoration practice. Flow and sediment transport, together with aquatic and riparian vegetation and geochemical processes, combine to create a complex and dynamic assemblage of habitats or "geodiversity" within river systems (Brierley and Fryirs, 2005) over a range of spatio-temporal scales (Newson, 2002).

Understanding links between river behaviour and ecological improvement are required for effective decision making and associated river management and restoration efforts. This requires effective means of assessing river habitat quality in a way that recognises the complex linkages between the biotic and abiotic components of the river environment. Recently, the REFORM hydromorphological framework has been developed by Gurnell *et al*., (2016) to draw upon the strengths of existing methods and fill key gaps to provide a practical and clear framework to guide river management. The majority of existing assessment and restoration methods are fundamentally underpinned by assumptions that morphological changes can drive a real ecological response (Vaughan and Ormerod, 2010).

One common assumption of most types of hydromorphological assessment methods is that surveys of mesoscale geomorphic features such as pools, riffles, and glides can help to explain ecological populations and diversity (Newson and

Newson, 2000). The theory behind this is that geomorphic units have distinctive physical (e.g. substrate) and hydraulic (e.g. velocity, flow depth) properties and are therefore likely to be utilized by organisms of different types for different purposes such as predating, resting, and reproduction (Maddock, 1999; Jowett, 2003). A number of studies have demonstrated their ecological relevance in broad terms (Padmore, 1997; Kemp *et al.*, 1999; Padmore *et al.*, 1998; Kemp *et al.*, 2000; Harper *et al.*, 2000; Newson and Newson, 2000; Harvey *et al.*, 2008), and the geomorphic unit represents a convenient spatial scale for assessing the habitat use of aquatic organisms (Vezza *et al.,* 2014; Wilkes *et al.,* 2012), for predicting the habitat suitability and for the focus of river restoration strategies.

The geomorphic unit is an attractive scale from a practical perspective since they can be visually identified relatively easily in the field, and initial research in this area suggested that features such as pools, riffles, glides, etc., could be distinguished on the basis of Froude number (Jowett, 1993). However, research by Clifford *et al.* (2006) has shown that this is problematic as distinctions between units can vary with stage and different combinations of velocity and depth can produce identical Froude number values. More fundamentally, the ecological relevance of Froude number for organisms is questionable, since these values are based on temporally and spatially variable hydraulic factors such as the local, instantaneous, near-bed shear stresses (Sand‐Jensen and Pedersen, 1999; Cotel *et al.,* 2006; Fenoglio *et al.,* 2013; Hockley *et al.,* 2014; Asaeda and Rashid, 2016). Despite this, hydraulic habitat assessments for river appraisal and restoration design have largely focused on temporally and spatially averaged flow properties rather than more complex descriptors of turbulence that are known to directly influence aquatic organisms (Lacey *et al.,* 2012). This partly reflects the complex nature of these properties and high frequency flow measurement required to derive them. Recent research by

Harvey and Clifford (2009) and Wilkes (2014) has gone some way to addressing this issue by characterizing the hydraulic characteristics of geomorphic units using more sophisticated, ecologically relevant metrics such as turbulence intensity and eddy size. In particular, by analysing turbulence intensity, and the periodicity, orientation and dimensions of coherent flow structures (Harvey and Clifford, 2009; Wilkes, 2014), variations in flow complexity and spatial heterogeneity of flow hydraulics both within and among geomorphic units has been demonstrated. These studies have revealed distinctions between some geomorphic units on the basis of hydraulic complexity that varies with flow stage. Nevertheless, the results of the studies were not consistent. For example, Harvey and Clifford (2009) found pools to contain the highest amount of hydraulic variability, whereas Wilkes (2014) found pools to be the least heterogeneous habitat. However, the results show different levels of spatial variability in the analysed geomorphic units. Also, these studies are based on sampling of a limited number of geomorphic units at a small number of sites in the UK (4 and 8 morphological features in the works of Harvey and Clifford (2009) and Wilkes, (2014) respectively); furthermore, little is known about the hydraulic characteristics and potential ecological relevance of the wider range of geomorphic units found in European rivers.

This suggests assessment of the high order (turbulent) flow properties of geomorphic units across a wider range of European river types, could improve understanding of the linkages between hydromorphological conditions and ecological functioning that underpin prevailing approaches to habitat assessment and restoration (Clifford *et al.,* 2006). Research is required to provide insights into scales of variability in turbulence properties that have direct ecological relevance, helping to inform river assessment and restoration efforts. This would contribute to the critical evaluation of the usefulness of visual surveys of geomorphic units for ecological purposes, and where necessary, identification of adaptations.

This thesis will explicitly quantify the key turbulence properties* and their spatial organization across different spatial scales (reach, geomorphic unit and hydraulic patch) and temporal scales (change with increasing flow stage or vegetation cover) for rivers with different gradients, and explores direct links between turbulence properties and fish behaviour under field conditions.

Note

Turbulence involves significant mixing and the transfer of momentum by eddies or vortices and is usually confined to the dissipative range of fluid energy at higher frequencies and smaller spatial scales. In this thesis, the complex nature of flow and its importance in relation to aquatic life has been explored by high frequency flow characteristics and coherent flow structures (CFS). High flow properties are accessible through advanced instrumentation; while CFS aims to detect periodic patterns of flow by via long-standing statistical methods.

1.2 Thesis structure

This thesis structure comprises eight chapters. Chapter 2 presents a review of existing literature on the two-way interactions between flow hydrodynamics and aquatic biota, and the key methodological approaches used in their quantification. The chapter reveals a critical need for more explicit consideration of turbulence in river assessment and restoration. The chapter is framed around a new holistic approach to identifying key ecologically relevance turbulence properties proposed by Lacey *et al*. (2012), and highlights important knowledge gaps, leading to the identification of the aims of this research. Research questions are introduced at the end of the chapter 2 in Table 2.2. An adapted version of this chapter has been accepted as an 'advanced review' article for the Wiley review journal WIREs Water.

Chapter 3 provides an overview of the research design including the descriptions of field sites and applied methodology. Certain aspects of the methodology are common to all results chapters, and these are included in Chapter 3. Specifically, this includes the sampling design used to capture the topographic, high order flow velocity and geomorphic unit data across reach of different gradients, together with data pre-processing protocols and computation of turbulence properties. Methods that are specific to each individual results chapter are included in that chapter.

To address the research questions, four distinct but related research projects (Figure 1.1) were developed and are reported in Chapter 4 - 7. Each results chapter is written as a semi-independent chapter including a short introduction with review of key literature direct relevant to that chapter, methods, results and discussion.

Chapter 8 summarize the conclusions and recommendations for future research.

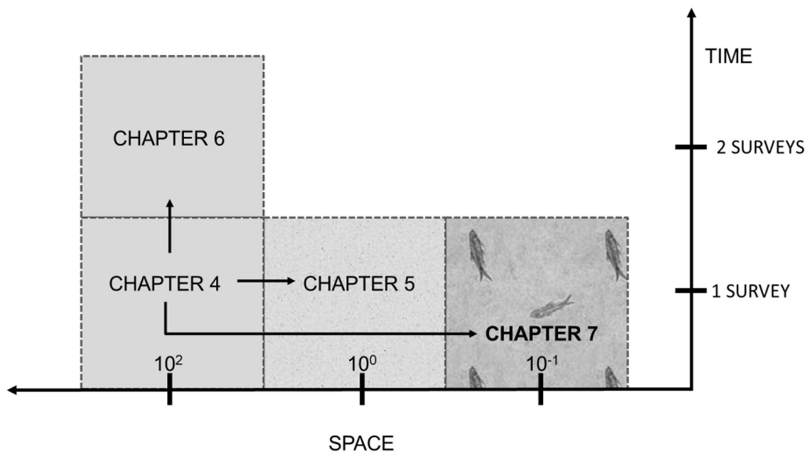

Figure 1.1 Conceptual scheme for chapters.

Chapter 4 investigates the high order flow properties at the reach scale across low, intermediate and high gradient reaches during low flow conditions and evaluates their spatial organisation in relation to bedforms and other characteristic roughness elements.

Chapter 5 explores the relationships between geomorphic units and turbulence properties more explicitly, by quantifying the turbulence characteristics of geomorphic units at low flow, examining the utility of turbulence parameters in predicting geomorphic unit occurrence, and assessing variability outside the scales of GUs.

Chapter 6 explores temporal variations in turbulence properties in two ways. For the high gradient reach, changes in the spatial organisation of turbulent flow properties are assessed with respect to increasing flow stage. For the low gradient reach, two seasonal periods are compared to explore changes in the spatial organisation of turbulent flow properties with increasing vegetation cover.

Chapter 7 takes an experimental approach, applying Lacey *et al.*'s framework to explore interactions between turbulence and fish habitat use around large wood under low flow conditions.

CHAPTER 2: Literature review

Chapter synopsis

This chapter provides a review of the current state of knowledge of interactions between biota and hydrodynamics in rivers in order to demonstrate the need for more explicit consideration of hydrodynamics in river assessment and restoration design. An overview of the approaches to research design is provided and the key elements of turbulent boundary layer theory and parameters are outlined. The main ways in which key groups of river organisms (aquatic vegetation, macroinvertebrates and fish) interact with the turbulent properties of river flow are discussed, recognising the two-way interactions between aquatic biota and hydrodynamics, and identifying the key benefits of turbulence and how organisms exploit these and the threats that turbulent flow can pose. The chapter concludes by discussing key knowledge gaps and introducing the research objectives to be addressed by the thesis. An adapted version of this chapter has been accepted by the Wiley review journal WIREs Water:

Trinci G, Harvey GL, Henshaw AJ, Bertoldi W, Hölker F (2017) Life in turbulent flows: interactions between hydrodynamics and aquatic organisms in rivers. *WIREs Water*.

2.1 Introduction

The mechanics of fluid flow exert a fundamental influence on river plants and animals, and aquatic organisms themselves modify hydrodynamics properties of flow (Vogel, 1994). In fluid dynamics, a fundamental distinction can be drawn between laminar flow regimes comprising parallel layers of fluid that 'slide' over one another with no significant mixing between layers, and turbulent flow regimes which involve significant mixing and the transfer of momentum by swirling flow structures known as eddies or vortices. Turbulent flow regimes are more mathematically complex, and are ubiquitous within rivers. The dimensionless Reynolds number (the ratio between inertial forces (mass) and viscous forces) is used to identify whether flow is laminar or turbulent, and can also be used to describe the interaction between aquatic organisms and the viscous forces of the fluid, with larger and more hydrodynamically rough body morphologies associated with higher Reynolds numbers (Figure 2.1). Turbulent flows, however, encompass a wide range of environmental conditions and a universally accepted definition of turbulence remains elusive. A suite of common attributes can be identified including: enhanced mixing, sensitivity to initial conditions and small perturbations (deterministic chaos), a large range of interacting spatial and temporal structures, motions in directions other than the applied shear, rotationality, intermittency and irregularity (Clifford *et al*., 1993c; Warhaft, 2002; Davidson, 2004; Nikora, 2010).

There has been a proliferation of turbulence studies in laboratory and field settings following the publication of accessible key texts on turbulence and boundary layer theory during the 1990s (e.g. Clifford and French, 1993c; Vogel, 1994); advances in instrumentation such as Acoustic Doppler Velocimetry, (Nortek, 1998; Lane *et al.,* 1998; Voulgaris and Trowbridge, 1998; García *et al*., 2005; Chanson, 2008); and development of analytical approaches to characterising turbulent properties (Farge, 1992; Torrence and Compo, 1998; McLelland and Nicholas, 2000; Goring and Nikora, 2002). Methodological advancements in quantifying turbulence have developed largely through a combination of laboratory experimentation (Nezu and Nakagawa, 1995; Adrian, 2007; Hardy *et al.*, 2009; Jiménez, 2011) and high-resolution field measurements over relatively small reaches (< 5 m) of natural channels.

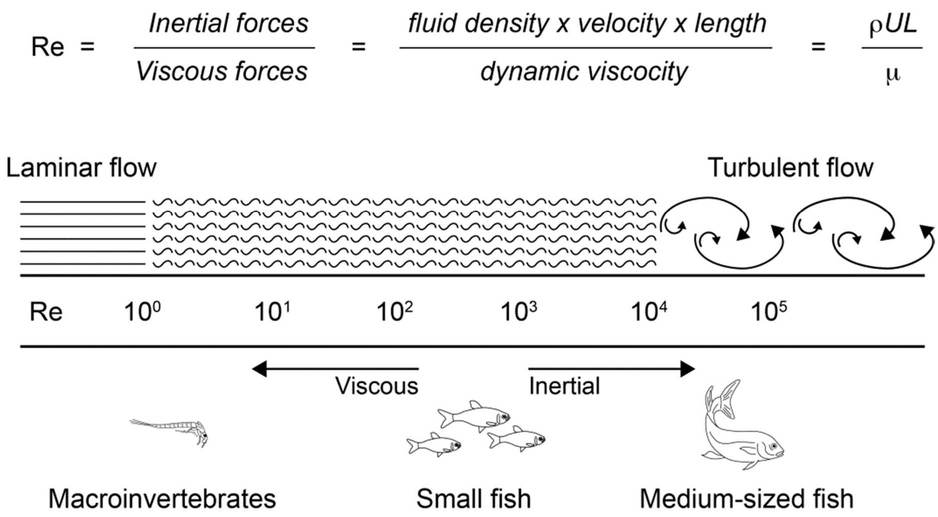

Figure 2.1 Definition of Reynolds number, laminar and turbulent flow, with example Reynolds numbers for different types of organisms interacting with the flow. Figure redrawn by E. Oliver, Cartographer, School of Geography, Queen Mary University of London.

Turbulence is known to exert a significant influence on river flora and fauna. For example, the presence of vegetation profoundly modifies the mean and turbulent properties of flow (Nepf, 2012), while the direct consideration of turbulence has been shown to add explanatory power when assessing habitat preferences of fish (Smith *et al.*, 2014) and invertebrates (Morris *et al.*, 2015). In spite of this, there remains a disconnect between standard approaches to habitat assessment (which often rely on visual observation and/or averaged flow properties e.g. River Habitat Survey (Raven *et al.*, 1998), River Habitat Index (IHF) (Pardo *et al.*, 2002; Fernández *et al.*, 2011) (see review of Rinaldi *et al.*, 2013a,b) and detailed investigation of hydrodynamics. This results in a lack of understanding of the links between turbulence and aquatic organisms at the 'mesoscale' of rivers (Wilkes *et al.*, 2013) defined as valid approach to integrate variations across hydraulic variables and channel form (Newson and Newson, 2000; Thomson *et al.*, 2001) where habitat assessment and restoration tends to be focused (Newson and Newson, 2000).

2.2 Approaches to research design

There is considerable diversity in the research approaches applied to the study of interactions between turbulence and aquatic organisms. This arises from several sources: (i) studies may involve field measurement, laboratory experimentation or hydraulic modelling; (ii) turbulence may be simulated in laboratory studies using a number of different mechanisms; (iii) laboratory experimentation may employ living or artificial organisms, and (iv) eco-physiological impacts and energy costs for swimming and turbulence-mediated behaviour may be quantified in a range of ways. Laboratory studies are by far the most common approach, reflecting the opportunities offered for detailed observations of organism behaviour and responses to perturbations and perhaps more importantly the advantages of tight experimental control. The latter is particularly attractive since a multitude of factors other than turbulence will influence habitat selection and bioenergetics in aquatic organisms in 'real' rivers, including endogenous factors (e.g. life cycle stage/size, physiological state, parasite load and disease) and environmental context (e.g. light levels, temperature, availability of oxygen and nutrients, presence of toxicants, competition)

(Liao, 2007; Hockley *et al.*, 2014). Accounting for these influences under field conditions is inherently challenging.

Even within laboratory flume settings, numerous options are available for simulating and quantifying turbulence, meaning that drawing comparisons between results arising from different experimental designs can be problematic. Mechanisms for turbulence generation within laboratory settings include varying the degree of flume boundary roughness (Nikora *et al.*, 2003), modulation of flow pumps (Enders *et al.*, 2003) and the positioning of cylindrical or spherical flow obstructions ('bluff bodies') within the flow field (Liao *et al.*, 2003; Maia *et al.*, 2015). Turbulent properties may be quantified through point measurements of velocity sampled at high frequencies (e.g. 20 Hz) using a range of sensor types (Clifford and French, 1993b; Lane *et al.*, 1998; Lane *et al.*, 1999; Buffin-Bélanger and Roy, 2005; Sulaiman *et al.*, 2013; Stewart and Fox, 2015) or visualised and estimated using Particle Image Velocimetry (PIV) which is more straightforward to implement in the laboratory (Creutin *et al.*, 2003; Adrian, 2005) than in the field (Tritico *et al.*, 2007; Fox and Patrick, 2008). Recent advances in acoustic Doppler current profiling can provide detailed 3-dimensional hydraulics by capturing high resolution vertical profiles of semi-continuous velocity points (Nystrom *et al.*, 2002; García *et al.*, 2005; Rusello *et al.*, 2006; Chanson, 2008). A range of hydrodynamic characteristics may then be derived (see Section 2.3). The same technologies can be deployed in the field, and both field and laboratory studies must consider a number of sources of error in the sampling design: the degree of disturbance introduced into the flow by the sampling equipment, probe orientation, the sampling volume, the measurement frequency and record length (Buffin-Bélanger and Roy, 2005; Wilkes *et al.*, 2013), and post-processing accuracy.

Numerical modelling approaches can also be applied and recent reviews have examined the role of numerical modelling in ecohydraulics (Tonina and Jorde, 2013) and the simulation of turbulent flow (Argyropoulos and Markatos, 2015). Numerical modelling of turbulence involves solving the system of partial differential equations that represent momentum and the conservation of mass (the Navier-Stokes equations). Direct Numerical Simulation (DNS) solves the equations at the smallest scales of turbulence but the approach is computationally expensive and ecohydraulics applications have been relatively limited as a result of the lack of ecological and geomorphological understanding at this scale (Tonina and Jorde, 2013). Many applications have instead used the less computationally intensive Reynold's averaged Navier-Stokes (RANS) equations to represent temporally averaged turbulence properties. Alternative approaches such as Large Eddy Simulation (LES) show promise for achieving a balance between accuracy and applicability, and computational demand (Argyropoulos and Markatos, 2015), LES can be used to resolve the Navier-Stokes equations for most scales of interest (Rodi *et al.*, 2013). Numerical modelling has been used to provide useful information on, for example, the turbulence structure of river confluences (Bradbrook *et al.*, 1998; Rhoads and Sukhodolov, 2004; Constantinescu *et al.*, 2011), secondary flow circulation due to the presence of obstacles (Brevis *et al.*, 2014) and sediment dynamics (Wu *et al.*, 2000; Duc *et al.*, 2004).

Laboratory studies have used living organisms or physical models (inanimate surrogates) to explore interactions between hydrodynamics and aquatic life, while field studies naturally focus on the former. Physical models of submerged and emergent vegetation include rigid or flexible plastic rods or blades that achieve a similar geometry and rigidity to species of interest, with or without foliage, and usually fixed to a board or the flume bed (Nepf and Vivoni, 2000; Wilson *et al.*, 2003; Ortiz *et al.*, 2013; Li *et al.*, 2014). Physical models of animals have also been used, for example artificial trout to assess the hydrodynamics of entraining behaviour (Przybilla *et al.*, 2010) and late instar Blackfly larva (*Simulium vittatum*) constructed from capillary tubing (Chance and Craig, 1986). Physical surrogates have the advantages of alleviating practical issues around husbandry and acclimatisation, cost, replication, abundance/density and positioning within the flow field as well as allowing very detailed measurements in close proximity to the 'organism' (Johnson *et al.*, 2014). They are, however, a simplification of the physical structure of live organisms, capable of mimicking morphological characteristics but necessarily overlooking important biomechanical, physiological, and behavioural interactions with the flow field and with other organisms (see Johnson *et al.*, (2014) for a full discussion of the use of surrogates and live animals in laboratory experimentation). For example, live animals enable detailed bioenergetics studies, with a number of options available for estimating turbulence-related energy costs. Visual observation can be used to record the critical flow rate (the velocity at which a fish fatigues) (Lupandin, 2005), while underwater videography captures behaviour and responses to perturbations continuously (Standen and Lauder, 2007; Tritico and Cotel, 2010), and respiratory experiments can directly quantify oxygen consumption and thus energetic losses (Enders *et al.*, 2003). Limitations of experimental approaches, however, include set-up costs, fitness-for-purpose of different equipment specifications, differences in the biogeochemical constituents of water, and difficulties in extrapolating results from short-duration, small–scale studies to greater temporal and spatial scales (Thomas *et al.*, 2014).

2.3 Turbulence theory and parameters

The diversity in definitions of turbulent flows is mirrored in the variety of studies of impacts of such flows on aquatic organisms. However, quantitative descriptions of turbulence can be usefully separated into two main approaches (Wilkes *et al.*, 2013; Cotel and Webb, 2015): (i) statistical description (Clifford, 1993a); and (ii) the use of spatially and temporally correlated turbulence properties to describe three dimensional coherent flow structures (CFS) or ‘eddies’ (Richards, 1979; Kirkbride and Ferguson, 1995; Roy *et al.*, 2004). The first approach considers turbulence as a stochastic (random) phenomenon and identifies aggregated or bulk properties of the flow. When fluid motion is viewed in a Eulerian frame (i.e. observing a specific location in space through which the fluid passes), the turbulent flow field may be represented by a velocity vector with three orthogonal components (streamwise, u; cross stream, v; and vertical, w), each of which can be decomposed into mean (U, V, W) and fluctuating (u’, v’, w’) parts. The second approach uses spatially and temporally correlated turbulence properties to describe three dimensional coherent flow structures (CFS) or ‘eddies’ (Kirkbride and Ferguson, 1995; Roy *et al.*, 2004). Coherent flow structures can be identified through time series analysis, flow visualisation or numerical modelling (Best *et al.*, 2001; Roy *et al.*, 2004) and encompass small scale structures shed from individual roughness elements such as bed material grains (Clifford *et al.*, 1992; Best, 1993; Roy *et al.*, 1996), to large-scale ejections of fluid away from the river bed and inrushes of fluid towards the bed (Hardy *et al.*, 2009). Such turbulent macrostructures may be important in initiating and modifying river bedforms (Thompson *et al.*, 1998; MacVicar and Roy, 2007b). Mathematical definition of vortices is challenging, leading to the development of a range of different algorithms for investigating the presence and nature of vortices in the flow. Applications within ecohydraulics have included a combination of Eulerian vortex detection methods such as the Q criterion (based on the magnitude of vorticity) and Langragian methods such as the Finite-time Lyapunov exponent (FTLE) method which tracks individual fluid trajectories through time (Marjoribanks *et al.*, 2016).

A recent paper by Lacey *et al*. (2012) proposed a framework for exploring ecologically-relevant turbulent properties in river channels, focusing specifically on fish. The “IPOS” framework (Lacey *et al.*, 2012) presents four categories of turbulent characteristics: intensity, periodicity, orientation and scale (Table 2.1), which can be computed from high frequency velocity time series. The representation of these properties is explored briefly below before the two-way interactions between biota and turbulent characteristics are discussed. The *intensity* of velocity fluctuations along the three components (u, v, w) can be explored by computing the root mean square of the fluctuations (RMS_u, RMS_v, RMS_w), which may be normalised by the shear velocity to provide a relative measure of the intensity of turbulent fluctuations. Turbulent Kinetic Energy (TKE) combines all three components to provide an overall measure of the kinetic (movement) energy of eddies in the flow, while the Reynolds shear stresses describe the frictional forces of flow that characterize sediment mobilization and transport (Davidson, 2004; Pope, 2000; Wilkes *et al.*, 2013).

Periodicity refers to the predictability of the flow, and the occurrence of dominant frequencies in the velocity record. A simple indicator of predictability can be gained through inspection of the kurtosis of the turbulent residuals (u’, v’, w’) (Wilkes, 2014). Second order autoregressive modelling can also be applied to high frequency velocity time series with the aim of deriving a length scale for the dominant eddy (see below). This approach requires series to satisfy a condition for pseudo-periodicity that reflects pseudo-cyclic sine oscillations (Richards, 1979) which may also provide an initial indication of time series predictability. Two further approaches can be used to identify the dominant periodic structure (eddy size) or range of structures present. Spectral density analysis decomposes the velocity signal into frequencies using the Fourier Transform and can be used to provide global information on the dominant period (converted to an eddy size or 'length scale' by multiplying by the mean velocity; see below) (Pope, 2000). In contrast, wavelet analysis uses the Continuous Wavelet Transform (CWT) to decompose the time series into time and frequency domains simultaneously, detecting and extracting the periodic signals in the record and how they vary through time (Torrence and Compo, 1998). It has been suggested that the latter approach is more appropriate for coherent flow structures which may be intermittent and evolve through time and space (Lacey *et al.,* 2012).

An initial indicator of flow 'orientation' can be derived from the skewness of the u', v' and w' components, which indicates the shape of the frequency distribution of the magnitude of turbulent fluctuations. Positively skewed turbulence residuals indicate the presence of a small number of high magnitude fluctuations, which may generate favourable conditions for sediment transport (Bagnold, 1966; Leeder, 1983). More complex analysis can assign instantaneous 2D velocity measurements to one of four turbulent 'events' based on Quadrant Analysis using the relative sign of paired values of u' and w' (Lu and Willmarth, 1973). In order to isolate the strongest events from those with negligible contribution to the Reynolds stress, a threshold or 'hole' may be applied, commonly twice the standard deviation of u'w' (Clifford, 1993; Clifford *et al.*, 1996; Harvey and Clifford, 2009; Wilkes et al., 2013). The cumulative duration and stress contribution can then be explored.

Commonly, eddy dimensions (scale) are represented by the length and the diameter that describe the extension and maximum rotation of the swirl of current movement, respectively. The integral eddy length scale is calculated as the product of mean velocity (U) and the integral time scale (t): the temporal scale of turbulent eddies or period over which velocity is autocorrelated (Lacey and Roy, 2008a). This assumes Taylor's 'frozen turbulence' hypothesis that a sequence of changes in velocity at a fixed location may be interpreted to represent the movement of an unchanging pattern of turbulence past that location (Taylor, 1938). The autoregressive modelling approaches described above can provide a means of computing the integral time scale (period) for the dominant eddy structure in the time series (Clifford and French, 1993a). This can also be compared to the size of aquatic organism (e.g. fish length) to give a momentum ratio (Lacey *et al.*, 2012; Cotel and Webb, 2015). The eddy diameter refers to the maximum extent of the rotating flow structure, often measured directly through laboratory visualisation.

Table 2.1 IPOS categories (intensity, periodicity, orientation, scale) identified by Lacey *et al.,* (2012) with example variables and descriptions. * denotes additional variables to those directly identified in Lacey *et al.,* (2012). Where x = u, v, w components, N are the number of observations and ρ is the water density, u', v' and w' are the turbulent residuals and U, V, W are the mean velocities along the three components. Methods for computation of turbulence parameters are provided in Chapter 3 (Table 3.8).

	Parameter	**Description**	**Variables/ notation**
INTENSITY	*Turbulence intensity* (absolute)	Root mean square of the turbulent fluctuations (Reynolds normal stresses in the u, v and w dimension).	*RMSu, RMSv, RMSw*
	Turbulence intensity (relative)	Normalised (by shear or mean velocity) values for u, v, w	*Tiu, TIv, TIw*
	TKE	Combines RMSu, RMSv, RMSw	*TKE*
	Reynolds Shear Stresses	Represent the turbulent flux of momentum – may affect organisms but rarely reported.	*u'v', v'w', u'w'*
	Vorticity (tendency to rotate)	2 x Ω Where Ω represents the angular velocity or rotational speed of the fluid	*ω*
PERIODICITY	*Predictability*	Kurtosis of the turbulent residuals (u', v', w') used as an initial indicator (Wilkes, 2014). Here, AR(2) models were applied and the condition for pseudo-periodicity derived	u'_{kurt}, v'_{kurt}, w'_{kurt} *fu, fv, fw* *Pu, Pv, Pw* *ITSu, ITSv, ITSw*

	Energy spectra	(Richards, 1979) (average eddy frequency, and period, and integral time scale)	
		Fourier transform (spectral density/ wavenumber spectra) traditionally applied to qualitatively explore the shape of spectra and derive the kinetic energy maximum	KE_{max}
		Wavelet analysis – a newer method, better for intermittent/evolving flow structures (dominant frequency)	*dfu, dfv, dfw*
ORIENTATION	*Skewness*	An initial, basic indicator of flow ‘orientation’ can be derived from the skewness of the u’, v’ and w’ components, describing the asymmetry of the frequency distribution of the magnitude of turbulent fluctuations	u'_{skew}, v'_{skew}, w'_{skew}
	Event structure	Duration and/or contribution to stress of each type of ‘event’: Q1 (outward interactions), Q2 (ejections of fluid away from the bed), Q3 (inward interactions) and Q4 (inrushes of fluid towards the bed)	$Q1_{dur}$, $Q1_{stress}$ $Q2_{dur}$, $Q2_{stress}$ $Q3_{dur}$, $Q3_{stress}$ $Q4_{dur}$, $Q4_{stress}$
	Direction of dominant fluctuation	Axis of eddy rotation (angle between the direction of dominant fluctuation and the streamwise direction)	*Alpha*
SCALE	*Eddy length scale*	Average eddy length	*Lu, Lv, Lw*
		Spatial extent of the region of correlation (“wedges” of fluid)	*ILSu, ILSv, ILSw*

	Fish momentum: wedge momentum ratio	Derived from the length scale and fish length.	*Mf*
	Eddy diameter	Spatial extent of rotating fluid, often directly measured using PIV techniques in the laboratory	*Du, Dv, Dw*

2.4 Biotic feedbacks on turbulence

Before considering the ways in which aquatic organisms (plants, invertebrates, fish) are influenced by turbulent flow, it is important to recognise that aquatic biota themselves also modify the flow field (Figure 2.2). Perhaps the most important of these interactions, within the scope of this chapter, is the influence of the biomechanical properties of aquatic vegetation on turbulence (Figure 2.2). At the scale of stems and branches, aquatic plants convert mean kinetic energy into turbulent kinetic energy through the generation of wakes, with the nature and fractional contribution to turbulence dependent upon the morphology and flexibility of the stems (Nepf, 1999). For flexible and long-leaved plants (e.g. *Sparganium emersum*), the development of wakes around individual stems may be locally important in the near-bed region but the dominant mechanism of turbulence generation is related to vortex shedding in the shear zone at leaf surfaces (Naden *et al.*, 2006; Nikora, 2010). Macrophytes can 'rescale' turbulence by breaking larger eddies into smaller ones (Madsen *et al.*, 2001), as reflected in the smaller eddy sizes found within plant stands (Nepf, 1999). Turbulence intensity may increase within sparse vegetation, but tends to then decrease with increasing density as the mean flow velocity decreases within vegetation stands (Nepf, 1999; Green, 2005). This relationship also reflects plant morphology, however, with longer and more flexible leaves capable of generating higher turbulence intensities (Sand-Jensen and Pedersen, 1999). Stem vibration and fluttering/ flapping can act as an additional source of turbulence at scales intermediate between the stem and canopy (Nikora, 2010).

At the canopy scale, the interaction between the plant stand and the flow generates a shear layer and different regions of turbulence can be identified. Nepf and Vivoni (2000) distinguished between submerged and emergent regimes. Submerged regimes comprised a zone of vertical exchange with the overlying water generated by shear, and a zone of longitudinal exchange dominated by advection, while emergent regimes were characterised by the longitudinal exchange zone only. Siniscalchi *et al.* (2012) identified three zones for artificial plants in flume experiments. Shear-generated zones of increased turbulent energy may be present upstream and along the canopy surface, associated with high turbulence intensities for some species (Sand-Jensen and Pedersen, 1999; Green, 2005), combined with longitudinally homogeneous zones of negative Reynold's stresses (on the streamwise and vertical plane), and an exit region at the transition to open channel conditions. Different plant morphologies can also result in different mechanisms of turbulence generation. Rigid, emergent vegetation has been shown to deflect flow in the horizontal plane, leading to the development of periodic patterns of twisting vortices known as a von Kármán vortex street, with reduced downstream turbulence intensity, while flexible submerged vegetation generates vertical and horizontal shear layers downstream as a result of strong vertical circulation (Ortiz *et al.*, 2013).

As a result, depending on plant morphology, density and environmental context, vegetation-induced changes to turbulence can alter sediment transport processes and either enhance or reduce fine sediment deposition (Nepf, 2012).

Animals also modify the flow field, although these impacts are generally considered less significant in relation to other roughness elements (Cotel and Webb, 2015). Flow separation around lotic invertebrates modify velocity gradients and drag and lift forces (Statzner *et al.*, 1988) and suspension feeding invertebrates may both passively and actively modify the flow field, generating supplies of particulate food resources. For example, turbulence surrounding the feeding appendages of larval blackfly alter particle interception rates and the flow paths taken by individual particles (Hart *et al.*, 1996) and can lead to considerable local modifications to the flow field (Thomson *et al.*, 2004), while mayfly larvae can generate vortices to enhance feeding opportunities (Figure 2.2, see section below). Fish generate and use their own eddies in swimming through the interactions of different fins (Webb and Cotel, 2010b) and, through schooling, can produce biotically-generated flows characterised by vortices shed from the propulsive wakes of individuals (Liao, 2007). The main ways in which animals exploit these interactions are explored further below.

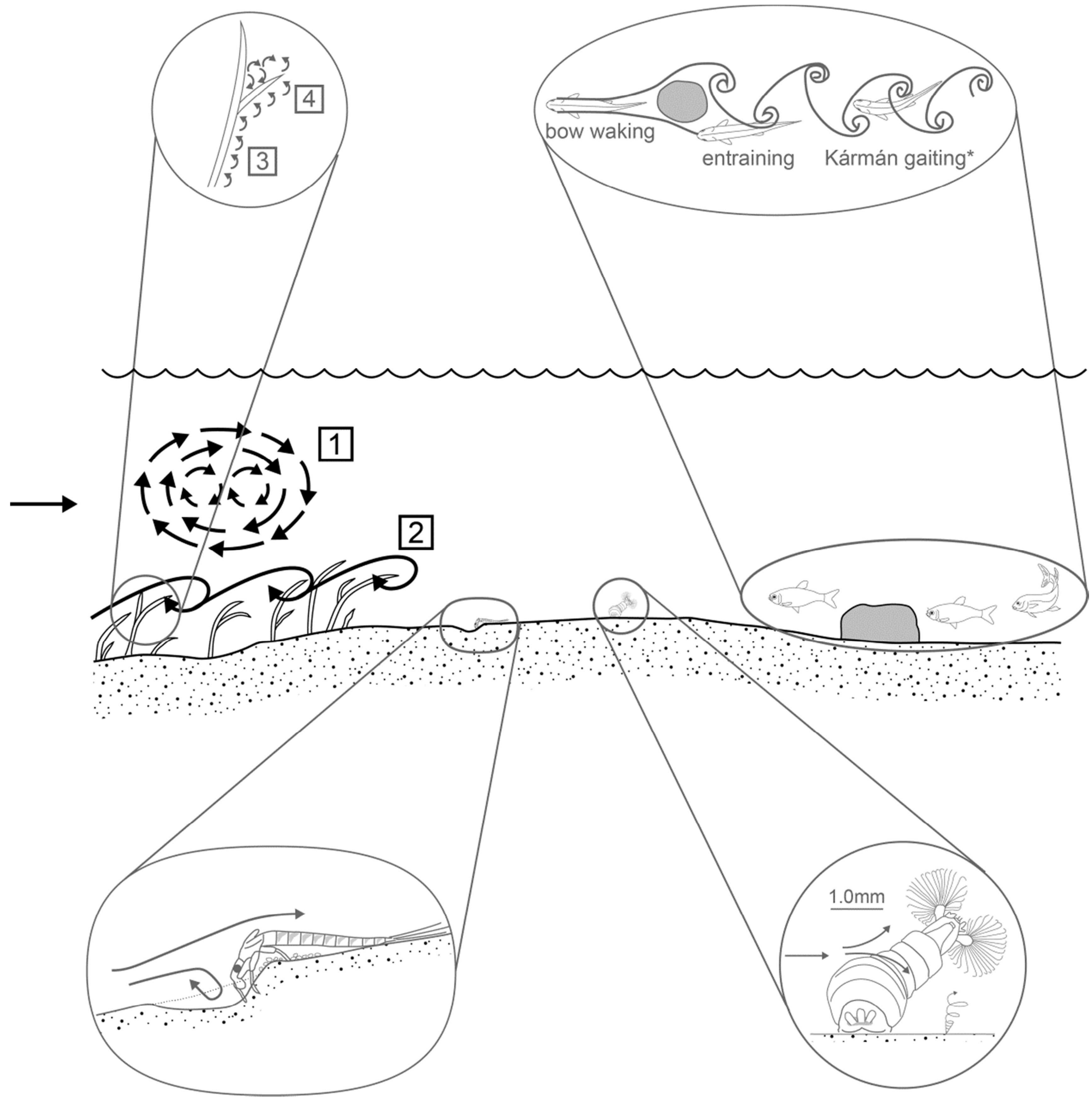

Figure 2.2 Interactions between flow hydrodynamics and aquatic organisms at small scales in rivers. For aquatic plants this include: [1] depth-scale shear generated turbulence formed above vegetation, [2] canopy scale shear generated turbulence, [3] turbulence generated at the scale of individual stems and [4] at the scale of individual leaves, modified from Nikora (2010). Additional sources of turbulence associated with plant motion occurring at scales intermediate between the stem and canopy are not shown here. Also showing exploitation of turbulence flow structures for feeding by mayfly larvae (modified from Soluk and Craig, 1990) and blackfly larvae (modified from Chance and Craig, 1986) and by trout (modified from Liao, 2007) for efficient locomotion in the vicinity of bluff bodies. * denotes that Kármán gaiting in trout has been observed In laboratory flume with D-shape cylinder than natural river channels. Figure redrawn by E. Oliver, Cartographer, School of Geography, Queen Mary University of London.

2.5 Exploitation of turbulent flow properties

Turbulent flow facilitates access to food, maintenance of adequate oxygen levels, removal of wastes, locomotion and predator evasion (Vogel, 1994; Hart *et al.*, 1996; Quinn *et al.*, 1996; Robinson *et al.*, 2000; Brooks *et al.*, 2005; Ferner and Weissburg, 2005; Rice *et al.*, 2008; Webb and Cotel, 2010a; Webb *et al.*, 2010b; Webb and Cotel, 2011). As such, turbulence can represent a benefit rather than a constraint in many circumstances (Liao, 2007), and can be an important consideration in aquaculture in relation to disease reduction (Liao and Cotel, 2013). Some studies indicate that even hydrodynamic conditions traditionally expected to represent a stressor or limitation can benefit some organisms. For example, in marine environments, whelks have been shown to effectively detect the odour signals of prey in flows with higher turbulence intensity that are known to confuse larger crustaceans (Ferner and Weissburg, 2005). In rivers, higher (average) velocities can somewhat counterintuitively reduce drift in some invertebrate species, which may reflect the gains in feeding efficiency and reductions in predation pressure that can be experienced in higher velocity areas (Fenoglio *et al.*, 2013). With respect to aquatic plants, turbulence preferences may differ according to plant morphology (Tonetto *et al.*, 2014; Tonetto *et al.*, 2015), but turbulent flows facilitate exchanges of solutes between plants and surrounding water to aid growth, and stimulate the epiphytic communities of bacteria, microalgae and invertebrates on plant surfaces (Sand-Jensen and Pedersen, 1999).

A range of animals either make vortices or use those generated by other roughness elements for movement and feeding (Vogel, 1994). Perhaps the largest body of work exploring the importance of turbulence for aquatic organisms centres on fish, reflecting a combination of factors including the practicalities of measuring effects on larger animals as well as wider public and commercial interests. There are two main mechanisms by which rheophilic fish can exploit turbulent flows (Liao, 2007). First, individuals can use regions of reduced velocity behind cylindrical or spherical 'bluff bodies' as flow refugia, and for station holding or 'entraining' (maintaining their position within the flow field, Figure 2.2). By tilting the body into the mean flow direction at a certain angle, some species may be able to maintain their position close to flow obstructions without corrective body or fin motions for short periods of time, thereby minimising energy costs (Przybilla *et al.*, 2010). Similarly, fin motions can generate lateral wakes helping fish to maintain balance and avoid rolling (Gazzola *et al.*, 2014; Maia *et al.*, 2015). The second mechanism involves capturing the energy of discrete vortices, and is dependent upon the interaction between vortex size and fish body length (Liao, 2007). Predictable patterns of vortex shedding (as opposed to chaotic wakes) are considered to be important here (Lacey *et al.*, 2012), such as the repeating pattern of eddies known as a 'von Kármán vortex street' that may be generated downstream of flow separation around stationary D-shaped cylinders in laboratory flumes (Figure 2.2). Under these conditions, eddies are shed at a certain frequency and are constrained to a relatively small range, allowing fish to recognise and anticipate flow structures (Liao and Cotel, 2013). Laboratory experiments have demonstrated that trout will adapt a novel mode of motion (the 'Kármán gait') in order to slalom in between predictable patterns of vortices shed from upstream objects (Liao *et al.*, 2003). This type of movement requires a lower tail beat frequency and allows individuals to use only the anterior axial muscles, decreasing the energetic costs of locomotion (Liao *et al.*, 2003). Turbulence generated by the propulsive movements of other fish can also be exploited in a similar way (Liao, 2007).

Studying the exploitation of turbulent flow structures by invertebrates is challenging as a result of the difficulties of flow measurement at the scale of individual organisms (Blanckaert *et al.*, 2013) and within the near-bed region inhabited by benthic organisms (Hart *et al.*, 1996). Despite this, several examples of the importance of turbulent flow properties for invertebrates are available. Passive suspension feeders are an exemplar here since they depend upon the hydrodynamic properties of flow for the supply of food particles. Interactions between feeding appendages and other body parts, flow and transport of particulate matter are, therefore, highly important (Hart and Finelli, 1999). Blackfly larvae (*Simulium vittatum*), for example, can twist their bodies in order to position their specialised feeding fans at different points in the flow field. This allows them to exploit paired vortices generated by the flow across their bodies, with one fan capturing vortex-entrained particulate matter from the substrate, and the other filtering water from the top of the boundary layer (Chance and Craig, 1986). Mayfly larvae can take advantage of flow perturbations generated by their bodies to excavate and utilise pits in the river bed for feeding. For example, *Pseudiron centralis*, can face upstream into the flow and assume an arched position, thus generating energetic horseshoe vortices which excavate a pit and expose prey such as small burrowing and interstitial invertebrates (Soluk and Craig, 1990). In contrast, *Ametropus neavei* have been shown to orientate themselves upstream and excavate a pit which is then used in combination with their head, antennae and elevated forelegs to generate a vortex that deflects flow downward (Soluk and Craig, 1988). This enhances feeding in at least two ways: by trapping material within the swirling vortices and hence increasing the probability of capture, and by resuspending material from within the pit. It is suggested that these mechanisms may enhance opportunities for feeding in fine-sediment dominated rivers that lack the hard substrates generally required for anchoring by filter-feeders (Soluk and Craig, 1988). Multiple organisms positioned adjacent or in the streamwise direction can exploit mutually generated hydrodynamic conditions, for example to enhance their feeding rate by concentrating flows (Chance and Craig, 1986), or in the case of fish schooling by exploiting von Kármán trails generated by individuals upstream individuals that can reduce the energy costs of swimming (Shaw, 1978; Svendsen *et al.*, 2003; Fish, 2010; Muñoz-Mas *et al.*, 2015).

2.6 Turbulence as a threat to growth and survival

The physiological and energetic costs of turbulence to aquatic organisms are perhaps better documented than the benefits. In terms of physiological effects, intense turbulence impacting upon aquatic plants may cause tissue damage, increase respiratory costs as a result of leaf movements (Sand-Jensen and Pedersen, 1999), and inhibit metabolic activities and growth (Asaeda and Rashid, 2016). For animals, turbulence may lead to passive dislodgement from habitats. It has been shown that benthic invertebrates (e.g. *Aeshna cyanea* and *Somatochlora flavomaculata*) are sensitive to peak values of shear stress related to discrete turbulent ‘events’, specifically ejections of fluid away from the bed (generating upward lift forces) and inrushes of fluid towards the bed (generating lift and drag), where flow structures scaled on flow depth and hence exceeded invertebrate body size (Blanckaert *et al.*, 2013). In extreme cases, high shear stresses can cause disorientation, injury or mortality in fish (Odeh *et al.*, 2002; Deng *et al.*, 2005; Silva *et al.*, 2012), but more commonly turbulence may cause linear translation of the body (i.e. displacement or drift downstream), and/or deformation which alters the kinematics, for example via increases in tail-beat amplitude (Liao, 2007). Turbulence can also alter predator-prey relationships in complex and contrasting ways. Intense turbulence can diminish the accuracy of strikes (and hence successful captures) as a result of reduced predictability of the location of both predator and prey, which can be costly for the predator (Higham *et al.*, 2015). Conversely, turbulence may also disrupt the lateral line system used by prey fishes to detect predators and hence potentially increase the probability of capture (Higham *et al.*, 2015).

The influence of turbulence on fish bioenergetics (consumption, metabolism and growth) and swimming performance has received considerable attention in the literature, and has generated what appears at first glance to be contradictory conclusions (Cotel and Webb, 2015). For example, high turbulence intensity may increase susceptibility of perch (*Perca fluviatilis*) to downstream displacement (Lupandin, 2005), increase swimming costs of Atlantic salmon *Salmo salar* (Enders *et al.*, 2003) and negatively impact upon the dynamic stability of brown trout (Cotel *et al.*, 2006; Tritico and Cotel, 2010), but Nikora et al. (2003) found no influence of turbulence intensity on Inaga (*Galaxias maculatus*). Closer inspection, however, indicates that this likely reflects the variations in various aspects of the research design: the mechanism of turbulence generation, the exact properties investigated, their relation to the physiological traits (e.g. scale) of the species and the influence of behavioural responses such as acclimatisation and learning (Lacey *et al.*, 2012; Smith *et al.*, 2014; Maia *et al.*, 2015; Cotel and Webb, 2015). Life cycle, sex and health may also play a role: larger and smaller guppies (*Poecilia reticulata*) have been shown to prefer differing levels of average velocity and turbulence, with males selected lower velocity regions possibly due to fin-induced drag, and parasite infected smaller fish selected the most stable and predictable areas of low turbulence intensity and Reynolds stresses indicating a need to offset infection related energy costs (Hockley *et al.*, 2014).

While a number of studies have focused on the influence of turbulence intensity or turbulent kinetic energy on fishes, there is increasing evidence to suggest that the size of vortices relative to fish size is one of the key factors influencing energy costs (Webb and Cotel, 2010a; Silva *et al.*, 2012; Cotel and Webb, 2015), Figure 2.3. Fish length is generally used to represent size, reflecting the importance of the 'lateral line' system of sense organs that runs lengthwise from the gills to the tail and is required for orientation, predation and coordinated swimming (schooling). Webb and Cotel (2010a) note the inverse relationship between eddy size and frequency and suggest that the largest and smallest eddies may be less significant for fish, since the largest flow structures may be perceived as similar to still water and the smallest are unlikely to generate stability problems. Eddies in the intermediate range may (depending on their size relative to fish body length), however, require corrections to stabilise position or may even overwhelm the ability of a fish to stabilise itself (Webb *et al.*, 2010b). For example, Silva *et al*. (2012) emphasised the importance of eddies roughly equal to the body size of adult Iberian barbel (*Luciobarbus bocagei*), while vortices approximately 2/3 fish length affect the balance of perch (*Perca fluviatilis*) leading to stabilising fin movements that increase hydraulic resistance and decrease swimming speeds (Lupandin, 2005). Similarly, Tritico and Cotel (2010) found that stability challenges were not identifiable until the largest eddies reached 76% of the fish body length. Under such conditions fish lost postural control, spinning and translating downstream along the rotational axis of the largest eddies ('spilling'). A related quantity, the length of time a fish is exposed to the eddy, may also be important and can be considered as 'persistence' or the number of eddy rotations that occur during the time it takes a fish to move one body length through the flow (Cotel and Webb, 2015).

The orientation of flow structures can also exert important influences on fish behaviour and energetics (Lacey *et al.*, 2012). Streamwise vortices (where the axis of rotation is aligns with the main flow directions) can be expected to cause rolling (perhaps the most costly), cross stream, horizontal vortices are associated with pitching and vertical vortices with yawing (Maia *et al.*, 2015). Streamwise vortices have been shown to destabilise bluegill sunfish (*Lepomis macrochirus*), causing an increased frequency of spills and unsteady swimming manoeuvres (e.g. forward acceleration and side-to-side movements) and hence increased oxygen consumption, although fish could partially adapt after a period of acclimatisation (Maia *et al.*, 2015). The horizontal component of the Reynolds shear stress has been identified as a key parameter in hydraulic habitat selection for smaller Iberian barbel (*Luciobarbus bocagei*), suggesting that this could be an important consideration in artificial fishway design (Silva *et al.*, 2011).

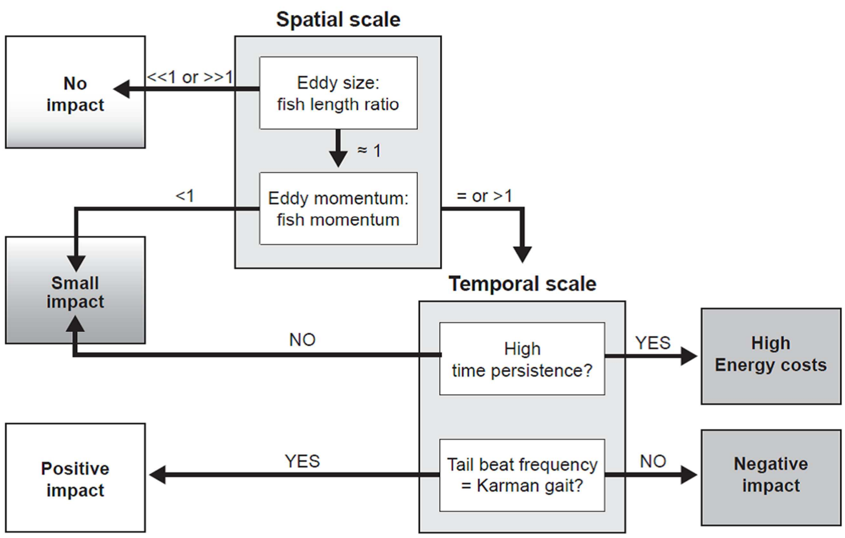

Figure 2.3 Decision tree illustrating how the spatial and temporal scales of eddies, combined with fish dimensions, influence the nature and magnitude of impacts on fish bioenergetics. Modified from Cotel and Webb (2015).

2.7 Knowledge gaps and research questions

This review has demonstrated the wide ranging and important interactions between high frequency flow properties and aquatic plants and animals in rivers, illustrating the importance of turbulence in generating suitable hydraulic habitat conditions and how organisms exploit different properties of the flow to maximise feeding and energy efficiency. The number of studies explicitly considering turbulent properties within the context of river habitat assessment and improvement, however, are relatively few (Lamarre and Roy, 2005; Wilcox and Wohl, 2007; Legleiter *et al.*, 2007; MacVicar and Roy, 2007a; MacVicar and Roy, 2007b; Harvey and Clifford, 2009; Roy *et al.*, 2010; David *et al.*, 2013; Wilkes, 2014). This partly reflects the practical difficulties associated with extensive field measurement of flow velocity at frequencies and record lengths sufficient to derive turbulent parameters (Buffin-Bélanger and Roy, 2005), as well as across different flow stages and at scales relevant to individual organisms (Hart *et al.*, 1996; Blanckaert *et al.*, 2013). As a result, approaches to habitat assessment tend to focus on spatially and temporally averaged conditions (e.g. average velocity, flow depth) at a single point in time (e.g. low flow) instead of the 'higher order' properties of the flow (Harvey and Clifford, 2009) over varying discharges.

Relationships between average flow velocity and turbulence, however, are complex and unclear, ranging from positive correlations (Wilkes, 2014; Tullos and Walter, 2015) to negative correlations (Cotel *et al.*, 2006; MacVicar and Roy, 2007a), and are influenced by additional factors such as bedform roughness (Wohl and Thompson, 2000). This suggests that standard hydraulic variables such as velocity and depth cannot be universally applied to provide reliable estimates of more complex turbulent flow properties which have greater ecological relevance (Lacey *et al.*, 2012). This may partly explain why aquatic communities (e.g.

macroinvertebrates) appear to ‘map’ onto visually identifiable geomorphic units in rivers (e.g. riffles, pools, cascades), while the hydraulics of those units have been difficult to define (Baker *et al.*, 2016). Direct consideration of turbulence has been shown to add discriminatory power when exploring habitat preferences and distributions of both fish (Smith *et al.*, 2014) and invertebrates (Morris *et al.*, 2015), illustrating the potential benefits of achieving better integration of “hydrodynamics into ecohydraulics” (Wilkes *et al.*, 2013).

Despite the inherent challenges, further work is urgently required to provide an improved understanding of the turbulent properties of geomorphic units and their interactions with river biota in order to support effective river habitat assessment and sustainable river management and restoration. The thesis aims to address some of the key knowledge gaps identified above, specifically: the relative lack of field studies relative to laboratory experimentation; the lack of explicit consideration of high frequency flow properties in habitat assessment at the reach and geomorphic unit scale; scales of variability in turbulence properties in space and time; and improved understanding of links between hydrodynamics and behaviour of aquatic organisms under field conditions.

2.8 Research aim and objectives

The overall aim of the research is:

to advance scientific understanding of the hydrodynamics of rivers at the geomorphic unit scale in order to inform effective habitat assessment and restoration.

This aim is addressed through four principal research elements and 14 objectives using field-based research at different spatio-temporal scales. The research questions, associated objectives and chapters in which findings are reported are provided in Table 2.2. The overall research design is described in Chapter 3 and details of methods specific to each research element are provided in the respective results chapters.

Table 2.2 Research objectives.

Spatial/ temporal scale	Research element(s)	Research objective(s)	Chapter(s)
Reach scale Low flow	Characterisation of reach-scale hydraulic habitat using turbulence properties	Compare turbulence intensity across reaches of different gradient, and explore their relationship with mean flow velocity.	4
		Identify differences in the predictability, orientation and scale of coherent flow structures across reaches of different gradient.	4
		Explore whether scales of variability in turbulence properties correspond with bedforms and/or other roughness elements.	4
		Identify the principal gradients in turbulence properties and their relationship with reach gradient.	4
Geomorphic unit Low flow	Hydraulic characterisation of geomorphic units across different gradient rivers	Quantify higher-order (turbulent) flow properties associated with key GUs (steps, riffles and pools) across reaches of different gradient.	5
		Evaluate the utility of turbulence variables in predicting the	5

		occurrence of geomorphic units.	
		Explore variation in turbulent properties in transitional areas and/or variations outside the scale of GUs.	5
Reach scale vegetated/ unvegetated season	Influence of changes in flow stage and aquatic vegetation cover on turbulence properties and their spatial organisation	Quantify the effects of increased flow stage on turbulence properties (intensity, periodicity, orientation and scale).	6
		Explore changes in the spatial organisation of turbulent properties associated with an increase in flow stage.	6
		Quantify the effects of aquatic vegetation growth on turbulence properties (intensity, periodicity, orientation and scale).	6
		Explore changes in the spatial organisation of turbulent properties with aquatic vegetation growth.	6
Geomorphic units Low flow	Interactions between turbulence and wood habitat features, and implications for fish habitat use	Characterize the IPOS turbulence properties around wood patches.	7
		Quantify fish preferences, behaviour and activity costs using underwater videography under field conditions.	7
		Explore the exploitation of hydraulic habitat around wood by fish.	7

CHAPTER 3: Field sites and research design

3.1 Introduction

The data presented in this thesis is based on field research conducted at three reaches spanning low, intermediate and high gradient rivers. The field sites, data collection and methods used to compute turbulence properties are common among the results chapters. This chapter therefore provides an overview of the field sites, description of the sampling design used for topographic, velocity surveys and geomorphological surveys and finally the details for the computation of turbulence parameters. Furthermore, the spatial and temporal scales of investigations are described. Chapter 4 and 5 consider analysis of all the three field sites while the chapter 6 describes the temporal variations of turbulence properties for the low and high gradient reaches and finally the chapter 7 considers only the intermediate reach (Table 3.1). Where methodological details differ from those presented in this chapter, descriptions are provided in the relevant results chapter.

Table 3.1 Details of spatial and temporal scales, type of surveys and rivers used for each chapter. GUS refers to the Geomorphic Units survey and classification System (Belletti *et al.*, 2015b) which is explained in further detail in Section 3.3.

Space	Time	Surveys	Datasets	Chapter
Reach	Low flow	Topography Velocity GUS	All 3 rivers	4
Geomorphic	Low flow	Topography Velocity GUS	All 3 rivers	5
Reach/ Geomorphic	Low flow and high flow OR vegetated and non-vegetated	Topography Velocity GUS	Vermigliana, Frome	6
Patch	Low flow	Topography Velocity Video	Tagliamento	7

3.2 Field sites description

Three field sites were selected in two countries, Italy and the United Kingdom. All three have suffered relatively low levels of management within the European context and achieve coverage of lowland, low gradient riffle/glide-pool morphology, intermediate gradient piedmont reach with riffle-pool morphology and high gradient step-pool morphology (Figure 3.1). For all three field sites, topography, velocity and geomorphic surveys were carried out during low flow conditions and a further velocity survey was undertaken for the low and high gradient reaches during high flow (high gradient reach) and for winter die back versus peak vegetation cover for the low gradient reach.

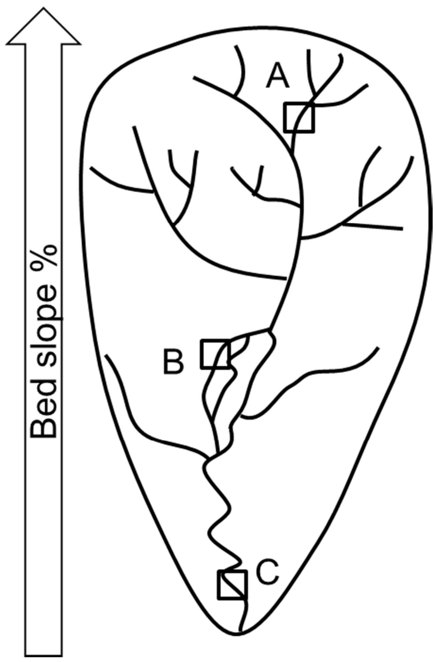

Figure 3.1 Catchment visualization for the three river sites from high gradient reach (A, Vermigliana), intermediate (B, Tagliamento) and low gradient reaches (C, Frome).

3.2.1 The Vermigliana Creek

The high gradient research site was a 64 m reach of the Vermigliana Creek (Figure 3.2), a tributary of the Noce River located in the Trentino Region of north-eastern Italy. The flow regime is pluvio-nival characterized by high seasonal variability with low flow during the winter and high flow in the summer (Table 3.2 and Figure 3.3).The creek flows from its source in the Presena glacier (3069 m a.s.l.) to join the Noce River at Ossana (950 a.s.l) and has a total length of 14 km and catchment area of 104 km^2. The steep hillslopes create a confined valley with an average channel slope of 1.5% (Zolezzi *et al.*, 2011). The bed substrate is predominantly composed of boulders and cobbles. The catchment can be described as semi-natural with relatively low levels of modification to the channel and riparian zone, although there is a small hydropower station and several sediment retention structures both located 2km downstream of the study site. Two flow surveys were carried out at two different flow stages (Table 3.7): one at 40% exceedance during August 2015 and the second at 10 % exceedance during May 2016.

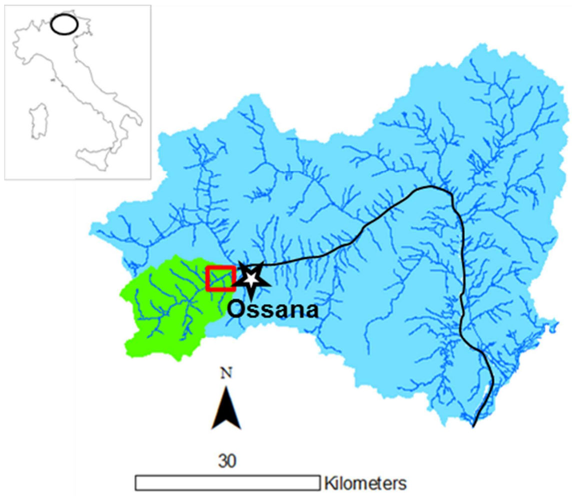

Figure 3.2 The Vermigliana Catchment (green area), included in the Noce catchment (blue area and black line) is located in the NE of Italy, Trentino Alto Adige. The red rectangle shows the location of the study site. Source: OpenData, (2014).

Table 3.2 Characteristics of study site. Hydrological data sourced by University of Trento, Department of Civil, Mechanical and Environment Engineering.

Reach Characteristics	Values
Q (50%) (m^3s^{-1}) (Main channel)	1.69
Bed slope	0.032
Reach Length (m)	64
Average Bankfull Width (m)	8
Average Water Depth (survey) (m)	0.5
Dominant substrate	Boulders and cobbles
Aquatic vegetation in the channel	Absent

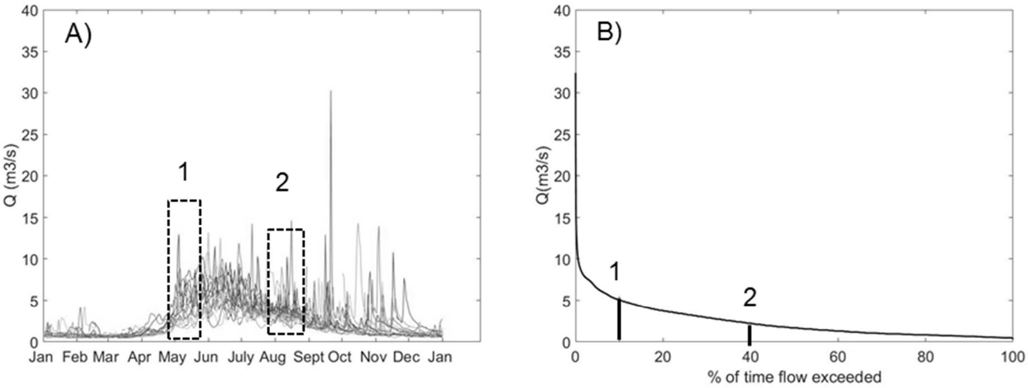

Figure 3.3 The Vermigliana Creek. A) Annual hydrograph of the Vermigliana Creek reveals an Alpine flow regime with low flow during the winter, and high flow during spring/summer. The black rectangles represent the two survey times: high flow at 10% exceedance (1) at the end of May ’16, and the low flow at 40% exceedance (2) during the dry period in early September. B) Shows the flow duration curve calculated for the validated available data (1996- 2012) with log-scale for x-axis. Source: University of Trento.

3.2.2 The Tagliamento River

The intermediate gradient field site was located on a side channel of the Tagliamento River in Italy. The Tagliamento is one of the last remaining pristine large gravel bed rivers in Europe (Müller, 1996). It is located in the Friuli Venezia Giulia region of North-East Italy (Figure 3.5b). The river flows from its source in the Dolomites National Park to the Adriatic Sea with a catchment area of 2540 km^2, and a total length of 172 km. The planform is predominantly braided, but the channel narrows and adopts a transitional to meandering style in the lower reaches (Gurnell *et al.*, 2000). In the braided sections, the river is highly dynamic and moves freely across a wider floodplain, developing a diverse range of morphological features and supporting a unique ecosystem (Ward *et al.*, 1999; Ward and Tockner, 2001). The Tagliamento is considered to be one of the last morphologically intact rivers in Europe, although it is not exempt from human intervention in the form of hydroelectric power plants, organic pollution and gravel abstraction in the upper reaches (Tockner *et al.*, 2003), and embankments downstream at Latisana. The hydrological regime is flashy pluvio-nival with higher flow during the spring and autumn caused by snowmelt and heavy rain respectively, with rapid changes in flow stage (Gurnell *et al.*, 2001). At Venzone, 20 km upstream from the study site, the mean discharge is approximatively 90 m^3s^{-1} (Tockner *et al.*, 2003).

The riparian vegetation is dominated by *Populus Nigra* (black poplar) and *Salix eleagnos (Karrenberg et al., 2003)*. The riparian zone is near-continuous in the braided section where there is a wide active floodplain of up to 1.5 km. There, sediments and driftwood deposited on gravel bars on the falling limb of flood events initiate vegetation colonisation and the formation of island landforms that protect and enhance the biodiversity of the river system (Ward and Tockner, 2001; Gurnell *et al.*, 2005; Gurnell and Petts, 2006). Wood inputs, together with hydraulics and sediment transport and deposition lead to the development of pioneer islands which grow and coalesce into larger, mature island features (Gurnell *et al.*, 2001; Gurnell and Petts, 2006) (Figure 3.4).

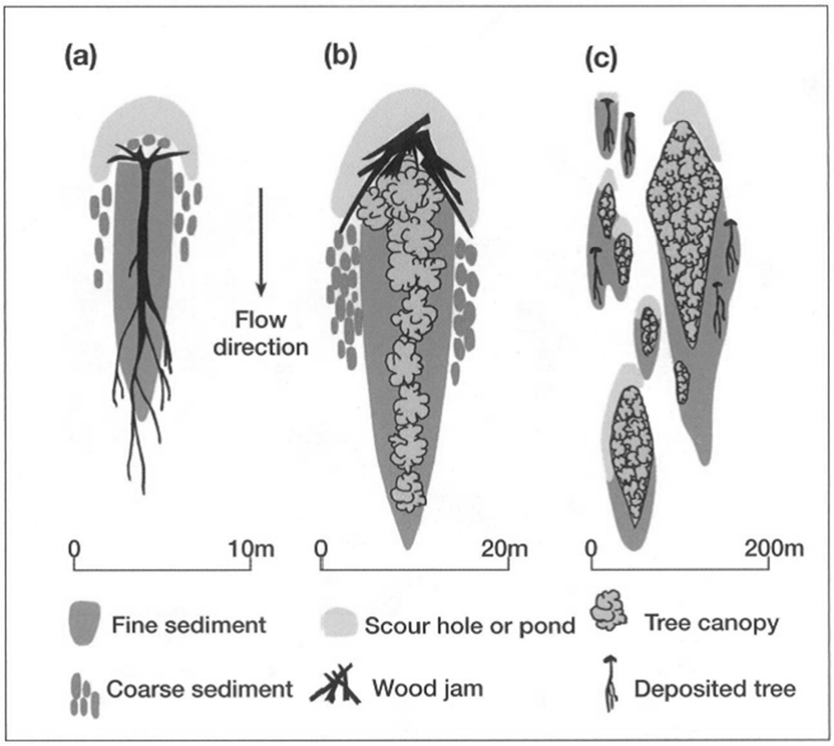

Figure 3.4 Developing of islands from living wood. (a) A deposited tree inducing the development of a suite of linked habitats; (b) a tree sprouting and inducing scour, deposition of fine sediment, and trapping of wood pieces to form a pioneer island; (c) an island complex with deposited trees, pioneer islands, and established islands distributed across an extensive gravel surface. Source: Gurnell *et al.*, (2005).

The study site of this research is located in the Flagogna reach, 3 km upstream from Pinzano (Figure 3.5). The river is braided in this section, with a wide active braid plain (maximum width = 900 m). The narrow 'pinch point' downstream at Pinzano gorge generates intensive upwelling that supports high vegetation growth rates in this section. The average slope is 0.012 and sediment size (D_{50}) is 40 mm. The research was carried out on a meandering anabranch of the main channel where, at low flows, a stable hydrological regime is regulated by groundwater maintaining undisturbed conditions (Sukhodolov and Sukhodolova, 2014). The survey was undertaken in July 2015 (Table 3.7). The discharge at the time of the survey was 3.52 m^3s^{-1} at the study section, and the flow at the upstream main section (Venzone gauge station) was 42 m^3s^{-1} (50% exceedance (Tockner *et al.*, 2003)) . The reach was 290 m long with average slope of 0.012 and water depth of approximately 45 cm. The reach receives a large input of wood, leading to the formation of wood jams and wood-associated morphological features such as gravel bars.

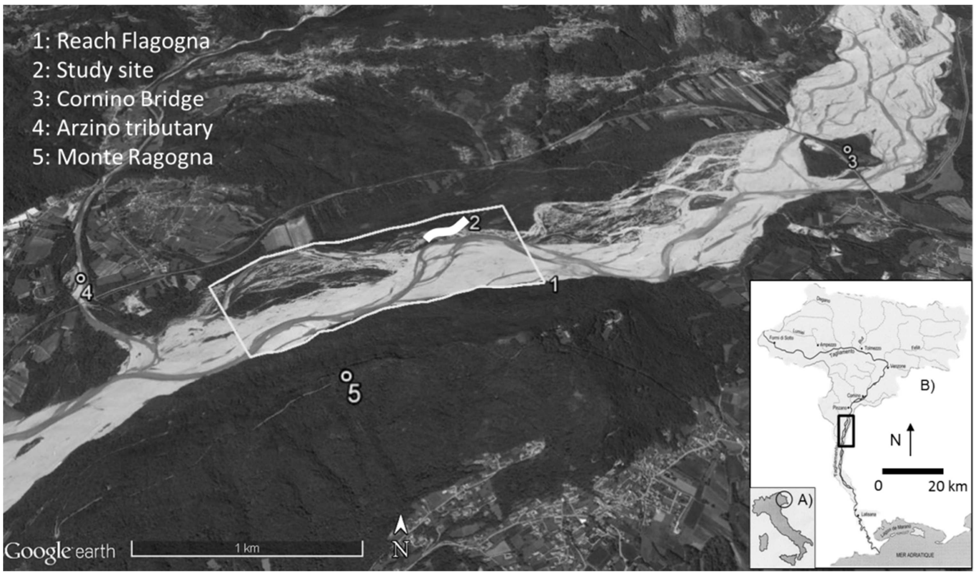

Figure 3.5 Location of the study site within the Flagogna reach and the Tagliamento catchment (B) in North East of Italy (A). The white line (2) shows the field site.

Table 3.3 Characteristics of study site. Source by Tockner *et al.*,(2003).

Reach Characteristics	**Values**
Q_{survey} (m^3s^{-1}) (side channel)	3.52
Bed slope	0.012
Reach Length (m)	290
Average Bankfull Width (m)	12
Average Water Depth (survey) (m)	0.45
Dominant substrate	Coarse gravel and cobbles
Aquatic vegetation	Living and dead wood

3.2.3 The River Frome

The low gradient field site was located on the River Frome in Dorset, southern England. The River Frome is a low gradient, lowland chalk stream. It rises at Evershot, passes through five small villages in the Dorset Downs area (Maiden Newton, Dorchester, Moreton, Wool and Wareham), and finally flows into Poole harbour. The total area of the catchment is 459 km^2 and its length is approximately 54 km. The upper Frome catchment is underlain by chalk systems, while the lower sections below Dorchester are characterized by mudstone and sandstone geology (Arnott *et al.*, 2009). Chalk streams are globally rare habitats, and the reach between Dorchester and Wareham is designated as Site of Special Scientific Interest (SSSI). The River Frome represents one of England's most productive rivers for Atlantic salmon (*Salmo Salar L.*) supporting a run of 1000 salmons (1997) that have been monitored by overlong time periods (> 30 years), although as is the case for many UK rivers, it has experienced a decline in the salmon population due to overfishing, loss of river habitats and artificial obstruction at the estuary (Welton *et al.*, 1999). Atlantic salmon (*Salmo Salar L.)* are most widespread along the middle and lower reaches while brown trout (*Salmo trutta*) are most abundant in the upper reaches (Environment Agency, 2010a).

Dominated by groundwater inputs from the underlying chalk aquifer, the Frome is rich in nutrients that support the growth of diverse and abundant communities of aquatic plants. The dominant species are *Ranunculus* spp, submerged macrophytes associated with high flow velocities in central channel areas (Gurnell *et al.*, 2006), and *Sparganium Erectum*, an emergent plant found at the channel margins. Both macrophytes influence flow hydraulics and sediment dynamics, for example by increasing water levels, and by generating regions of reduced flow velocities and fine sediment retention within plant stands (Wharton *et al.*, 2006) combined with intervening areas of high velocity where flow is concentrated (Gurnell *et al.*, 2006).

The research site was a 60 m long reach located in the upper part of the catchment near the town of Maiden Newton. The single thread channel is sinuous with dense riparian vegetation, and is characterized by riffle, pool and glide geomorphic units and abundant submerged macrophytes (*Ranunculus penicillatus subsp. pseudoluitans* (water crowfoot)) (Grabowski and Gurnell, 2014). Two velocity surveys were undertaken during peak vegetation growth (maximum vegetation cover) (September 2015) and winter die-back of vegetation (minimum cover; February 2016) as shown in Table 3.7 and Figure 3.6.

The average daily flow derived from 30 years of daily records at Dorchester gauging station 15 km upstream is 2.34 $m^3 s^{-1}$ (1971-2002). During spring 2015, the Environment Agency installed a new gauging station at Maiden Newton bridge to measure discharge and water level, but data were awaiting validation at the time of writing and hence the Dorchester record was used here.

Table 3.4 Characteristics of the study site. Source by Grabowski and Gurnell (2014).

Reach Characteristics	Values
Q (50%) (m^3s^{-1})	2.34
Bed slope	0.004
Reach Length (m)	60
Average Bankfull Width (m)	6
Average Water Depth (survey) (m)	0.33
Dominant substrate	Fine Gravel
Aquatic vegetation (seasonal)	*Ranunculus spp*

Figure 3.6 Photographs to illustrate seasonal change in macrophyte cover in a riffle tail on the River Frome: A) peak vegetation cover and B) minimum cover.

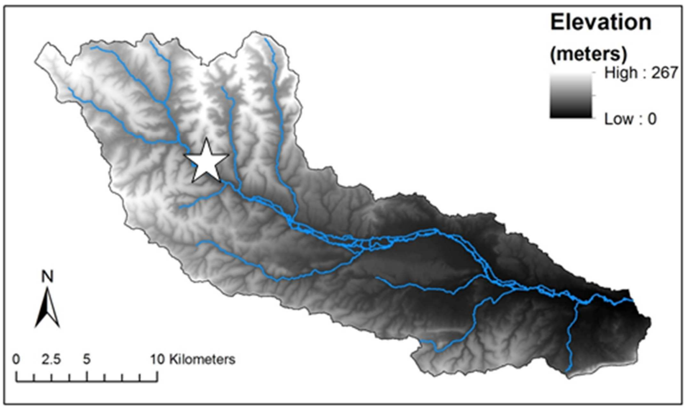

Figure 3.7 Frome catchment. Source: Graboswky *et al.*, (2014). The white star indicates the study site.

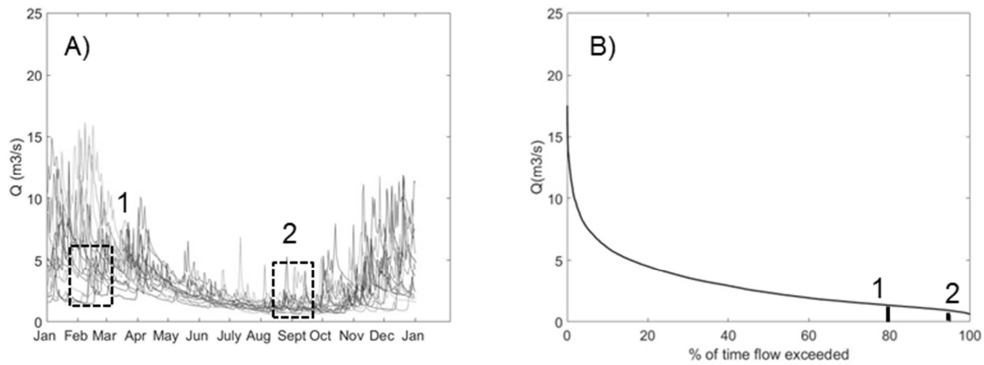

Figure 3.8 A) The daily flow of Frome. The dotted black lines represent the two sampling periods that reflect the die back period (1) (February 2016) and the peak of vegetation growth (2) in early autumn (September 2016). B) shows the flow duration curve (Log-scale for the x-axis) calculated for the available 30 years of gauging station data from Dorchester. Source: Environment Agency.

3.3 Identification of Geomorphic Units

In order to characterise geomorphic units in the channel (e.g. riffles, pools) at each of the three study reaches, rapid field surveys were carried out using the Geomorphic Units survey and classification System (GUS) (Belletti *et al.*, 2015b). The method is based on three different spatial scales (macro-units, units, and sub-units) within three different riverine areas (channel, margins, and floodplain), aiming to capture the diversity of geomorphic features within the river corridor as part of the wider Italian Morphological Quality Index (MQI) method for assessing morphological quality (Rinaldi *et al.*, 2015). Macro-units define the assemblage of homogeneous units with common textural features that can be identified by aerial images, while the units and sub-units capture greater detail on instream, marginal or floodplain features. Under this scheme, the channel represents the macro-unit, while bedforms (e.g. riffles, pools, glides, benches) represent recognisable units. Geomorphic Units (GUs) were delineated by visual assessment of process zones (erosion and deposition), landform configuration (channel slope, sediment organization, position within the channel) and natural riverine elements (bedrock, large wood), following elements of the classifications of (Brierley and Fryirs, 2013; Buffington and Montgomery, 2013). Table 3.5 presents the GUs surveyed under low flow conditions across the three study reaches of differing gradient. The low and intermediate gradient reaches where characterised by riffles and pools, while the high gradient reach was characterised by step-pool sequences.

Table 3.5 Brief description of Geomorphic Units surveyed across the three gradient reaches within an example of one step/riffle and one pool for each site (Belletti *et al.*, 2015b).

<table>
<tr><th></th><th>Low Gradient</th><th>Medium</th><th>High</th></tr>
<tr><td rowspan="2">Pools</td><td colspan="3">Channel spanning topographic depression in the channel bed; reversed bed slope; deep water; relatively slow velocity; finer sediment than adjacent units.</td></tr>
<tr><td></td><td></td><td>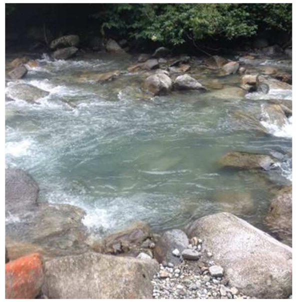</td></tr>
<tr><td rowspan="2">Steps/Riffles</td><td colspan="2">Shallow and fast flow; uniform sediment (gravel to small cobbles); undulating but unbroken standing waves; locally higher bed slope.</td><td>Bedrock steep channels; short unit; near vertical drops; span the entire width; tumbling flow; accelerating/ convergent flow.</td></tr>
<tr><td>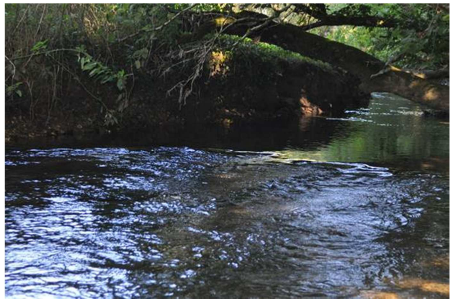</td><td></td><td>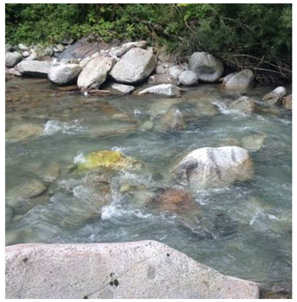</td></tr>
</table>

BASIC LEVEL *(page 4)*												
Bankfull channel Units												
Macro-unit type	P/A	N (or code)	L/A									
			1	2	3	4	5	6	7	8	9	10
Main channel (C)												
Secondary channel (S)												

Macro-Unit ID	Unit type	P/A	N (or code)	L/A									
				1	2	3	4	5	6	7	8	9	10
C	Pothole (CH)												
	Cascade (CC)												
	Rapid (CR)												
	Riffle (CF)												
	Step (CT)												
	Glide/run (CG)												

Figure 3.9 Example of the basic level form of GUS worksheet used to record the presence/absence of instream geomorphic units (Pothole, Cascade, Rapid, Riffle, etc.), by assigning a number or code and measuring their size. Source: Belletti *et al.*, (2015).

3.4 Topographic survey

Topographic surveys were conducted for each of the three research sites, under low flow conditions using a Leica Station T305. The survey was designed to capture bed elevations within the wetted channel, bank foot, and bank top locations. The survey resolution comprised a grid of approximately 1 m cell size (Morris *et al.*, 1990), and breaks in slope (Brasington *et al.*, 2000) were used to capture the variation in bed morphology. Detrended Digital Elevation Models (DEMs) were created for each of the three river reaches by removing the bank topography and extracting the channel centreline and thalweg of each site. Then, topographic residuals were linearly interpolating using a mesh of triangles to a 0.25 m^2, 1 m^2 and 0.21 m^2 resolution grid from a Triangulated Irregular Network (TIN) (Milne and Sear, 1997; Brasington *et al.*, 2000) developing topographic surface for the low, medium and high gradient reaches respectively. In addition, the analysis of positive and negative elevation residuals identified the presence of bedforms from the reach scale trends. Positive residuals may reflect deposition (riffles) while negative residuals may suggest the presence of depressions (pools) (Richards, 1976, Clifford *et al*, 2006). Geospatial analysis was completed in ArcGIS v. 10.2.

3.5 High frequency flow measurements

High frequency (32 Hz) flow velocity was recorded in 3 dimensions (streamwise, lateral, and vertical) using a Nortek/YSI (Vector) Acoustic Doppler Velocimeter (ADV) for a period of 120 s to ensure accuracy and robustness of turbulence measurements (Buffin-Bélanger and Roy, 1998, 2005; Wilkes, 2014). The Nortek Vector measures the 3 dimensional velocities in a small sampling volume with minimal effects on the flow (Nikora and Goring, 1998) using the Doppler Effect defined as the change in frequency for a sound wave produced by a moving source. The acoustic waves generated by the submerged probe hit suspended particles in the water and reflect back to the three orientated receivers. Additional measurements including temperature, pressure, orientation and position can also be collected.

In this research, the secondary circulations and microstructure of eddies (viscosity process) are not explored because they are less relevant to individual organisms (Webb and Cotel, 2010). The frequency and record length were selected to capture the majority of flow structures in the turbulent/ near-turbulent range following Buffin-Bélanger and Roy (2005). The flow meter was attached to a moveable mounting structure (Figure 3.11) designed with 'T' shape rod to vertically suspend the ADV in the flow and change the heights of velocity sampling based on the water depth ranging from 22 to 120 cm. Both horizontal and vertical planes had spirit levels to ensure accurate positioning within the flow field. This solid design ensured that the probe was orientated correctly in the flow, and stabilized the instrument under difficult environmental conditions (gravel or vegetated bed, high flows). The probe was orientated with respect to the bed and not to the flow streamline that may be orientated in several directions (towards the bed or the water surface). In fact, the presence of bedforms such as steps and pools sequences, vegetated features or river confluence increases the complexity of flow exhibiting streamlines which are not parallel to each other and means vertical velocities differ significantly from zero (Roy et al., 1994). Data were not rotated during the post-processing to facilitate the comparison between data. A stratified sampling approach was taken, with velocities sampled at three locations (30, 50, 70 % of channel width) along equally spaced cross sections in order to capture variability along the channel centreline and more marginal locations (Figure 3.12). Longitudinal cross sectional spacing was scaled on channel width: 3 m for the low and high gradient reaches; 5 m for the intermediate gradient reach. Each velocity measurement was captured at 0.6 of the water depth from the surface, in order to sample conditions in the central flow zone. This choice excludes the boundary layers with greatest intensity and shear stress but captures turbulent properties at the position in the velocity profile that is conventionally the focus of habitat studies. Flow measurement was not possible in areas where water depth was below 15 cm. Velocity measurements were obtained at two flow stages for the high gradient reach, and in two different seasonal periods for the low gradient reach. Discharge was estimated for each site at the upstream cross section and compared to stage data from historical records of the nearest gauge station. The water level was constantly monitored (every 10 minutes) in the upstream cross section to identify any changes in flow stage. Flow conditions were stable under all surveys. For low and medium gradient reaches, unfortunately, gauging stations were located some distance from the study site, but provide a broad hydrological context for the study.

Because ADVs are highly sensitive instruments, measurements are, however, subject to errors arising from probe orientation, sampling frequency, Doppler noise floor, and aliasing of the Doppler signal (Lane *et al.,* 1998). To ensure quality control, visual observation of time series plots was used to explore velocity variability and identify possible spikes (Chatfield, 2004). The WinADV (version 2.028) programme (US Bureau of Reclamation) was used to filter the velocity data for noise (spikes). Spikes are detected and replaced using the phase – space thresholding (PST) method based on a three-dimensional Poincaré map (Goring and Nikora, 2002). The Signal to Noise Ratio (SNR) and the Correlation (COR) parameters are the two key variables that can be used to evaluate the sensitivity of the beam's performance and the strength of the data linkage respectively. SNR values above 15 decibel (dB) and COR values above 70 represent an appropriate threshold above which spikes can be filtered and replaced (Goring and Nikora, 2002). In addition, stationarity tests were performed for each time series to identify the time series that were not stationarity and these were detrended using linear or second order regression (Clifford, 1993a; Harvey and Clifford, 2009). Data processing is presented in Figure 3.10.

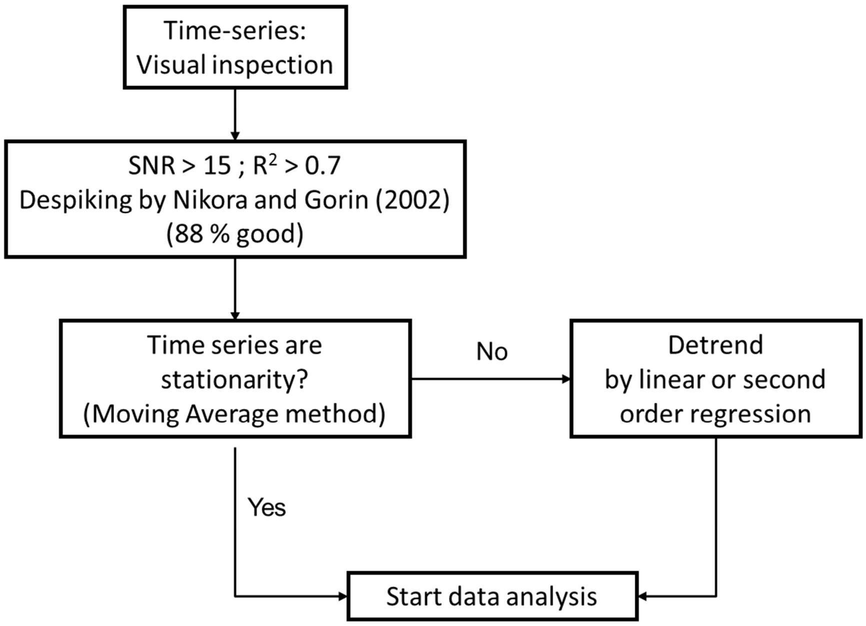

Figure 3.10 Process of data cleaning and detrending.

Following visual inspections and stationarity checks, 87 %, 93 % and 95 % of time series for low, medium and high gradient reaches respectively met the data quality requirements (Table 3.6). Those not meeting data quality requirements tended to be either close to aquatic plants (low gradient reach), highly turbulent areas (intermediate gradient reach) or shallow turbulent areas (high gradient reach).

Table 3.6 Summary of time series used for the study at the first and second surveys. For the low gradient reach, first survey reflected the die back vegetation period and the second the peak; while for the high gradient reach, the first survey represents the low flow stage and the second the high flow stage.

Rivers	Total surveyed measurements		Time series with visual errors		Time series used for analysis	
	1survey	2survey	1survey	2survey	1 survey	2 survey
Frome	62	62	7	8	55	54
Tagliamento	174	-	12	-	162	-
Vermigliana	51	51	2	4	49	47

Table 3.7 Time and discharge of surveys for each river. *Estimated by Tockner *et al.* (2003).

Gradient Rivers	Time of Survey	Q_{50} [m^3s^{-1}]	Q_{survey} [m^3s^{-1}]	Q percentile (%)
High	Low: August ‘15 High: May ‘16	1.69	Low: 1.82 High:5.53	48 10
Medium	July ‘15	42 (main channel)	3.52	50 (main channel)*
Low	Vegetated: September ‘15 Not vegetated: February ‘16	2.34	Vegetated: 0.58 Not vegetated: 1.45	95 80

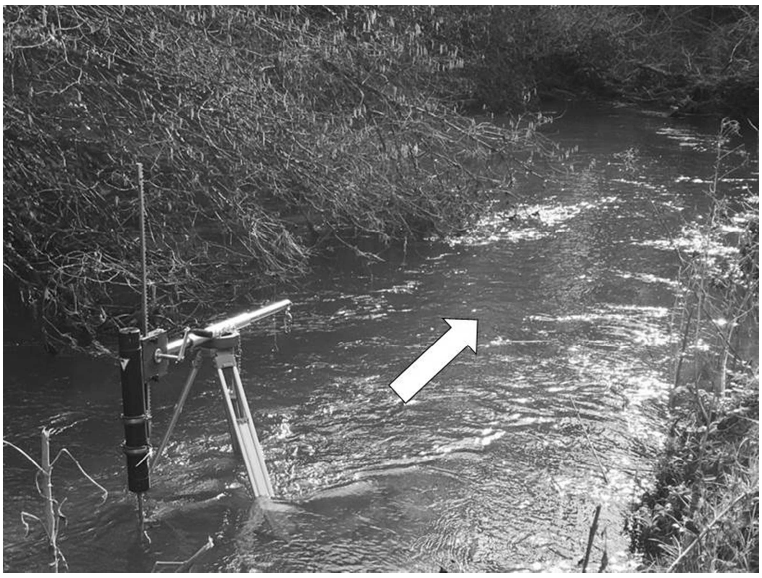

Figure 3.11 Mounting of the Acoustic Doppler Velocimeter formed by a tripod and a metallic mobile frame. The flow direction is represented by the white arrow.

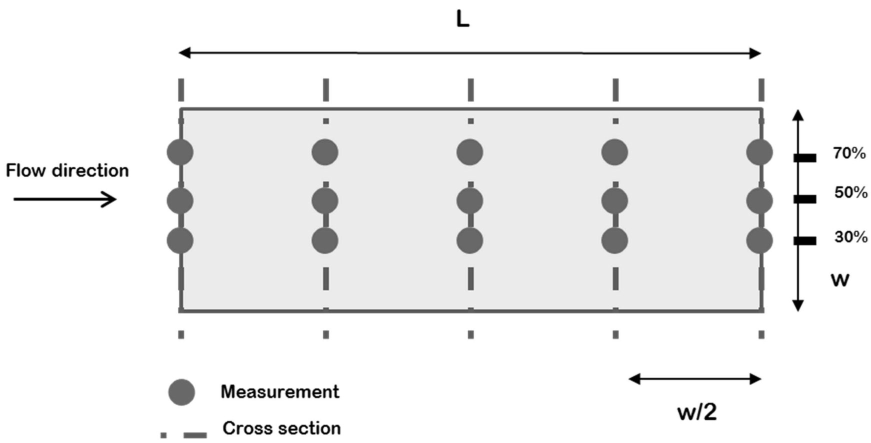

Figure 3.12 Sampling design for the velocity measurements was undertaken at each cross section (black dotted line), spacing on the channel width (w) for 3 points (30, 50, 70 % of channel width) at 0.6 from water surface. The black dots represent the location of 3D velocity measurements.

3.6 Limitation in the research design

The research design presented captures the hydrogeomorphology across three reaches of different gradients scaling on the size of the river. This approach may have implications on interpretations of result at small scales and represents a limitation to in relation to exploring turbulence generation at a scales smaller than individual boulders/aquatic vegetation stands. In addition, there were difficulties in collecting flow data under the same hydraulic conditions during the peak and die back vegetation periods due to weather conditions. This presents a limitation in relation to drawing comparisons between surveys andinterpretating results. Analysis using theManning coefficient, however supports the interpretation of the results. The sampling strategy was a compromise between time resources, instrumentation (ADV) and environmental conditions.

3.7 Computation of IPOS parameters

This section describes the computation of the ecologically relevant turbulence parameters explained in the Lacey *et al.,* (2012) IPOS (intensity, periodicity, orientation, scale) framework.

The IPOS framework has been informed by the results of laboratory and field studies of the influence of turbulence properties on fish behaviour and swimming performance. It offers a range of ecologically-relevant turbulent flow properties most of which can be readily computed from high frequency velocity time series. A range of variables falling within the four IPOS categories are presented in Table 3.8 and described in the following four subsections.

Table 3.8 IPOS categories (intensity, periodicity, orientation, scale) identified by Lacey *et al.* (2012) with example variables and descriptions. * denotes additional variables to those directly identified in Lacey *et al.* (2012). Where x = u, v, w components, N are the number of observations and ρ is the water density, u', v' and w' are the turbulent residuals and U, V, W the mean velocities along the three components.

	Parameter	Description
INTENSITY	*Turbulence intensity (absolute)*	Root mean square of the turbulent fluctuations (Reynolds normal stresses in the u, v and w dimension): $$RMS_x = \sqrt{\frac{1}{N}\left(x'^2_1 + x'^2_2 + \cdots + x'^2_N\right)}$$
	Turbulence intensity (relative)	Normalised (by shear or mean velocity) values for u, v, w: $$TI_x = \frac{\sigma_x}{X}$$
	TKE	Combines RMSu, RMSv, RMSw: $TKE = \frac{1}{2}\rho(RMS_x^2 + RMS_x^2 + RMS_x^2)$
	Reynolds Shear Stresses	Represent the turbulent flux of momentum – may affect organisms but rarely reported: $\tau_{uv} = \rho\overline{u'v'}$ $\tau_{uw} = \rho\overline{u'w'}$ $\tau_{vw} = \rho\overline{v'w'}$
	Vorticity (spinning speed)	$$\omega = 2\ angular\ velocity$$
PERIODICITY	*Predictability*	*Kurtosis** of the turbulent residuals (u', v', w') used as an initial indicator : $$K = \frac{\sum_1^N \left(\frac{x_i - \bar{x}}{\sigma}\right)^4}{N}$$ AR(2) models applied and the condition for pseudo-periodicity* derived (Richards, 1979). Average eddy frequency/ period (the *integral time scale*) can be derived (where R(t) is the normalized autocorrelation function and t is the time lag): $$ITS_{u,v,w} = \int_0^{\infty} R(\ t)dt$$
	Energy spectra	Fourier transform (spectral density/ wavenumber spectra) traditionally applied to qualitatively explore the shape of spectra and derive the kinetic energy maximum. Involves conversion of the frequency spectra into wavenumber spectra (k) using the frequency domain (fn): $$E\ (k) = \frac{U}{2\pi}\ S(f_n)$$

		$$k = \frac{2\pi f_n}{U}$$ Wavelet analysis – a newer method, better for intermittent/evolving flow structures (dominant frequency)
	Strouhal number	Dominant eddy frequencies in gravel-bed rivers could be linked to bed particle sizes (Clifford and French, 1993c), where Sl is the diameter of a body responsible for vortex shedding, S is the Strouhal number (~0.2) and f is the frequency of interest. $$S_l = \frac{SU}{f}$$
ORIENTATION	*Skewness**	An initial indicator of flow 'orientation' can be derived from the skewness of the u', v' and w' components (Wilkes, 2014): $$K = \frac{\sum_1^N \left(\frac{x_i - \bar{x}}{\sigma}\right)^3}{N}$$
	*Event structure**	Duration and/or contribution to stress of each type of 'event': Q1 (u'>0, w'>0; outward interactions), Q2 (u'<0, w'>0; ejections of fluid away from the bed), Q3 (u'<0, w'<0; inward interactions) and Q4 (u'>0, w'<0; inrushes of fluid towards the bed).
	Direction of dominant fluctuation	Axis of eddy rotation (angle between the direction of dominant fluctuation and the streamwise direction)
SCALE	Eddy length scale	Average eddy length or spatial extent of the region of correlation ("wedges" of fluid). The integral time scale (see above) can be converted to an average eddy length (L) using mean velocity (U) and t (time). $$L = Ut$$
	Eddy diameter	Spatial extent of rotating fluid, often directly measured using PIV techniques in the laboratory
	Length-scale ratio	Derived from the length scale (L_u) and fish length (L_f)
	Fish momentum: wedge momentum ratio	Derived from the length scale (L_u) and fish length (L_f) and convection velocity of the wedge (u_e) and fish velocity (u_f). $$\frac{Wedge\ momentum}{Fish\ momentum} = \frac{L_u * u_e}{L_f * u_f}$$

3.7.1 Intensity

The streamwise (u), cross stream (v) and vertical w velocity components can be decomposed into the mean (U, V, W) and the fluctuations (u', v', w') parts (Clifford and French, 1993a; Pope, 2000; Adrian *et al.*, 2000; Ömer, 2011) (Table 3.8).

Equation 3.1 $$u = U + u' \quad v = V + v' \quad w = W + w'$$

Within this framework, the mean refers to (relatively) longer-term variation at time intervals outside the range of turbulent fluctuations. For velocity time series exhibiting stationarity (i.e. unchanging mean, variance and autocorrelation through time), U, V and W are represented by the mean velocity for the series (Clifford and French, 1993a). However, velocity time series may exhibit low frequency variations associated with, for example, secondary circulations or vortex shedding from large roughness elements generating non-stationarity in time series. In this case, local detrending using linear or polynomial trends can be used to extract the turbulent residuals u', v' and w' (Soulsby, 1980).

The *Root Mean Square* provides a dimension indication of the magnitude of turbulent fluctuations, which can be computed separately for u, v, and w or presented as an average of the u' and v' components termed 'overall intensity' (Duncan, 1970). The *turbulent kinetic energy* is defined as the sum of the variance of the three components of velocity and represents the total amount of kinetic energy and is linearly dependent on the Reynolds shear stress (Pope *et al.*, 2006). Since turbulent flows are characterised by rotationality, with eddies defined as regions of finite vorticity, a *vorticity* metric can be used to describe the curve of the velocity vector.

3.7.2 Predictability (Periodicity)

Periodicity is defined as a tendency towards repeating flow patterns. Kurtosis of velocity residuals, the integral eddy time scale and meeting of the condition of pseudo-periodicity by second order autoregressive models represent variables that can be used to identify the periodic nature of turbulent flow. *Kurtosis* can be used to indicate the shape of the frequency distribution of turbulent fluctuations, with more leptokurtic (peaked) distributions indicating greater predictability. The integral of the autocorrelation function (ACF), or the *integral time scale* (Equation 3.2), represents the extent of the temporal window within which velocity values are highly autocorrelated (the quantity of time required for the passage of an eddy; Lacey and Roy, 2008), where *R* is the normalized autocorrelation function and *t* is the time lag.

Equation 3.2 $$ITS_{u,v,w} = \int_0^\infty R(\,t)dt$$

Assuming stationarity and a characteristic pseudo-periodicity in the time series, an autoregressive model (Equation 3.3) can be fitted to the velocity time series in order to compute the average frequency of vortex shedding (Equation 3.5; Clifford and French, 1993a). The condition of pseudo-periodicity defined by the Equation 3.4 indicates the tendency of phenomena to recur semi-regular intervals.

Equation 3.3 $$y_t = \emptyset_1 y_{t-1} + \emptyset_2 y_{t-2} + \varepsilon_t$$

Equation 3.4 $${\emptyset_1}^2 + 4\emptyset_2 < 0$$

Equation 3.5 $$Cos\ 2\pi f = \frac{\theta_1}{\sqrt{-\theta_2}}$$

The inverse of the frequency is the period (P), or time taken (in seconds) for the flow structure to pass the sensor.

However, the approach described above is based on characterising the average or 'dominant' eddy size in the time series but does not preserve any information on the distribution of eddies of varying size (MacVicar and Roy, 2007b) . In order to explore the contribution of eddies of varying size, the *spectral density function* of turbulent fluctuations (u', v', w') can be examined. The spectral density function is the Fourier transform of the autocorrelation function, and hence represents the distribution of eddy scales in the frequency domain (Clifford and French, 1993a). It represents the distribution of energy across frequencies in the time series, where the lowest frequency (fm) tend to be associated with the highest peaks reflecting the presence of larger, unstable vortices with higher magnitude kinetic energy, while the highest frequencies represent the low energy dissipative scale flow structures.

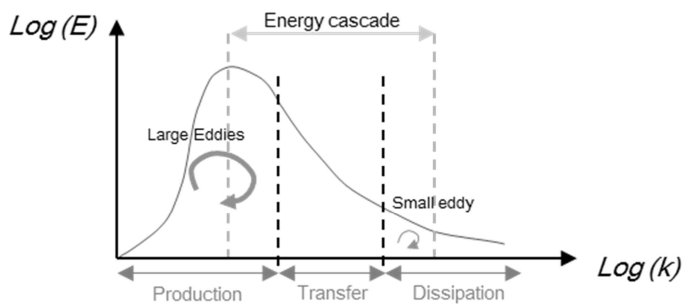

Figure 3.13 The energy cascade conceptum is represented by the energy spectrum of turbulent (E(k): Energy Spectral Density; k: wavenumber), modified from Davidson, (2004).

Conversion of the spectra density from the frequency domain (f_n) into spatial length scales can be achieved by computing the wavenumber spectra (Equation 3.6) where wavenumber (k) represents eddy size and $S(f_n)$ is the frequency of the spectra at the frequency $f_{n.}$

Equation 3.6 $$E\ (k) = \frac{U}{2\pi}\ S(f_n);\ k = \frac{2\pi f_n}{U}$$

The Wavelet Transform analysis is applied to detect the intermittent/evolving flow structures in a time series (Torrence and Compo, 1998; Zolezzi *et al.*, 2011) extrapolating the dominant temporal structure by scaling and shifting the signal on the window of a wavelet function. In this study, the Morlet wavelet was applied to estimate temporally and spatially variability. The Morlet wavelet has been identified as suitable for capturing semi-periodic patterns in geophysical processes (Torrence and Compo,1998). Subplots can be produced to reflect global and local properties of the signal energy describing the temporal velocity in the streamwise (u) dimension (Figure 3.14a), the Wavelet Power spectra (Figure 3.14b) with abscissa axis reflecting the length of the time series and ordinate axis the temporal length scale, the global wavelet spectra (GWS) (Figure 3.14c) and the average variance of the signal (Figure 3.14d). The dotted black line is the influence cone that reflects the significance level and confidence for the wavelet spectra.

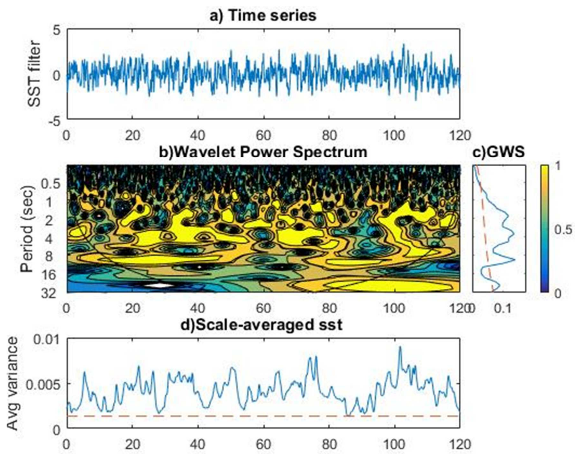

Figure 3.14 Example of the Wavelet analysis applied to time series of the one measurement along the streamwise component during survey at low flow. Graphs reflect: a) the time series, b) Power wavelet spectra, c) global wavelet spectrum (GWS) and d) scale-averaged time series.

3.7.3 Flow Orientation

A complementary approach to the time and frequency domain approaches described above is provided by application of quadrant analysis theory (Lu and Willmarth, 1973) to turbulence time series. This has been applied to identify the presence and contribution to the Reynolds shear stress of different types of turbulent 'events' as identified by the nature of fluctuations on the uw plane (Clifford, 1993; Harvey and Clifford, 2009 (Wilkes *et al.*, 2013). Research indicates that the highest magnitude 'events' are ejections (or 'bursts') of fluid away from the bed and compensatory sweeps (inrushes) of fluid towards the bed, with smaller contributions to the stress associated with outward and inward interactions (Roy *et al.*, 2004; Marquis and Roy, 2011; Robinson, 1991). Technically, the definition of burst-sweep events invokes the presence of streamwise 'streaks' of low momentum fluid within a viscous sublayer (Lu and Willmarth, 1973; Pokrajac *et al.*, 2007; Nakagawa and Nezu, 1977) which is unlikely to exist in hydraulically rough boundaries such as river beds where even the smallest particles may protrude above the limits of any such layer. However, the application of quadrant analysis can be usefully applied to gravel-bed rivers to statistically isolate turbulent flow structures and has been used to explore their form and intensity under controlled conditions (Lacey and Roy, 2008a; Hardy *et al.*, 2009; Marquis and Roy, 2011).

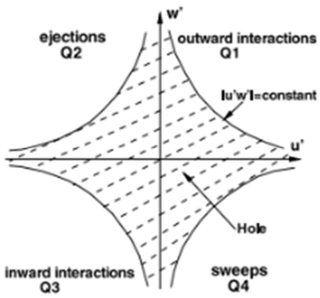

Figure 3.15 Structure of Reynolds stress. u' and w' are the fluctuation on the uw plane and the structure of the hole size by Yue *et al.*, 2007.

A 'hole size' (Equation 3.7) or threshold criteria can be applied in order to focus analysis on the stronger events (Yue *et al.*, 2007) and is defined by the relative shear stress for each region (where the bar over the elements represents the average value) (Figure 3.15).

Equation 3.7 $$H = \frac{|u\prime w\prime|}{|\overline{u\prime w\prime}|}$$

The fractional contribution of each quadrant to the shear stress is defined as by Equation 3.9, where S is the mean stress.

Equation 3.8 $$S_{i,H} = \frac{1}{T}\int_0^T u'w'(t) I_{i,H} dt \quad I_{i,H} = \begin{cases} 1 \; if \; (u', w') is \; in \; the \; quadrant \; i \\ \qquad |u'^{w'}| > H\overline{(u'w')} \\ 0 \qquad\qquad otherwise \end{cases}$$

(i = 1,2,3,4) represent the quadrant

Equation 3.9 $$S_{i,H}^{f} = \frac{S_{i,H}}{S}$$

3.7.4 Scale

Turbulence boundary layers encompass flow structures at a range of spatial scales, but the most commonly interested is the eddy length scale defined by the correlation length (Lu) or the integral length scale (ILS), that measures the spatial extent of the area over which velocity is correlated. Following the Equation 3.2 and assuming Taylor's (1935) hypothesis, the spatial length (Equation 3.10), or *integral length scale*, is given by the product of mean velocity (U) and the time delay (t).

Equation 3.10 $$L = Ut$$

While the eddy length measures the spatial extent over which the fluid velocity is correlated, the diameter measures the spatial extent of the rotation. A common way to calculate the eddy diameter (Equation 3.11) is to extract the information from the energy spectrum (Davidson, 2004) (k: wavenumber).

Equation 3.11 $$d = \frac{2\pi}{k}$$

It has been shown that the ratio of eddy size (rather than absolute eddy size) to fish size can be an important factor in fish energetics (Webb and Cotel, 2010a; Lacey *et al.*, 2012). To evaluate this, the length-scale (Equation 3.12) and momentum ratios (Equation 3.13) are two useful dimensionless parameters that can be used to estimate the likely nature and magnitude of impacts of vortices on fish:

Equation 3.12 $$\text{length scale ratio} = \frac{\text{eddy scale}}{\text{fish length}}$$

Equation 3.13 $$\text{Momentum ratio} = \frac{\mathrm{L_u * u_e}}{\mathrm{L_f * u_f}}$$

3.8 Statistical analysis

Multivariate statistical analysis was applied in order to explore the key trends emerging from the wide range of turbulence properties calculated. In total, 49 variables were computed to explore the turbulent properties of velocity time series. These range from time-averaged of the intensity of turbulent fluctuations and characteristics of ‘dominant’ eddies to energy spectra representing variability across flow structures of different frequency (size).

Given the large number of variables available, with potential for autocorrelation of variables, Principal Components Analysis was applied in several chapters in order to reduce the dimensionality and extract the key gradients in turbulent properties that explain the majority of variation in the data set. PCA describes how the covariance is structured through all variables of a dataset and identifies the direction(s) of variation, or eigenvector(s) which are linear combinations of the original variables (Jolliffe, 2002). PCA is a data reduction technique that can be used to reduce the dimensionality of a data set containing a large number of correlated variables (Legendre and Legendre, 2012). The eigenvectors, or principal components (PCs) represent the gradients of maximum variance and the principal component loadings describe the strength of correlation between each original variable to each new ‘variable’ (PC). The total number of PCs generated equals the number of original variables, but the first two or three are usually the most important in explaining the variance within the data set. The selection of PCs for further analysis takes place by assessing the eigenvalues (which should be > 1) and the amount of explained variance (ideally 70- 80%) and by visually observing the scree plot to identify breaks in slope.

Prior to PCA, Kaiser-Meyer-Olkin (KMO) and Barlett's test of Sphericity were analysed to identify redundant variables and check correlations between variables respectively. The KMO test assesses the sampling adequacy of the dataset and was used to check whether turbulence properties present were highly correlated with one another. Barlett's test checks the presence of redundancy between variables by identifying whether the observed correlated matrix is significantly different from the identity matrix. The KMO test ranges from 0 to 1 and values > 0.6 were considered acceptable. Barlett's test should return a result < 0.05 to enable an efficient PCA (Dziuban and Shirkey, 1974).

To explore the spatial organization of turbulence properties, geospatial analysis was performed for each reach using a semivariance approach based on the concept of a regionalized variable whereby closer observations (in space) are generally more similar. The theoretical semi-variogram model illustrates three parameters (range, sill and nugget) that help to identify the magnitude of variance and key scales of variation within the data set (Goovaerts, 1997). The range represents the distance beyond which the data are no longer correlated, the sill reflects the level of variance between observations and the nugget defines the variability at scales smaller than the sampling interval. The selection of the lag size, defined as the width of the distance observations, is important for accurate interpretation of results. In this study, the sampling grid used for each survey was used to select the correct lag size. The lag size used in the empirical semi-variograms computed by ArcGis 10.2 was 0.25 m for low and high gradient reaches and 1 m for medium gradient. A binning process was applied in which pairs of points were grouped by the distance from one another. The binned lags were associated with the distance between each cross section and they were 3 m for low and high gradient reaches and 5 m for the intermediate reach. Empirical semi-variograms were fitted with a semi-variogram model to assist interpretation. The model was fitted using a custom function written in MATLAB programming language by using a least squares fit of theoretical variograms (exponential) (Leigleter *et al.,* 2007; David *et al.,* 2013) in one dimension (streamwise).

CHAPTER 4: Characterization of reach-scale hydraulic habitat using turbulence properties

4.1 Introduction

Studies of turbulence in flume and field settings over the past 20 years have been facilitated by advances in instrumentation, such as Acoustic Doppler Velocimetry (ADV) (Nortek, 1998; Lane *et al.*, 1998; Voulgaris and Trowbridge, 1998; García *et al.*, 2005; Chanson, 2008); and quantitative analysis of turbulence (Farge, 1992; Torrence and Compo, 1998; McLelland and Nicholas, 2000; Goring and Nikora, 2002). A large body of important work has explored the spatial organisation, temporal dynamics and ecological importance of turbulent properties of flow in natural and artificial channels (Legleiter *et al.*, 2007; Nikora, 2010; Nepf, 2012; David *et al.*, 2013), including studies seeking to characterise the turbulent properties of visually identifiable channel Geomorphic Units to support river assessment, restoration and appraisal (MacVicar and Roy, 2007a; Harvey and Clifford, 2009; Roy *et al.*, 2010; Wilkes, 2014). Despite these developments there remains a lack of studies exploring turbulent properties at the reach-scale across different river styles. Likewise, understanding of the interactions between turbulence and fish is predominantly based on laboratory research that is known to generate different ranges of turbulent properties to those expected in natural channels (Lacey *et al.*, 2012).

Figure 4.1 and Table 4.1 summarise the spatial coverage and focus of published turbulence research based on a Google Scholar search constrained by article titles containing either “turbulent” or “turbulence” and either “river” or “stream” and the term “field” in order to illustrate the geomorphological context of field studies published to date.

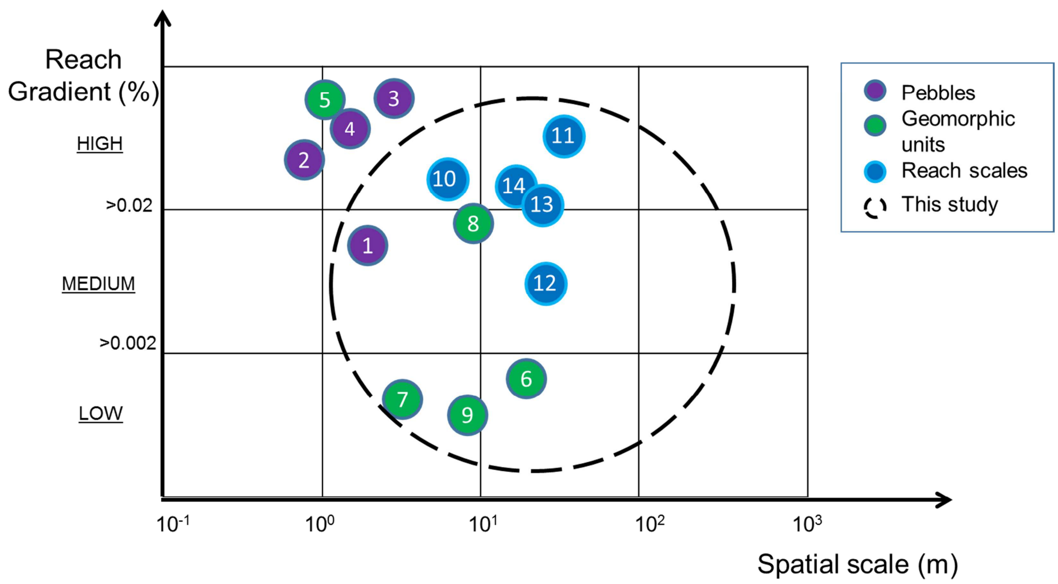

Figure 4.1 Previous studies on the variability of velocity and turbulence properties based on filed sites. Dotted line represents the coverage achieved in this thesis.

Table 4.1 Details of previous field studies of the variability in turbulent flow properties.

Bubble number	Papers	Gradient	Scale	Reach slope	Space (m)	Frequency (f) (Hz)	Time (sec)	Record length = f*time	Instrument
1	Lacey and Roy 2008	High	Pebble	0.013	5	30	100	3000	ADV
2	Tritico and Hotchkiss, 2005	High	Pebble	0.036	1	25	120	3000	ADV
3	Thompson, 2007	High	Pebble	0.07	8	10	180	1800	ADV
4	Buffin-Bélanger and Roy, 1998	Medium	Pebble	0.05	4.5	20	70	1400	ECMC
5	Wohl and Thompson, 2000	High	Geomorphic unit	0.03	3	20	360	7200	ECMC
6	Robert, 1997	High	Geomorphic unit	0.001	20	1	60	60	ECMC
7	Harvey and Clifford, 2009	Low	Geomorphic unit	0.002	6	16	30	480	ECMC
8	Roy *et al.*, 2010	Medium	Geomorphic unit	0.02	10	25	80	2000	ADV
9	Wilkes, 2014	Low	Geomorphic unit	0.003	10	25	90	2250	ADV
10	David *et al.*, 2013	High	Reach scale	0.04	6.5	1	180	180	ADV
11	Wilcox *et al.*, 2011	High	Reach scale	0.03	30	20	90	1800	ADV
12	MacVicar and Roy, 2007	Medium	Reach scale	0.012	25	20	120	2400	ADV

13	Lamarre and Roy, 2008	Medium	Reach scale	0.002	25	25	80	2000	ADV
14	Leigleter *et al.*, 2007	High	Reach scale	0.04	20	10	180	1800	ADV
	This study	High	Geomorphic/Reach unit	0.032	64	32	120	3840	ADV
	This study	Medium	Geomorphic/Reach unit	0.012	290	32	120	3840	ADV
	This study	Low	Geomorphic/Reach unit	0.004	60	32	120	3840	ADV

Lacey *et al.* (2012) proposed a framework for exploring ecologically-relevant turbulent properties in river channels. The paper notes the constraints of laboratory experimentation in simulating the flows fish (and other organisms) experience in natural channels and proposes four categories of turbulent characteristics that should be explored: intensity, predictability, orientation and scale ('IPOS'; Lacey *et al.*, 2012; see review in Chapter 2 and summary in Table 2.1).

This chapter presents high frequency flow data captured under low flow conditions from low, intermediate and high gradient rivers with different characteristic bedform sequences to explore the nature, variability and spatial organisation of turbulence properties at scales relevant to river assessment. In particular, the research addresses four objectives:

1. Compare turbulence intensity across reaches of different gradient, and explore their relationship with mean flow velocity.

2. Identify differences in the predictability, orientation and scale of coherent flow structures across reaches of different gradient.

3. Explore whether scales of variability in turbulence properties correspond with bedforms and/or other characteristic roughness elements.

4. Identify the principal gradients in turbulence properties and their relationship with reach gradient.

4.2 Methodology

4.2.1 Field data

Full details of the three field sites and sampling design are provided in Chapter 3 (Section 3.2) and a summary of the field site characteristics is provided in Table 4.2. A stratified sampling approach to velocity measurement was taken, with velocities sampled at three locations (30, 50, 70 % of channel width) along equally spaced cross sections in order to capture variability along the channel centreline and more marginal locations. See Chapter 3 (Research Design) Section 3.5 for full details of velocity measurement. Each velocity measurement was captured at 0.6 of the water depth (from the surface) in order to sample conditions in the outer flow zone. Velocity measurements were captured under low flow conditions for all three reaches.

Table 4.2 Details of three river sites including location, gradient, channel properties (slope, width, length, depth), Q_{50}, survey dates, discharges at time of surveys and number of surveyed points.

River	Vermigliana	Tagliamento	Frome
Location	Trentino Alto Adige, Italy	Friuli Venezia Giulia, Italy	Dorset, UK
Gradient	High	Medium	Low
Slope	0.032	0.012	0.004
Mean water surface width (m)	8	12	6
Mean flow depth at the survey time (m)	0.41	0.48	0.33
Length (m)	64	290	60
Dominant Substrate	Boulders and pebbles	Coarse gravel and cobbles	Fine gravel
Bedform spacing	8/10 m	15/20 m	10 m
Q50 ($m^3 s^{-1}$)	1.69	42 (main channel)	2.34
Survey dates	19 August 2015	13 July 2015	28 September 2015
Q ($m^3 s^{-1}$) (field measured) during the survey	1.82 (48% exceedance)	3.52 (50% exceedance based on main channel flow)	0.58 (95% exceedance)
Number of surveyed points	48	165	57

4.2.2 Data analysis

Turbulence parameters were computed (see Chapter 3 for full details) for all time series that met data quality as previous explained in Chapter 3 (see Table 3.6). Data were not normally distributed (Shapiro – Wilk: $p < 0.001$) and therefore non-parametric statistical tests were used. Spearman's Rank correlations were used to assess the relationships between variables and Kruskall Wallis with post hoc tests were used to identify significant differences between groups. Semi-variograms were used to explore the spatial organisation of turbulence properties. Semi-variance is a geostatistical approach used to explore the spatial correlation of individual variables between measured points at various distances. The approach is based on the concept of a 'regionalised variable', which assumes that points that are close to one another are more similar (Davis, 2002). Investigation of spatial dependence between samples of hydraulic properties has been linked to the structure of bedforms in previous studies (Clifford *et al.*, 2005) and semi-variograms of turbulence intensity have revealed strong stage-dependency of hydraulics and an important influence of channel location, in particular flow convergence or divergence areas appeared to influence turbulence (Leigleter *et al.*, 2007; David *et al.*, 2013). Semivariograms showing semi-variance in the streamwise direction were computed for 10 key hydraulics variables comprising the main turbulence descriptors defined by Lacey *et al.* (2012), topographic residuals (ΔZ) and mean velocity in three dimensions (U, V, W). The distance between observations (lags) was 3 m for low and high gradient reaches and 5 m for intermediate reach.

Multivariate statistical analysis (Principal Components Analysis; PCA) was used to identify the key gradients in turbulence properties within the data set. Prior to compute the PCA, Kaiser-Meyer-Olkin (KMO) and Barlett's test of Sphericity were analysed to check correlations between variables in the data set and the sampling adequacy were appropriate for PCA. Correlations between variables were checked using Spearman's Rho in order to remove any variables with particularly high correlations. This led to the removal of the mean velocity, RMS fluctuations, kurtosis and skewness for the three components (u, v, w) and the temporal and spatial eddy scales in the cross stream dimension (ITSv, ILSv) and cumulative duration and magnitude of inward/outward interactions (Q1, Q3) and power spectra. Bartlett's test of sphericity was then used to confirm that correlations between the remaining pairs of variables were sufficiently high to be included in the PCA. The final data set therefore include 12 variables: the resultant velocity, Reynolds shear stress on uv and uw planes, turbulent kinetic energy, magnitudes and duration of ejections and inrushes and spatial and temporal eddy scales on u and w directions.

Two PCAs were run, both based on Spearman's rho correlation matrix with orthogonal rotation (Varimax): a dimensionless PCA accounting for differences in magnitude for mean velocity and turbulence properties between the rivers singularly standardised by z-scores (Emery *et al.*, 2003; Wallis *et al.*, 2012), and a PCA based on 'raw' turbulence variables to account for absolute differences in magnitude of turbulence properties.

Semivariograms were computed for the PCA scores to explore the spatial organisation of turbulence properties. Statistical analyses were conducted in IBM SPSS version 22, ExcelSTAT Base 2016 and Matlab R2015b and geostatistical analysis was conducted in ArcGIS v10.2 and Matlab R2015b.

4.3 Results

4.3.1 Scale and variation of IPOS turbulence parameters and relationships with mean velocity

The absolute and relative intensity of velocity residuals along the three components (u, v, w), together with the Reynolds shear stresses and Turbulent Kinetic Energy (TKE) combining all three velocity components, provide key indicators of turbulence intensity (Figure 4.2). Considerable variability in values for all metrics was noted for the intensity parameters, but some trends were apparent. Across the three reaches, the absolute intensity (Figure 4.2A) was highest for the streamwise component (u), lowest in the vertical direction (w) and intermediate for the lateral (v) component. There was an overall increase in absolute magnitude with increasing gradient for all three components, which is also illustrated by TKE (Figure 4.2D). The reversal of this trend for relative intensity (standardised by mean velocity in each dimension respectively; Figure 4.2B) illustrates the high magnitude of fluctuations relative to v and w, and reveals a decrease in the magnitude of fluctuations relative to mean velocity with increasing gradient for u and v components.

Overall, values for Reynolds shear stresses increased with gradient, and the uv plane was associated with the highest and most variable values, followed by u'w' and v'w' (Figure 4.2C). Kruskall Wallis post-hoc tests showed significant differences between reaches in all parameters (Table 4.3), with the majority of parameters distinguishing between reaches. Exceptions were no significant differences in RMSu for the medium and high gradient reaches, and TIv and TIw where there was no significant difference between low and medium gradient reaches.

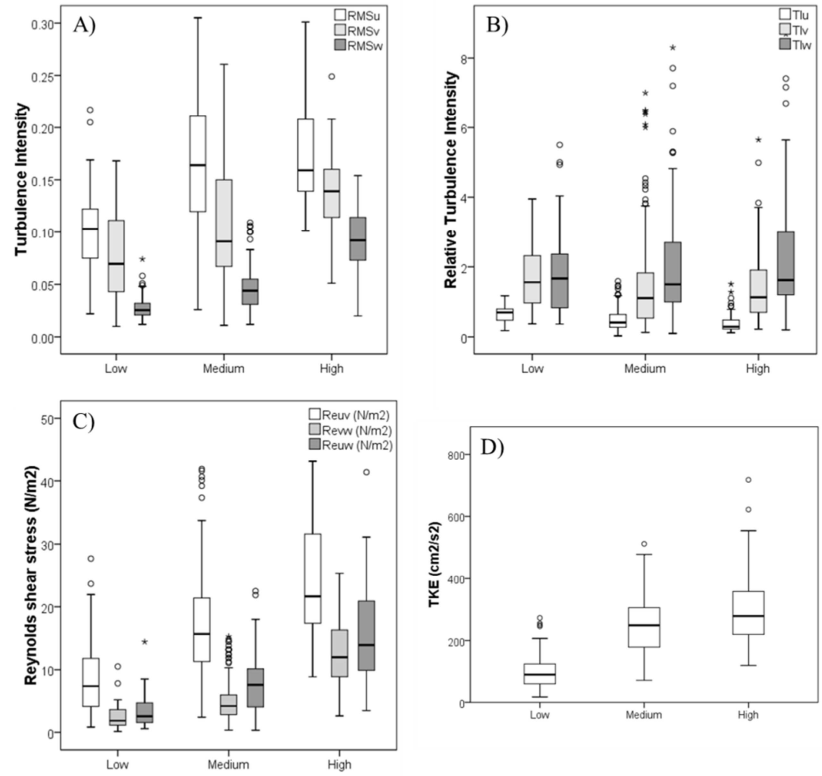

Figure 4.2 Distribution of the mean turbulence intensity (m s^{-1}) (A), the relative intensity (B) along the streamwise (u), lateral (v) and vertical (w) directions. Reynolds shear stress (Nm^{-2}) (C) on the three planes (uv, vw, uw) and the turbulent kinetic energy cm^2 s^{-2}) (TKE) (D) from low to high gradient rivers at low stage. Central line indicates the median; the lower and upper box limits indicate the 25 and 75 percentile and the whiskers show the 0 – 100% quartile range.

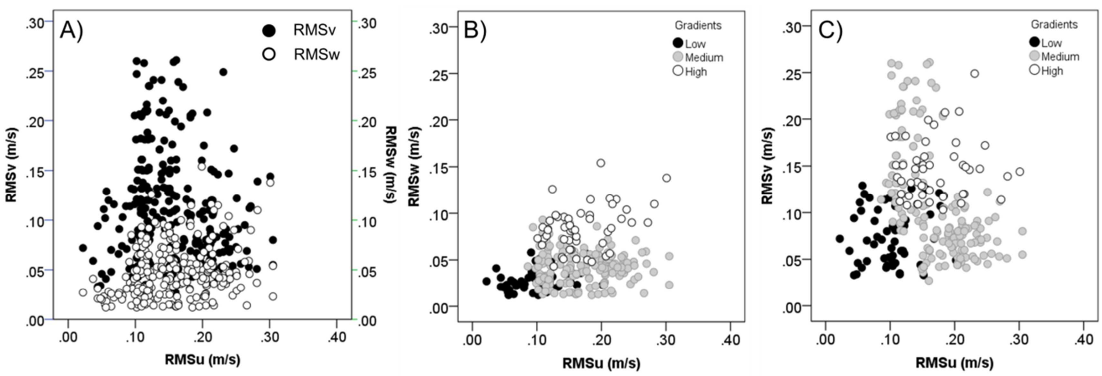

Figure 4.3 Relationships between fluctuation on streamwise (RMSu) and lateral (RMSv) and vertical (RMSw) components (A) and the exploration of fluctuations of all the three components between across different river gradients (B and C).

Table 4.3 Table of significant differences between parameters (Kruskall Wallis post-hoc tests where $p < 0.01$).

Parameter	Significant differences
RMSu	High/medium gradient > low gradient
RMSv	High gradient > medium gradient > low gradient
RMSw	High gradient > medium gradient > low gradient
Tlu	Low gradient > medium/high gradient
Tlv	Low gradient > medium/high gradient
Tlw	Low gradient > medium/high gradient
u’v’	High gradient > medium gradient > low gradient
v’w’	High gradient > medium gradient > low gradient
u’w’	High gradient > medium gradient > low gradient
TKE	High/medium gradient > low gradient

The relationship between the RMS of fluctuations in the u plane with fluctuations in w and v are explored in Figure 4.3 together with the exploration of RMS in all three components across different gradient reaches. There was no clear overall trend, which suggests that while the median intensity increased across all three velocity planes with gradient at the reach-scale, there was no clear correlation at the scale of individual measurements. There was a smaller range of intensity for the vertical component than the lateral component. Reach-specific behaviour indicates: (i) for the low gradient reach, a constrained range of values for RMSw, but considerable variability in RMSv in relation to increasing RMSu; and (ii) for the medium and high gradient reaches highly variable RMSw and RMSv with increasing RMSu and no linear relationship. Thus, higher intensities on the v and w planes were not necessarily associated with higher intensities on the u plane.

The RMS and Reynolds shear stresses are explored in relation to the resultant velocity in Figure 4.4. Across all three reaches there was an overall increase in RMS and Reynolds stresses with increasing resultant velocity. Bivariate correlations were generally weak (<0.50) and the strength of relationships is higher for the Reynolds stresses (0.46-0.49) compared to RMS (0.27-0.40) but all were statistically significant (Spearman's Rank: $p < 0.01$). Presence of linear relationships between resultant velocity and RMS/ Reynolds stresses were also explored for each river individually. Again these were generally weak (<0.2) although relatively stronger correlations were observed for the low gradient reach (0.38-0.49; $p<0.05$). Closer inspection of the plots indicates that two phases of the relationship account for the large amount of scatter for most of the plots, relating broadly to a lower gradient and higher gradient curve. Exceptions are RMSv and v'w' where a cluster of lower RMS/ higher v'w' values are observed outside of the main trend (black dot-dashed circles). The two phases are not explained by the three reaches and therefore spatial organisation of these properties was explored by visualisations using the relationships between resultant velocity and RMSu/ u'v' (Figure 4.5 and Figure 4.6).

Bi-plots were subdivided in 9 grid cells indicating specific ranges in order to assign measurements to the two broad phases (Figure 4.6). Phase 1 values were assigned to grid cells 1, 2, 4 and 7 for both bi-plots described by resultant velocity ranged from 0 to 0.29 m s^{-1} and all fluctuations/shear stress and by resultant velocity ranged between 0.29 and 0.60 m s^{-1} and fluctuations/shear stress above 0.20 m s^{-1} and 26 N m^{-2}. The remaining cells characterized by resultant velocity above 0.30 m s^{-1} and greater variability of fluctuations/shear stress were assigned to Phase 2.

For the low gradient reach, the majority of points are classed as Phase 1, with a smaller number of Phase 2 points located in narrower marginal areas constrained by aquatic plants, indicating higher fluctuations and increases in shear stress. For the intermediate gradient reach, Phase 1 points were largely associated with marginal locations on the right bank and in few areas of negative topographic residuals (pools) while Phase 2 points were mostly observed in the central part of the channel and left bank and areas with higher topographic residuals (i.e. riffle/run areas). For the high gradient reach, there was a more complex spatial organization: both phases were found in both central channel and marginal areas.

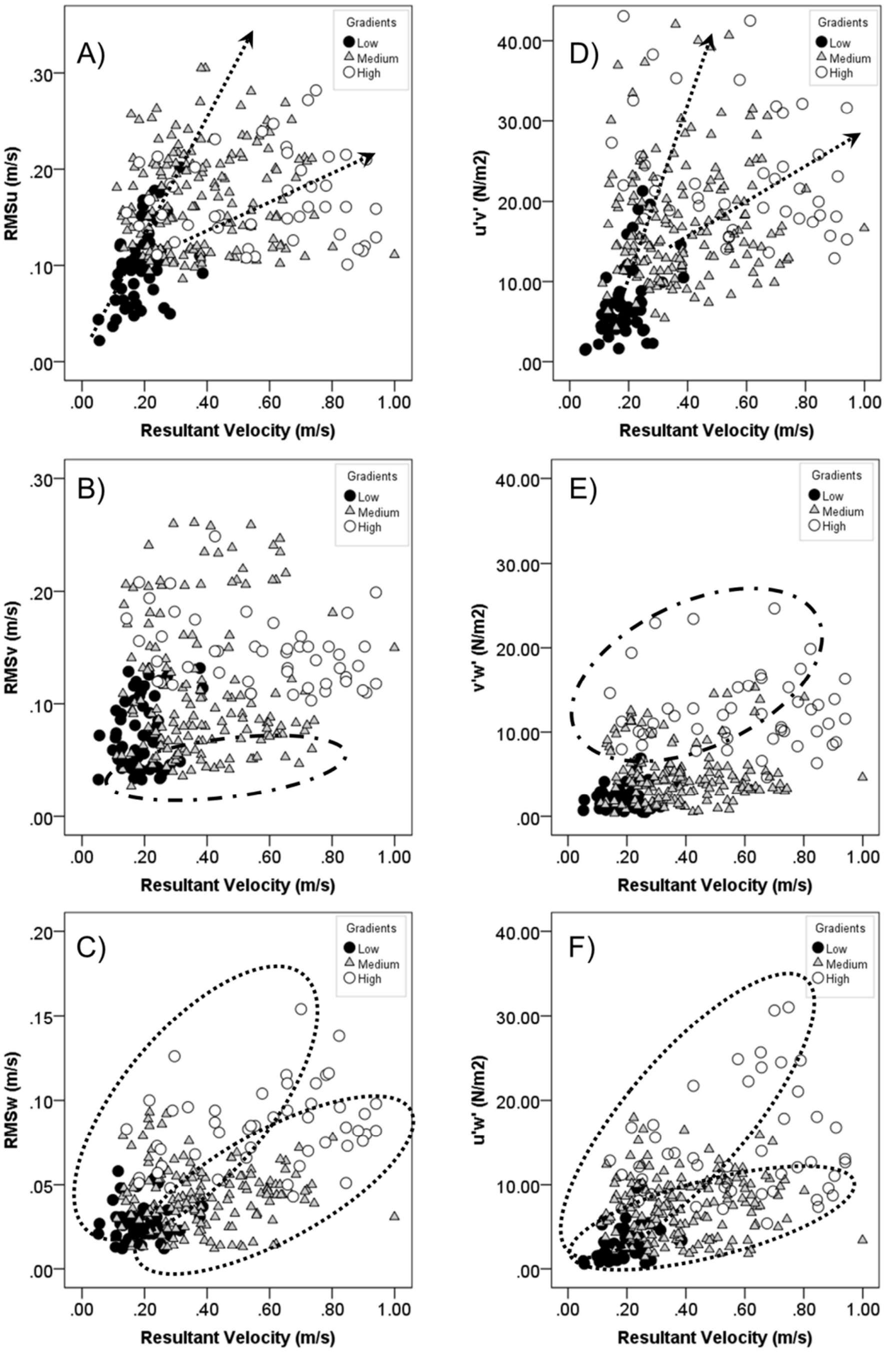

Figure 4.4 Comparison of root mean square values along the streamwise, lateral and vertical directions (A, B, C) and Reynolds shear stress along the uv (D), vw (E), and uw (F) planes to the resultant velocity respectively.

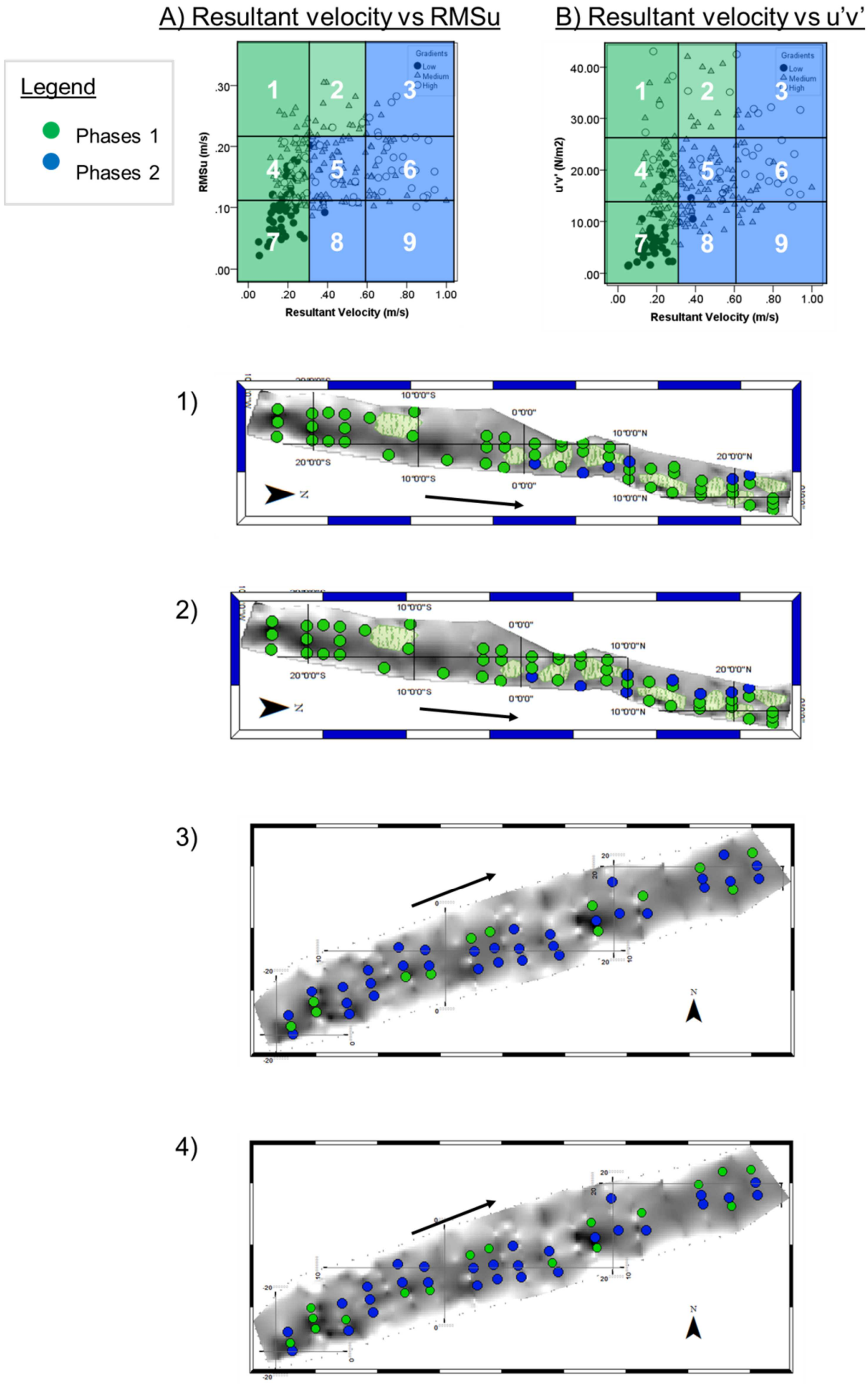

Figure 4.5 Subdivision of each bi-plots in grids reflecting specific range of resultant velocity and fluctuations on u component (A) and shear stress on uv plane (B). The spatial distribution for the two groups is explored for the low (1-2) and high gradient (3-4) reaches. The two phases (green and blue areas/dots) reflect the relationships between resultant velocity and RMSu (1, 3) and shear stress on uv plane (2, 4).

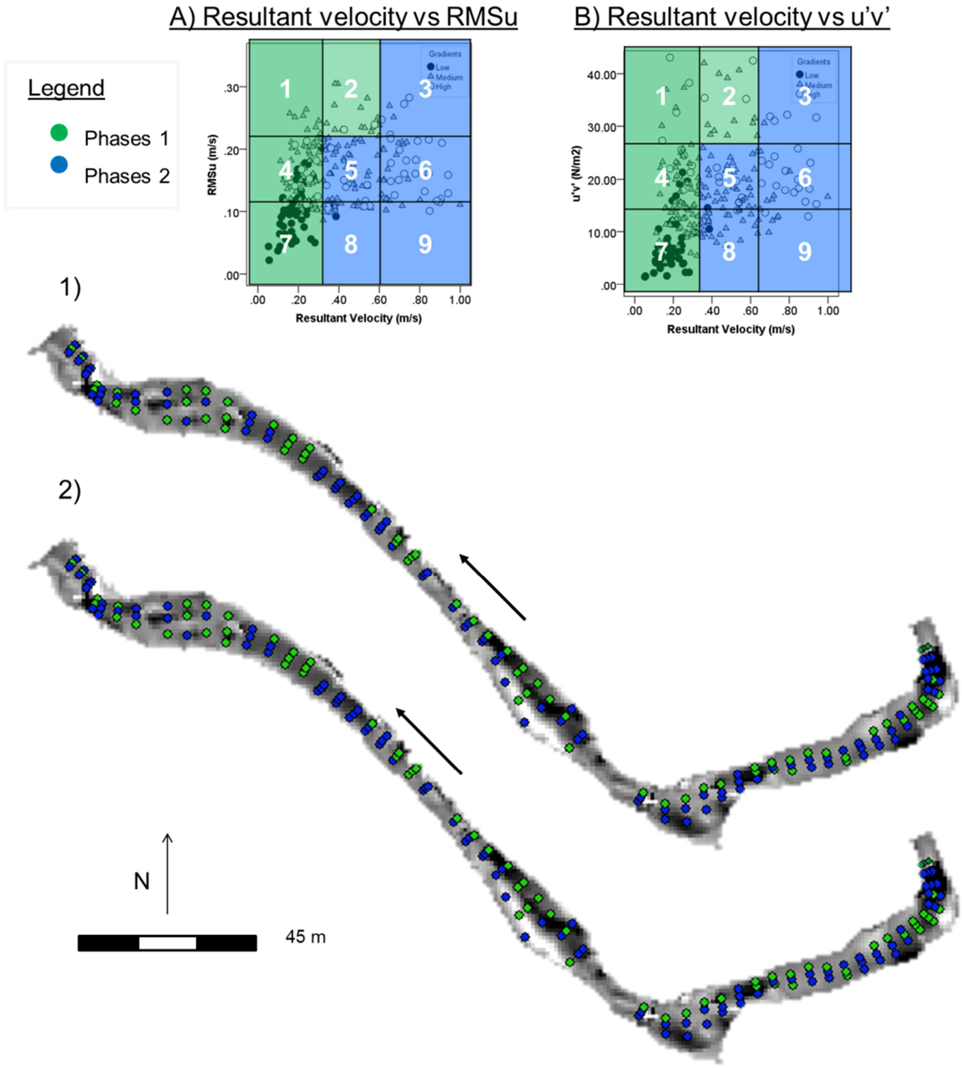

Figure 4.6 Subdivision of each bi-plots in grids reflecting specific range of resultant velocity and fluctuations on u component (A) and shear stress on uv plane (B). The spatial distribution for the two groups is explored for the intermediate (1-2) reach. The two phases (green and blue areas/dots) reflect the relationships between resultant velocity and RMSu (1) and shear stress on uv plane (2).

4.3.2 Predictability, orientation and scale of coherent flow structures

The kurtosis or 'peakedness' of the frequency distribution of turbulent residuals is presented in Figure 4.7A, providing an initial indication of the predictability of velocity series. There was a general trend of decreasing kurtosis with increasing gradient for each of the u, v and w turbulent residuals, although differences between reaches were not statistically significant at the 0.01 level with the exception of medium gradient < low gradient for the u component (Kruskall Wallis: $p < 0.01$). Figure 4.7B shows the distribution of the pseudo-periodicity parameter for time series in relation to the condition for pseudo-periodicity (see Chapter 3, section 3.6.2). Considerable differences were noted between reaches. Almost all of the velocity time series for the low gradient reach were classified as pseudo-periodic (91%), while a smaller proportion but still an overall majority (74%) of the intermediate gradient series were pseudo-periodic. In contrast, the majority of velocity series from the high gradient reach (64%) did not meet the condition for pseudo-periodicity indicating a lower level of 'predictability' in the flow structure (Table 4.4). Differences between the velocity components were less striking, with similar levels of pseudo-periodicity noted for each component across the three reaches.

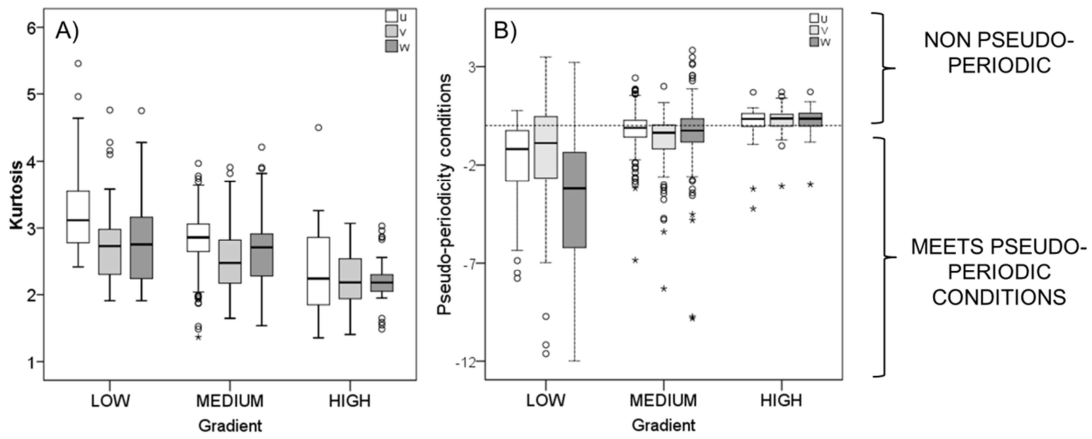

Figure 4.7 Boxplots for kurtosis of velocity time series along the streamwise (u), lateral (v) and vertical (w) components at different gradient reaches (A) and the distribution of condition for pseudo-periodicity across the reaches (B). The dotted line represents the pseudo-periodicity threshold. Negative values meet the condition for pseudo-periodicity.

Table 4.4 Numbers of velocity series that not satisfy the pseudo-periodicity conditions.

Gradient	Total number of series	Number of non pseudo-periodicity series			% series of non pseudo - periodicity
		u'	v'	w'	
High	147	13	12	18	64
Medium	501	31	19	18	26
Low	168	1	4	4	9

The skewness of turbulent residuals (u', v', w') is presented in Figure 4.8. There was considerable variability in the skewness of time series and a combination of positive and negative skewness values were noted for all three components across all three reaches. There was a tendency for positive skewness (indicating the presence of a small number of high magnitude fluctuations) in the medium and high gradient reaches (median > 0) which was more pronounced for the high gradient reach and for the u component. In contrast, the lower gradient reach had a median skewness <0 for all three components, indicating a tail of lower magnitude fluctuations in the frequency distribution. Differences between reaches were not statistically significant at the 0.01 level, however, with the exception of low /medium < high gradient for the u component.

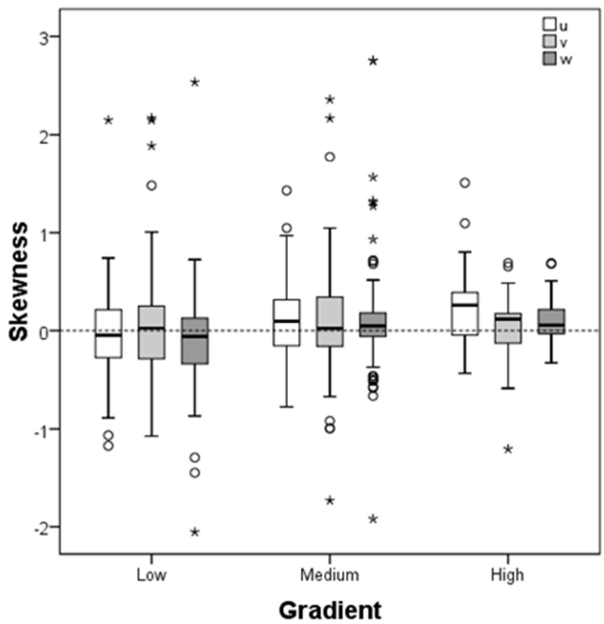

Figure 4.8 Boxplots of skewness of turbulent residuals for the streamwise (u), lateral (v) and vertical (w) components at increasing gradient rivers.

The cumulative duration and contributions to the Reynolds stress of each turbulent event type (Q1-Q4) are presented in Figure 4.9. There was an approximately linear relationship between the cumulative duration and cumulative stress contribution for each quadrant (Q1-t1: R^2 = 0.933, $p < 0.001$; Q2-t2: R^2 = 0.950, $p<0.001$; Q3-t3: R^2 = 0.903, $p < 0.001$; Q4-t4: R^2 = 0.966, $p < 0.001$), indicating that longer duration events generate larger contributions to the total stress, although stress contributions also become more variable at higher cumulative durations. There was considerable variability among time series for each reach, but the low gradient and high gradient reaches were associated with a higher proportion of longer-duration and higher magnitude ejections of fluid away from the bed (Q2) followed by inrushes of fluid towards the bed (Q4), while the medium gradient reach was associated with a higher proportion of longer-duration and higher magnitude outward interactions (Q1) and inward interactions (Q3).

Table 4.5 Table of significant differences between parameters (differences where p<0.001 for Kruskall Wallis post-hoc tests).

Parameter	Significant differences
Q1stress	Medium gradient > low/high gradient
Q2stress	Low gradient > high gradient > medium gradient
Q3stress	Medium gradient > high gradient > low gradient
Q4stress	High gradient > medium gradient > low gradient
Q1dur	Medium gradient > low/high gradient
Q2dur	Low gradient > medium /high gradient
Q3dur	Medium gradient > low/high gradient
Q4dur	High gradient > medium gradient > low gradient

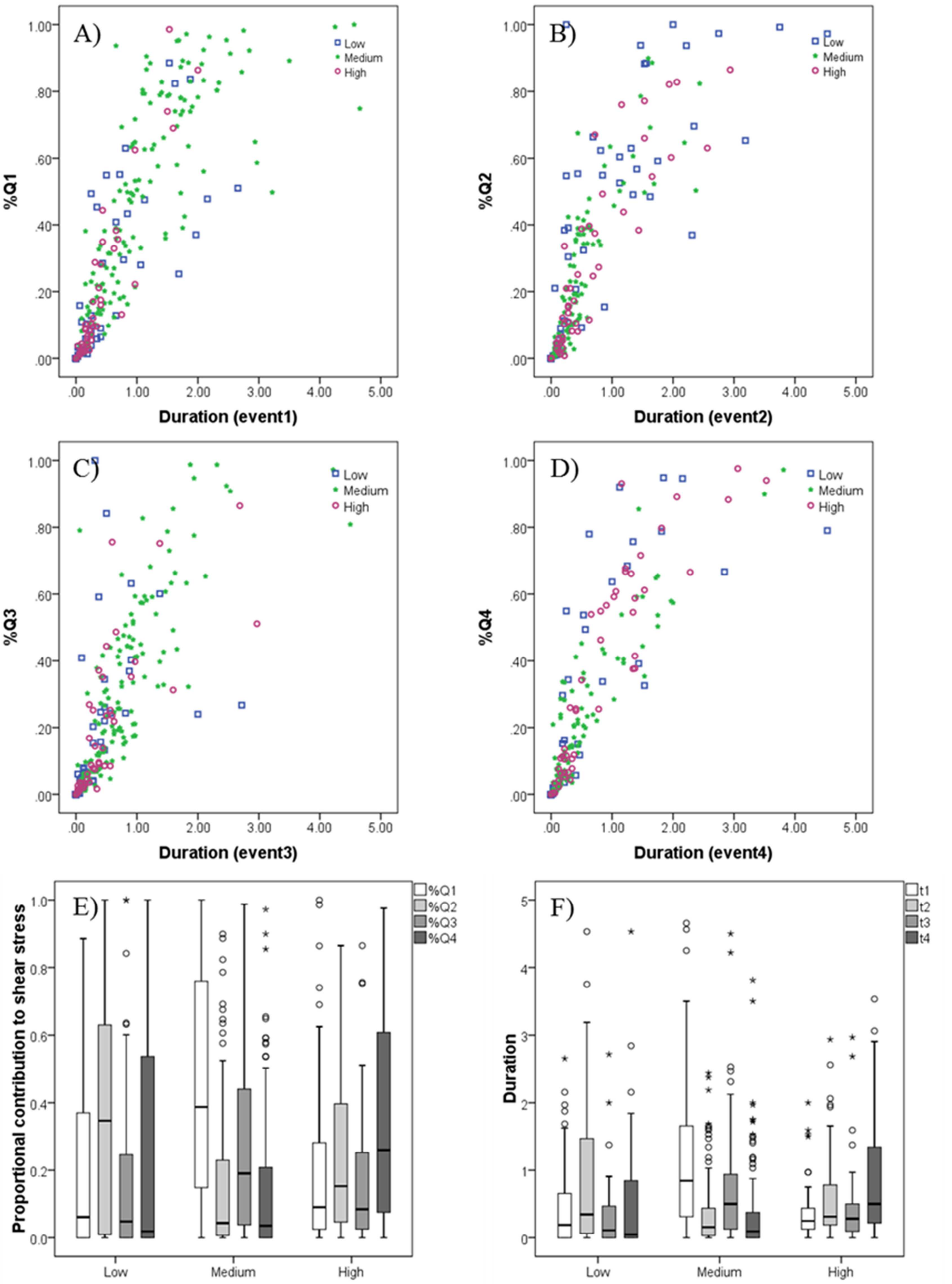

Figure 4.9 Scatter plots of each cumulative duration vs contribution to shear stress for each quadrant (A, B, C, D). Proportional contributions to shear stress from inwards (Q1), ejections (Q2), outwards (Q3) and inrushes (Q4) and respectively cumulative duration time for each event (E and F).

The orientation of the resultant velocity is illustrated visually using vectors superimposed on a detrended DEM in Figure 4.11, Figure 4.12 and Figure 4.13 and the angular velocity is presented in Figure 4.10. Changes in the magnitude and angle of velocity vectors in Figure 4.11 were observed to correspond broadly with channel constriction and local changes in roughness for the low gradient reach, in particular in the downstream section. Figure 4.12 revealed two dominant orientations at the reach scale representing the change in orientation of the channel from a SW flow direction (upstream section) to NW flow direction (downstream section). Within the relatively straight upstream section before the meander bend, channel width and planform was relatively homogeneous and resultant velocity vectors ranged between -5º and 15º with respect to the main flow direction. In the downstream section after the meander bend, there was greater variability in flow orientation corresponding to changes in channel width and planform. In the high gradient reach, (Figure 4.13), there was considerable spatial variability in flow orientation over small distances, suggesting the presence of steps/boulders generated more complex changes in flow orientation. These changes may reflect the choice of orientated the probe with respect to the bed instead to the streamline.

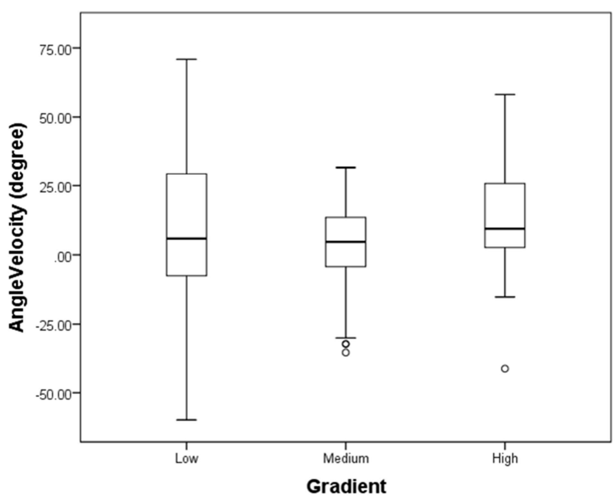

Figure 4.10 Distribution of the velocity's angles referred to the upstream-downstream direction (x axis) for each river.

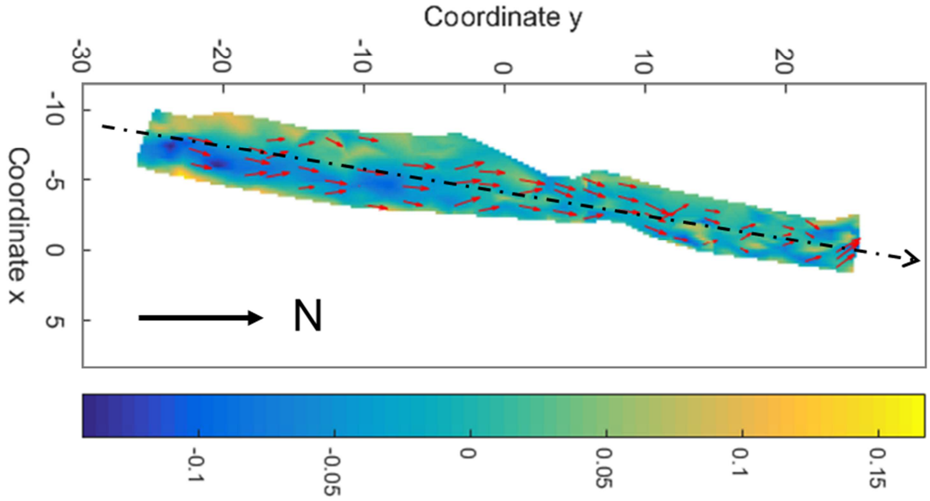

.

Figure 4.11 Detrended DEM of low gradient reach (Frome) within the orientation of the velocity (red arrows) calculated respect to the x axis of the velocity degree (0º) identified by the dotted black arrows.

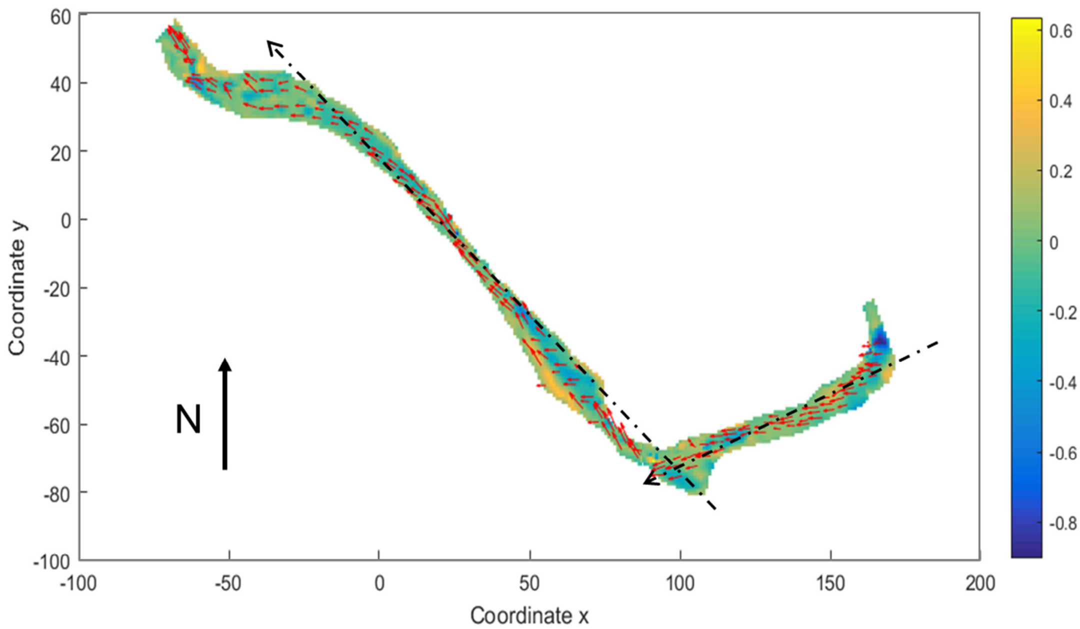

Figure 4.12 Detrended DEM of intermediate gradient reach (Tagliamento) within the orientation of the velocity (red arrows) calculated respect to the x axis of the velocity degree (0º) identified by the dotted black arrows.

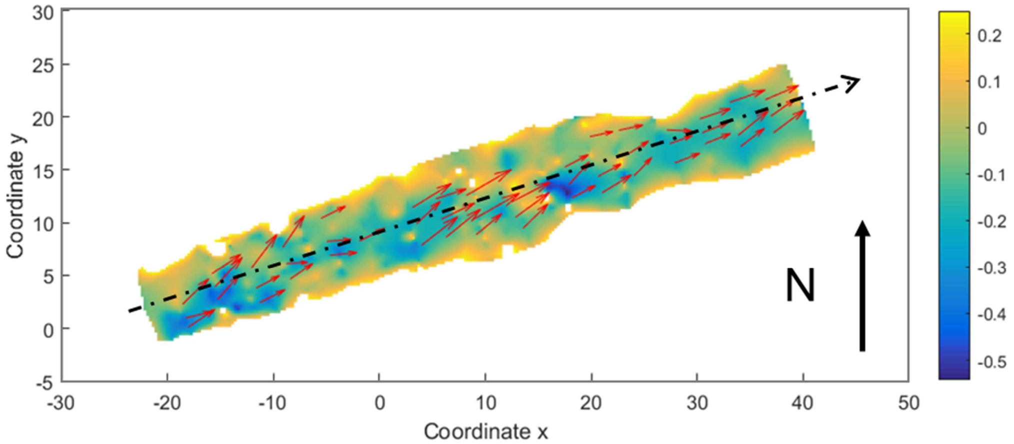

Figure 4.13 Detrended DEM of high gradient reach (Vermigliana) within the orientation of the velocity (red arrows) calculated respect to the x axis of the velocity degree (0º) identified by the dotted black arrows.

The eddy length scale along all the three components (u, v, w) is explored across the three gradient reaches in Figure 4.14. Across the three reaches, median values were lowest for the eddy length on the vertical component (w), highest for the streamwise (u) and intermediate for the lateral (v) components. An overall increase in eddy length scales was noted from the low, to intermediate, to high gradient reach across all the three components. Kruskall Wallis tests exhibited significant differences between reaches in all parameters (Table 4.6), with all three eddy lengths distinguishing between reaches.

The relationship between eddy length scale on all the three components and mean water depth is explored in Figure 4.15. Across the three components, there was a different tendency of increasing eddy size with mean water depth. For the streamwise component, there was considerable scatter, with eddy scales both greater than and less than the flow depth. For the lateral and vertical components, there was less variability and eddy scales were considerably smaller than the flow depth for both components. Table 4.7 compares dominant eddy length scale with key roughness elements: sediment size (D_{50}), channel width and Manning roughness coefficients for each of the three reaches. Bed material size was estimated from visual classifications using the Wentworth scale (Buffington and Montgomery, 1999; Bunte and Abt, 2001; Latulippe *et al.*, 2001). Channel width and depth are averaged measurements of wetted width and water depth at the time of survey. The Manning's roughness coefficient takes into account several factors including channel geometry and irregularities, planform (e.g. meandering or straight), flow obstructions, bed material shape/size and distribution, and vegetation density. Manning's n was estimated for each reach using Limerinos, 1970.

Larger clast sizes resulted in a higher Manning's n value for the intermediate and higher gradient reaches, but the Manning's value for the low gradient reach was relatively similar to the other two reaches as a result of the presence of aquatic plants. For the high gradient reach, the Manning value was highest due to the presence of boulders without vegetation in channel within steep banks and trees and bushes along the banks. The estimated Manning's value for the intermediate gradient reach was in between the other two. For the streamwise component, eddy length scales were much larger than the bed material size for all three reaches, but smaller than channel width, indicating that flow structures scale on larger microtopography elements e.g. larger clasts, pebble clusters, macrophytes. For all the three reaches, the streamwise (u) eddy scales were similar to the average water depth measured during the survey. For the lateral and vertical components, eddy length scales were more similar to bed material size for the low and medium gradient reaches, while the eddy length scales for the high gradient reach were 20 times smaller than the bed material size.

Table 4.6 Table of significant differences between parameters (differences where $p < 0.001$ for Kruskall Wallis post-hoc tests).

Parameter	Significant differences
Lu	High gradient > medium gradient > low gradient
Lv	High gradient > medium gradient > low gradient
Lw	High gradient > medium gradient > low gradient

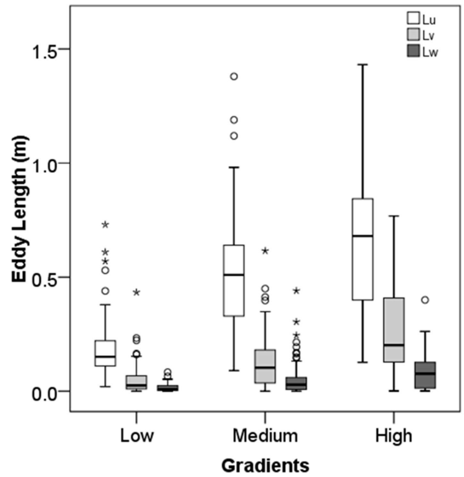

Figure 4.14 Distribution of the eddy length across the three gradient rivers from low to high.

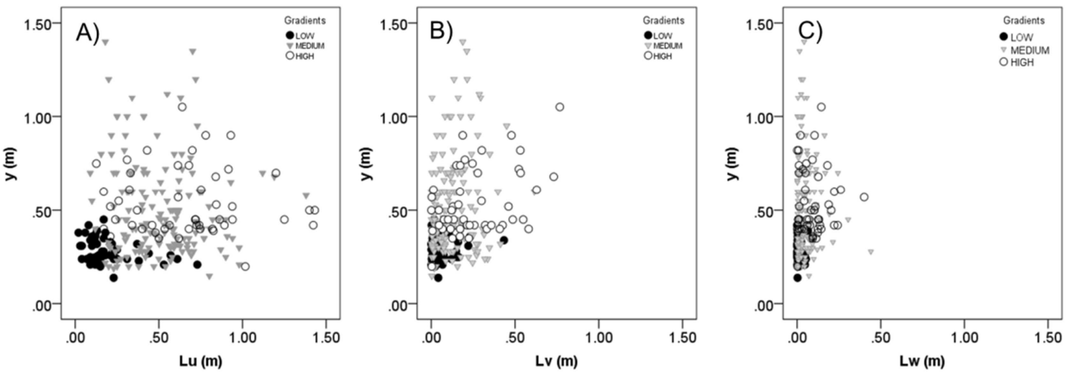

Figure 4.15 Biplots of eddy dimension for all the three components and mean water depth across the three gradient reaches.

Table 4.7 Characteristics of dominant range of eddy length (Lu), D_{50} (estimated from visual assessment), mean water depth, mean channel width and roughness for each river.

Reach Gradient	Lu (m)	Lv (m)	Lw (m)	D_{50} (m)	y_m (m)	Channel width (m)	Roughness (manning)
Low	0.1- 0.3	<0.2	<0.2	0.04	0.33	6	0.0034
Medium	0.3 – 0.7	<0.3	<0.2	0.09	0.48	12	0.0040
High	0.4 - 1	<0.4	<0.2	> 0.25	0.41	8	0.0050

4.3.3 Identification of principal gradients in turbulence properties

PCA analysis was carried out for two global data sets including data from all the three reaches: (i) dimensionless hydraulic variables made by z-scores method (Emery *et al*., 2003); and (ii) the raw dataset. Both PCA analyses were performed on a reduced number of hydraulic variables that satisfied the Kaiser Meyer Olkin (KMO) and Barlett tests (dimensionless data set: KMO: 0.58 and $\chi^2_{critical}$: 84.45, $p < 0.0001$; raw data set: KMO: 0.64 and $\chi^2_{critical}$: 85.96, $p < 0.005$) including: resultant velocity, TKE, Reynolds shear stress (uv and uw), eddy period and length scale, and flow structure events of second and fourth quadrant (Q2, Q4) and correspondent duration time (t2, t4).

For the dimensionless data set, 4 PCs had eigenvalues greater than 1.6 and cumulatively explained 70% of the variance in the data set. Inspection of the scree plot revealed an inflection point after the 4th PC, and hence the first 4 PCs were retained for further analysis. PC loadings were used to interpret the meaning of each principal component (Figure 4.16b). PC1 defines an increasing gradient of the temporal and spatial scale of eddies along the streamwise (u) and vertical (w) components. PC2 represents a gradient of turbulence intensity (kinetic energy and shear stress on two planes uv and uw). PC3 describes a gradient of decreasing mean velocity and increasing magnitude and duration of ejection events (Q2, t2). PC4 is a gradient of the magnitude and cumulative duration of inrushes (Q4, t4).

For the raw data set, 5 PCs had eigenvalues greater than 1 and cumulatively explained 82% of the variance in the data set. Inspection of the scree plot revealed an inflection point after the 5th PC, and hence the first 5 PCs were retained for further analysis. PC1 defines an increasing gradient of kinetic energy and shear stress on two planes uv and uw and hence represents a turbulence intensity gradient. PC2 represents a gradient of increasing eddy period and length scale for the vertical (w) component while the PC3 is a gradient for eddy period and length scale for streamwise component and decreasing gradient for resultant velocity. PC4 reflects a gradient of increasing magnitude and cumulative duration of inrushes, while PC5 represents increasing magnitude and duration period of ejections. Overall, both PCAs therefore derive key axes that map onto three of the four IPOS categories, with PCs representing ‘intensity’, ‘scale’ and two PCs to represent ‘orientation’.

For the dimensionless data set, the three reaches occupy broadly the same areas of the biplots for both PCs 1 and 2, and PCs 3 and 4, with some variation in the extent of variability within reaches (Figure 4.17), which tended to be greatest for the intermediate gradient reach. No statistically significant differences were observed for principal components and Figure 4.19A shows similar mean and errors across the three gradient reaches.

For the raw data set, the three reaches occupy broadly different areas of the biplots for PCs 1 and 2 (although with overlap) but differences between reaches on the basis of PCs 4 and 5 are less clear. Hence, absolute magnitudes of turbulence intensity increase from low to high gradient reaches and differences between reaches for PC1 were statistically significant (KW: $p < 0.01$). Greater variability within reaches is observed for absolute eddy scale (PC2), although the low gradient reach appears to be constrained to a narrower range of (larger) eddy sizes. PC3 was associated with considerable overlap in values across the three reaches. PC5 showed great variability within reaches. Statistically significant differences were identified between low/medium and medium/high gradient reaches (KW: $p<0.01$) indicating lower magnitude and shorter duration inrushes for the medium gradient reach compared with both low and high gradient reaches, which were in Figure 4.18B.

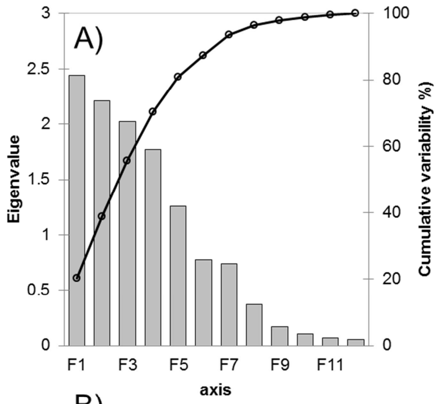

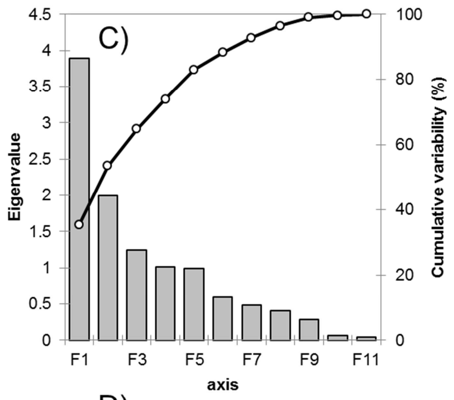

B)

	PC1	PC2	PC3	PC4
Vel tot	0.268	0.233	**-0.360**	-0.115
TKE	0.016	**0.921**	-0.061	-0.019
u'v'	-0.127	**0.856**	-0.016	0.009
u'w'	0.124	**0.617**	-0.042	-0.022
Q2	0.005	0.005	**0.953**	-0.117
Q4	-0.013	-0.016	-0.089	**0.959**
t2	0.073	-0.034	**0.939**	-0.038
t4	-0.048	-0.025	0.005	**0.966**
ITSu	**0.608**	-0.305	-0.023	-0.023
ITSw	**0.838**	0.171	0.085	0.038
Lu	**0.675**	-0.114	-0.251	-0.176
Lw	**0.816**	0.234	0.111	0.062

D)

	PC1	PC2	PC3	PC4	PC5
Vel tot	0.548	-0.036	**-0.654**	0.074	-0.111
TKE	**0.855**	0.025	0.160	-0.019	-0.180
u'v	**0.923**	0.006	0.009	0.019	-0.067
u'w	**0.843**	0.122	-0.059	0.113	0.072
Q2	-0.014	0.348	-0.387	-0.037	**0.974**
Q4	0.026	0.142	-0.194	**0.858**	-0.046
T2	-0.046	0.178	0.012	-0.071	**0.851**
T4	0.056	-0.005	0.286	**0.652**	-0.056
ITSu	-0.072	0.297	**0.681**	-0.019	0.056
ITSw	-0.008	**0.908**	0.192	0.014	-0.010
Lu	0.266	0.205	**0.832**	-0.106	-0.081
Lw	0.239	**0.900**	0.213	0.011	0.077

Figure 4.16 Scree plot (A) and factors loadings (B) for the dimensionless PC analysis and for raw data set (C,D).

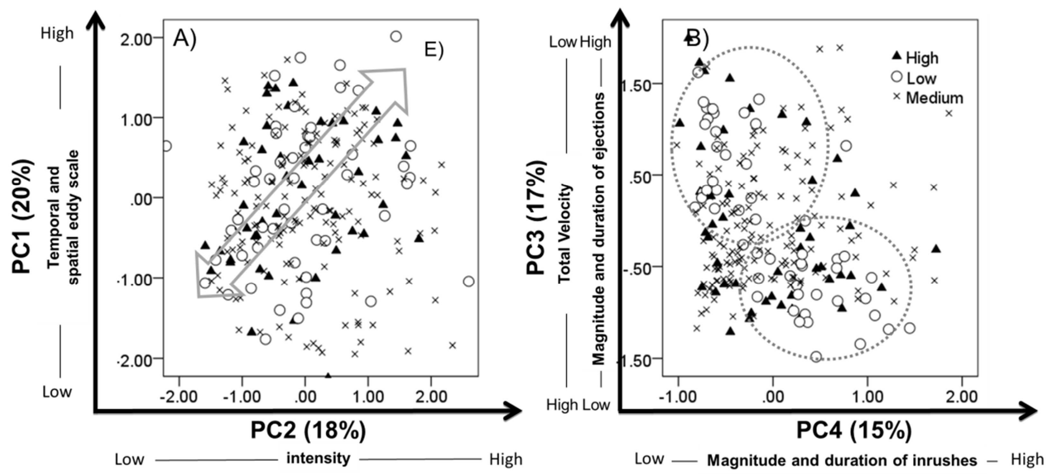

Figure 4.17 Scatter plots of first and second PCs (A) and third and fourth (B) principal components across three gradient reaches of dimensionless turbulence variables.

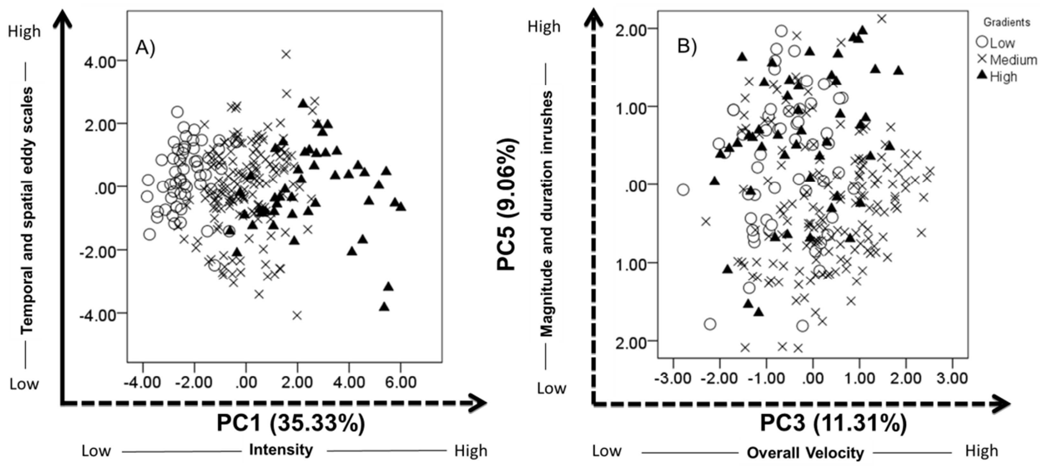

Figure 4.18 Scatter plots of first and second PCs (A), and fourth and fifth (B) principal components across three gradient reaches of dimensionally turbulence variables. Dotted lines represent the principal component that shows statistical significance between at least two gradient reaches.

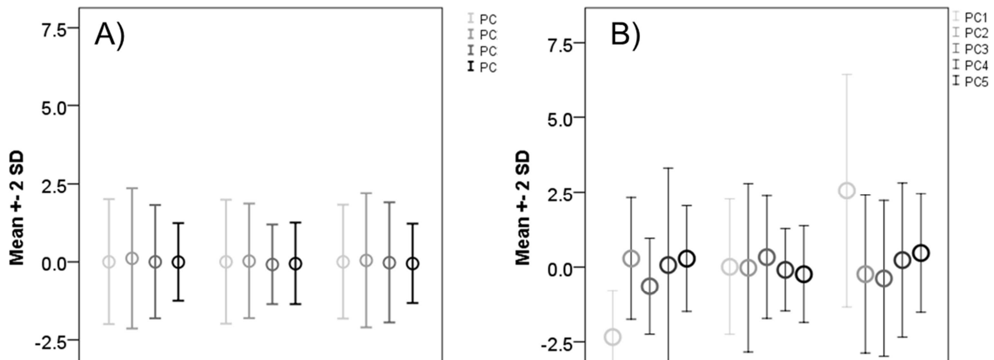

Figure 4.19 Errors bar for dimensionless (A) and dimension (B) PC analysis. Circles are means and the whiskers the 2 standard deviations.

4.3.4 Spatial organisation of turbulence properties

Model semivariograms were fitted to spatially referenced data for bed elevation, mean water depth, mean velocity (Figure 4.20), turbulence intensity parameters (Figure 4.21) and predictability, orientation and scale parameters (Appendix I). There was considerable variability in the form of semivariograms between parameters and across sites but some key trends emerge. All plots showed a nugget effect to some degree, indicating spatial variation at scales smaller than the sampling interval. Variograms are complex in form across most parameters for each reach, characterised by a lack of pronounced sill and a 'spiky' profile indicating spatial correlation at multiple scales.

For the low gradient reach some pronounced decreases in semivariance appeared to broadly correspond with the spacing of either bedforms (~10 m) or macrophyte patches (generally ~2 m) for some parameters (RMS, TKE, Skewness, Kurtosis), but the intervening features of the variograms have no obvious eco-morphological explanation. For the medium and higher gradient reaches there was a clearer correspondence with bedform spacing, with mean velocity, RMS, Z and TKE profiles aligning with double riffle/pool spacing (~ 30/40 m) for the medium gradient reach and mean, RMS, Z and TKE aligning with step/pool spacing (~ 10 m) for the higher gradient reach. However, variograms for predictability and orientation exhibit more complex variation across smaller scales (see Appendix I).

The morphology of semivariograms revealed overall smoother shapes for mean velocity at low gradient and RMSv,w at medium and high gradient indicating smoother changes across the reach while sharp variations in form were observed

for turbulent kinetic energy, kurtosis and flow events suggesting less predictable changes in spatial variation through the reaches.

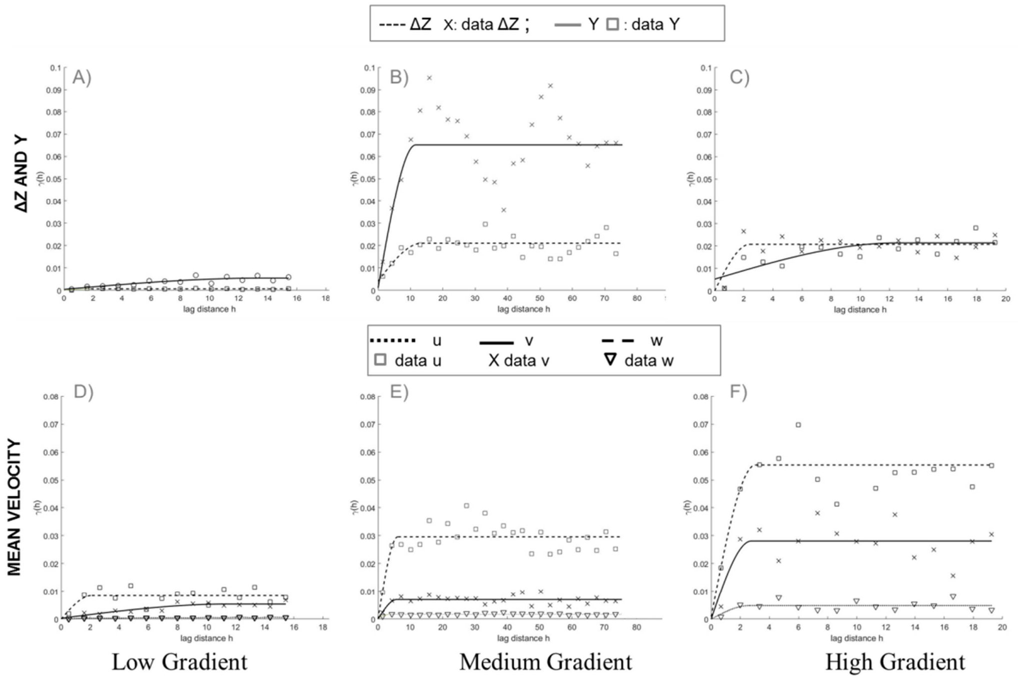

Figure 4.20 Descriptions of fitted model and experimental semivariograms for topographic residuals (ΔZ) and mean water depth (Y) (A, B, C) and mean velocity along the streamwise (u), lateral (v) and vertical (w) directions (D, E, F) across low, medium and high gradient reaches.

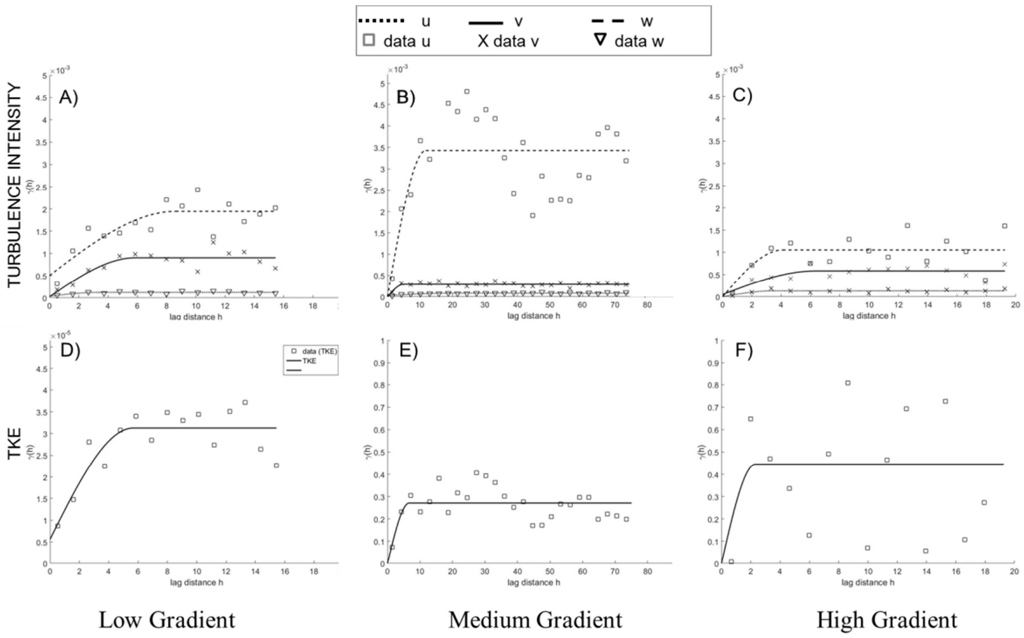

Figure 4.21 Semivariograms of turbulent intensity (RMSu,v,w) (A,B,C) and turbulent kinetic energy(D, E, F) across low, medium and high gradient reaches.

The spatial organisation of PC scores was explored using experimental semivariograms (Figure 4.22 - 4.25) for each reach and for each of the four PCs. For the low gradient reach, variance in PC scores was highest for PC2 (intensity) and lower for the two orientation gradients (PC3 and PC4). PC1 (eddy length scales) revealed different shape semivariogram with a linear increase indicative of complex spatial organization without clear spatial autocorrelation. GIS visualisations reveal the highest intensities (PC2) occur around aquatic plants, while eddy scales (PC1) tend to be smaller along the thalweg compared to marginal channel locations. Spatial organisation of Q2 and Q4 events (PC4) was more complex with no clear patterns.

For the intermediate gradient reach, semivariogram morphology is similar among the PCs, but the variance shown by the sills was lowest for the magnitude of inrushes (PC4) compared to eddy scale (PC1), ejections (PC3) and intensity (PC2). Geospatial analysis revealed that the lowest intensity and smallest eddy scales were associated with negative topographic residuals, mostly in the central area of the channel while higher turbulent intensity and lower magnitude ejections and inrushes were observed in positive topographic residuals in the straight section.

For the high gradient reach, the variance was highest for turbulence intensity (PC2), followed by eddy scale (PC1) and magnitude of ejections (PC3), and lowest for the contribution to shear stress of inrushes (PC4). Also the higher range for PC2 suggests that the spatial distribution of turbulence intensity was complex and affected by the presence of boulders that diverged the flow and developed wakes. The experimental data in the semivariogram trends for PC2 and PC4 reveal the presence of similar pattern with distance of 4 lags (12 m) that might reflect the bedform spacing (~10 m). Figure 4.25 indicates that there was no clear difference between the central part of the channel and marginal area.

Table 4.8 Parameters of semi-variogram models for principal components at low gradient reach (Frome).

	Range	Sill	Nugget
PC1	83.05	1.48	0.76
PC2	6.70	1.45	0.15
PC3	2.10	0.91	$1\ 10^{-5}$
PC4	2.02	0.38	$1\ 10^{-5}$

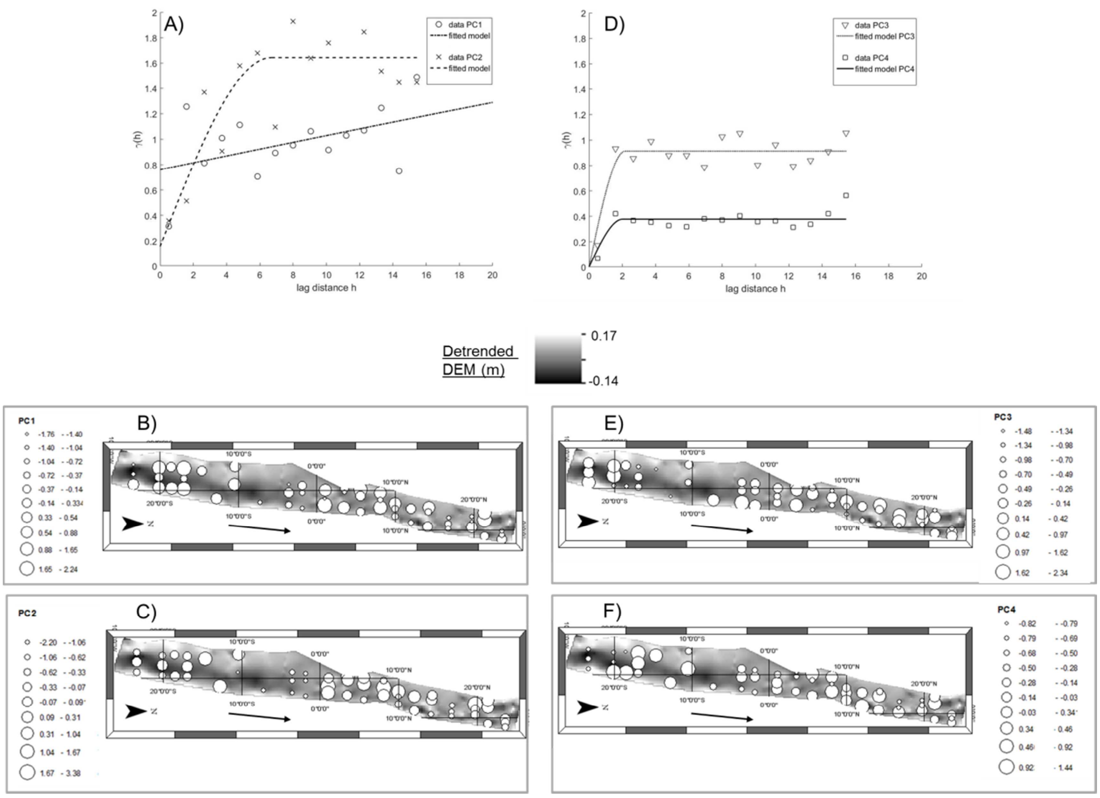

Figure 4.22 Graduate symbol maps and semivariograms for non-dimensional principal components: PC1 (B), PC2 (C), PC3(E) and PC4 (F) for the low gradient river (Frome) at low flow. Black arrow shows the direction of the flow. A is the semivariograms for the first and second PCs and B for the third and fourth PCs.

Table 4.9 Parameters of semi-variogram model for principal components at the medium gradient reach (TAG).

	Range	Sills	Nugget
PC1	7.55	0.64	0.200
PC2	7.06	0.96	0.058
PC3	0.71	0.87	0.004
PC4	1.26	0.41	0.025

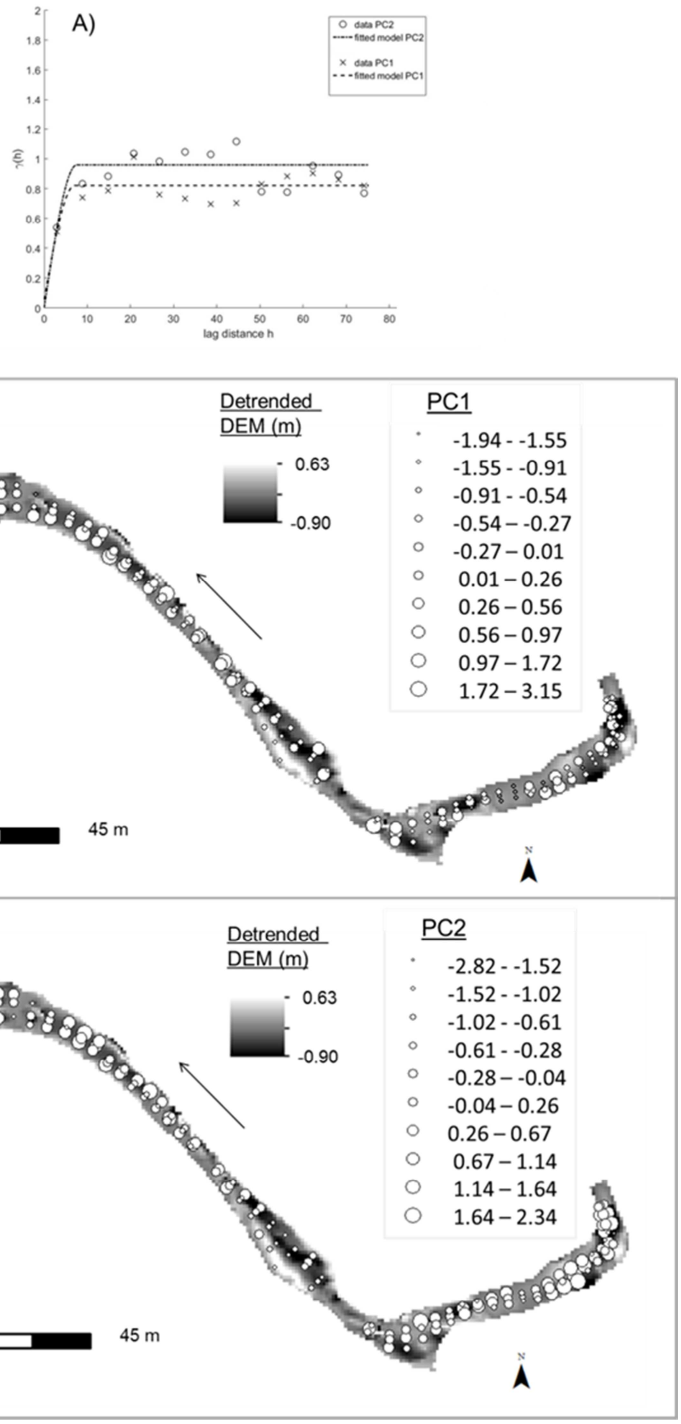

Figure 4.23 Graduate symbol maps and semivariograms of non-dimensional principal components 1 (B) and 2 (C) for the intermediate gradient river (Tagliamento) at low flow. A is the semivariograms for the first and second principal components.

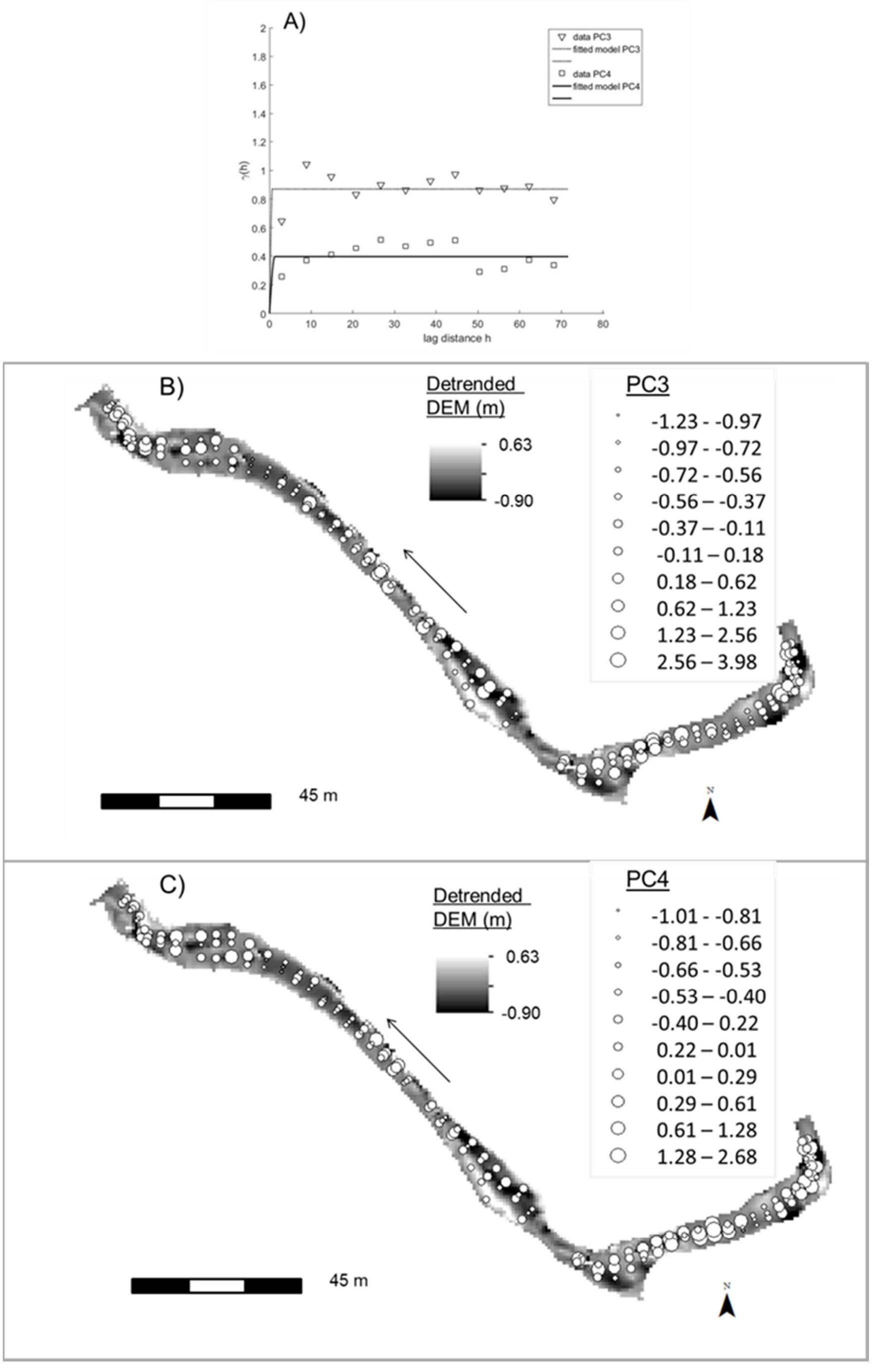

Figure 4.24 Graduate symbol maps and semivariograms of non-dimensional principal components 3 (B) and 4 (C) for intermediate gradient river (Tagliamento) at low flow. A is the semivariograms for the third and fourth principal components.

Table 4.10 Parameters of semi-variogram model for principal components at the high gradient reach (Vermigliana).

	Range	Sills	Nugget
PC1	2.91	0.85	$3.4\ 10^{04}$
PC2	3.52	1.09	$6.6\ 10^{-03}$
PC3	2.30	0.84	$1.2\ 10^{-02}$
PC4	3.52	0.42	$1.1\ 10^{-02}$

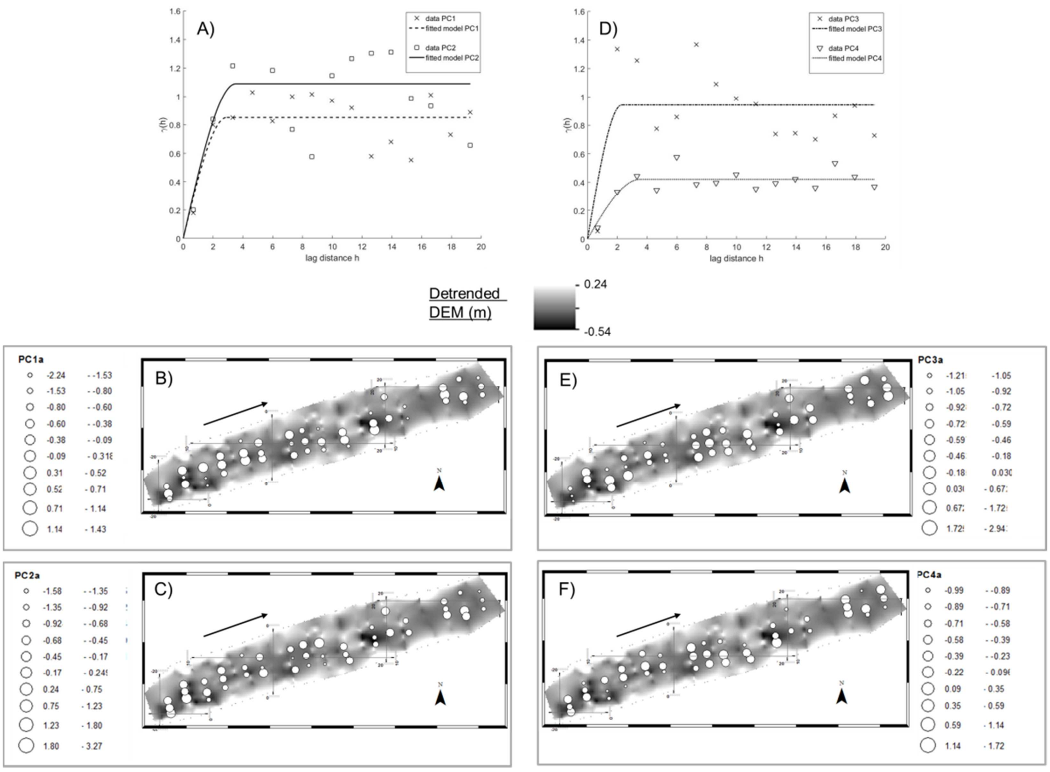

Figure 4.25 Graduate symbol maps and semivariograms of non-dimensional principal components: PC1 (B), PC2 (C), PC3 (E) and PC4 (F) for high gradient river (Vermigliana) at low flow. A is the semivariograms for the first and second PCs and B for the third and fourth PCs.

4.4 Discussion

4.4.1 Spatial variability of turbulence intensity and relationship with mean velocity

Across the three reaches, the absolute intensity was lowest for the vertical component (w), largest in the streamwise direction and intermediate for the lateral (v) component and there was an overall increase in absolute magnitude of fluctuations with increasing gradient for all three components, which is also illustrated by TKE. The reverse was true for relative intensity and this illustrates the high magnitude of fluctuations relative to v and w respectively. Despite consistent increases in RMSu, v and w with gradient there were no clear linear relationships between the velocity components indicating that the intensity of the components is not spatially correlated – higher intensities on the v and w planes were not necessarily associated with higher intensities on the u plane. This contrasts with clear linear trends between the RMSu and RMSw/RMSv ($R^2 > 0.70$) reported by Wilcox and Wohl (2007) in a high gradient river at multiple discharges, suggesting that the nature of such relationships may vary in space, and underlining the insights that can be gained from field measurement in 3 dimensions.

Overall, values for Reynolds shear stresses increased with gradient, and the uv plane was associated with the highest and most variable values, followed by uw and vw. Experiments on juvenile rainbow trout (Smith *et al.*, 2005) indicated that fish were able to control their holding position under higher magnitude stresses in the uv compared to the uw plane, suggesting the uw plane as a potentially important parameter for fish bioenergetics. Across all three reaches there was an overall increase in RMS and Reynolds stresses with increasing resultant velocity but scatter in the relationship creates at least two phases of behaviour for most of the variables: phase 1 whereby intensities increased rapidly with resultant velocity, and phase 2 where a lower magnitude and/or more variable increase in turbulence intensity with increasing resultant velocity was observed. These two phases did not correspond with the different reaches but instead represented sub-reach scale variability. For the low and intermediate gradient reaches, there was some broad spatial organisation of the two phases, associated with either macrophytes (low gradient reach) or bedform spacing (intermediate gradient reach). In contrast, the high gradient reach was characterised by high spatial variability. These data confirm previous observations that standard hydraulic variables such as mean velocity, cannot be applied universally to 'predict' higher order turbulent flow properties (Raven *et al.*, 1998; Pardo *et al.*, 2002; Rinaldi *et al.*, 2013a), supporting more explicit incorporation of turbulence properties and the IPOS framework into river habitat assessment and design protocols.

4.4.2 Predictability, orientation and scale of coherent flow structures

Predictability of the flow structure generally decreased with increasing gradient, represented by decreasing kurtosis and increasing incidence of non-pseudo-periodicity in time series. These trends were relatively consistent across the three velocity planes. In all three reaches there was considerable variation in skewness, with both positive and negative values recorded. Median skewness values for the low gradient reach were centred around zero skewness indicating an approximately normal distribution. In contrast, the medium and high gradient reaches tended towards positive skewness indicating a small number of very high magnitude fluctuations were present in time series (Lacey and Roy, 2008a).

Longer-duration turbulent events tended to generate greater contributions to the shear stress, although there was some variability in the magnitude of the longer-duration events as also noted in other studies (Lamarre and Roy, 2005; MacVicar *et al.*, 2007b; Harvey and Clifford, 2009). Ejections and inrushes of fluid dominated the event structure in both low and high gradient reaches while the medium gradient reach was associated with more longer-duration/ higher magnitude inward and outward interactions. Previous works found that ejections and inrushes events are typically associated with turbulent bursting in the near bed environment (MacVicar *et al.*, 2007b), and around flow obstructions such as boulders (Lacey and Roy, 2008a) providing a possible explanation for higher magnitude of ejections and inrushes for areas with higher roughness. For the low gradient reach, vegetation was present as a key roughness element, capable of dissipating flow energy, which helps to explain the increased occurrence of inrushes of fluid towards the bed (Q4, inrushes) and the decrease in fluid moving rapidly away from the bed (Q2, ejections) in vegetation patches (Devi and Kumar, 2016). High presence of inrushes has been shown to be important in sediment resuspension, increasing the mobilisation and transport of sediment and associated nutrients (Finnigan, 2000; Pan *et al.*, 2014), thereby providing food sources to aquatic organisms as well as assisting predator evasion.

Eddy length scales in three dimensions increased in magnitude with increasing in gradient for all three reaches. This supports previous work e.g. Lamarre and Roy (2005) that related eddy length scale and duration to bed morphology at the reach scale. There are very few reach scale field studies of the spatial organisation of turbulence properties, but some recent studies at smaller, sub-reach scales have indicated length scales between 0 and 1.3 m (Harvey and Clifford, 2009; Roy *et al.*, 2010; Wilkes, 2014) which are similar to those reported here.

Correspondence between eddy dimensions in the streamwise component and estimated average sediment D_{50} differed among the reaches. For the low and medium gradient reaches, the average D_{50} was an order of magnitude lower than the eddy length scales in the u dimension. This is to be expected since eddies often scale on larger elements of microform roughness (e.g. pebble clusters; Buffin-Bélanger and Roy, 1998) as well as aquatic plant stands and bedforms (Nepf, 1999). In contrast, for the high gradient reach the D_{50} is of the same order of magnitude as the eddy length scales (u), indicating that individual boulders may be a key driver of turbulence generation which may be explained by vortex shedding processes (Lamarre and Roy, 2005; Lacey and Roy, 2008b). The average sediment D50 may affect the eddy propagation near bedforms and could explain the elements responsible for the turbulence generation (Clifford *et al.,* 1997) and reproduces small-scale form resistance as microtopographic features (Clifford *et al*., 1992). However, in this study, the grain size has been estimated by visual assessment and could not use for in-depth analysis in relation to of eddy propagation.

4.4.3 Principal gradients in turbulence properties

Both PCA analyses revealed gradients that largely correspond with three IPOS categories, which were, in order of contribution to the overall variance in the data set: ‘scale’, ‘intensity’ and two ‘orientation’ gradients for the dimensionless PCA; and ‘intensity’, two ‘scale’ gradients, and two ‘orientation’ gradients for the raw data PCA. The majority of predictability variables had to be removed so that the PCA met the key statistical assumptions of the analysis technique, and therefore were not fully represented in this multivariate analysis. The results suggest that grouping of a large number of turbulence properties under the IPOS categories accurately reflects the principal sources of variance in turbulent time series as well as the ecological relevance of those properties, emphasising the utility and potential applications of the framework.

PC scores based on absolute (raw) values showed broad patterns that distinguished between low and high gradient reaches while the intermediate revealed greater variability. Turbulent intensity increased from low to high gradient reaches within higher magnitude for inrushes at low and high gradient reaches compared with intermediate gradient reach.

4.4.4 Scales of spatial variability in turbulence properties

A combination of a geostatistical analysis of turbulence properties (semi-variance) and DEMs of bed topography provide a useful means of assessing spatial patterns at reach scale (Clifford *et al.*, 2005; Lamarre and Roy, 2005). The presence of a nugget effect for most of data sets highlights variability at scales smaller than the sampling interval, such as pebble clusters and individual clasts which were not captured in this study. Spatial variation in all turbulence properties occurred at scales smaller than the sampling interval emphasising the well-known importance of microscale roughness elements on turbulence generation (Roy *et al.*, 2004; Tritico and Hotchkiss, 2005; Smith and Brannon, 2007).

Spatial organisation of turbulence properties was complex in the low gradient reach, where aquatic macrophytes appear to be the key influence on the variation in values for a number of key turbulence properties. Aquatic plants can distinctly alter the velocity profile and flow resistance inside the canopy (Nepf, 2012) as well as the spatial distribution of velocity across the channel, often intensifying velocities and turbulence between patches and generating wakes (Meire et al., 2014). This is explored in further detail in Chapter 6.

For the medium gradient reach there was a clearer correspondence with bedform spacing (~ 20 m) with mean velocity, RMS and Z profiles aligning with riffle/pool spacing, consistent with some previous research at this scale (Clifford *et al.*, 2005; Legleiter *et al.*, 2007). Also, some of the 'orientation' parameters, including skewness of turbulent residuals and event structure, revealed a periodic recurrence that could reflect the undulating topography of bedforms/ geomorphic units (the riffles/pool). This is explored in further detail in Chapter 5.

For the high gradient reach, the geostatistical analysis for mean velocity, Z and TKE aligned with step/pool spacing (~ 10 m) illustrated by a reduction in semi-variance occurring at lags approximating step/pool spacing. Flow diversions around boulders are known to generate high localized turbulent areas with shedding vortex that interact with fluid, sediment particles, nutrients and micro-organisms (Lacey and Roy, 2008b; Lacey and Roy, 2008a). In contrast, semi-variance for the cumulative duration of flow events decreased at lags approximating double the bedform spacing, which corresponds with the spacing of the most pronounced pools.

CHAPTER 5: Hydraulic characterization of geomorphic units across different gradient rivers

5.1 Introduction

Existing river assessment methods use different terminology to describe key river features at different spatial scales, often leading to confusion and reducing the potential for drawing comparisons between rivers in different countries (Brierley and Fryirs, 2013; Rinaldi *et al.*, 2013a). The range of geomorphic units considered may also vary according to assessment method, with implications for assessing true geomorphic diversity (Belletti *et al.*, 2015a). The Geomorphic Units survey and classification System (GUS) (Belletti *et al.*, 2015b) is a new classification system designed to try to overcome some of these issues and facilitate comparisons of geomorphic units across different environments. The classification incorporates a greater variety of geomorphic units for different river types (ranging from low to high gradient river styles) and integrates existing definitions and descriptions of spatial scales in fluvial geomorphology (e.g. Montgomery and Buffington, 1997; Church, 1992; Buffington and Montgomery, 2013).

Geomorphic units (GUs) have been defined as an "*area containing a landform created by erosion or deposition of sediment, sometimes in association with vegetation*" (Gurnell *et al.*, 2016, p.10), identified by distinct sediment shape and dimensions, hydraulic properties (water depth and velocity) and also by the presence of vegetation/wood. Geomorphic units (e.g. riffles, pools, runs, steps) have been proposed as a convenient spatial scale for assessing habitat use/ availability in relation to various aquatic organisms (Vezza *et al.*, 2014; Wilkes *et al.*,

2012) and have been linked to ecologically-relevant 'functional habitats' within rivers (Harvey *et al.*, 2008). Some species show a preference for specific GUs, for example greater abundance of mayfly nymphs *Ephemeroptera* was found in riffles compared with pools indicating their preference for shallow water, clearer water and bed roughness (Logan and Brooker, 1983; Brooks *et al.*, 2005).

As a result GUs may represent a practical scale for river management and restoration design strategies (Fryirs and Brierley, 2016; Brierley and Fryirs, 2013). Despite this, and the importance of turbulence properties for aquatic biota outlined in Chapter 2, descriptions of the hydraulic properties of GUs largely rely on spatially and temporally averaged velocity, water depth and substrate (Jowett, 1993; Kemp *et al.*, 2000; Wallis *et al.*, 2012; Baker *et al.*, 2016).

Recent research by Harvey and Clifford (2009) and Wilkes (2014) has gone some way to addressing this issue by characterizing the hydraulics of GUs using more sophisticated, ecologically relevant metrics such as turbulence intensity and eddy size. In addition, the Lacey *et al*. (2012) IPOS framework has now established a clear and ecologically validated framework for analyzing turbulence properties. These studies revealed distinctions between some geomorphic units on the basis of hydraulic complexity that varies with flow stage. Nevertheless, the results of the studies were somewhat inconsistent. For example, Harvey and Clifford (2009) found pools to be associated with the highest levels of hydraulic variability, whereas Wilkes (2014) found pools to be the least heterogeneous habitat in terms of hydrodynamics. Further work is required to further investigate the hydraulic characteristics of GUs, including those already sampled in lowland UK rivers and across the wider range of European river types, to evaluate their distinctiveness in terms of ‘higher order’ turbulence properties (Harvey and Clifford, 2009). This would assist critical evaluation of the utility and robustness of visual surveys of GUs for ecological purposes and identify whether adaptations to existing approaches to hydraulic habitat assessment may be required.

This chapter explores the relationships between turbulence properties and GUs across different hydraulic environments (morphological sequences in reaches of different gradient) under low flow conditions. In particular, the research addresses three research objectives:

1. Quantify higher-order (turbulent) flow properties associated with key GUs (steps, riffles and pools) across reaches of different gradient.

2. Evaluate the utility of turbulence variables in predicting the occurrence of geomorphic units.

3. Explore variation in turbulent properties in transitional areas and/or variations outside the scale of GUs.

5.2 Methodology

5.2.1 Field data

Full details of the three field sites and sampling design are provided in the Research Design chapter (Chapter 3, Section 3.2) and a summary of the field site characteristics is provided in Chapter 4 (Table 4.2). The three reaches are characterised by riffle-pool (low and intermediate gradient), and step-pool (high gradient) morphologies. GUs were identified visually in the field following Belletti *et al.* (2015b) focusing on instream units only. Features were delineated by visually examining process zones (erosion and deposition), landform configuration (channel slope, sediment organization, position with respect to the channel) and presence of natural riverine elements (bedrock, large wood), following the classifications of Brierley and Fryirs (2005) and Buffington and Montgomery (2013). Each measurement location in the surveyed reach was assigned to one GU under low flow conditions.

A stratified sampling approach to velocity measurement was taken, with velocities sampled at three locations (30, 50, 70 % of channel width) along equally spaced cross sections in order to capture variability along the channel centreline and more marginal locations. The sampling design enabled sufficient replication of measurements within the key geomorphic units characteristic of each reach (step-pool or riffle-pool sequences). See Chapter 3 (Research Design, Section 3.5) for full details of velocity measurement. Each velocity measurement was captured at 0.6 of the water depth (from the surface) in order to sample conditions in the outer flow zone. Velocity measurements were recorded under low flow conditions for all three reaches.

5.2.2 Data analysis

Turbulence parameters were computed (see Chapter 3 for full details) for all time series that met data quality requirements as previously explained in Chapter 3 (see Table 3.6). Data were not normally distributed (Shapiro - Wilk: $p < 0.001$) and therefore non-parametric statistical tests were used. Multivariate statistical analysis (Principal Components Analysis; PCA) was used to identify the key gradients in turbulence properties within the data sets. Prior to PCA, Kaiser-Meyer-Olkin (KMO) and Barlett's test of Sphericity were analysed to identify redundant variables and check correlations between variables respectively. The following variables were retained for the PCA: resultant velocity, turbulent kinetic energy, shear stress on the uv and uw planes, and temporal and spatial eddy scales (ITSu,w and ILSu,w), together with event structure derived from quadrant analysis ((ejections (Q2) and inrushes (Q4)). Separate PCAs were conducted for each reach.

Generalised linear modules (logistic regression) can be used to predict the probability of a sample or observation falling within a category of a binary response based on a set of explanatory variables (Hosmer Jr and Lemeshow, 2004). In this case, the four derived Principal Components (PCs) were used as explanatory variables, in order to predict the GU response variable (riffle/pool or step/pool) depending on the reach. Multiple logistic regression was applied to each site individually. ROC (Receiver Operating Characteristics) curves were used to check the performance of each model and its accuracy is represented by the area under the curve (AUC). The Hosmer-Lemeshow test was used to evaluate the goodness-of-fit.

Agglomerative hierarchical cluster analysis (HCA) was used to objectively identify the number of homogeneous groups of velocity measurements based on their turbulence properties (PC scores). HCA was performed using Ward's method and the Euclidean distance measure (Emery *et al.*, 2003). Three main clusters were identified from the dendrogram for each reach and used in a K-means cluster analysis. All analysis were performed in either XLSTAT Base Microsoft 2016, SPSS v22 and Matlab R2015b.

5.3 Results

5.3.1 Turbulent flow properties associated with key GUs

Across the three reaches, riffles or steps accounted for a larger proportion of channel area than pools (Table 5.1). Paired comparisons (riffle-pool and step-pool) of turbulence intensity parameters are provided in Figure 5.1. Across sites, absolute intensity, TKE and absolute shear stress were lowest for the pools in the low gradient reach compared to the intermediate/high gradient reaches, while considerable variability in values was observed for riffles and steps.

For the low gradient reach, TKE and shear stress on the uv plane were lower and less variable for the pools but differences between riffles and pools were not statistically significant. Absolute intensity on streawise (u) direction was higher for the riffles while turbulent intensity on the v and w dimensions, and relative intensity, was similar across riffles and pools. For the intermediate gradient reach, the streamwise (u) intensity was very high for the riffles while intensity on v and w components was low, and the v intensity was higher for the pools. Variability and median values for shear stress for uv and vw planes was also higher for pools than riffles, but relative intensity and TKE were similar across riffles and pools. For the high gradient reach, absolute intensity was similar across steps and pools, but relative intensity and TKE were lower and less variable for steps compared to pools. Median values for shear stress on uv and vw planes were higher for pools compared with steps, while the stress on uw was similar.

Kruskall Wallis tests showed some significant differences between geomorphic units, but not for all parameters (Table 5.2) and not consistently among pairs of GUs. Only RMSu distinguishes between pairs of GUs within the same reach. Some parameters distinguish between reaches, but not between pairs of GUs within each reach: RMSw, v'w', v'w'. Other parameters separate the lower gradient reach GUs from the intermediate and high gradient reaches: TKE, Tlu, u'v'.

Table 5.1 Total areas for each gradient reach and percentage of area covered by steps/riffles and pools.

Gradient reach	Total area (m^2)	% Area covered by Steps/Riffles	% Area covered by Pools
Low	240	52	48
Medium	2806	56	44
High	501	55	45

Table 5.2 Table of significant differences between parameters (Kruskall Wallis post-hoc tests where $p < 0.01$). L: low; M: medium; H: high gradient.

Parameters	Significant differences
RMSu	$Step_H$/ $Riffle_M$ > $Riffle_L$ /$Pool_H$/ $Pool_M$ > $Pool_L$
RMSv	$Step_H$/$Pool_H$/$Pool_M$ > $Riffle_M$ /$Riffle_L$/$Pool_L$
RMSw	$Step_H$/$Pool_H$ > $Riffle_M$/$Pool_M$ > $Riffle_L$/ $Pool_L$
Tlu	$Riffle_L$/ $Pool_L$ > $Riffle_M$/$Pool_M$ / $Step_H$/$Pool_H$
Tlv	Not statistically significant
Tlw	Not statistically significant
u'v'	$Pool_H$/$Step_H$/$Pool_M$ > $Riffle_M$ > $Riffle_L$/ $Pool_L$
v'w'	$Pool_H$/$Step_H$> $Pool_M$/$Riffle_M$ > $Riffle_L$ >$Pool_L$
u'w'	$Pool_H$/$Step_H$/$Pool_M$ > $Riffle_M$ > $Riffle_L$/ $Pool_L$
TKE	$Pool_H$/$Pool_M$/$Step_H$/$Riffle_M$ > $Riffle_L$/ $Pool_L$

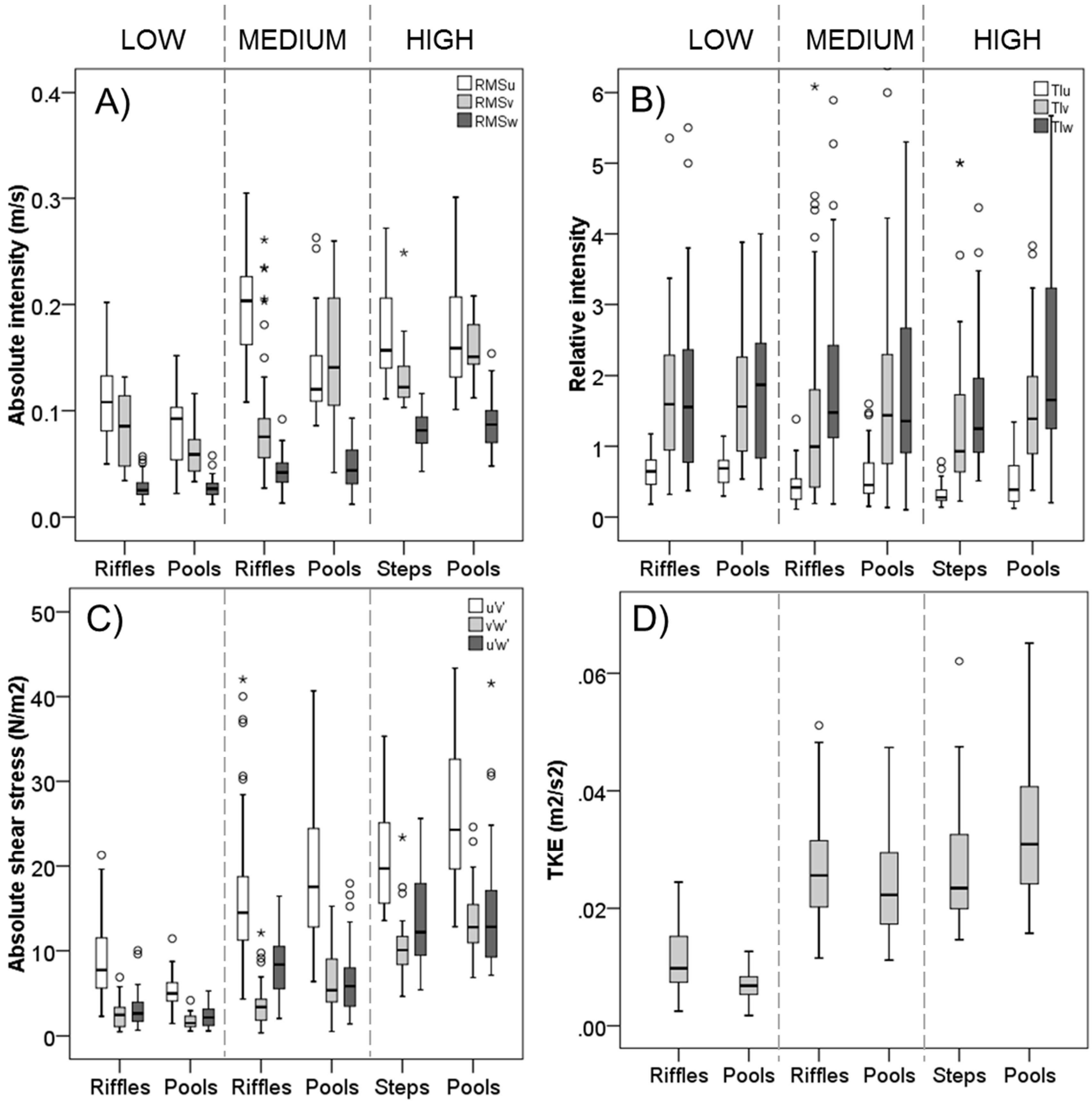

Figure 5.1 Distribution of the mean turbulence intensity (A), the relative intensity (B) along the streamwise (u), lateral (v) and vertical (w) directions. Reynolds shear stress (C) on the three planes (uv, vw, uw) and the turbulent kinetic energy (TKE) (D) across riffles, pools grouped by low, medium and high gradient reaches.

The relationships between the overall resultant velocity and shear stress on uv plane with fluctuations in u, v and w directions are presented in Figure 5.2. There was considerable variability in values for geomorphic units in medium and high gradient reaches (riffles/pools and steps/ pools) for resultant velocity. Fluctuations and shear stress were higher in riffles than pools at low gradient. This suggests that while across the sites there was no clear overall tendency, there was some trend across the geomorphic units. These are explored further in Figure 5.2.

Overall, there was considerable overlap in values for all of the plots in Figure 5.2, however, clusters of outliers from the predominant linear trends can be identified and these correspond with particular GUs at particular study sites. In most cases, the riffles and pools in the intermediate gradient reach are distinct from the other GUs, for example in the relationships between resultant velocity and RMSu, RMSv and Reynolds stress on uv plane. For the Reynolds stress on the vw plane, the steps and pools in the high gradient reach are more distinct from the other GUs at the two other study sites.

Bivariate correlations for overall velocity and the RMS fluctuations were generally weak (< 0.52) across geomorphic units. The strength of linear relationships was highest for RMSu in pools for low and medium gradient reaches, and for riffles for the medium gradient reach and all of these correlations were statistically significant (Spearman's Rank: $p < 0.01$). Correlations were also higher (0.52 – 0.88) for the relationships between Reynold shear stress u'v' and the RMSu and RMSv, and again these were statistically significant (Spearman's Rank: $p < 0.01$), with exception for RMSv for high gradient pools. RMSw values were below 0.22 with exceptions for riffles (0.65) at low gradient (Table 5.3).

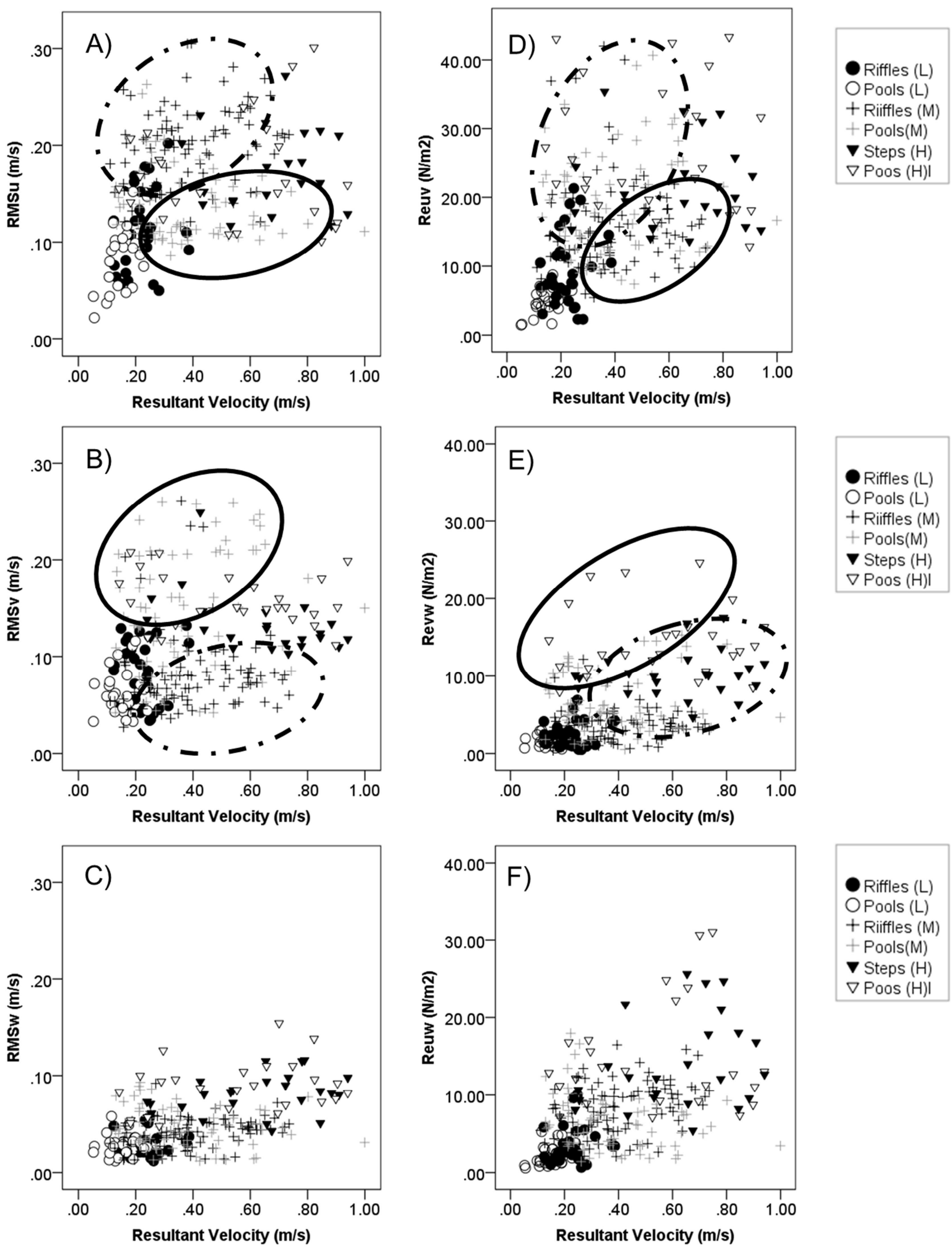

Figure 5.2 Comparison the resultant velocity with the root mean square values for u, v and w components (A,B,C) and to the Reynold shear stress on uv, vw and uw planes (D, E, F) grouped by different geomorphic units for each gradient reach. There was apparent trends for pools (black) and riffles (black dotted) at intermediate gradient and high gradient reaches.

Table 5.3 Bivariate correlation coefficients (Spearman) for the RMS fluctuations related to overall velocity and Reynolds shear stress on uv plane. Values displayed in bold text are significant for $p < 0.01$.

	Overall velocity to:			*Reynolds shear stress (u'v') to:*		
	RMSu	*RMSv*	*RMSw*	*RMSu*	*RMSv*	*RMSw*
Pools$_L$	**.518**	.012	.092	**.669**	**.579**	.113
Pools$_M$	**.319**	.057	**.440**	**.523**	**.750**	.142
Pools$_H$	.130	.257	.271	**.885**	.104	.217
Riffles$_L$	.246	-.131	.032	**.624**	**.765**	**.626**
Riffles$_M$	**.256**	.074	-.108	**.806**	**.717**	.089
Steps$_H$	.193	-.402	.327	**.870**	**.536**	.202

The kurtosis, integral time scale and pseudo-periodicity for turbulent residuals on the three velocity components are presented in Figure 5.3. Kurtosis was positive across all geomorphic units and ranges were similar for GUs within the same reach. The highest variability was associated with high and low gradient pools, followed by riffles in the low gradient reach. Differences between pools for kurtosis (u) were statistically significant only between low and medium/high gradient reaches (KW: $p<0.01$), showing a gradient of decreasing kurtosis (u) from high/intermediate to low gradient pools. This indicates a peaked distribution and more predictable flow structure for low gradient pools compared to high gradient.

The integral eddy time scale revealed a decrease in magnitude for ITSu from low to high gradient reaches indicating that dominant flow structures had a longer period in the lower gradient GUs compared to higher gradient GUs. In addition, for low gradient, there was no statistically significant difference between riffles and pools but in combination these were distinct from the other GUs, possessing the highest median values for ITSu and similar range for ITSv and ITSw. This indicates a more predictable flow structure compared to the intermediate and high gradient reaches. For both intermediate and high gradient reaches, pools revealed longer eddy periods (ITS) along the u and w components compared with riffles/steps, although these differences were not statistically significant. Statistically significant differences were observed for geomorphic units at low flows compared with medium/high gradient reaches (KW: $p < 0.01$) as shown in Table 5.4.

The observation of the percentage of time series that meets the criteria of pseudo-periodicity is presented in Figure 5.5. The highest number of time series that meets the condition was identified for low gradient riffles (u and w components) and pools (v component), while the values were lowest for the pools along all the three components at high gradient. Overall, more series met the pseudo-periodicity condition within riffles compared to pools for the low and intermediate gradient reaches (u and w series) and steps compared to pools in the high gradient reach (v and w series).

For skewness (Figure 5.4A), both positive and negative values were observed for each GU, but there was a trend for negative skewness in pools, and positive skewness in riffles and steps reflecting a small proportion of higher magnitude fluctuations in those environments. Significant differences were identified between high/low gradient pools only (KW: $p < 0.01$).

The cumulative duration and contributions to the Reynolds stress of each turbulent event type (Q1-Q4) are presented in Figure 5.4. Relative contributions to the shear stress of the different event types were highly variable and were not consistent among the GUs. There were no consistent differences between riffle-pool or riffle-step pairs; each GU group displays a different event type signature, although riffles and pools in the intermediate gradient site are most similar.

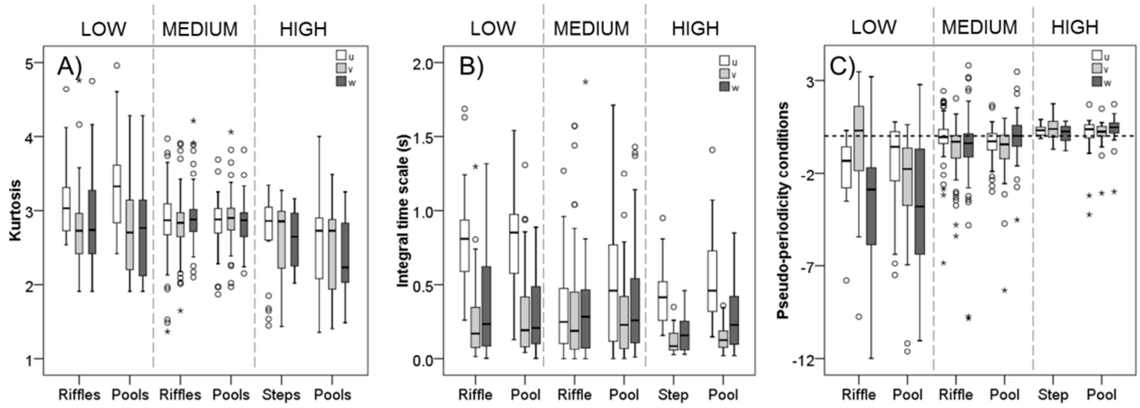

Figure 5.3 Boxplots of kurtosis (A), Integral time scale (B) and pseudo-periodicity conditions (C) of time series along the streamwise (u), lateral (v) and vertical (w) components for geomorphic units across reaches of different gradients.

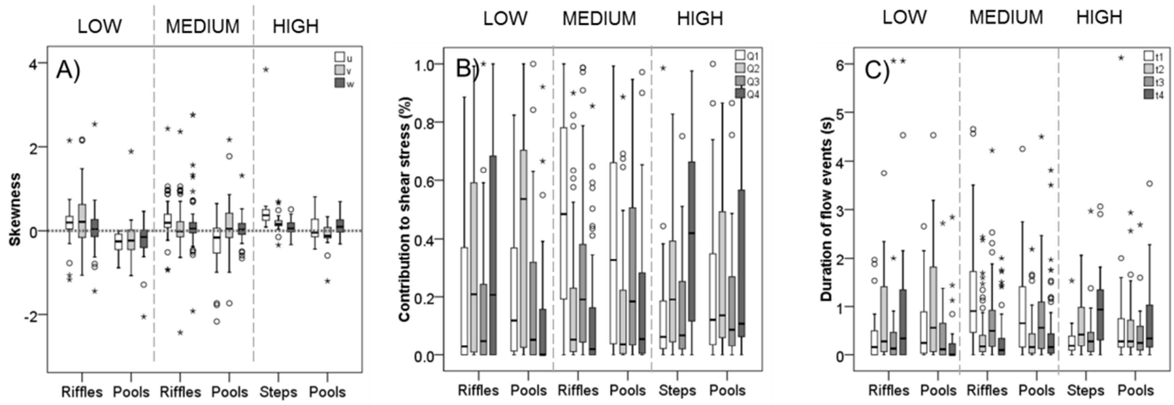

Figure 5.4 Skewness (A), contributions to shear stress (B) from inwards (Q1), ejections (Q2), outwards (Q3) and inrushes (Q4) and respectively cumulative duration time for each event (C) across geomorphic units in different gradient reaches.

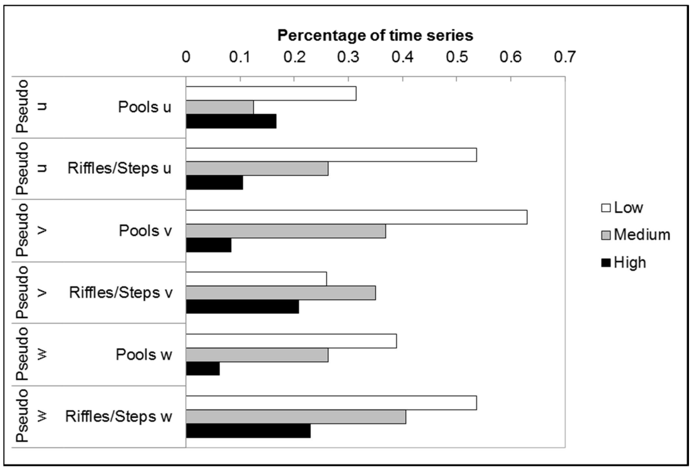

Figure 5.5 Percentage of time series that meets the condition of pseudo-periodicity on all the time series along the streamwise (u), lateral (v) and vertical (w) components for each geomorphic units across different gradients.

The eddy length scales in three dimensions (u, v, w) across the geomorphic units is explored in Figure 5.6. When considered together, reach gradient exerted a stronger influence on eddy scale than individual GUs at low gradient reach, but statistically significant differences were identified between pairs of GUs in the high and medium gradient reaches (Table 5.5). Length scales in the u dimension tended to be smaller within the pools compared to respective riffles/ steps (KW: $p<0.01$). Length scales for v and w components were less variable and lower with stronger influence at reach scale.

The eddy length along the three components is explored in relation to mean water depth in Figure 5.7 (A-C). There was no clear trend across geomorphic units, but again some GUs at particular sites cluster in certain areas of the biplots. In particular, the pools at the intermediate gradient reach are associated with restricted eddy lengths in the u and v dimension, but with high flow depths. The steps in the high gradient reach are associated with longer eddy lengths for shorter water depths compared to the pools.

Table 5.4 Table of significant differences between parameters for integral time scale (ITS) along the three components (Kruskall Wallis post-hoc tests where $p < 0.01$). L: low; M: medium; H: high gradient.

Parameters	Significant differences
ITSu	$Pool_L$/$Riffle_L$ > $Pool_H$ /$Step_H$ / $Pool_M$ / $Riffle_M$
ITSv	No statistical differences
ITSw	No statistical differences

Table 5.5 Table of significant differences between parameters (differences where $p < 0.01$ for Kruskall Wallis post-hoc tests).

Parameter	Significant differences
L_u	$Step_H$ / $Riffle_M$ > $Pool_H$ /$Pool_M$ > $Riffle_L$/$Pool_L$
L_v	$Step_H$/$Pool_H$ > $Riffle_M$/$Pool_M$ > $Riffle_L$/$Pool_L$
L_w	$Step_H$/$Pool_H$ > $Riffle_M$/$Pool_M$ / $Riffle_L$/$Pool_L$

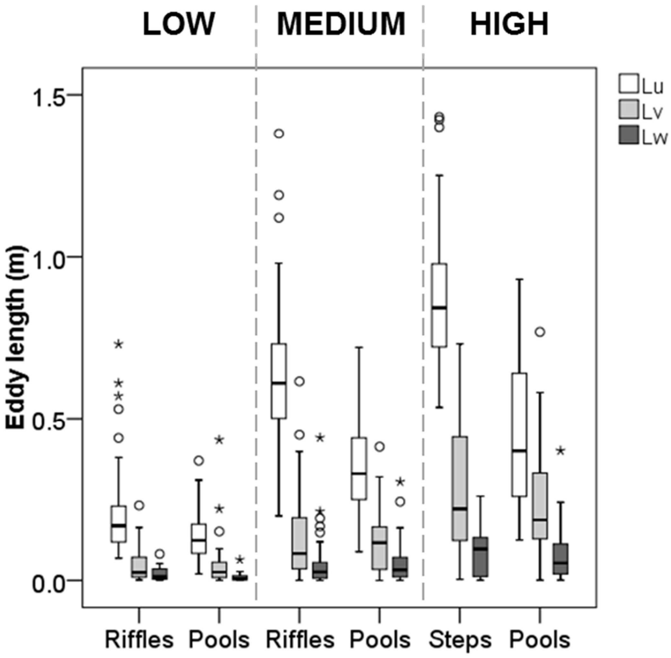

Figure 5.6 Distribution of the eddy length across geomorphic units surveyed in three gradient rivers from low to high.

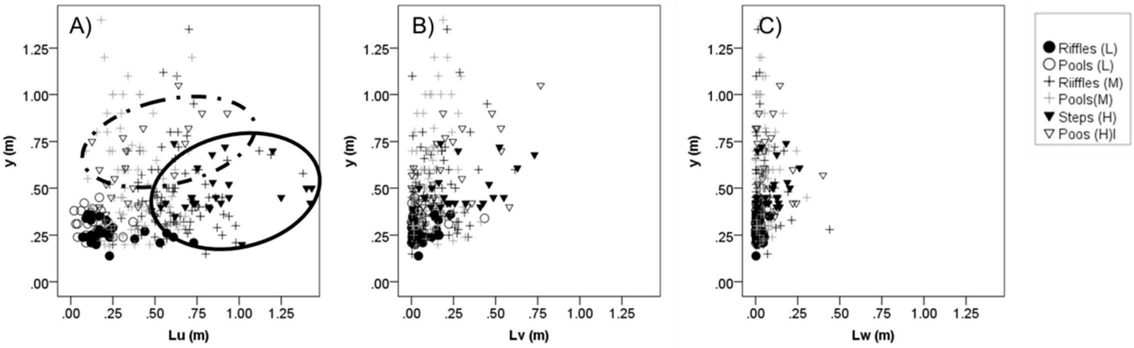

Figure 5.7 Relationships between eddy length and water depth along the streamwise (A), lateral (B) and vertical (C) components.

5.3.2 Gradients in turbulent properties and prediction of GUs

PCA was conducted separately for each reach using the following variables: resultant velocity, TKE, Reynolds shear stress on uv and uw planes, eddy period and length scale for u and w dimensions, and event structure (Q2 and Q4). PCs had eigenvalues greater than 1 for each site and cumulatively explained 74% (low gradient), 73% (intermediate gradient) and 54% (high gradient) of the variance in the data set. Inspection of the scree plot (Figure 5.8 (A-C)) revealed an inflection point after the 3rd, 4th and 2nd PC for each reach respectively. As a result, the first three, four and two PCs were retained for further analysis for the low, intermediate and high gradient reaches respectively. PC loadings were used to interpret the meaning of each principal component (Figure 5.8 (D-F)). Table 5.6 summarizes the principal components derived for each analysis describing what they represent.

For the low gradient reach, PC1 defines a gradient of turbulence intensity, while PC2 defines a gradient of spatial and temporal eddy scales on u and w dimensions. PC3 defines a gradient of increasing magnitude of ejections (Q2) and decreasing magnitude of inrushes (Q4). For the medium gradient reach, PC1 defines a gradient of eddy scale (u and w components). PC2 defines a gradient from low to high magnitude of turbulence intensity represented by kinetic energy (TKE) and shear stress on uv plane. PC3 defines a gradient of decreasing magnitude of ejections (Q2) and associated increase in magnitude of inrushes (Q4). PC4 defines a gradient of low to high Reynolds stress on uw plane. For the high gradient reach, PC1 describes a gradient of turbulence intensity represented by kinetic energy (TKE) and shear stress on uv and uw planes. PC2 defines a gradient of spatial eddy scale for streamwise (u) and vertical (w) components.

The extent to which PCs discriminated between GUs appeared to vary across the three reaches. For the low gradient reach (Figure 5.9 (A, B)), riffles were associated with larger eddy scales (PC2) and higher turbulence intensity (PC1) than pools, but there were no clear differences in PC3 between GUs. In the intermediate gradient reach (Figure 5.9 (C, D)), there were high levels of variability in PC scores for all PCs, however significant differences between GUs were identified for PCs 1 and 4, indicating larger eddy size and greater shear stress in riffles compared to pools. For the high gradient reach (Figure 5.9 (E, F)), steps were associated with significantly higher scores on PC2, indicating larger eddy scales (u), but there was considerable overlap between the two GUs in terms of PC1 scores.

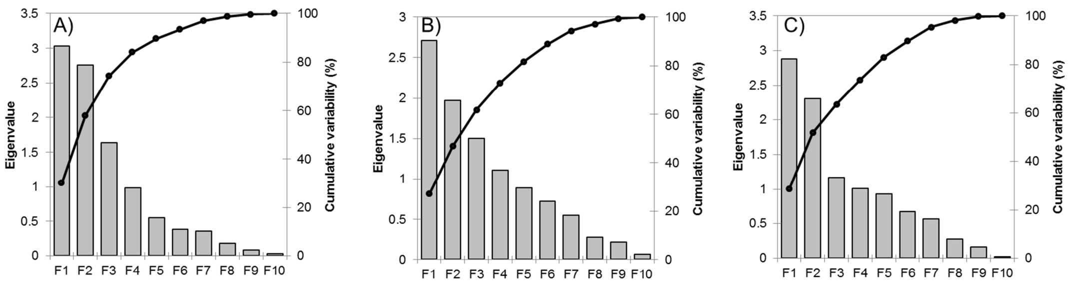

D)

	PC1	PC2	PC3
Tot vel	**0.549**	0.374	-0.468
TKE	**0.933**	-0.100	-0.128
uv	**0.868**	-0.139	-0.149
uw	**0.839**	-0.142	-0.082
Q2	0.139	-0.500	**0.543**
Q4	0.089	0.691	**-0.699**
ITSu	-0.220	**0.778**	-0.014
ITSw	0.315	**0.602**	0.280
ILSu	-0.150	**0.774**	-0.091
ILSw	0.452	**0.509**	0.272

E)

	PC1	PC2	PC3	PC4
Tot vel	0.337	**0.435**	-0.471	-0.146
TKE	0.109	**0.864**	0.296	0.137
uv	-0.079	**0.821**	0.306	0.010
uw	0.193	0.349	0.036	**0.563**
Q2	0.145	-0.331	**-0.581**	0.567
Q4	-0.600	-0.157	**0.562**	0.050
ITSu	**0.617**	-0.288	0.020	0.437
ITSw	**0.755**	-0.078	0.478	-0.384
ILSu	**0.782**	0.034	-0.419	0.131
ILSw	**0.773**	-0.103	0.497	-0.269

F)

	PC1	PC2
Tot vel	0.056	**0.680**
TKE	**0.887**	-0.312
uv	**0.814**	-0.365
uw	**0.895**	0.098
Q2	-0.400	-0.371
Q4	0.107	0.274
ITSu	0.143	0.353
ITSw	0.348	-0.408
ILSu	0.302	**0.841**
ILSw	0.469	**0.537**

Figure 5.8 Scree plots and loading factors for low (A and E), medium (B and F) and high (C and F) gradient reaches.

Table 5.6 Summary of which parameters reflect the first four principal components for each river.

Gradient	PCs	PCs name	Included variables
Low	PC1	Resultant velocity and intensity	Resultant velocity/ TKE/ Reynolds shear stress
	PC2	Temporal and Spatial eddy scales on u and w directions	ITSu, ILSu, ITSu, ITSw
	PC3	Contribution to shear stress	Q2, Q4
Medium	PC1	Time and Spatial eddy scales	ITSu, ITSw, ILSu, ILSw
	PC2	Resultant velocity and intensity	Resultant velocity, TKE, shear stress on uv plane
	PC3	Contribution to shear stress	Q2, Q4
	PC4	Partial intensity	Shear stress uw plane
High	PC1	Intensity	TKE, Shear stress on uv and uw planes
	PC2	Resultant velocity and spatial eddy scale	Resultant velocity, ILSu, ILSw

Table 5.7 Summary of principal components across the three reaches subdivided by four main categories: turbulence intensity (resultant velocity, TKE, u'v', u'w'), contribution to shear stress (Q2, Q4), spatial eddy scale (ILSu, ILSw) and temporal eddy scale (ITSu, ITSw).

Gradient reach	Intensity	Contribution to shear stress	Spatial eddy scale	Temporal eddy scale
Low	PC1	PC3	PC2	PC2
Intermediate	PC2 + PC4	PC3	PC1	PC1
High	PC1	-	PC2	-

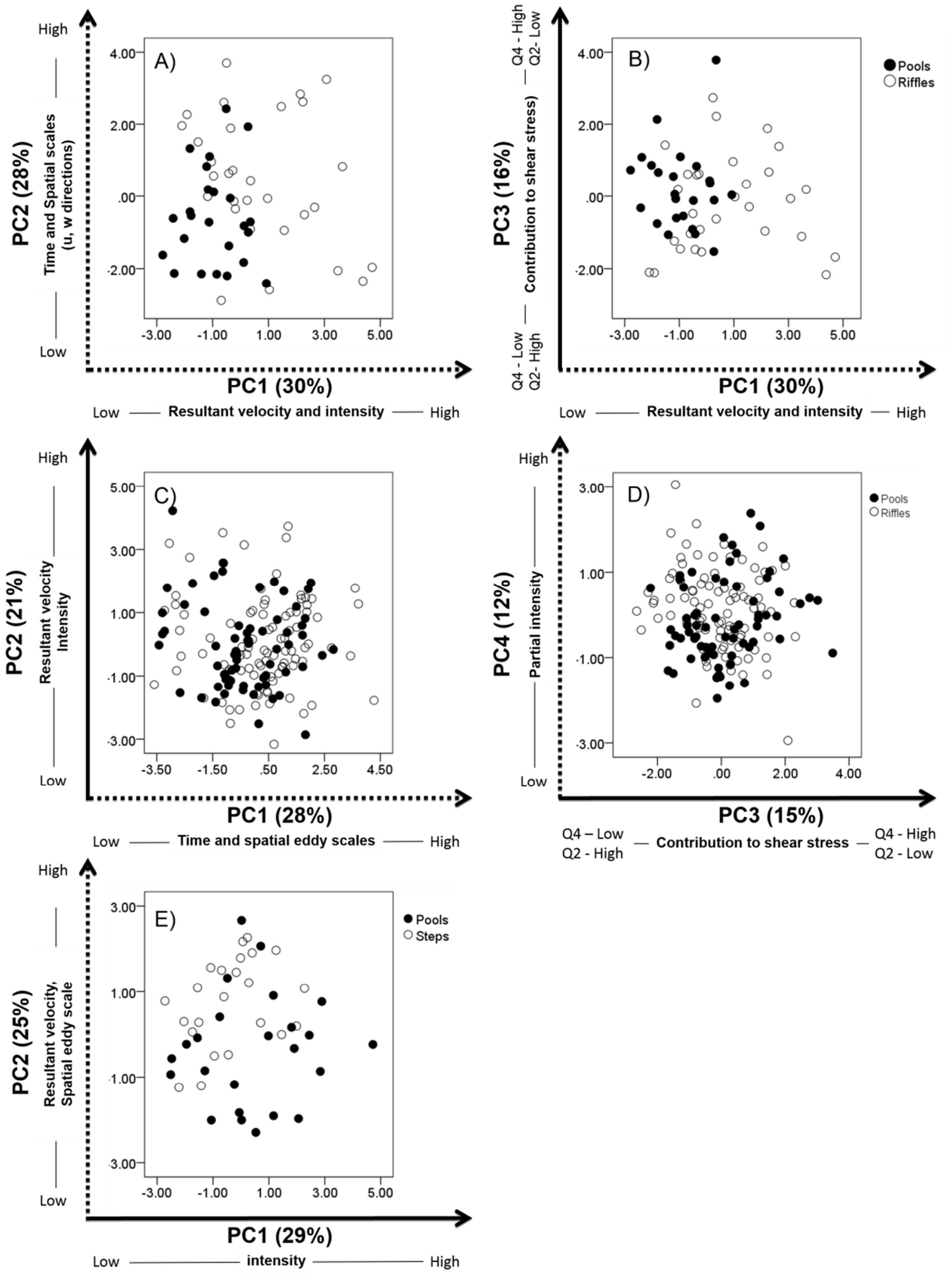

Figure 5.9 Bi-plots of principal components for low (A-B), medium (C-D), and high (E) gradient reaches with dotted lines (as x or y axis) representing the principal components statistically significant across riffles (steps) and pools.

Multiple logistic regression was applied in order to assess the ability of turbulence properties to predict the occurrence of different GUs. The model parameters are presented in Table 5.8. Across the three gradient reaches, the AUC values were all positive and above the 0.6 threshold for acceptable model fit, with particularly high values (> 0.7) for the low gradient reach (0.86) and high gradient reach (0.74). Models across the three reaches were statistically significant ($p < 0.01$) for at least one principal component and explained 43% of the variance in the low gradient reach, 8% in the intermediate gradient reach and 25% in the high gradient reach (Nagelkerke R^2). Model parameters and standardised coefficients enable identification of the variables that best predict riffles and pools or steps and pools. Different PCs were mostly effective in predicting the occurrence of GUs depending on reach gradient/GU type. For the low gradient reach, PC1 and PC2 were significant, indicating that higher turbulence intensity and larger scale were associated with an increased likelihood of riffle (pools) occurrences. For the intermediate gradient reach, PC1 was significant, indicating that larger scale eddies were associated with increased likelihood of riffle (pools) occurrence however the explained variance was low. For the high gradient reach, PC2 was significant, indicating that higher overall velocity and spatial eddy scale were associated with an increased likelihood of step (pools) occurrence.

Table 5.8 Parameters of logistic regression model used to predict the geomorphic units (riffles and steps) at low, medium and high gradient reaches. Values in brackets are the parameters for predicted pools.

Descriptions	Values	Standard error	Wald Chi^2	p	Odds ratio
FROME					
Constant	0.32 (-0.32)	0.35	0.85	0.35	
PC1: Resultant velocity and intensity	0.77 (-0.77)	0.28	7.74	0.005	3.8 (0.46)
PC2: Time and spatial scale (u component)	0.69 (-0.6)	0.26	7.03	0.008	3.3 (0.49)
PC3: Contribution to shear stress	0.18 (-0.18)	0.25	0.54	0.46	1.3 (1.2)
TAGLIAMENTO					
Constant	0.38 (-0.38)	0.17	5.37	0.02	
PC1: Time and spatial eddy scales	0.28 (-0.28)	0.11	6.41	0.01	1.32 (0.76)
PC2: Resultant velocity and intensity	0.13 (-0.13)	0.12	1.11	0.29	1.14 (0.88)
PC3: Contribution to shear stress	-0.07 (0.07)	0.15	0.11	0.74	0.95 (1.05)
VERMIGLIANA					
Constant	-0.12 (0.12)	0.32	0.14	0.02	
PC1: Intensity	-0.22 (0.22)	0.20	1.31	0.25	0.80 (0.84)
PC2: Resultant velocity, spatial eddy scale	0.78 (-0.78)	0.28	7.46	0.006	2.19 (0.26)

5.3.3 Objective identification of spatial clusters based on turbulence properties

Agglomerative Hierarchical Cluster Analysis (HCA) was applied separately for each reach to the PCs derived from PCA and used to explore the structure of the data set. Ward's algorithm and the Euclidean distance measure were used to perform the analysis and the structure of cluster dendograms revealed the presence of three clusters. On this basis, velocity time series were then partitioned into one of three classes using k-means cluster analysis using the centroid method. Summary statistics for three clusters describing the means and standard deviations across the main turbulence gradients represented by the PCs are presented in Table 5.9, together with brief descriptions of what they represent and their approximate positions within the channel. Figure 5.10 presents the distribution of the clusters for each reach. In addition, Kruskall Wallis test with post hoc was then applied to the three clusters separately for each river to identify which clusters had statistically significant differences across the PCs (Table 5.10).

For the low gradient, cluster 1 exhibits intermediate turbulence intensity, largest eddy scale with high presence of inrushes described by positive orientation gradient. Cluster 2 was broadly described by negative mean values for intensity, spatio-temporal eddy scales and orientation of flow structure that identify a class with the lowest intensity and the flow motion away from the bed (ejections). Cluster 3 was the highest turbulent intensity, smaller eddy scales and flow events moving towards the bed (inrushes). Kruskall Wallis test indicated that cluster 1 exhibited statistically differences for all turbulent gradient components compared with cluster 2 and 3 while there was no statistically difference for eddy scales and orientation of flow structure between cluster 2 and 3.

For the intermediate gradient reach, cluster 1 reflects the intermediate turbulent intensity, smallest eddy scales and the presence of flow events moving to the bed (inrushes). Cluster 2 exhibits the highest intensity, intermediate eddy size and duration with the presence of ejections while cluster 3 was characterized by low intensity, bigger eddy and flow events moving towards the bed (inrushes). All the three classes exhibited differences in eddy period and spatial scales (KW: $p < 0.001$). However, cluster 1 and 3 were similar for overall intensity and orientation of flow structure indicating the presence of similar flow structure (inrushes) in areas with both small and big eddy size with low/intermediate intensity.

The distribution of each cluster was below the 50 percent for each reach indicating a uniform presence of the three classes. For the low gradient reach, cluster 2 (low intensity and ejections) was dominant compared with the intermediate/high turbulent classes. Cluster 3 (high intensity and small eddy size and ejections) suggesting an increase of turbulence in localized areas. For the intermediate gradient, turbulent classes were uniform in percent with a slightly dominance for cluster 2 reflecting high intensity and larger eddy size and duration. For the high gradient reach, cluster 3 reflects the dominant group defined by high intensity and small eddy size.

Table 5.9 Summary statistics of means and standard deviations of the four principal components with briefly description of their location compare with the channel.

Reach gradient	Cluster	Description	Location	PC1 mean (SD)	PC2 mean (SD)	PC3 mean (SD)	PC4 mean (SD)
Low				Intensity	Spatio-temporal eddy scales	Orientation	-
	1	Intermediate intensity; higher eddy scales; inrushes	Marginal areas	0.22 (1.32)	1.49 (1.33)	0.69 (1.45)	-
	2	Low intensity; ejections	All other areas	-1.06 (0.88)	-0.54 (1.31)	-0.35 (0.95)	-
	3	High intensity; smaller eddy scales; ejections	Around Macrophytes	2.74 (1.41)	-1.36 (1.18)	-0.33 (1.08)	-
Intermediate				Spatio-temporal Eddy scales	Resultant velocity and Intensity	Orientation	Partial intensity u'w'
	1	Intermediate intensity; Smaller eddy scales, inrushes	Riffles and margins	-1.78 (0.96)	-0.08 (1.48)	0.39 (1.15)	-0.15 (1.02)
	2	High intensity; Intermediate eddy scales; ejections	Predominantly riffles	0.45 (0.86)	0.67 (1.24)	-0.69 (0.95)	0.38 (0.81)
	3	Low intensity; bigger eddy scales; inrushes	Pools and transitional zones	1.30 (1.07)	-0.78 (1.08)	0.48 (0.95)	-0.33 (0.93)
High				Intensity	Resultant velocity; spatial eddy scale	-	-
	1	Intermediate intensity; bigger eddy scale	Marginal areas	0.30 (1.09)	1.87 (0.86)	-	-
	2	Low intensity, smaller eddy scale	Margins and transition zones	-1.39 (0.83)	-0.53 (0.91)	-	-
	3	High intensity, smaller eddy scale	Largely central channel locations	1.94 (1.05)	-0.59 (1.32)	-	-

Table 5.10 Table of significant differences between parameters (principal components) across 3 clusters (differences where p < 0.001 for Kruskall Wallis post-hoc tests).

Gradient reach	PCs descriptions	Significant differences
Low	PC1: Overall velocity and intensity	Cluster 3> cluster 1 > cluster 2
	PC2: Time and spatial scale (u and w components)	Cluster 1 > cluster 2 / cluster 3
	PC3: Contribution to shear stress (ejections/inrushes)	Cluster 1 > cluster 2/cluster 3
Medium	PC1: Time and spatial eddy scales	Cluster 3 > cluster 2 > cluster1
	PC2: Overall velocity and intensity	Cluster 2 > cluster1/cluster3
	PC3: Contribution to shear stress (ejections/inrushes)	Cluster1/cluster 3 > cluster 2
	PC4: Partial intensity	Cluster 2 > cluster 1/ cluster 3
High	PC1: Intensity	Cluster 3 / cluster 1 > cluster 2
	PC2: Overall velocity, spatial eddy scale	Cluster 1 > cluster 2 / cluster 3

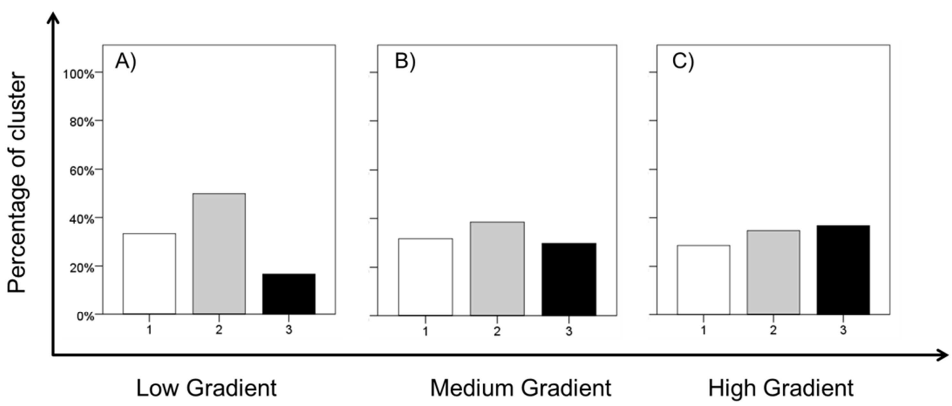

Figure 5.10 Bar charts for percentage of number of observations for each cluster across the low (A), medium (B) and high (C) gradient reaches.

Figure 5.11 and Figure 5.12 present GIS visualisations to show the spatial location of clusters for each reaches.

For the low gradient reach, cluster defined by the highest turbulent intensity, flow events moving away from the bed (ejections) and smaller eddy size (3) was associated with areas around aquatic macrophyte patches suggesting that they influenced the development of eddy patterns. The low turbulent intensity within variable eddy scale cluster (2) was associated generally with channel areas within margins and vegetated patches, while the intermediate intensity (1) with the presence of inrushes was related with margins. Figure 5.11B shows no correspondence between the three clusters and geomorphic units, this evidence suggests that clusters may be reflect smaller sub-units directly associated with aquatic vegetation.

For the intermediate gradient reach, riffles and pools habitat were broadly discriminated by higher intensity, larger eddy scales and ejections (2) and low intensity, variable eddy and flow events moving towards the bed (inrushes) (3), respectively, while areas with the intermediate intensity, smaller eddy scales and inrushes (1) reflect partially riffles and marginal regions.

For the high gradient reach, the three clusters present a complex spatial organisation without clear relations with steps and pools, although few spatial trends were noted. Marginal areas were associated with intermediate intensity and bigger eddy size (1), while transitional and marginal regions were related to cluster with lower intensity and smaller eddy scales (2) and finally largely central channel locations to the highest intensity and smaller eddy scales high intensity (3).

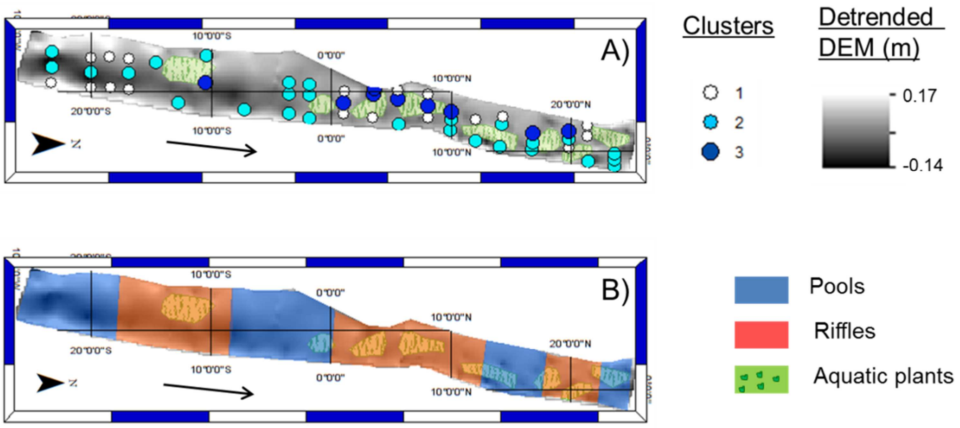

Figure 5.11 Spatial visualization of 3 clusters below the detrended DEM (A) and the spatial organization of pools/riffles for the low gradient reach. Black arrow is the direction of the flow.

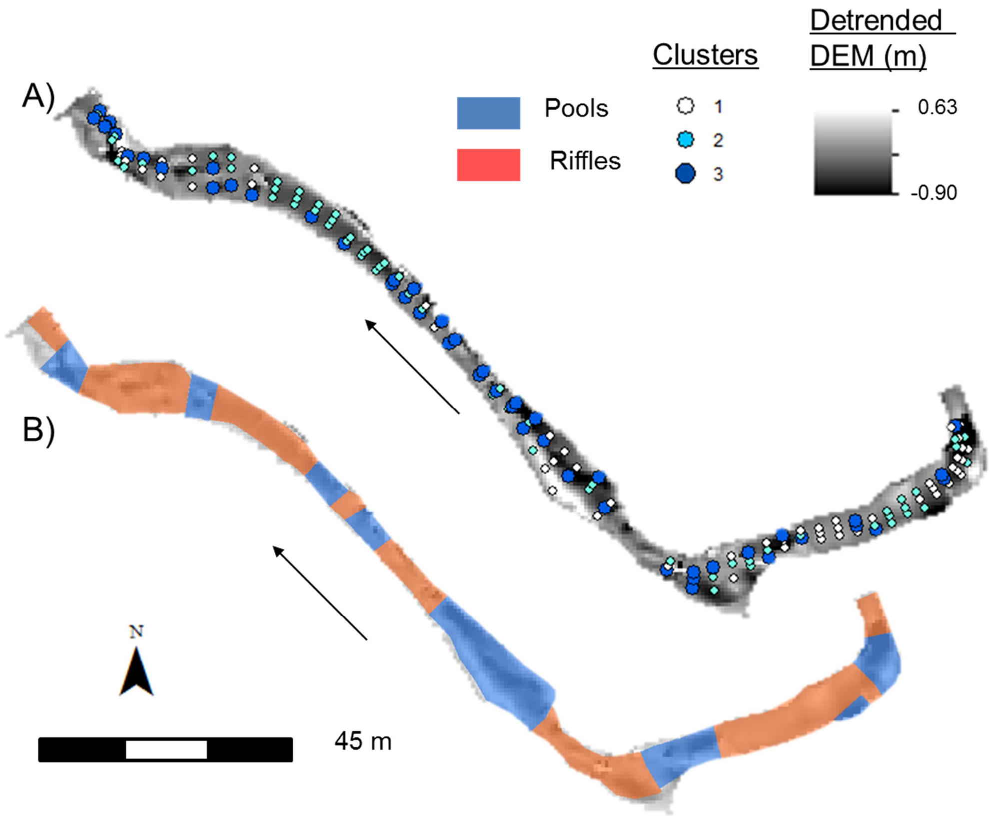

Figure 5.12 Spatial organization of 3 clusters below the detrended DEM (A) and the spatial organization of pools/riffles (B) for the medium gradient reach. Black arrow is the direction of the flow.

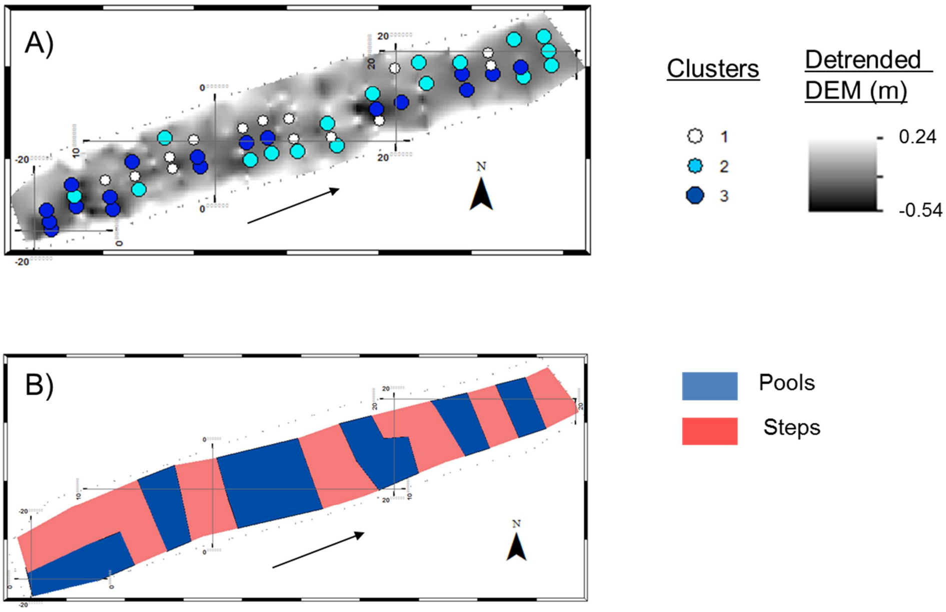

Figure 5.13 Spatial visualization of 3 clusters below the detrended DEM (A) and the spatial organization of pools/steps (B) for the high gradient reach. Black arrow is the direction of the flow.

5.4 Discussion

5.4.1 Turbulent flow properties associated with key GUs

The results of higher-order (turbulence) flow properties associated with key geomorphic units highlight different turbulence variability for geomorphic units in reaches of different gradients. The IPOS framework has been applied to provide a full detailed investigation of turbulence properties based on four groups of parameters: intensity, periodicity, orientation and scale.

Turbulence characterization of geomorphic units in natural rivers is still relatively scarce. A small number of previous studies on higher-order flow properties have explored turbulence properties across riffles, glides and pool in different environment considering few hydraulic variables. Table 5.11 summarizes the hydraulic parameters on which previous works have been focused highlighting not all previous works analysed all the turbulence variables applied in this thesis. For the low gradient, geomorphic units (riffles, pools and glides) were investigated on turbulence intensity by fluctuation on streamwise (u) and vertical (w) components, overall intensity, event structure and eddy size (Harvey and Clifford, 2009), while Wilkes (2014) included turbulent kinetic energy and Reynolds shear stress on the three planes for the intensity parameters, and added variables on the orientation of flow structures and periodicity. For intermediate and high gradient reaches, previous research have distinguished differences between riffles (steps) and pools by the distribution of the turbulence intensity (turbulent kinetic energy), periodicity (temporal scale of eddy (ITS)) and orientation (shear stress) (Wilcox and Wohl, 2007, Roy *et al.*, 2010).

Overall, the results presented in this chapter suggest that reach gradient has a stronger influence on turbulence properties than GUs. The capacity for IPOS variables to distinguish between GUs varied between the different IPOS categories. For example, turbulence intensity did not show any clear or consistent trends between GUs in the three reaches, and patterns varied depending on the individual variable studies. This may partly reflect that pools can be highly spatial heterogeneous flow environments (Mac Vicar and Roy, 2007b; Harvey and Clifford, 2009). Furthermore, pools can represent more tranquil environments under low gradient conditions, but in high gradient reaches, flow acceleration over steps may generate a more energetic flow environment in pools (Wohl and Thompson, 2000, Wilcox and Wohl, 2007).

Predictability variables showed some gradients among the same GUs in different gradient reaches, with greater predictability in low gradient pools compared to high gradient pools illustrated by kurtosis and integral time scale variables. This is consistent with previous research in high and low gradient pools (Mac Vicar and Roy, 2007b; Wilkes, 2014). For orientation variables, there were no clear differences between GUs with each unit revealing a unique event signature. Eddy scale showed some differences among GUs, with smaller eddies (u dimension) in pools relative to riffles/steps at the intermediate and high gradient reaches respectively. This is consistent with previous findings from low gradient rivers (Harvey and Clifford, 2009; Wilkes, 2014).

Table 5.11 Summary of results on turbulence characterization of riffles and pools for previous studies together with this study. Values are mean values (or range in italics). * referred to overall velocity and not turbulent kinetic energy.

	Harvey and Clifford, 2009	Wilcox and Wohl, 2007	Roy *et al*, 2010	Wilkes, 2014	This thesis		
Reach Gradient	Low	High	Medium	Low	Low	Medium	High
Intensity TKE [$cm^2\ s^{-2}$]							
Pools	2* – 100*	300-600	67	< 90	60-100	180-280	240-410
Riffles/Steps	4* – 120*	40-320	145	50 -120	80-150	200-300	200-340
Periodicity			ITSu,w [s]	ITS u,w [s]	ITS u,w [s]	ITS u,w [s]	ITS u,w [s]
Pools	N/A	N/A	0.69 / 0.35	4.7 / 2.3 2.3 / 2.2	0.6-10 0.2-0.4	0.4-0.8 0.2-0.5	0.35-0.75 0.25-0.41
Riffles/Steps	N/A	N/A	0.33 / 0.25	0.4 / 0.2 0.1 / 0.1	0.7-1.3 0.2-0.6	0.15-0.4 0.15-0.3	0.15-0.42 0.12-0.20
Orientation	Skewness u,w		u'w' [$N\ m^{-2}$]	u'w' [$N\ m^{-2}$]	$Ske_{u,v,w}$ [Nm^{-2}]	$Ske_{u,v,w}$ [Nm^{-2}]	$Ske_{u,v,w}$ [Nm^{-2}]
Pools	-0.4 – 0.8 -0.35 – 0.4	Deceleration	9.7	0.1	-0.4 - -0.4 -0.4 - 0 -0.3 - 0	-0.6 – 0.05 -0.2 – 0.44 -0.1 – 0.1	-0.1 – 0.35 -0.25 – 0.05 0 – 0.30
Riffles/Steps	-0.2 – 0.7 -0.4 – 0.42	High velocity jet	30.7	1.9	0.1 - 0.3 -0.1 - 0.5 -0.1 - 0.2	0.1-0.4 -0.15 – 0.2 -0.05 – 0.2	0.3 – 0.6 0.2 – 0.3 0 – 0. 25
Scale Lu [m]							
Pools	0.05 – 0.7	N/A	N/A	0.02 / 0.33	0.1 – 0.25	0.3 – 0.75	0.35 – 1.00
Riffles/Steps	0.75 – 1.05	N/A	N/A	0.18 / 2.16	0.2 – 0.35	0.45 – 0.9	0.70 - 1.25

5.4.2 Gradients in turbulent properties and statistical identification of GUs

PCA was carried out individually for each site to identify principal gradients in the data and relate these to groupings of GUs. PCs represent gradients in intensity, scale and orientation, consistent with the IPOS framework. The majority of predictability variables had to be removed so that the PCA met the key statistical assumptions of the analysis technique, and therefore were not fully represented in these multivariate analyses. The results confirm that the IPOS categories accurately reflect the principal sources of variance in turbulent time series across different sites. For the low and intermediate gradient reaches, gradients represented intensity, scale and orientation, while for the higher gradient reach only two gradients were derived, representing intensity and scale variables.

PCs did not fully distinguish GUs at any of the sites, but greater distinction between GUs on the basis of PC scores was observed for the low gradient reach, and the largest overlap in values between GUs was observed for the high gradient reach. Logistic regression models were applied to assess the ability of PCs to predict the occurrence of GUs at each site. All regression models were statistically significant, but different PCs were important depending on the site and GU combination. For the low gradient reach, intensity was the best predictor of GUs, while for the intermediate and high gradient reaches eddy scale was the best predictor.

Cluster analysis was applied to objectively group sample locations on the basis of their PC scores. Three clusters were identified at each reach, representing differences in intensity, orientation and scale. At the low and high gradient reach, clusters appeared to correspond with sub-GU scale patches. For the low gradient reach clusters appeared to distinguish between locations around aquatic plant stands and marginal channel areas. This likely reflects the influence of aquatic vegetation on local turbulence properties including enhanced intensity, breaking down eddies and hence reductions eddy scale, and wake generation (Nepf, 1999; Zong and Nepf, 2010; Nepf, 2012; Ortiz *et al.*, 2013). For the high gradient reach the spatial organisation of clusters was more complex, perhaps relating to hydraulic variation driven by individual flow obstructions such as large boulders. Areas immediately above and below steps have been identified as producing distinct hydraulic zones in step-pool morphologies, representing an additional source of sub-GU scale variability (Wohl and Thompson, 2000).

CHAPTER 6: Influence of changes in flow stage and aquatic vegetation cover on turbulence properties and their spatial organization

6.1 Introduction

It is common for field assessments of river habitat quality to be undertaken under low flow conditions during the period of maximum vegetation growth (Raven *et al.*, 1998; Rinaldi *et al.*, 2013b; Rinaldi *et al.*, 2016), to enable to capture of the full range of instream and riparian features. However, considering hydraulics under one discharge condition does not provide a full understanding of hydrodynamics at the habitat scale and relationships with bedforms and other roughness elements that may be strongly stage dependent (Kondolf *et al.*, 2005). A small number of studies have explored the hydraulics of physical biotopes at different discharges but these have largely focused on standard hydraulic variables (average velocities, water depth and substrate). The assemblage of instream hydraulic units changes with flow stage, for example with both pool and riffle units becoming more similar to run or glide units at higher flows (Padmore, 1998) although more pronounced bedforms may retain hydraulic distinction at higher flows (Wallis *et al.*, 2012).

Padmore *et al.* (1997) identified maximum hydraulic diversity at low flow while Wallis *et al.* (2012) found that intermediate flow had the higher level of hydraulic diversity. In contrast, Clifford *et al.* (2002; 2009) found lower levels of hydraulic diversity at the intermediate-high flow stage as morphological controls on instream hydraulics were ‘drowned out’. Studies directly exploring temporal variability in turbulence properties are even fewer. Changes in the turbulence properties of geomorphic units under different flow conditions (low and intermediate) were investigated by Harvey and Clifford (2009) and Wilkes (2014) in low gradient rivers. The two studies both revealed differences in the levels of internal complexity of geomorphic units on the basis of a range of turbulence properties, although the relative complexity of different combinations of units differed. Harvey and Clifford (2009) identified a gradient of increasing complexity from glide (less variable), to riffle to pool, while Wilkes (2014) identified riffles as the most hydraulically complex and pools as the most uniform, perhaps reflecting differences in the type of pools studied.

It is not only flow stage that may cause temporal variations in hydraulic habitat. In lowland rivers in particular, annual cycles of growth and senescence of submerged and emergent aquatic plants can dramatically alter the spatial organisation of flow velocities and erosion and deposition patterns at the reach scale (Gurnell *et al.*, 2006; Wharton *et al.*, 2006), see review in Chapter 2), creating changes in the mosaic of habitat patches available and potentially leading to the construction of landforms through sediment retention (Gurnell, 2014). This adds an additional element of spatiotemporal complexity to habitat assessment in these rivers that must be considered.

Understanding of temporal dynamics of hydraulic habitat is important in terms of assessing habitat suitability for different species, and as a consideration in the design of river restoration schemes. This chapter explores changes in the nature and spatial organisation of turbulence properties in relation to (i) changes in flow stage (high gradient reach) and (ii) changes in aquatic plant cover (low gradient reach). In particular, the research aims to address the following research objectives:

1. Quantify the effects of increased flow stage on turbulence properties (intensity, predictability (periodicity), orientation and scale).

2. Explore changes in the spatial organization of turbulent properties associated with an increase in flow stage.

3. Quantify the effects of aquatic vegetation growth on turbulence properties (intensity, predictability, orientation and scale).

4. Explore changes in the spatial organization of turbulent properties associated with aquatic vegetation growth.

6.2 Methodology

6.2.1 Field data

Variations in turbulence properties with flow stage (Objectives 1 and 2) were assessed for the high gradient reach (Vermigliana Creek) while variations associated with aquatic vegetation growth were assessed for the low gradient reach (River Frome). Full details of the two field sites, including catchment characteristics are provided in the Research Design chapter (Chapter 3). For each reach, velocity surveys were recorded under two different conditions. For the flow stage analysis on the high gradient reach, the surveys were undertaken under relative low flow (Q = 1.82 m^3 s^{-1}; 48% exceedence) and high flow (Q = 5.53 m^3s^{-1} 10% exceedence) conditions. For the vegetation analysis on the low gradient reach, the surveys were carried out in two different seasonal periods, while attempting to conduct surveys under similar relative low flow conditions (exceedence between 95% and 80%). One survey was undertaken during peak vegetation cover (early/mid September; 95% exceedence) and the second during the period of winter die-back (mid-February; 80% exceedence) (Table 6.1).

A stratified sampling approach to velocity measurement was taken, with velocities sampled at three locations (30, 50, 70 % of channel width) along equally spaced cross sections in order to capture variability along the channel centreline and more marginal locations. The distance between longitudinal cross sections was scaled on channel width and was 3 m for both rivers. The sampling design enabled sufficient replication of measurements within the key geomorphic units characteristic of each reach (step-pool or riffle-pool sequences). Each velocity measurement was captured at 0.6 of the water depth (from the surface) in order to sample conditions in the outer flow zone. See Chapter 3 (Research Design) for full details of velocity measurement.

Table 6.1 Details of discharge during the survey (Q_{survey}), average water depth (y_m), mean velocity (V_m) and time period of surveys for the high gradient reach at low and high flows and for the low gradient reach at high and minimal vegetation cover. * calculated by Manning equation (Limeniros, 1972) V_m=1.486/n R^(2/3) S^(1/2) where S is the channel slope and R is the hydraulic radius (respectively 0.033 and 0.029 for non vegetated and vegetated periods).

High gradient	Low flow	High flow
Q_{survey} (m^3 s^{-1})	1.82 (48 %exceedence)	5.53 (10% exceedence)
y_m (m)	0.48	0.61
V_m (m s^{-1})	0.60	0.76
Time period survey	August 2015	May 2016
Low gradient	Low vegetation cover	High vegetation cover
Q_{survey} (m^3 s^{-1})	1.45 (80% exceedence)	0.58 (95% exceedence)
y_m (m)	0.41	0.38
V_m (m s^{-1})	0.52	0.19
Roughness (Manning)*	0.0009	0.0034
Time period survey	February 2016	September 2015

6.2.2 Data Analysis

Turbulence parameters were computed for all time series that met data quality requirements as previous explained in the Research Design (see Table 3.6). Data were not normally distributed (Shapiro – Wilk: $p < 0.001$) and therefore non-parametric statistical tests were used. Spearman's Rank correlations were used to assess the relationships between variables and Kruskall Wallis tests (with post hoc tests) were used to identify significant differences between groups. Multivariate statistical analysis (Principal Components Analysis; PCA) was used to identify the key gradients in turbulence properties within the data set to reduce the dimensionality of the data set and examine whether the principal components reflect the IPOS turbulence groups (intensity, predictability, orientation and scale). Prior to PCA, Kaiser-Meyer-Olkin (KMO) and Barlett's test of Sphericity were analysed to identify redundant variables and check correlations between variables respectively. Following this, the following variables were retained for use in the PCA: turbulent kinetic energy, shear stress on uv and uw planes, and temporal and spatial eddy scales (ITSu,w and ILSu,w) together with event structure magnitude and duration derived from quadrant analysis (ejections (Q2, t2) and inrushes (Q4, t4)). PCA was conducted separately for each reach. Two PCAs were run with orthogonal rotation (Varimax): one combining the two data sets for each reach (standardised by z-scores; (Emery *et al.*, 2003; Wallis *et al.*, 2012)) and one for each survey at each reach separately (using raw data). Geospatial analysis was performed separately for each reach and survey condition by producing experimental semivariograms for PC scores and fitting appropriate semivariogram models (Legleiter *et al.*, 2007; David *et al.*, 2013).

Sample locations were separated into two groups depending on magnitude of change using frequency distributions: (i) 'high change' showing those with a large amount of change (positive or negative), represented by sample locations falling above the 75th or below the 25th percentiles respectively; and (ii) 'low change' showing those with a smaller level of change (between 25th and 75th percentiles).

Wavelet analysis was applied to both data sets from the low and high gradient reaches. This was used to identify levels of flow predictability using the presence of intermittent/evolving flow structures (by identifying the dominant frequency in the velocity time series) over the sampling period ranging from 0 to 90 seconds. Full details on the Wavelet analysis are described in Chapter 3 (Section 3.6.2).

The common fish species for the high and low gradient reaches was brown trout, *Salmo trutta,* (Betti, 2001; Environment Agency, 2010a). This species was used to represent average fish size (length) and swimming speed to explore relationships between fish characteristics and eddy size and implications for fish stability. These parameters were used to calculate eddy: fish length scale and momentum ratios using Equations 3.12 and 3.13 explained in Chapter 3 (Section 3.6.4).

Statistical analyses were conducted in IBM SPSS version 22, ExcelSTAT Base 2016, Matlab R2015b and geostatistical analysis was performed initially in ArcGIS 10.2 version and after using customised functions written in Matlab R2015b. Wavelet analysis was performed using default functions written in Matlab R2015b.

6.3 Results

6.3.1 Effects of increased flow stage on turbulent properties (high gradient reach)

Figure 6.1 illustrates the overall changes in velocity and depth throughout the high gradient reach associated with the increase in flow stage. Water depths increased and became more homogenous throughout the reach. Mean velocities in the U and V dimensions increased overall with flow stage and some higher magnitude outliers were identifiable, while lower levels of change were noted for the W component. Figure 6.2 presents the key parameters for turbulence intensity across the two flow stages. Similar distributions were noted for the absolute intensity along the streamwise (u) component while the range of values for the lateral (v) and vertical (w) components increased under high flow conditions. Relative intensity showed minimal change with flow stage for all three components. Both TKE and the shear stress on vw and uw planes increased under high flow conditions, although the differences between flow stage were not statistically significant (Mann Whitney U: $p > 0.05$).

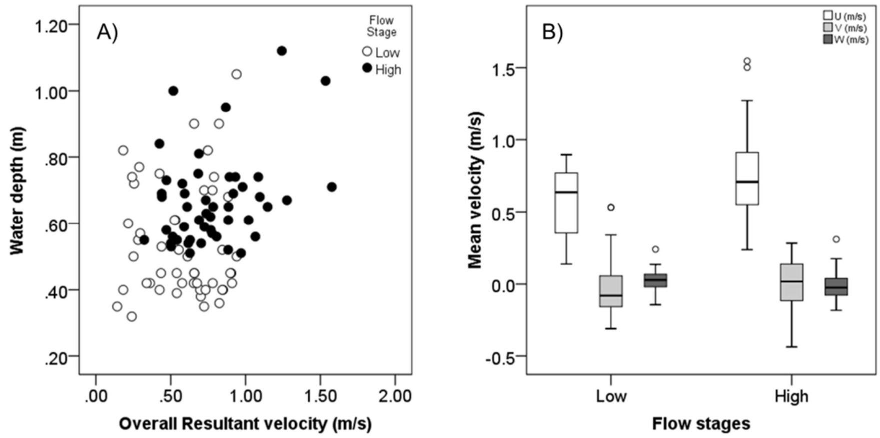

Figure 6.1 Scatter plots of resultant velocity and water depth grouped by low/high flows (A) and the distribution of average velocity in u, v and w directions (B) across the two flow stages.

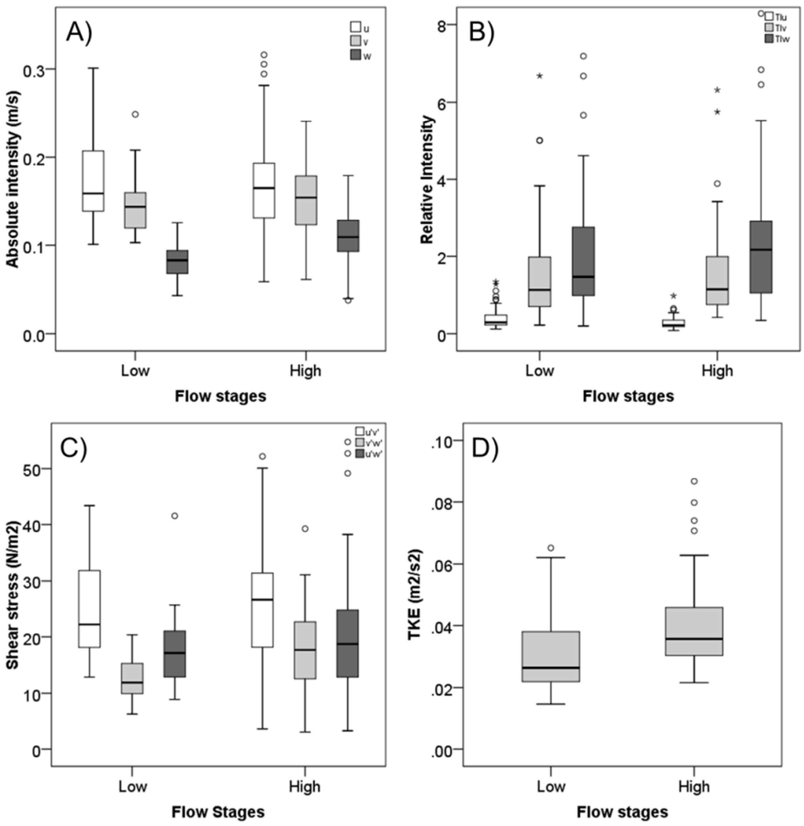

Figure 6.2 Distribution of key turbulent intensity: A) the absolute and B) relative turbulence intensity for all three components, C) Reynolds shear stress for uv, vw and uw planes across the two flow stages.

The predictability and periodicity of velocity series described by the kurtosis, the pseudo-periodicity condition and the integral time scale for the two flow stages is shown in Figure 6.3. The predictability of time series is also explored by the results of the wavelet analysis (Figure 6.4). Kurtosis values for the higher flow stage occupy a narrower range of higher values, indicating that the frequency distributions of turbulent fluctuations on u, v and w components were more consistently associated with a 'peaked' form. This indicates a tendency for a more uniform, predictable velocity structure throughout the reach, in comparison to greater spatial variability in kurtosis values at the lower flow stage. Differences in kurtosis values between flow stages were statistically significant for all three velocity components (Mann Whitney U: $p<0.05$). Despite this, the majority of time series for both low and high flow stage did not satisfy the criteria for pseudo-periodicity. There is a pronounced reduction in the integral time scale for eddies on the u component, and to a lesser extent on the w component with increasing flow stage, and in both cases these differences were statistically significant (Mann Whitney U: $p < 0.05$).

Wavelet subplots reflect global and local properties of the signal energy, describing the temporal velocity structure for the streamwise (u) velocity component. Example plots are provided in Figure 6.4 showing (a) the raw u time series, (b) the Wavelet power spectra showing the correlation between the raw time series and different temporal length scales of the wavelet across the length of the time series, (c) the global wavelet spectra, showing the presence of significant periods in the record and (d) the variance of the dominant period through time. For each sample point, wavelet analysis was used to derive a dominant wavelet period, and the frequency distributions for the wavelet period for low and high flow surveys are shown in Figure 6.5. Average (median) dominant period of oscillations increased from low to high flow, but the form of frequency distribution also changed. The narrower more peaked distribution at low flow suggests greater spatial homogeneity in dominant period, while the broader distribution at high flow suggests greater spatial heterogeneity. However, it was noted through qualitative visual inspection of global wavelet spectra that some time series showed a clear significant peak, while others were characterised by multiple peaks, and hence the derivation of a dominant peak may be more appropriate to some sample locations than others. There was a difference in number of time series with single/multiple peaks between low and high flows. Most of time series at low (61%) had simple peaks while only 39% of time series were observed with single peaks at high flows indicating an increase in multiple peaks at high flow suggesting more complex flow period.

The flow orientation defined by skewness, and the cumulative magnitude and duration of the four turbulent event types (ejections, inrushes, inward interactions, outward interactions) are presented in Figure 6.6 to illustrate changes in orientation attributes. Skewness values ranged from positive to negative for both flow stages, indicating a combination of series largely dominated by lower magnitude fluctuations (skewness < 0) and series largely dominated by higher magnitude fluctuations (skewness >0). Overall, median skewness values were positive across all three components, but skewness values decreased at the higher flow stage, towards median values approaching zero. The difference between flow stages was statistically significant for the streamwise (u) and lateral (v) components (Mann Whitney U: $p < 0.05$). Quadrant analysis revealed similar proportional contributions to the total shear stress from the four event types at both low and high flow stages, but the cumulative duration of events increases significantly at the higher flow stage for all four event types (Mann Whitney U: $p <0.05$). This indicates a tendency for lower magnitude events (but of longer cumulative duration) at the higher flow stage, consistent with patterns identified for skewness. Figure 6.7 illustrates the relationship between magnitude and duration for Q4 (inrushes) and Q2 (ejections), showing that shorter duration events account for considerably greater contributions to shear stress at the lower flow stage.

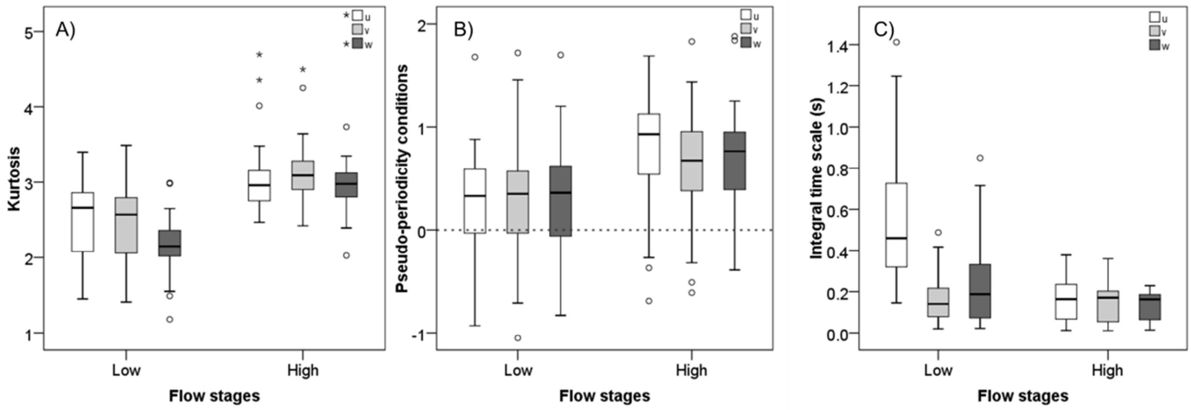

Figure 6.3 Predictability and periodicity of velocity time series by kurtosis (A), pseudo-periodicity (B) and integral time scale (C) across the two flow stages.

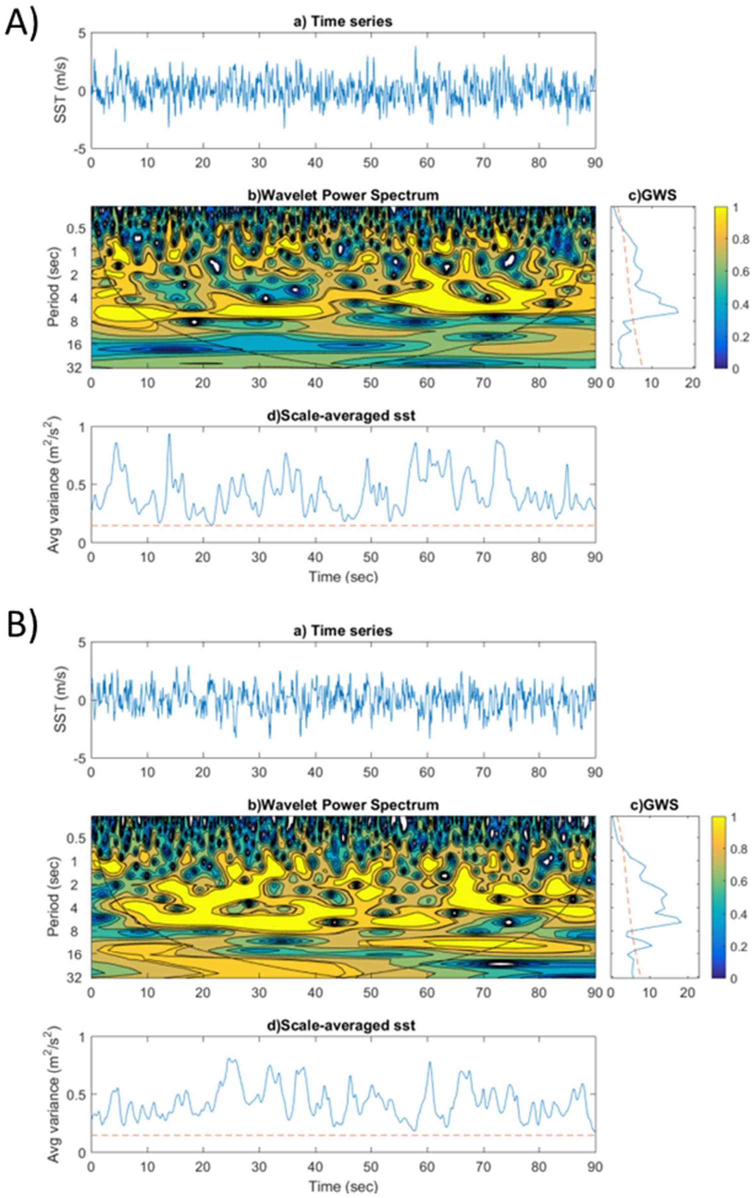

Figure 6.4 Example of the Wavelet analysis for low flow (A) and high flow (B) stages. Graphs reflect: a) the original (u) time series (sst); b) Wavelet power spectrum (dotted black line shows influence cone that reflects the significance level and confidence for the wavelet spectra indicating the disturbed areas/error); c) global wavelet spectrum; and d) the variance explained by the dominant wavelet period through the time series.

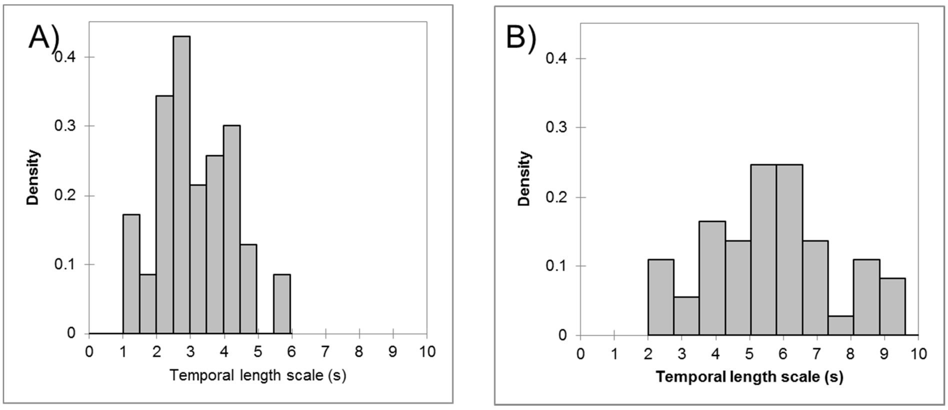

Figure 6.5 Frequency distribution of dominant temporal length scale extracted by Wavelet spectra for the low flow (A) and high flow (B) stages.

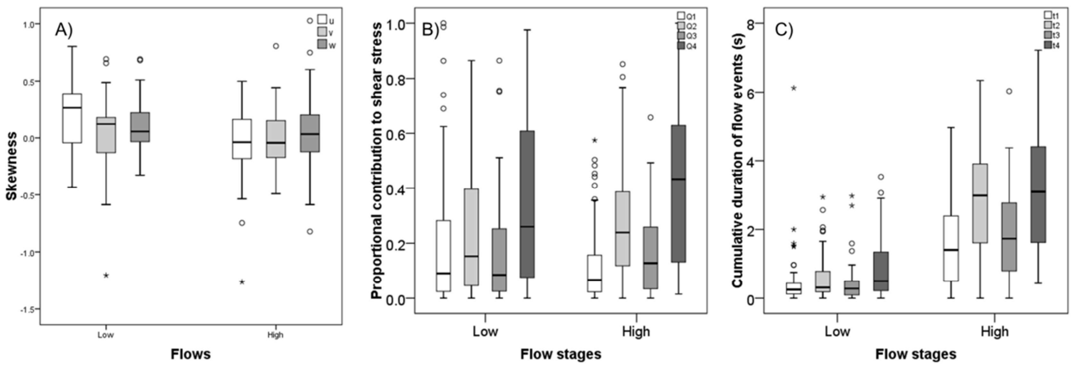

Figure 6.6 Distribution of skewness of turbulent residuals (A), magnitude (B) and cumulative duration (C) of flow structures.

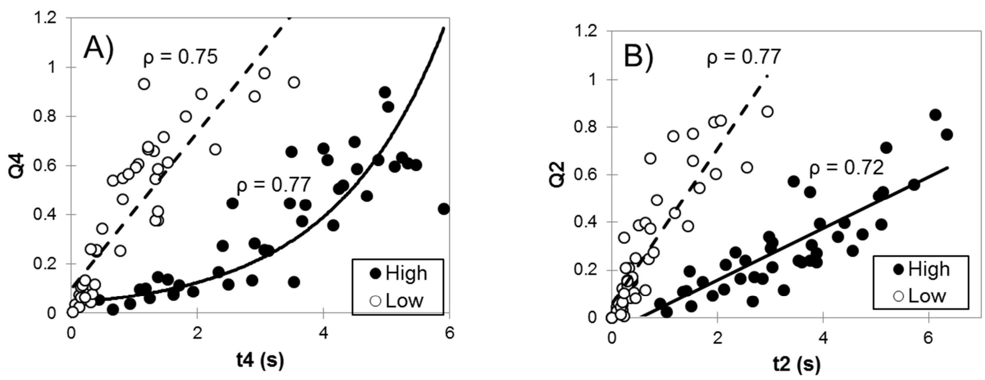

Figure 6.7 Scatter plots of cumulative duration and contribution to shear stress for inrushes (A) and ejections (B).

Figure 6.8 presents key turbulence parameters describing the scale of flow structures (length and diameter) and the eddy length:fish length and eddy momentum: fish momentum ratios. There is a pronounced reduction in the median and range of dominant eddy length on the u and w components, while less change was observed for the v component. There were no statistically significant differences for eddy diameter, but a decrease in size was noted with respect to increasing flow stage. The size of dominant eddy structures was significantly different between flow stages for u and w (Mann Whitney U: $p < 0.05$). Eddy scales become more similar across the three components at the higher flow stage, suggesting that eddy shape was more elongated at low flow.

Brown trout , *Salmo trutta*, body length ranges from 5 to 35 cm with a mean value of 16.1 cm while the critical swimming speed ranges between 81 and 135 cm s^{-1} (Peake, 2008). The fish momentum was therefore calculated using the formula 3.13 in Research Design Chapter with a fish length equal to 16.1 cm and the minimum swimming speed of 81 cm s^{-1}.

The observations of ratios between eddy and fish variables revealed values below 0.5 for the length scale ratio and below 0.15 for the momentum ratio with a few outliers above these thresholds but never equal to 1. This suggests that the flow structures would not adversely affect the representative species *Salmo trutta*.

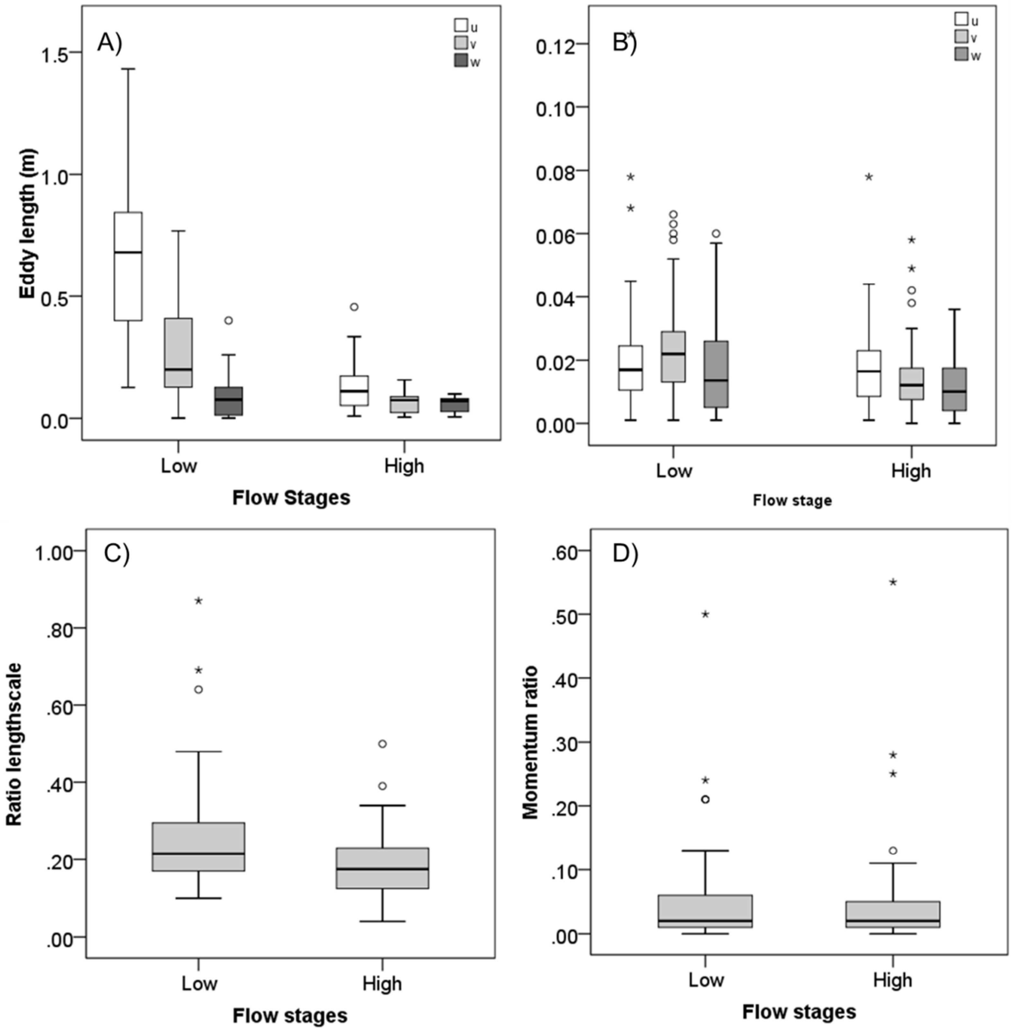

Figure 6.8 Distribution of eddy size (length (A) and diameter (B)) for the three components (u, v, w) and results of ratio length scale (C) and momentum (D) at low and high flow stages.

6.3.2 Spatial organisation of changes in turbulent properties with flow stage (high gradient reach)

Low and high flow data sets were standardized to generate z-scores, allowing the two sets of measurements to be combined into a single dataset. PCA was conducted using 11 dimensionless turbulence variables: turbulent kinetic energy (TKE), shear stress on uv and uw planes, flow structure (magnitude and duration) for Q2 and Q4 events and eddy period and length scale on u and w components. The first four principal components had eigenvalues above 1.6 and cumulatively explained 76% of the variability in the data set. The scree plot in Figure 6.9 revealed an inflection point after the 5th component but only the first four components were used for the investigation because the loadings for 5th component were weak compared to the other four and there was no clear physical explanation for this gradient in the data set. PC loadings were used to interpret the meaning of each principal component (Table 6.2).

PC1 defines a gradient of increasing turbulence intensity represented by turbulent kinetic energy and shear stress on the uv and uw planes. PC2 defines a gradient of increasing eddy scale on the u dimension and PC3 defines an orientation gradient of increasing in magnitude and duration for inrushes. PC4 reflects a gradient of eddy temporal and spatial scale on the vertical (w) component.

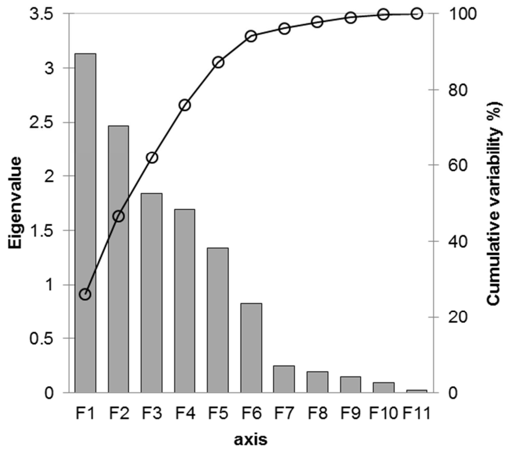

Figure 6.9 Scree plot for the global dataset of low and high flows.

Table 6.2 Summary of PC scores and identification of the turbulence variables reflect the first four principal components.

	PC1	PC2	PC3	PC4	PC5
	INTENSITY	SCALE (u)	ORIENTATION	SCALE (w)	-
TKE	0.474	0.131	-0.246	0.258	-0.288
u'v'	0.881	-0.071	-0.088	-0.072	-0.257
u'w'	0.899	-0.052	-0.101	0.018	-0.239
Q2	0.243	0.625	-0.189	0.110	-0.270
Q4	-0.126	-0.192	0.896	0.005	-0.323
t2	-0.072	0.796	-0.289	-0.042	-0.412
t4	-0.215	0.093	0.849	0.011	-0.435
ITSu	-0.245	0.781	0.083	0.024	0.019
ITSw	-0.014	-0.073	0.060	0.939	0.633
ILSu	0.419	0.630	0.372	0.059	-0.028
ILSw	0.053	0.244	-0.032	0.955	0.533

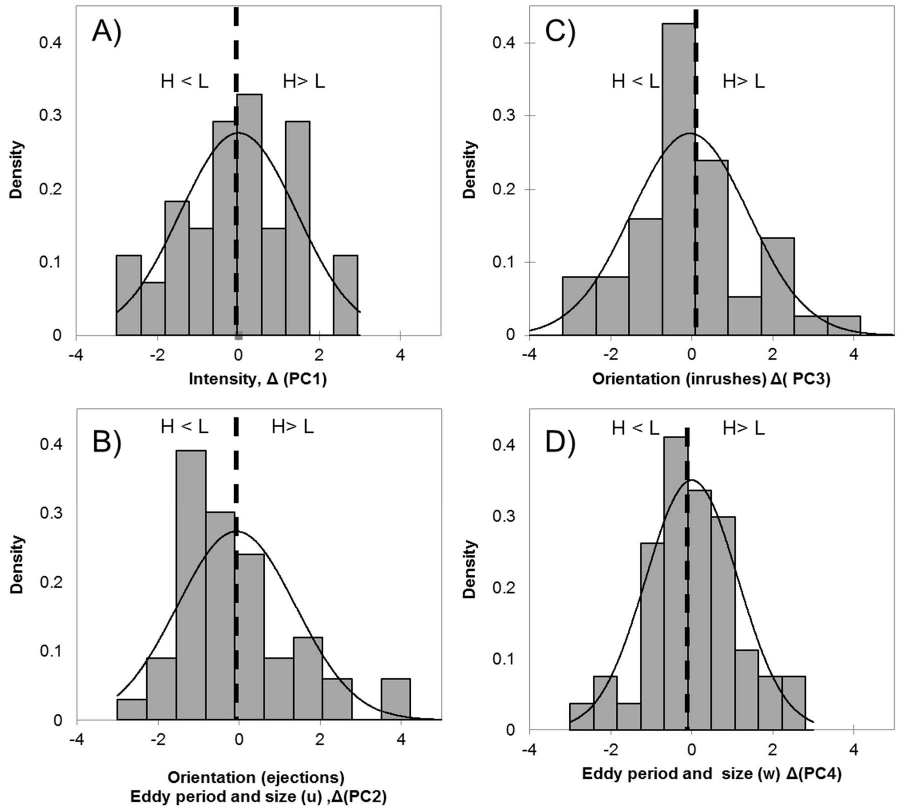

Figure 6.10 Frequency distribution of the variation of principal components from low (L) to high (H) flows.

Table 6.3 Statistical descriptors of delta of principal components.

Description	PCs	Median	Standard deviation	Skewness	Kurtosis
Intensity	PC1	0.02	1.44	-0.21	-0.49
Orientation (ejections) + eddy period and size u	PC2	-0.38	1.46	1.05	0.97
Orientation (inrushes)	PC3	-0.18	1.44	0.49	0.55
Eddy period and size w component	PC4	-0.02	1.10	0.02	0.18

The change in PC scores between low and high flow stage is expressed as a frequency distribution for each PC in Figure 6.10 with supporting descriptive statistics in Table 6.3. All four PCs show both positive and negative change for each of the PCs, with medians generally around zero. Skewness is most pronounced for PC2 (eddy magnitude, u), however, reflecting a reach-level reduction in the magnitude of flow structures on the u components. In contrast, for the remaining 3 PCs, levels of positive and negative change are more similar, indicating a combination of flow intensification/increasing flow structure size in some channel areas, and reductions in other areas.

Spatial organization of change in PC scores between flow stages is presented in Figure 6.11. Sample locations were separated into two groups depending on magnitude of change: (i) ‘high change’ showing those with a large amount of change (positive or negative), represented by sample locations falling above the 75^{th} or below the 25^{th} percentiles respectively; and (ii) ‘low change’ showing those with a smaller level of change (between 25^{th} and 75^{th} percentiles). For PC1 (intensity), substantial changes in intensity occurred over relatively large zones, but was not associated in particular with pool or step areas. In contrast, for PCs 2, 3 and 4 representing scale and orientation parameters, the spatial organisation of magnitude of change was more patchy indicating boulder-scale and pool margin effects. This may reflect the increasing flow depth and submergence of larger roughness elements at the higher flow stage which begin to interact with the flow.

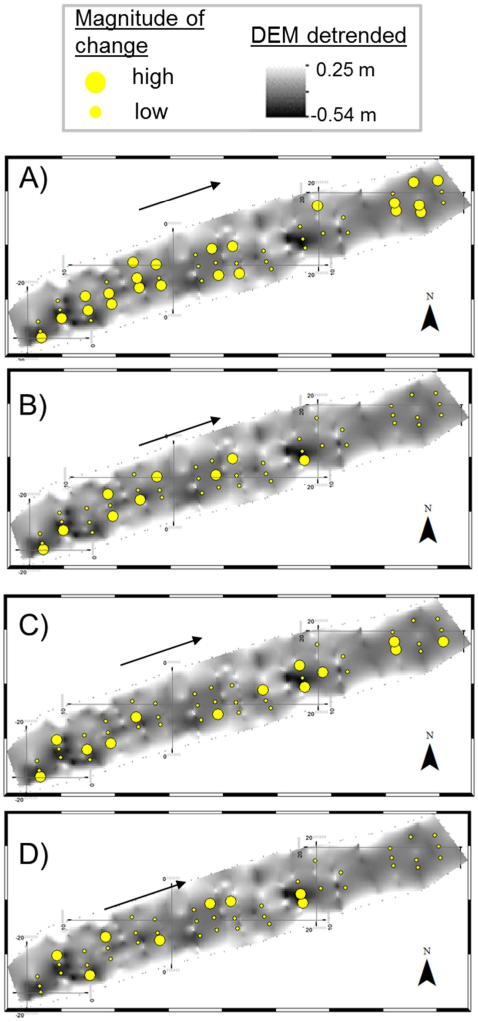

Figure 6.11 Spatial organization of delta of principal components classified by big yellow dots as delta above 25% and below 75% and small yellow dots as delta between 25 and 75%of turbulence changes. PC1 (A), PC2 (B), PC3(C) and PC4 (D).

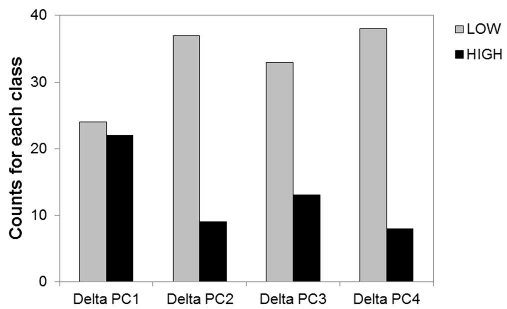

Figure 6.12 Bar chart for the number of measures classified as lower (between 25 and 75%) and /higher (below 25% and above 75%) of turbulent changes.

Experimental semivariograms for the principal components across the two flow stages are explored in Figure 6.13, together with the coefficients for modelled semivariograms in Table 6.4. The ranges, sills and nugget assist in the interpretation of spatial organisation of turbulence properties at the reach scale. The range represents the lag distance at which the semivariogram reaches the sill, and points at lag distances smaller than the range being most highly correlated. The sills is the level at which the semivariogram level off and the nugget describes the variability at lag distances smaller than the sampling spacing scale.

For PC1 (intensity) and PC3 (orientation (inrushes)), there is only a slight change in the sill with increasing flow stage. The range decreased at the higher stage for PC1 suggesting more uniform distribution of turbulent intensity across the reach, and it increased at the higher stage for PC3 indicating reduced correlation at shorter lag distances. For PCs 2 and 4, a greater different in the sill was observed across the two flow stages. For PC2 (eddy scale, u), the sill increased, indicating increased variability at the higher flow stage, while the reverse was true for PC4 (eddy scale, w).

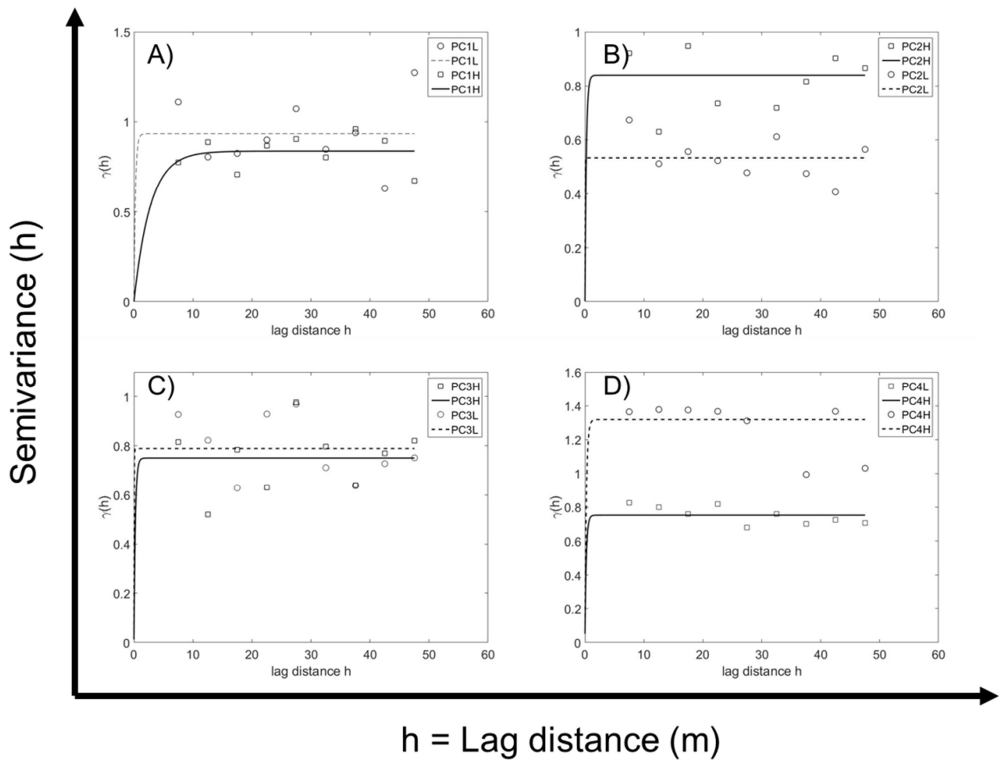

Figure 6.13 Semivariance of PC changes across the two flow stages: PC1 (A), PC2 (B), PC3 (C) and PC4 (D). Dotted line and squares are the condition at high flow stage.

Table 6.4 Parameters for the semivariogram model for the turbulent variation across the two flow stages.

	Low Flow			High Flow		
	Range	Sill	Nugget	Range	Sill	Nugget
Intensity (PC1)	2.75	0.93	0.2^{-6}	0.24	0.83	0.5^{-4}
Orientation (ejections) and period and scale eddy (u) (PC2)	0.048	0.52	0.1^{-4}	0.22	0.83	1.6^{-4}
Orientation (inrushes) (PC3)	0.03	0.77	0.02	0.23	0.73	0.01
Eddy period and length scale (w) (PC4)	0.24	1.25	0.06	0.23	0.23	0.05

6.3.3 Influence of aquatic vegetation growth on changes in turbulence properties (low gradient reach)

Table 6.1 compares also the roughness by the Manning equation for the two vegetated periods exhibiting two significantly different values. As expected, the peaked vegetation period showed highest value compared with the die back season due to the presence of aquatic plants that increase the flow resistance. This result reflect the effects of vegetation on flow discharge and explaining the difference in flow velocity and stage for the two seasons and allows comparison between the two datasets. Figure 6.14 illustrates the overall changes in velocity and depth throughout the low gradient reach associated with the change in vegetation cover (vegetated, V; minimal vegetation, NV). Water depths are higher and more variable in the NV period, although this may partly reflect the slightly higher flow stage (80% compared to 95% exceedance). Mean velocities in the u and v dimensions reduced with increasing in vegetation cover and became less variable for the u component, while a more subtle increase in values was observed for the v component. For the w component, the V period was associated with positive values, and the NV period with negative values indicating a change from predominantly downwelling to predominantly upwelling flow.

The absolute and relative intensity, together with the shear stress and turbulent kinetic energy for the die back and peak vegetation cover periods are presented in Figure 6.15. Median values were higher in the vegetated period for absolute and relative intensity (u component) together with TKE and shear stress on uv plane and variability was also higher. Differences between vegetated and unvegetated periods for these variables were statistically significant (Mann Whitney U: $p<0.001$). In contrast, absolute turbulence intensity on the vertical (w) component and the shear stress on vw and uw planes were higher during the un-vegetated period (Mann-Whitney $p < 0.001$).

Figure 6.16 explores relationships between RMSu, RMSw and TKE. A positive linear relationship was observed between RMSu and RMSw for the unvegetated period (Spearman, ρ =0.76), while in contrast, for the vegetated period there was no clear trend (Figure 6.16 A). The relations between RMSu and TKE revealed a strong positive correlation for both unvegetated and vegetated periods (Spearman, ρ = 0.88 and 0.74, respectively).

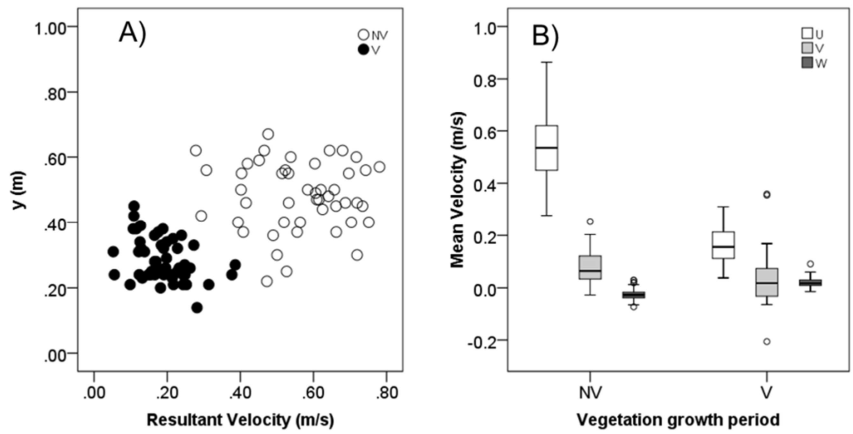

Figure 6.14 Scatter plots of the resultant velocity and water depth grouped by two different seasonal period (A) and the distribution of average velocity in u, v and w directions (B). NV = minimal vegetation, V= vegetation.

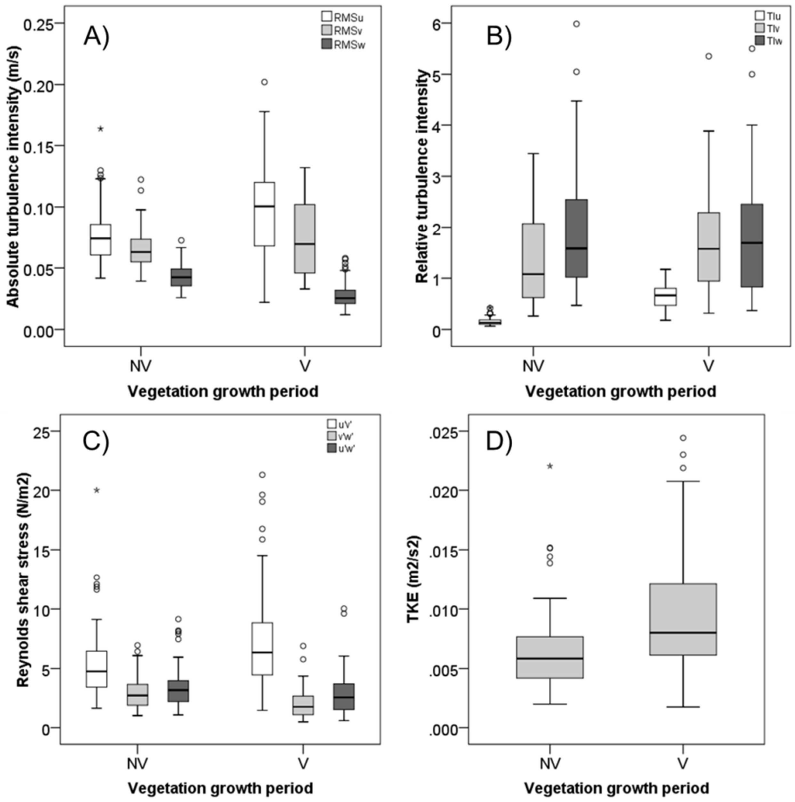

Figure 6.15 Comparison of the distribution of absolute (A), relative (B) turbulence intensity together to shear stresses on uv, vw and uw planes (C) and turbulent kinetic energy (D) across die back (NV) and peak (V) vegetation growth periods.

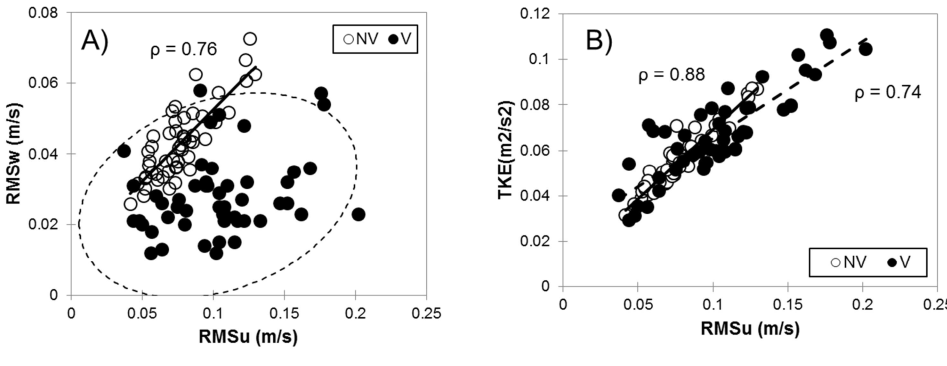

Figure 6.16 Bivariate plots of fluctuations on streamwise (u) and vertical (w) (A) components and also turbulent kinetic energy (B) across peak (V) and die back vegetation growth (NV) periods.

The predictability and periodicity of velocity of time series are presented in Figure 6.17, Figure 6.18 and Figure 6.19. Kurtosis values were strongly positive for both datasets. Median values were similar along the streamwise (u) and vertical (w) components for vegetated and unvegetated periods but the range of kurtosis values was greater for the vegetated period greater spatial variation in the form of frequency distributions of turbulent residuals (Figure 6.17 A). All time series met the condition for pseudo-periodicity for the unvegetated period, while a number of time series for the vegetated period did not meet the condition for pseudo-periodicity, indicating a less predictable flow structure under the vegetated scenario.

The time scale (period) of the dominant eddy as derived from autoregressive modelling was considerably higher for the unvegetated period compared to the vegetated period. Mann Whitney U tests revealed statistically significant differences between vegetated and unvegetated scenarios for kurtosis (u component) and integral time scale for all three components. Results of Wavelet analysis are presented in Figure 6.18 showing (a) the raw u time series, (b) the Wavelet power spectra showing the correlation between the raw time series and different temporal length scales of the wavelet across the length of the time series, (c) the global wavelet spectra, showing the presence of significant periods in the record and (d) the variance of the dominant period through time. The peak plant cover exhibited greater variability in period compared to the minimum plant cover, indicating an increase in spatial heterogeneity in the dominant wavelet period with increasing vegetation cover (Figure 6.19). There was an increase in number of peaks for dominant period with increasing vegetation cover. For unvegetated period, single and double peaks were observed in 82% of time series while multiple (>2) peaks in 17%. A reversal trend with higher number of multiple peaks (57%) and less single/double (43%) peaks was noted for the vegetated period suggesting more complex flow period with higher vegetation period.

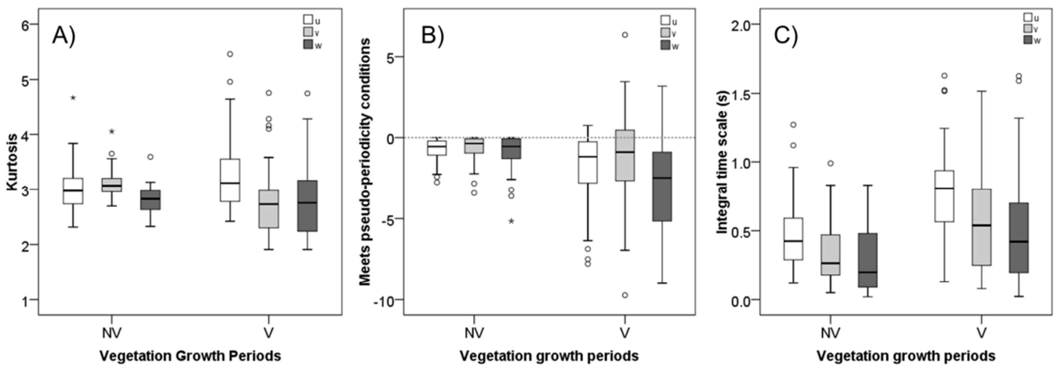

Figure 6.17 The distributions of predictability and periodicity described by kurtosis (A), the condition of pseudo-periodicity (B), the integral time scale (C) across die back (NV) and peak (V) vegetation growth periods.

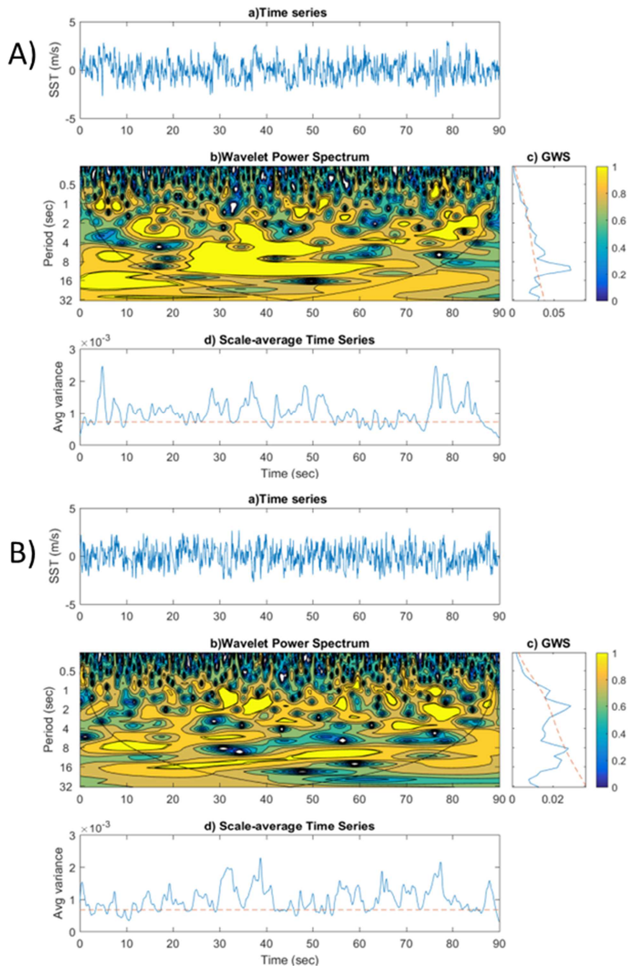

Figure 6.18 Example of Wavelet spectra for unvegetated (A) and vegetated (B) periods showing: a) the original (u) time series (sst); b) Wavelet power spectrum (dotted black line shows influence cone that reflects the significance level and confidence for the wavelet spectra indicating the disturbed areas/error); c) global wavelet spectrum; and d) the variance explained by the dominant wavelet period through the time series.

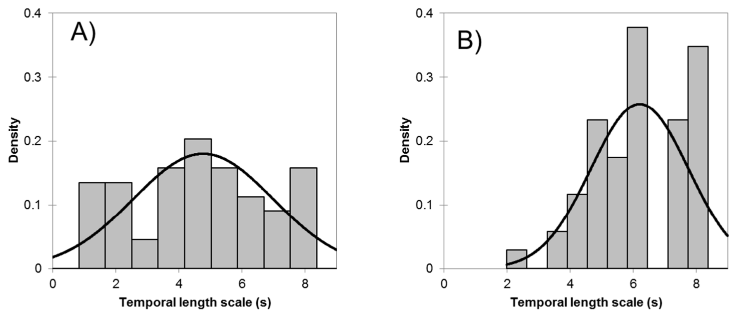

Figure 6.19 Frequency distribution of dominant temporal length scale extracted by Wavelet spectra for the unvegetated (A) and vegetated (B) periods.

Orientation parameters (skewness of velocity time series, and the stress contribution and duration of turbulent event types) are explored in Figure 6.20 (A, B and C). Skewness values ranged from positive to negative for both unvegetated and vegetated periods for all three components, indicating a combination of series with a small proportion of relatively lower magnitude fluctuations (u, v) (skewness < 0) and series with a small proportion of relatively higher magnitude fluctuations (w) (skewness > 0). There was an increase in skewness values, towards more positive values for the vegetated period, while in contrast skewness decreased (towards more negative values) for the w component. Differences between the groups (vegetated/ unvegetated) were statistically significant for skewness on both u and w components (Mann Whitney U: $p < 0.05$). There were also differences in the magnitude and duration of different event types between the two vegetation periods. For the unvegetated period, Q4 events (inrushes) are dominant, with smaller and more equal contributions from Q2 and Q3 events, while for the vegetated period, ejections (Q2) and inrushes (Q4) were dominant in terms of both stress contributions and cumulative duration.

Bivariate plots of magnitude and duration of inrushes and ejections are shown in Figure 6.21. For minimum vegetation cover, the relationship between duration and magnitude of inrushes was non-linear (Q4; Spearman ρ: 0.87, $p < 0.0001$) while a linear relationship was observed for ejections (Q2; Spearman ρ: 0.84, $p < 0.0001$). For peak vegetation cover relationships between magnitude and duration of inrushes and ejections were weaker (Spearman: $\rho < 0.67$).

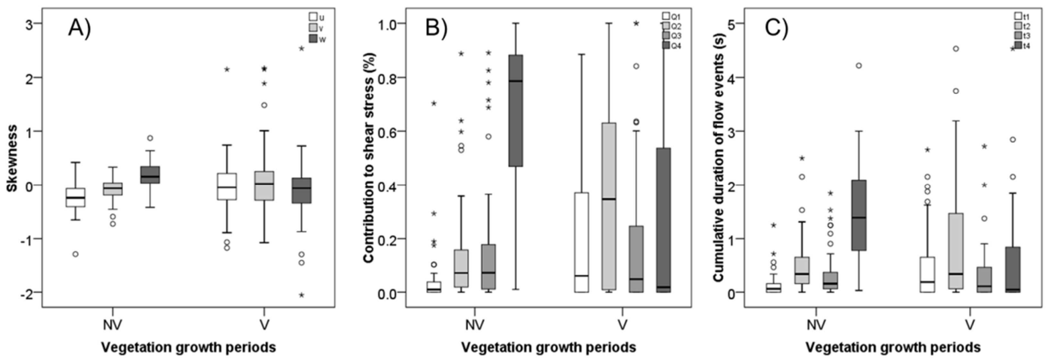

Figure 6.20 Distribution of skewness (A), magnitude (B) and cumulative duration of flow structures (C) for the unvegetated (NV) and vegetated (V) growth periods.

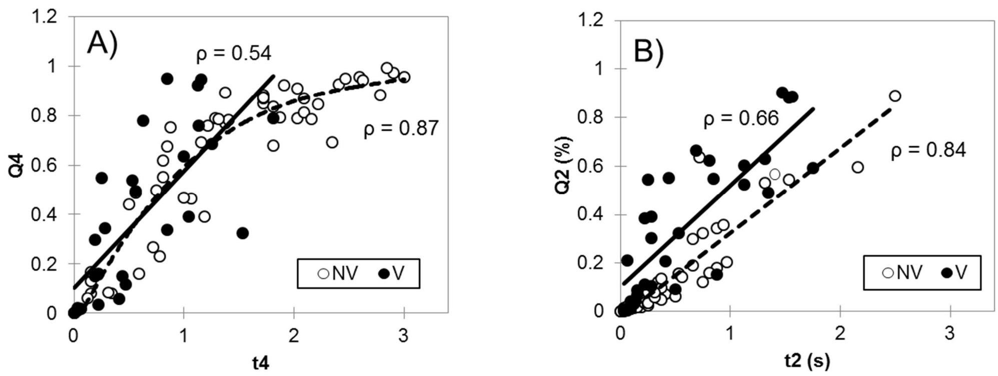

Figure 6.21 Bivariate plots of the magnitude and cumulative duration for inrushes (Q4) and ejections (Q2) across peak (V) and die back vegetation growth(NV) periods.

Dimensions of the dominant eddy structure (length and diameter) derived from u, v and w components are presented in Figure 6.22 (A, B). The range of eddy sizes (length and diameter) decreased (v and w directions) when vegetation cover was higher, and there was a reduction in the variability of eddy sizes throughout the reach. Mann Whitney tests showed significant differences for eddy size on the v and w components for eddy length ($p < 0.0001$) and on all the three components for eddy diameter ($p < 0.005$).

Brown trout, *Salmo trutta*, body length ranges from 8 to 28 cm with a mean value of 15 cm while the critical swimming speed ranges between 81 and 135 cms^{-1} (Environment Agency, 2010b). The fish momentum was therefore calculated using the formula 3.13 in Research Design Chapter with a fish length equal to 15 cm and the minimum swimming speed of 81 cm s^{-1}.

The results of length scale and momentum ratios between eddy and fish sizes are explored in Figure 6.22 (C, D). Higher median values for both parameters were observed for the unvegetated period with a small number of sample locations with values equal to 1. For the peak vegetation period median values were below 0.30 for length scale ratio and below 0.15 for momentum ratios indicating higher length/momentum values for fish compared with eddy. Ratios were significantly different between the two vegetation periods (Mann Whitney: $p < 0.05$). The upper quartile shows values above 1 for both size and momentum ratios for the die-back vegetation season suggesting greater similarity in eddy and fish size that could destabilize the control systems of fish.

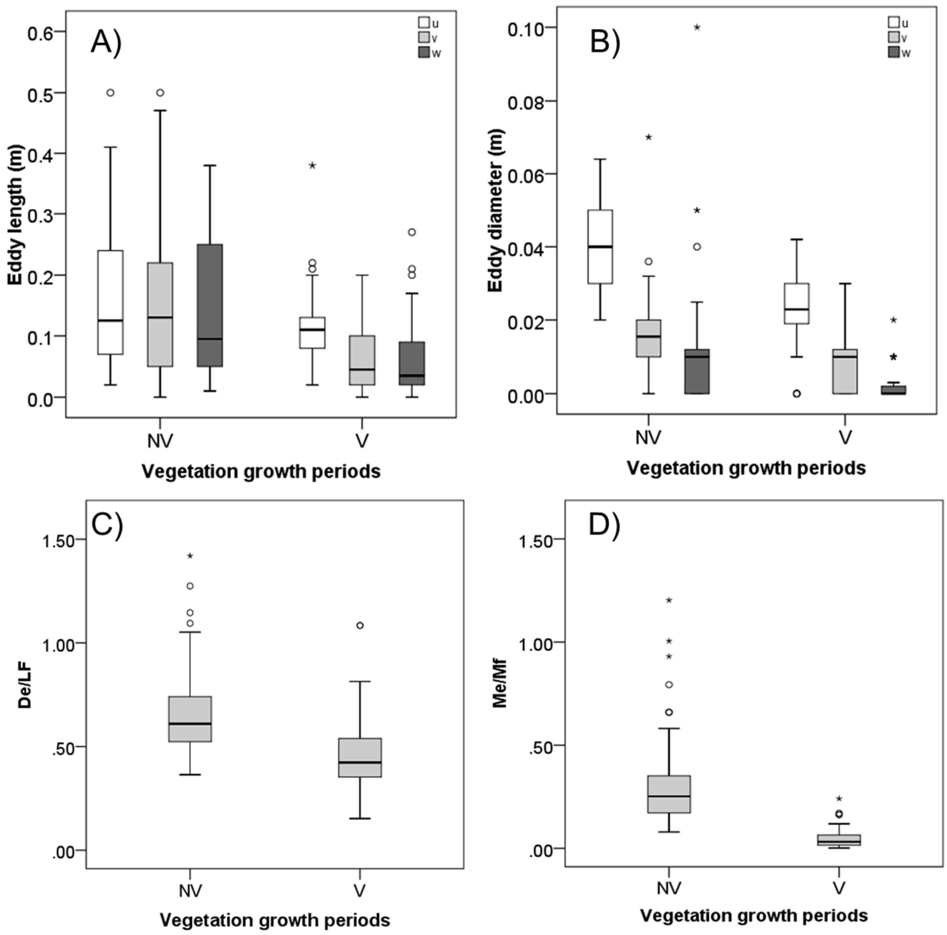

Figure 6.22 Distribution of eddy size (length (A) and diameter (B)) for the three components (u, v, w) and results of ratio length scale (C) and momentum (D) across the minimal vegetation cover (NV) and peak cover (V) periods.

6.3.4 Spatial organisation of changes in turbulent properties with vegetation growth (low gradient reach)

Spatial organisation of changes in turbulent properties with vegetation cover were assessed by standardising the unvegetated and vegetated data sets for the low gradient reach using z-scores to create one global dataset. PCA was conducted using 11 turbulent dimensionless variables: turbulent kinetic energy (TKE), shear stress on uv and uw planes, magnitude and duration of Q2 (ejections) and Q4 (inrushes) events and eddy period and length scale. (Barlett test's: $chi^2_{critical} = 84.82$, $p < 0.001$). The first four principal components had eigenvalues above 1.5 and cumulatively explained the 86% of variability in the data. The scree plot in Figure 6.23 revealed an inflection after the 4th component and the first four components were therefore retained for further investigation. PC loadings were used to interpret the meaning of each principal component (Table 6.5). PC1 defines a gradient of increasing magnitude and duration for ejections and inrushes, while PC2 represents a gradient of increasing turbulent kinetic energy and shear stress on uv and uw planes. PC3 and PC4 define gradients of eddy scale relating to the w and u components respectively.

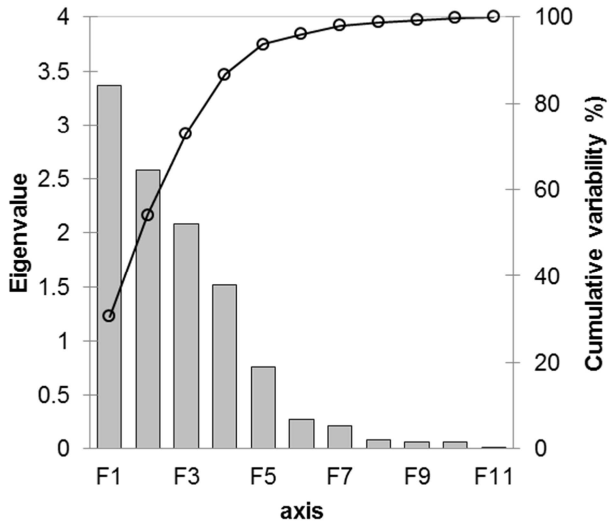

Figure 6.23 Scree plot for the global dataset across the two seasonal periods.

Table 6.5 Factor loadings of PC analysis with global datasets across the two seasonal periods and description of which turbulence variables reflect the PCs.

	PC1	PC2	PC3	PC4
	ORIENTATION	INTENSITY	SCALE w	SCALE u
TKE	0.002	0.921	0.002	0.012
u’v’	0.002	0.901	0.002	0.002
u’w’	0.001	0.809	0.005	0.003
Q2	0.881	0.008	0.012	0.000
Q4	0.480	0.004	0.006	0.378
t2	0.785	0.013	0.006	0.033
t4	0.414	0.008	0.004	0.319
ITSu	0.001	0.015	0.003	0.745
ITSw	0.005	0.004	0.949	0.016
ILSu	0.002	0.000	0.152	0.661
ILSw	0.003	0.006	0.954	0.012

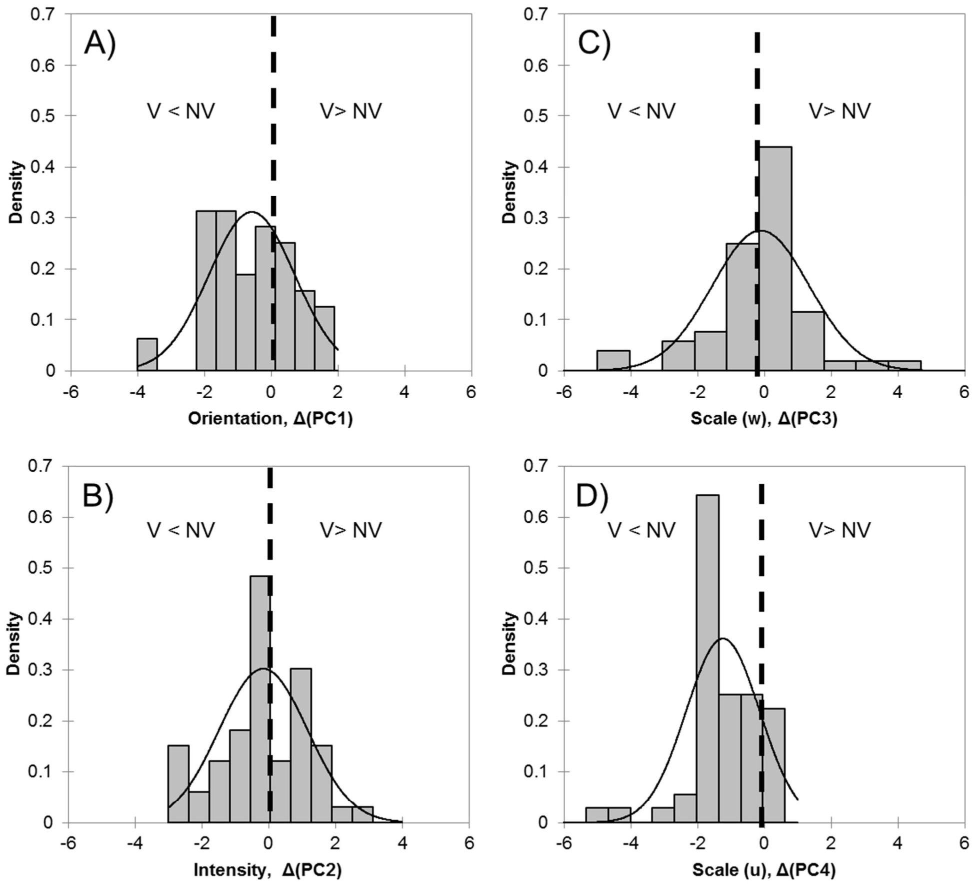

Figure 6.24 Frequency distribution of variation of principal components across the two seasonal periods.

Table 6.6 Statistical descriptors of principal components.

Name PCs	PCs	Median	Standard deviation	Skewness	Kurtosis
Orientation	PC1	-0.50	1.28	-0.23	-0.38
Intensity	PC2	-0.21	1.32	-0.07	-0.37
Scale w	PC3	0.05	1.45	-0.19	2.93
Scale u	PC4	-1.44	1.10	-0.88	2.18

The change in PC scores between the two vegetation periods can be expressed as a frequency distribution with associated descriptive statistics (Figure 6.24 and Table 6.6). PC1 (orientation) has a broad distribution, with values either side of zero indicating increases and decreases occur in the magnitude and duration of inrushes and ejections at different locations within the reach in association with vegetation growth. A negative skewness indicates greater frequency of negative change (smaller magnitude-duration events) for the unvegetated scenario. PC2 had lower skewness, with a large proportion of values around zero indicating minimal change in intensity with vegetation cover. PC3 (eddy scale, w) the majority of values were close to zero, while for eddy scale (u) (PC4), the vast majority of values are below zero suggesting that eddy size in the u dimension decreases throughout the reach when vegetation is present.

The spatial variation in turbulence properties across the reach is explored in Figure 6.25 highlighting two groups defined by the level of turbulence changes: (i) ‘high change’ identifying those with a large amount of changes by sample locations falling above the 75th or below the 25th percentiles respectively; and (ii) ‘low change’ showing those with a smaller level of change (between 25th and 75th percentiles). By observing the bar charts of turbulent changes (Figure 6.26), a large number of sample locations revealed low degrees of change for PCs 2, 3 and 4, while a relatively large proportion of the reach experienced more extreme change (positive or negative) for PC1.

The spatial organisation of change in PC scores is explored in Figure 6.25. The largest magnitude change (either positive or negative) is associated with the orientation (PC1), intensity (PC2) and eddy scale on u component (PC4) gradients.

Lower magnitude change throughout the reach was noted for eddy scale on the w component (PC3). For PCs 1, 2 and 4, there is a tendency for the higher magnitude change to be associated with areas around vegetation stands, although vegetation is relatively ubiquitous throughout the reach meaning it is difficult to identify more detailed patterns.

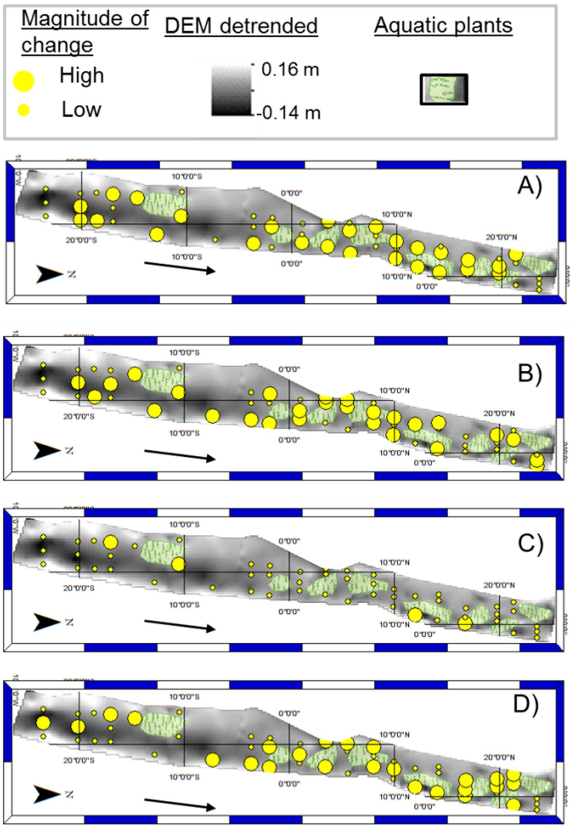

Figure 6.25 Spatial organization of delta of principal components classified by big yellow dots as the high class and small yellow dots as the low class of turbulence changes.

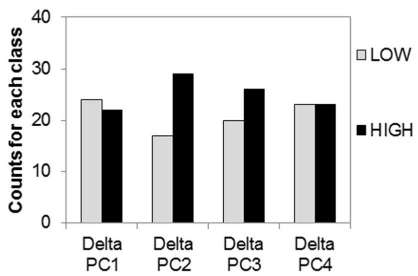

Figure 6.26 Bar charts of the two groups showing the lower and higher turbulent changes.

Semivariograms for each of the four PCs for the unvegetated and vegetated period are presented in Figure 6.27, and the coefficients of modelled semivariograms are presented in Table 6.7. Both unvegetated and vegetated semivariograms were fitted with an exponential model describing linearly the behaviour close to the origin and reflecting the high level of variability in a short range. Levels of semivariance were lower overall for the die back vegetation period, indicating more uniform spatial variation across the reach in the absence of vegetation.

Semivariograms for PC1 (orientation) revealed a pronounced increase in the sill for the vegetated period, indicating overall higher levels of spatial variation. Also, the range increased from 10.60 to 15.79 indicating lower spatial correlation for vegetation period. The nugget was small for both vegetation cover periods. Semivariograms for PC2 (intensity) presented higher values in variance shown by the sill and a longer range for peaked vegetation period, indicating a higher spatial correlation. For both vegetation periods, the nugget was around zero. The variogram for PC3 (eddy scale, w) revealed an increase in the sill for peak vegetation cover, indicating an increase of levels of spatial variation and showed a pronounced decrease in the range from 19.97 to 3.68. The nugget values were greater for the vegetated period compared to the unvegetated period reflecting the increased variation at smaller spatial scales. For PC4 (eddy scale, u), the peak vegetation growth period had a lower sill (variance) and larger range, indicating that higher spatial correlation. The shape of the variogram also differs between periods, with a linear trend for the unvegetated period indicating an continual increase in semivariance with distance. In contrast the vegetation period is characterised by the more common S-shaped curve with a pronounced sill. The nugget effect due to measurement errors or spatial sources of variation at smaller scale was observed in both periods.

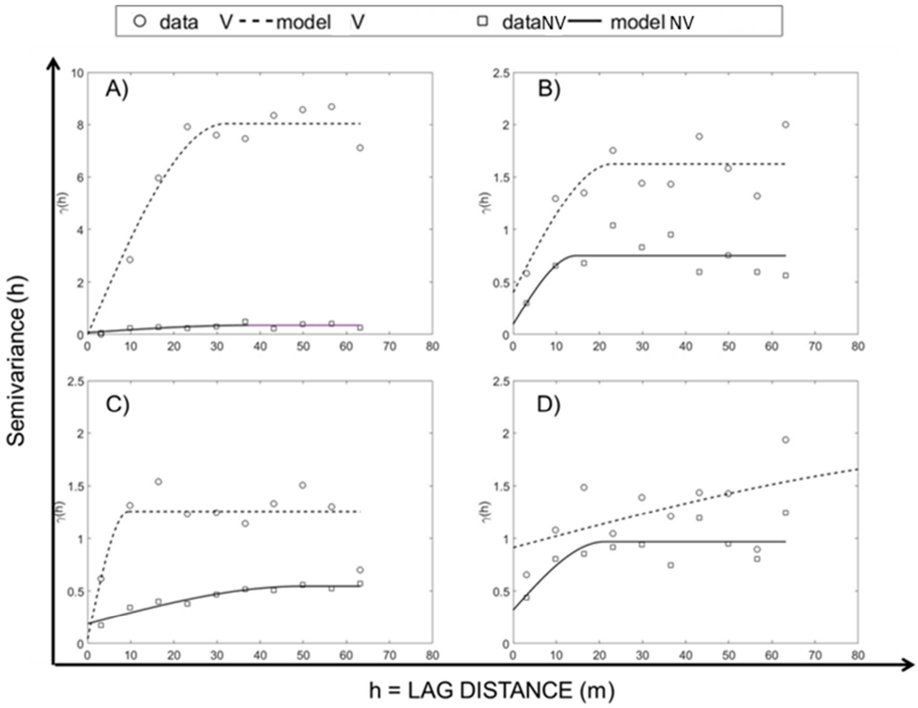

Figure 6.27 Semivariograms for PC changes: flow orientation (PC1) (A), intensity (PC2) (B), eddy period and length on vertical (w) (PC3) (C) and streamwise (u) PC4 (D) components during the unvegetated (NV) (black line and black squares) and peaked vegetation (V) (dotted line and black circle) seasons.

Table 6.7 Parameters for the semivariogram model for the turbulent variation across the two flow stages.

	Die back vegetation			Peak vegetation		
	Range	Sill	Nugget	Range	Sill	Nugget
Orientation (PC1)	10.60	0.34	4.5^{-4}	15.79	8.61	6.2^{-6}
Intensity (PC2)	5.10	0.75	6.6^{-4}	7.14	1.60	0.1
Scale eddy (w) (PC3)	19.97	0.44	0.2	3.68	1.26	0.4
Scale eddy (u) (PC4)	9.25	0.76	0.3	6.46	1.14	0.2

6.4 Discussion

6.4.1 Effects of increased flow stage on turbulent properties (high gradient reach)

The statistical analysis of hydraulic properties across the entire reach for two flow stages provided insights into changes in turbulence in relation to the flow stage in a high gradient reach. As expected, the water depth and mean velocity increased throughout the reach as observed in other step-pool reaches (Wohl and Thompson, 2000), but more complex changes were observed in the IPOS variables identified by Lacey *et al.*, (2012). Changes by IPOS category (intensity, predictability, orientation and scale) are summarised in Table 6.8 and discussed below.

The higher flow stage was associated with increased intensity in some variables (e.g. TKE and shear stress on vw and uw planes) but no statistically significant differences were identified between flow stages. This finding is consistent with previous studies that did not identify significant differences in turbulent fluctuations on the streamwise, vertical and lateral velocity components between flow stages (Wilcox and Wohl, 2007; Chin and Wohl, 2005) and suggest that while discharge influences mean velocities turbulent fluctuations can remain relatively constant (Chin, 2003).

For predictability, the simpler kurtosis metric based on the frequency distribution of the turbulent residuals indicated a more predictable flow structure, but in contrast the majority of time series for both flow stages failed to satisfy the criteria for pseudo-periodicity. The analysis of wavelet power spectra revealed that the dominant wavelet period increased from low to high flow stages. This suggests longer period structures at the higher flow, reflecting the proportionality between the evolution of flow structures and flow velocity (Hardy *et al.*, 2009). However, qualitative analysis indicated that some time series were characterised by multiple peaks in global wavelet spectra and hence a more complex flow structure and these largely related to high flow stage.

For orientation, proportional contributions to the shear stress from the four event types were similar across flow stages, while the cumulative duration of events increased significantly for the higher flow stage. Thus, longer-duration and lower magnitude events became more significant at the higher flow stage indicating the four quadrant events had equal role in the shear stress process without reflecting ejections/inrushes model (MacVicar and Roy, 2007b; Wilkes, 2014), in contrast to the low flow condition.

For the scale variables, there was an overall reduction in the median and range of eddy dimensions across the three velocity components and additionally dimensions became more similar across the three components as water depth increased. Results of dimensionless ratios used to estimate the influence of turbulent flow structures on fish revealed values that were consistently either greater than or less than 1 indicating minimal impacts on their body stability and locomotion. Values around 1 (i.e. when flow structure size is approximately equal to fish size) have been shown to have the most adverse impacts on fish stability and trajectory (Tritico and Cotel, 2010; Cotel and Webb, 2015). Interpretation of both ratios, however, should be cautious since fish properties (length and swimming speed) were applied from previous studies and was not based on fish measurements undertaken at the field site.

6.4.2 Spatial organisation of changes in turbulent properties with flow stage (high gradient reach)

The PCA analysis revealed gradients that largely correspond with three IPOS categories: intensity, eddy scale (u), orientation and eddy scale (w). The majority of predictability variables had to be removed so that the PCA met the key statistical assumptions of the analysis technique, and therefore were not fully represented in this multivariate analysis. The change in PC scores between low and high flow was explored visually, revealing high magnitude changes (either positive or negative change) throughout the reach for intensity in contrast to small patches of high magnitude changes in the scale and orientation PCs. For scale and orientation, the spatial organisation of high magnitude change suggests that individual roughness elements such as boulders, as well as roughness at pool margins drove the highest magnitude changes in scale and orientation of flow structures. This is interpreted to reflect increasing flow depth and submergence of larger roughness elements such as the largest clasts/step features at the higher flow stage. These features would then be able to interact with the flow and generate local changes in eddy size (Lamarre and Roy, 2005) and turbulence generation through vortex shedding (Roy *et al.,* 1999).

Semivariograms revealed reduced sills (overall variance) for the higher flow stage for intensity, orientation and scale (w), although this was much more pronounced for the scale (w) gradient. This indicates greater spatial similarity in flow properties at the higher flow stage, consistent with observations of overall increases in homogeneity reflecting gross morphology with increasing discharge (Lamarre and Roy, 2005; Legleiter *et al.*, 2007; David *et al.*, 2013). In contrast the sill for the scale (u) gradient increased with flow stage, indicating reduced spatial correlation in eddy scale at the higher flow stage which may reflect the boulder-scale influences discussed above. In addition, these findings may reflect the relationship between intensity and shear layer (Clifford, 1997) highlighting the explicit influence of boundary profiles.

6.4.3 Influence of aquatic vegetation growth on changes in turbulence properties (low gradient reach) and spatial organization

The statistical analysis of hydraulic properties across the entire reach for two flow seasonal periods provided insights into changes in turbulence in relation to the increasing vegetation cover in a low gradient reach. Changes by IPOS category (intensity, predictability, orientation and scale) are summarised in Table 6.9 and discussed below.

For intensity parameters, some metrics showed statistically significant increases in intensity with increasing vegetation cover (e.g. TKE, u'v') while others showed statistically significant decreases in intensity with increasing vegetation cover (e.g. RMSw, v'w', u'w'). This may partly reflects more powerful longitudinal and lateral fluctuations compared with vertical motions and increasing spatial diversity around the vegetated patches. The highest overall intensity areas were found at the centre of vegetation patches, higher lateral intensities at the transitional regions and lower values at the end of the patches (Devi and Kumar, 2016). This may facilitate transfer of sediment and nutrients laterally within the channel (Nepf, 1999; Finnigan, 2000). Vegetation dissipates flow energy reducing flow momentum on the vw and uw planes (Ortiz *et al*., 2013), however the u'v' shows higher median values compared with unvegetated period. This may due to the presence of dense vegetation and detailed spatial patterns above individual stands cannot be assessed.

For predictability, the peak vegetation period was associated with greater spatial variability in kurtosis values, and an increased incidence of time series that did not meet the condition for pseudo-periodicity. Wavelet analysis revealed increased variation in the dominant wavelet period for the peak vegetation cover period. Together, these findings suggest greater heterogeneity in predictability of flow with vegetation growth. This may reflect the continuous natural movement of plants that does not generate semi-periodic flow oscillations (Cameron *et al*., 2013). However, qualitative analysis indicated that some time series were characterised by multiple peaks in global wavelet spectra and hence a more complex flow structure and these largely related to higher vegetation cover.

For orientation, the no vegetation period was characterised by a higher proportional contribution from inrushes, with lower magnitude contributions from ejections and outwards (Q3) events. In contrast, the peak vegetation period was characterised by more equal contributions from ejections and inrushes that dominate momentum and kinetic energy transfers providing enhanced resuspension and sediment transport (Raupach *et al*., 1996). The range of eddy sizes decreased with increasing vegetation cover, as well as the absolute dimensions for the majority of length and diameter metrics with the exception of length scale on the u component. This is consistent with the known role of macrophytes in breaking down eddy sizes (Nepf, 2012). For all sample locations under the vegetated scenario, eddy scale: fish scale ratios were considerably less than 1, while for the unvegetated period a number of locations were associated with ratios around 1. As noted above, values around 1 (i.e. when flow structure size is approximately equal to fish size) have been shown to have the most adverse impacts on fish stability and locomotion, and these appear reduced during the vegetated period indicating a potential beneficial habitat impact during the spring/ summer period that may be relevant for juvenile growth and survival (Environment Agency, 2010a). This may represent an additional improvement to habitat diversity generated by aquatic plants (Kemp *et al.*, 2000; Champion and Tanner, 2000).

6.4.4 Spatial organisation of changes in turbulent properties with vegetation growth (low gradient reach)

The PCA analysis revealed gradients that largely correspond with three IPOS categories: orientation, intensity, scale (w) and scale (u). The majority of predictability variables had to be removed so that the PCA met the key statistical assumptions of the analysis technique, and therefore were not fully represented in this multivariate analysis. The change in PC scores between the unvegetated and vegetated periods was explored visually and indicated higher magnitude change in areas around the vegetation patches for the orientation, intensity and scale (u) gradients. In contrast there was lower magnitude change throughout the reach for scale (w). Since most of the reach was vegetated, detailed spatial patterns around individual stands cannot be assessed, but semivariograms indicated increased overall variance for all PCs for the vegetated period indicating higher spatial variation when vegetation is present.

Table 6.8 Summary of the variations of hydraulic parameters with increasing flow stage for the high gradient river.* denotes the significant differences between the two flow stages (Mann Whitney $p < 0.001$).

Depth, velocity and Froude number	Turbulent intensity	Predictability and periodicity	Orientation	Scale
↑ y ↑ U	↑ TKE ↑ u'w'; ↑ v'w'	↑ Kurtosis* ↓ Pseudo-periodicity	↑ (t) all four event types* ↓Skewness(*u,v)	↓eddy length*

Table 6.9 Summary of the variations of hydraulic parameters with increasing vegetation cover for the low gradient reach. * denotes the significant differences between the two vegetation periods (Mann Whitney $p < 0.001$).

Depth, velocity and Froude number	Turbulent intensity	Predictability and periodicity	Orientation	Scale
↓ y ↓ U,V ↑ W	↑ RMSu*,↑TKE* ↓ RMSw* ↑ u'v'* ↓ u'w'*; ↓ v'w'*	↑ Kurtosis*(u) ↓Kurtosis*(v,w) ↓ Pseudo-periodicity	↑ (% and t) ejections (Q2) ↑skewness (u)* ↓skewness (w)*	↓ eddy length (v,w)*

CHAPTER 7: Interactions between turbulence and wood habitat features, and implications for fish habitat use

7.1 Introduction

Plants, including trees and associated wood features, play a crucial ecosystem engineering role in river systems, altering geomorphological and hydraulic processes (Gurnell, 2014; Comiti *et al.*, 2016) and providing a diverse range of habitat functions (Bisson *et al.*, 1987; Manners *et al.*, 2007; Hrodey *et al.*, 2008; Pilotto *et al.*, 2014). Instream wood features can influence stream morphology (Comiti *et al.*, 2006), increase the frequency of pools (Gurnell and Sweet, 1998) and increase pool area (Lisle, 1995) as well as altering local hydraulics (Smith *et al.*, 1993; Wallerstein *et al.*, 2002). As a result of these and other functions (e.g. provision of food resources and shelter from predation), wood can contribute to the initiation and maintenance of habitats suitable for a diverse range of organisms, and enhance river habitat diversity (Abbe and Montgomery, 1996).

Previous studies have included exploration of flow hydraulics around single pieces of wood (Gippel, 1995) and wood accumulations (Manners *et al.*, 2007); the effects of wood-induced erosion and deposition on channel morphology (Abbe and Montgomery, 1996; Montgomery *et al.*, 2003); and the provision of suitable habitat for aquatic organisms, in particular fish (Zika and Peter, 2002; Rifflart *et al.*, 2009) and macroinvertebrates (Schneider and Winemiller, 2008; Pilotto *et al.*, 2014).

Reintroducing wood as part of sustainable river restoration design can help to improve physical habitat and support ecological improvements (Abbe *et al.*, 2003; Bernhardt *et al.*, 2005; RRC, 2013). For instance, large wood can provide flow refugia and food sources for aquatic communities, minimise energy expenditure, reduce exposure to predation and increase taxa richness (Schneider and Winemiller, 2008). As shown in Chapter 2, turbulent flow properties play a crucial role in the life cycle of rheophilic fish, influencing swimming stability, energy expenditure, spawning and egg survival rates (Webb and Cotel, 2010a; Silva *et al.*, 2011). Previous research has explored swimming costs and loss of orientation by observing changes in fish behaviour in artificial habitats created in laboratory flumes (Enders *et al.*, 2003; Tritico and Cotel, 2010; Lacey *et al.*, 2012; Wilkes, 2014).

Laboratory experimentation overcomes may of the practical challenges associated with detailed field study, and the findings provide an improved understanding of swimming performance under controlled conditions. It is widely acknowledged, however, that behaviours observed under laboratory conditions may differ to those observed in natural channels (Lacey *et al.*, 2012). The results of advanced laboratory and field studies were brought together by Lacey *et al.* (2012) to develop the new IPOS framework which groups turbulence properties into four groups that directly influence fish: Intensity, Predictability (Periodicity), Orientation and Scale. The IPOS framework has not yet been widely applied within ecohydraulics research (an exception being Wilkes, 2014). This study represents one of the first complete applications and provides a rare insight into fish behaviour over short timescales under field conditions.

This chapter presents the results of a field investigation of the interactions between wood, turbulence and fish habitat use in a natural channel. The study employs an innovative combination of field measurement and underwater videography to reveal patterns in fish abundance and activity around two marginal wood features.

In particular, the research addresses three objectives:

1. Characterize the IPOS turbulence properties around wood patches.

2. Quantify fish preferences, behaviour and activity costs using underwater videography under field conditions.

3. Explore the exploitation of hydraulic habitat around wood by fish.

7.2 Methodology

7.2.1 Study site

The research was carried out in a side channel of the large, multi-thread Tagliamento River in Italy (Figure 7.1). The study section was located in the upstream part of the reach analysed in Chapters 4 and 5 and details of catchment characteristics and data sets are provided in the Research Design chapter (Chapter 3). The riparian corridor is a floodplain forest (largely *Populus Nigra*, *Alnus incana* and *Salix sp.*). The study section was 20 m long and two marginal patches containing wood features were selected for survey (Figure 7.2). Discharge at the time of survey was 3.52 $m^3 s^{-1}$ at the study section, and flow at the upstream main channel gauging station at Venzone was 42 $m^3 s^{-1}$ (50% exceedance). The reach was accessible for topographic, hydraulic and fish observational surveys, and the channel substrate and water depth were suitable for mounting camera equipment in the channel.

The first patch (P1) was located on the right bank downstream of a meander bend (Figure 7.1-1). The bed material was coarse gravel (range 10 to 26 mm). Roots and living branches extended into the water from the riparian zone creating marginal wood features. The size of the patch was 2.25 m^2. The diameters of submerged dead wood pieces and roots were less than 0.15 m and lengths ranged from 0.2 to 1 m. The second patch (P2) was on the left bank, 12 m downstream from P2 (Figure 7.1-2). Tree roots from riparian vegetation combined with submerged dead wood pieces provided the marginal wood features. Submerged branches and roots ranged from 0.06 to 0.15 m in diameter and from 0.2 to 0.6 m in length. The size of the patch was 3.75 m^2.

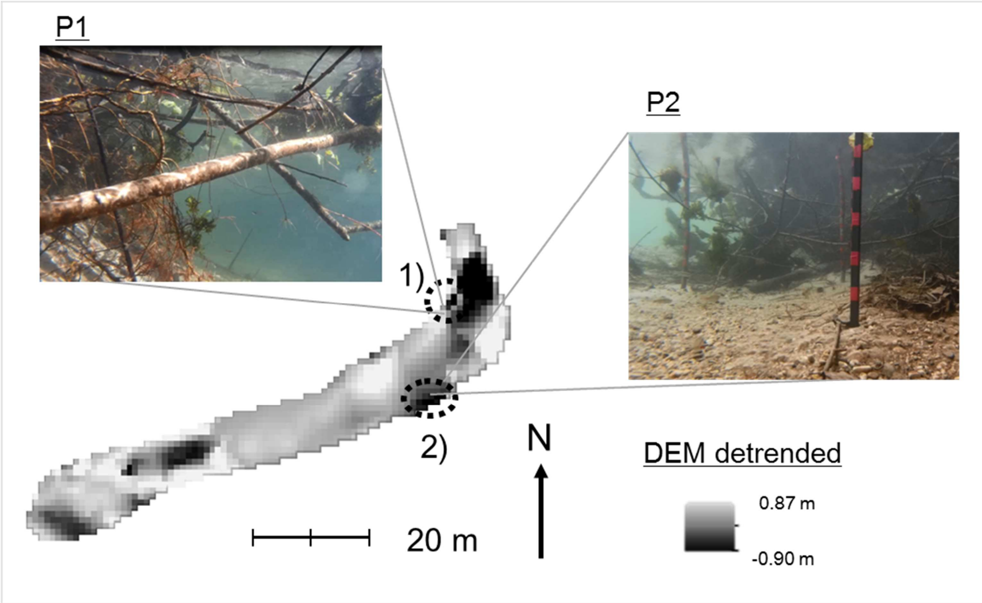

Figure 7.1 Detrended DEM (Digital Elevation Model) of the upstream reach in the Tagliamento with a grid resolution of 1 m. The black dotted circles represent the two patches used for the fish investigation.

Figure 7.2 Description of two patches. Patch (1) on the right bank above (A) and under the water surface (B). Downstream patch (2) above (C) and under the water surface (D).

7.2.2 Velocity measurements and underwater videography

In order to characterise the turbulent properties within each patch, instantaneous velocity measurements were captured at 0.6 of the flow depth (from the water surface) using an Acoustic Doppler Velocimeter (see Chapter 3 Research Design) within a measurement grid of 0.5 m x 0.5 m. The measurement grid was scaled on the patch size, yielding 6 within-patch measurements at P1 and 9 within-patch measurements at P2. Velocity was recorded at a frequency of 32 Hz for 120 seconds. Full details of velocity measurement are provided in Chapter 3 (Research Design), Section 3.5.

For each patch, underwater video was captured at 3 hour intervals throughout the day between 08.00 and 20.00. Night recordings were attempted using an infrared underwater video camera (Pond Camera 3.6mm. 500TVL) but the image resolution was not sufficient to detect fish movements. After velocities had been measured, the location was marked using a wading rod to enable orientation in video frames. The measurement grids used for each patch are illustrated in Figure 7.3. Underwater videography was used to observe fish presence and swimming behaviour around wood features. Recordings were captured over the course of one week in July 2015. One high resolution (10 MP) underwater camera (Umox SJ4000) was deployed immediately above the river bed (0.05 m) 1 m downstream of each patch and close to the bank (1 m from the bank for P1, 1.5 m for P2; Figure 7.3). The camera can capture images at a rate of 30 frames per second with 32 GB memory and a battery life of 80 minutes, although in practice this was reduced to 40 minutes as a result of relatively low water temperatures.

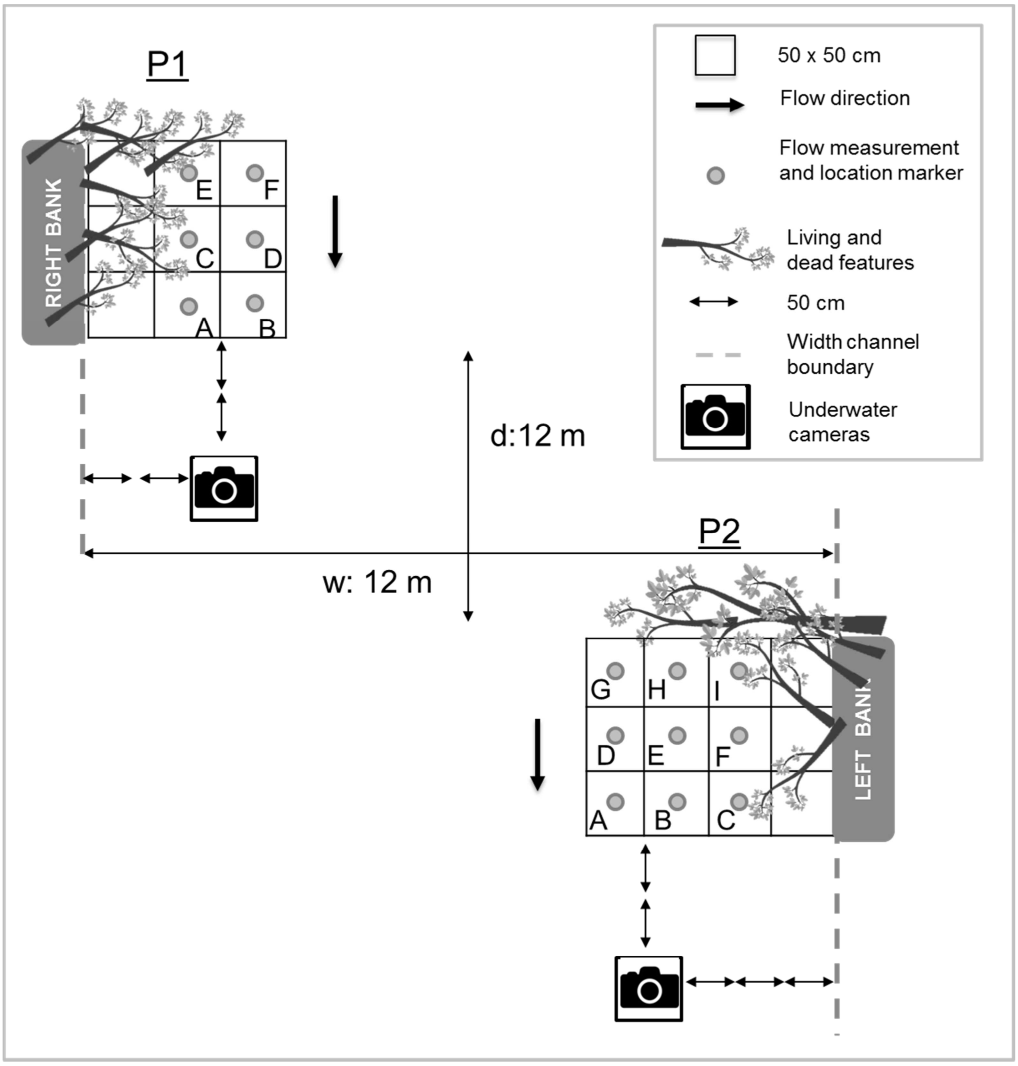

Figure 7.3 Sampling design of flow measurements and video recordings in the two patches. The distance between the two locations and the channel width are not scaled respect to the grid resolution of flow measurements. No measurements nearest the bank were densely vegetated and did not allow taking measurements.

7.2.3 Image capture and analysis

Six 30-minute videos were collected for each patch, but two videos (14.00 and 20.00) were lost due to battery failure, leaving four videos for analysis in patch 1 and six videos for patch 2. In total, 64000 frames were captured for each video. Recent advances in video processing systems provide rapid, automated techniques for identifying, counting and tracking movements of fish (Spampinato *et al.*, 2010; Delcourt *et al.*, 2013; Dell *et al.*, 2014). However, since the videos were captured under field conditions, a range of factors including luminosity, turbulence, air bubbles, water turbidity and movement of the wood features within the flow limited the use of auto-tracking software in this study. Instead, videos were observed manually at 60 s intervals (generating 30 observations per video; 180 observations for each patch) in order to record fish abundance and density, together with their position in the grids.

In order to explore relationships between energy expenditure and turbulence, fish behaviour over 30 s was observed (Hart, 2003) to estimate the main activities and the swimming speed of fish. Two main activities were identified (Table 7.1): station holding and exploring. Station holding referred to fish maintaining the same position in the flow for a period of 10 s or more and is usually associated with energy conservation and predator avoidance behaviour. Exploring behaviour was determined by the distance covered within the observational period, and usually reflects foraging activity.

Fish swimming speed refers to the speed at which the fish moved during the exploring and resting activities. Swimming speed is calculated by considering two swimming patterns: forced swimming, defined as the unidirectional flow velocity against which they swim and the spontaneous (directed) swimming speed that reflects the observed fish swimming speed (Boisclair and Tang, 1993). For exploring activity, the speed was described by the forced swimming speed and directed swimming defined as the ratio between distance and the time used for the movement while for fish in station holding, it was estimated using forced swimming speed that reflects the flow velocity.

Table 7.1 Fish activity selected by time and area of occupancy of the two patches.

Activity	Description	Parameters used to identify the activity
Station holding	Ability to maintain the position in the flow field without focusing on any specific object (Liao, 2007)	Time and area of occupancy in the same hydraulic patch >10 s
Exploring	Swimming long distances	Crosses >1 cell in the measurement grid

7.2.4 Fish species and video-derived variables

Fish identified by underwater videography were native European minnow, *Phoxinus phoxinus*, a member of the Cyprinidae family commonly found in freshwater habitats including rivers, ponds and large lakes and noted for shoaling behaviour (Pitcher, 1986; Barber and Wright, 2001). *P. phoxinus* is a slim, small-scaled fish with varied colour from green to brown with small black dots on the back (Figure 7.4) (Mills and Eloranta, 1985). Adults are typically 60-100 mm in length, although individuals up to a maximum of approximately 140 mm in length have been recorded (Ward and Krause, 2001). The diet of *P. phoxinus* includes algae, river plant debris, molluscs, crustaceans and insects (Billard, 1997). They can tolerate water temperature ranges from 4 to 20 ºC and average water temperatures at the time of survey were 15 ºC. Suitable habitat for *P. phoxinus* includes river reaches with coarse substrate, fast-flowing, well oxygenated water combined with more tranquil pool habitats (Kottelat and Freyhof, 2007). Predators are a key threat (Boutorina and Reznik, 2014) and shoaling behaviour reduces the risk of predation (Hamilton, 1971).

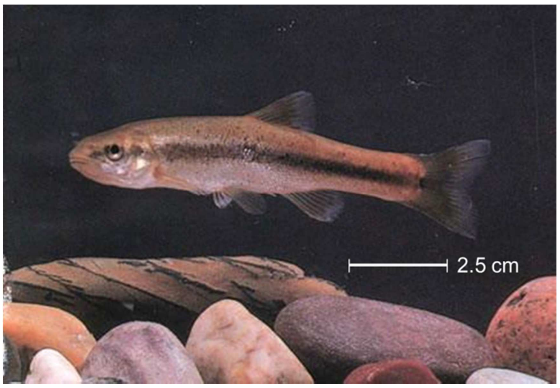

Figure 7.4 European minnow species (*Phoxinus phoxinus*). Source: Chinese Academy of Fishery Science, 2006.

To quantify the influence of turbulence on fish energy expenditure, the net swimming cost is indirectly estimated by empirical equations using the swimming speed and parameters related to the fish species in question (Boisclair and Tang, 1993). This approach provides a valid alternative to estimate the energy spent by the fish free-swimming under field conditions. More accurate estimates involve laboratory studies which can measure activity costs by respirometer experiments but these require tightly controlled boundary conditions (Enders and Boisclair, 2016).

Fish biomass can be estimated by mass-length equations (Equation 7.1), in this case for the cyprinid, using observed body lengths (Froese, 1998; Miranda *et al.*, 2006). The total mass (W) was computed from a combination of experimental parameters (a = 0.0042) and (b = 3.42) for the *P. phoxinus* (Oscoz *et al.*, 2005) with total length (L) in cm.

Equation 7.1 $$W = 0.0042 * L^{3.42}$$

A dimensionless metric expressing the ratio of eddy length to fish body (length ratio; LR) has been proposed as an important parameter in assessing the impacts of turbulence on fish (Cotel and Webb, 2015). It is defined by Equation 3.12 (Chapter 3, section 3.6.4) as the ratio of eddy size to fish size.

The net swimming cost, defined as the energy required by the animal for external movements, was estimated from fish mass, swimming speed and flow speed by applying empirical relationships. This was achieved by (i) estimating fish velocity based on video data in relation to field markers; (ii) based on the direction of travel, identifying the velocity measurement location that the fish was moving towards; (iii) computing the resultant velocity and flow direction at that measurement location, derived from the streamwise and lateral components; (iv) computing fish swimming speed and applying one of two net swimming cost equations based on the relationship between the direction of travel of the fish and the flow direction, following Boisclair and Tang (1993). If the velocity vector was opposing the direction of travel of the fish, fish swimming speed was estimated as the sum of the fish velocity and the flow velocity. In this case, the forced swimming equation (7.2) was used to estimate the net swimming costs. According to Boisclair and Tang (1993), forced swimming refers to swimming against the prevailing flow direction. If the velocity vector was similar to the direction of travel of the fish, fish swimming speed was estimated by subtracting the flow velocity from the fish velocity and the equation for directed swimming (Equation 7.3) was applied. According to Boisclair and Tang (1993), directed swimming refers to straight line movement from one location to another under still water conditions and therefore is more appropriate to use in situations where the fish is unimpeded by the prevailing flow direction.

Equation 7.2 $\log_{10} C = 0.80 \log_{10} W + 1.21 \log_{10} S - 2.43$

Equation 7.3 $\log_{10} C = 0.36 \log_{10} W + 1.10 \log_{10} S - 1.46$

(C: net energy cost (C, mgO^2h^{-1}), W: fish body mass (mg) and S: swimming speed (cm s^{-1}))

7.2.5 Data Analysis

Data were not normally distributed (Shapiro – Wilk: $p < 0.001$) and therefore non-parametric statistical tests were used. Mann Whitney tests were used to identify significant differences between patches.

7.3 Results

7.3.1 Characterising turbulence around wood patches

The distribution of key IPOS variables is presented in Table 7.2. The two wood-related patches revealed differences in their high frequency flow properties, although in many cases differences were not statistically significant. P1 was characterised by ponded/rotational flow, with negative streamwise velocities indicating flow in the upstream direction at all measurement locations. In contrast, P2 was characterised by positive streamwise velocity indicating the main direction of flow was downstream. Mean streamwise velocity was -0.11 ms^{-1} in P1 and 0.18 ms^{-1} in P2, and lateral flow velocities indicated preferential flow deflection towards central channel areas. Reynolds stresses were overall higher for P1 compared to P2, while TKE was on average lower in P2, but also more variable, and vorticity was higher and more variable in P2.

The predictability, orientation and scale of flow structures show some differences between the patches. The majority of velocity time series in P2 meet the condition for pseudo-periodicity, indicating a more predictable flow structure, while almost all w series, and 3 (out of 6) v series together with 4 (out of 6) u series for P1 do not meet the condition, indicating a less predictable flow structure. For P1, there was a tendency for higher magnitude ejections (Q2) and inrushes (Q4) throughout the patch, and lower magnitude inward and outward interactions, while for P2 the contributions of different event types were variable among sampling points without any clear trends. Eddy length and diameter in the streamwise dimension were larger for P2 compared to P1, while dimensions in the v and w dimension were constrained to a narrower, lower range indicating increased elongation of eddies in the streamwise dimension. For P2, eddy dimensions were more similar across the three dimensions and particularly for u and v components.

Statistically significant differences (Mann Whitney U) were observed between the two patches for mean velocity (u and v components) and the magnitude of inwards interactions.

Table 7.2 Summary statistics of the key IPOS parameters across the two patches. Bold font refers to statistically significant (Mann Whitney: $p< 0.001$).

	Variables	Patch	Minimum	Maximum	Mean	SD	p value
Mean velocity ($m\ s^{-1}$)	U ($m\ s^{-1}$)	1	-0.186	-0.067	-0.11	0.044	**0.012**
		2	0.103	0.407	0.18	0.112	
	V ($m\ s^{-1}$)	1	0.049	0.093	0.08	0.015	**0.025**
		2	-0.015	0.095	0.03	0.036	
	W ($m\ s^{-1}$)	1	-0.037	0.040	-0.01	0.036	0.724
		2	-0.077	0.027	-0.02	0.032	
Intensity	TKE ($m^2\ s^{-2}$)	1	0.025	0.055	0.04	0.012	0.239
		2	0.016	0.052	0.03	0.012	
	Reuv ($N\ m^{-2}$)	1	1.030	4.670	2.34	1.412	0.239
		2	0.390	4.500	1.65	1.398	
	Reuw ($N\ m^{-2}$)	1	0.520	3.830	1.53	1.277	0.193
		2	0.250	2.470	0.97	0.860	
	Vorticity (s^{-1})	1	0.070	0.170	0.11	0.041	0.157
		2	0.060	0.330	0.19	0.101	
Orientation	%Q1	1	0.009	0.890	0.29	0.305	0.905
		2	0.079	0.720	0.29	0.215	
	%Q2	1	0.045	0.728	0.32	0.269	0.852
		2	0.063	0.366	0.22	0.109	
	%Q3	1	0.020	0.140	0.06	0.044	**0.010**
		2	0.070	0.517	0.223	0.156	
	%Q4	1	0.008	0.897	0.35	0.333	0.724
		2	0.057	0.562	0.26	0.188	
Predictability	Pseudo -period. u	1	-3.290	-0.300	-1.65	1.272	0.316
		2	-1.380	0.200	-0.47	0.422	
	Pseudo -period. v	1	-2.950	-0.180	-1.49	1.121	0.340
		2	-1.590	0.810	-0.33	0.801	
	Pseudo -period. w	1	-2.220	0.210	-0.93	1.036	**0.025**
		2	-1.530	0.870	0.11	0.715	
Scale	Lu (m)	1	0.068	0.312	0.17	0.089	0.126
		2	0.117	0.293	0.21	0.068	
	Lv (m)	1	0.059	0.149	0.12	0.034	0.088
		2	0.013	0.150	0.05	0.051	
	Lw (m)	1	0.020	0.080	0.04	0.022	0.556
		2	0.001	0.042	0.02	0.015	

	Du (m)	1	0.020	0.040	0.03	0.010	0.157
		2	0.025	0.080	0.05	0.016	
	Dv (m)	1	0.020	0.070	0.04	0.018	0.085
		2	0.010	0.055	0.03	0.015	
	Dw (m)	1	0.010	0.030	0.02	0.009	0.429
		2	0.005	0.031	0.02	0.008	

The spatial organisation of flow properties is explored in Figure 7.5 and Figure 7.6. For both patches, there is a tendency for lower turbulence intensity closer to the wood features, and higher turbulence intensity in outer flow areas, particularly two points in each patch at the upstream end of the sampling area (E and F for P1; D and G for P2). In both patches these points were located further from the wood features. Greater spatial variation in the contribution of different event types to the shear stress was noted for P1 with higher magnitude ejections and inrushes associated with upstream points E and F.

Eddy dimensions showed similar patterns for sampling points within the two patches. Eddies located in the outer zone were smaller in size than eddies located in the less turbulent areas closer to the wood features, with larger dimensions in the lateral (v) dimension compared to u (streamwise). In addition, eddy diameters in outer zone points were higher for the v dimension, while eddy dimensions in the inner areas closer to the wood features were higher for the streamwise (u) dimension.

Power spectra for the streamwise (u) component are explored in Figure 7.7 for points in P1 and Figure 7.8 for points in P2. For P1, the highest peaks were observed at lowest frequency spanning from 0.025 to 0.045 for the outer points further away from the wood (B, D and F) with smaller peaks at higher frequency, while several peaks at lower frequency were observed at inner points closer to the wood (A, C, E) suggesting complex flow structure for points close to the bank. For P2, spectral density plots were more complex, with no obvious spatial organisation.

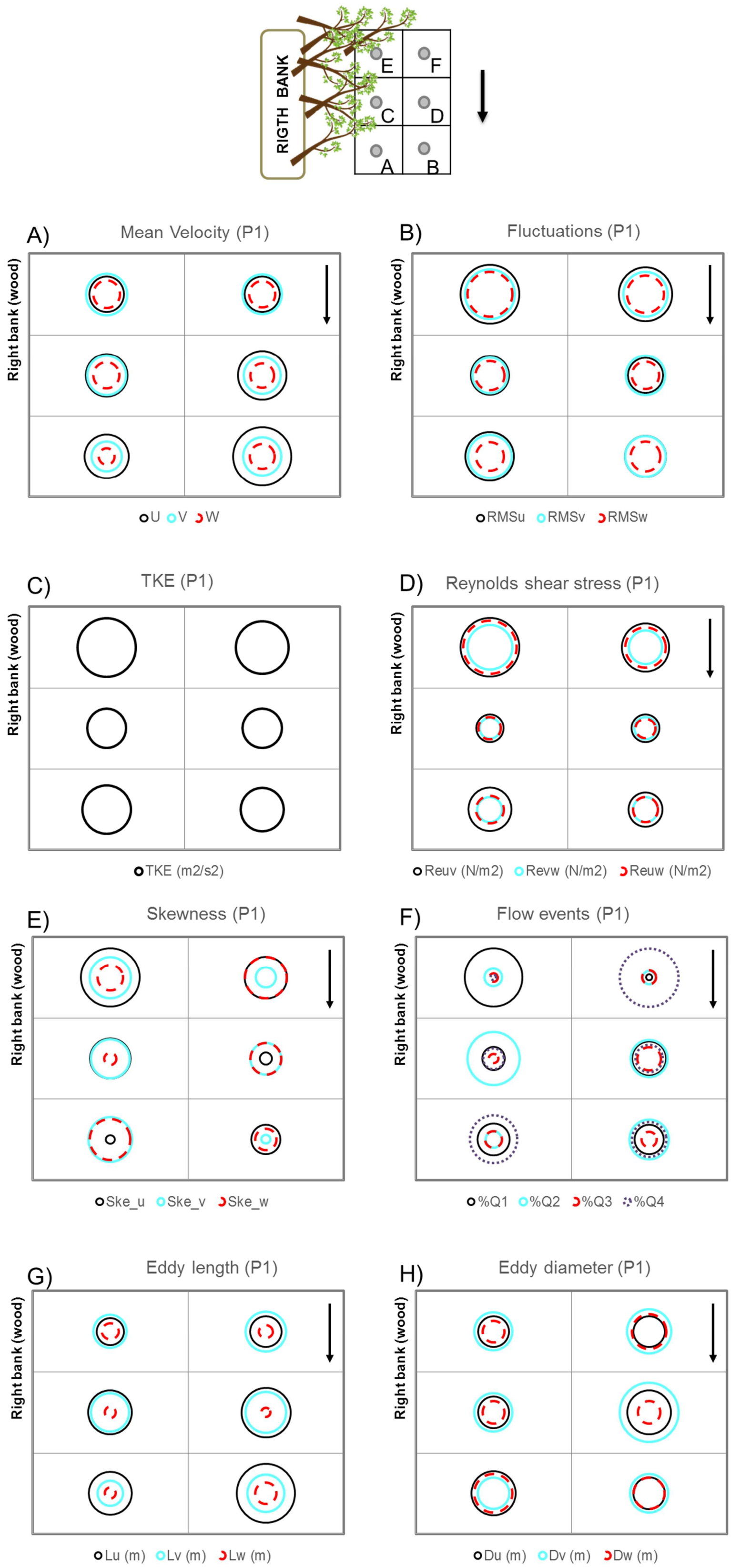

Figure 7.5 Key flow properties for patch 1 (P1).

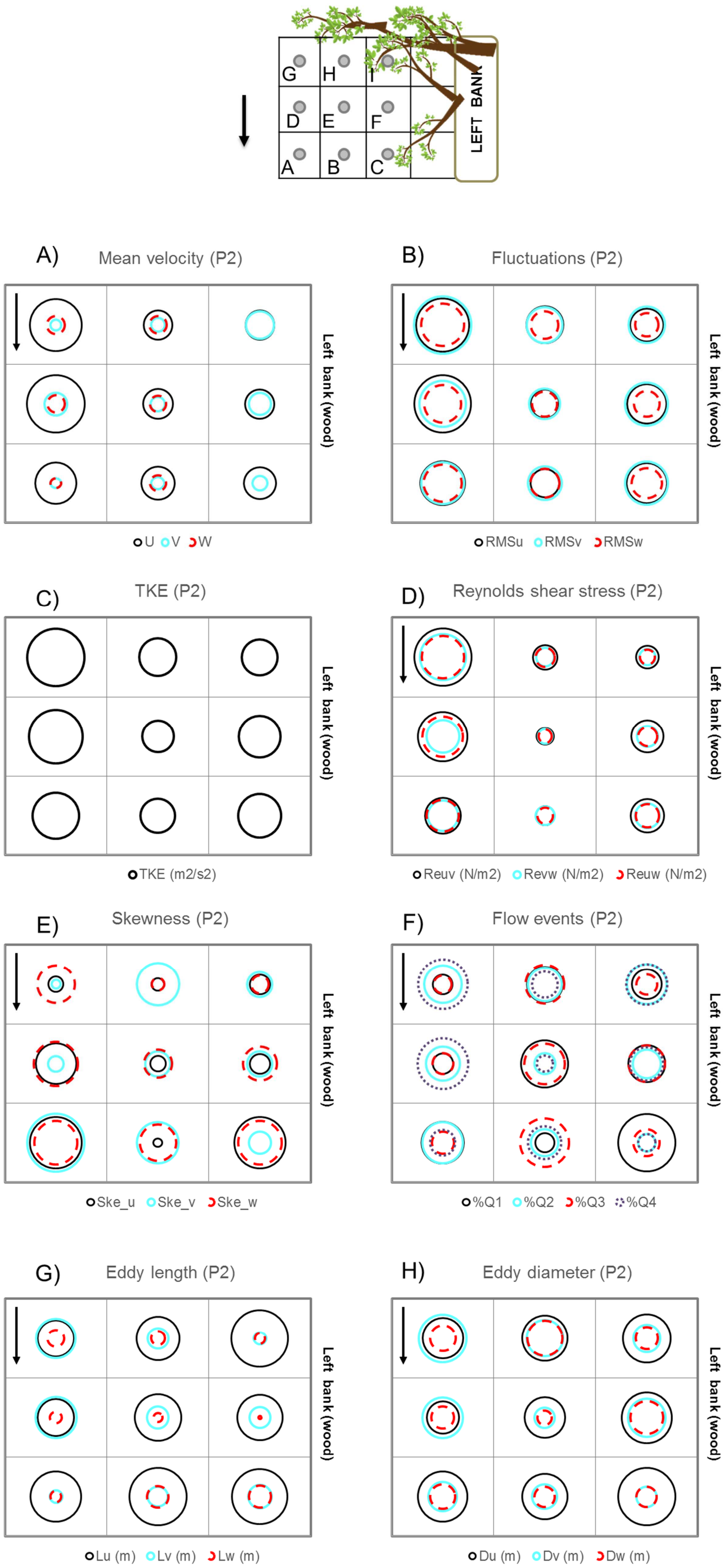

Figure 7.6 Key flow properties for patch 2 (P2).

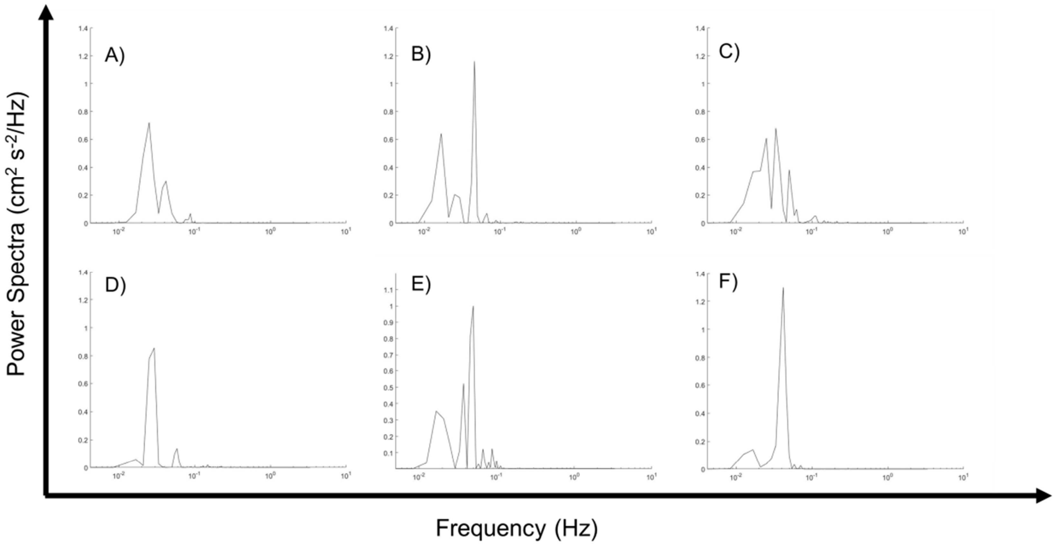

Figure 7.7 Power spectra for time series along the streamwise (u) component at patch 1. A, C, E are the inner points close to the bank and B, D, F are the outer closer to the channel.

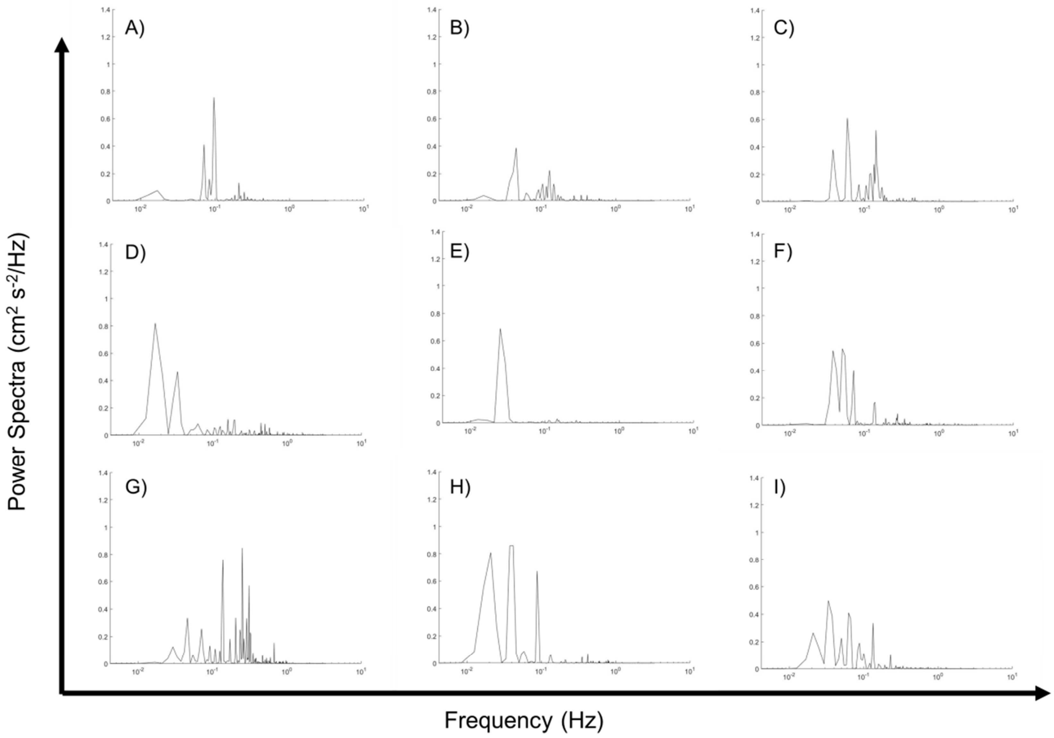

Figure 7.8 Power spectra for time series along the streamwise (u) component at patch 2. C, F, I are the inner points close to the bank and A, D, G are the outer points.

7.3.2 Habitat use and swimming costs of *P. phoxinus* in the two patches

The abundance and average size of fish occupying areas within the two patches through the sampling period are presented in Figure 7.9. *P. phoxinus* were more abundant at P1 (median 16 individuals; maximum 25) compared to P2 (median 8 individuals; maximum 21), and were considerably smaller in P1 (mean: 0.05 m) compared to P2 (mean: 0.14 m). Observations of the distribution of fish presence and size throughout the day in both patches indicated a lower concentration of small fish during the period of maximum exposure to light (14.00) and before sunset (20.00) (Figure 7.9 B-D). Average body size was most variable in the late afternoon (17.00) and least variable during the evening (20.00). P1 was characterized by similar sized individuals throughout most of the day although data for 14.00 and 20.00 are missing due to battery failure. There was an increase in fish abundance from early morning to mid-afternoon in P1. Fish size was more variable in P2 throughout the day, with a peak in average size at 17.00 corresponding with an increased abundance of fish (10). Fish abundance did not change considerably throughout the day, with one exception during sunset (20.00) where the abundance and size of individuals decreased markedly in P2 (Figure 7.9 C-D).

Two types of fish activity were observed: station holding and exploring actions (Table 7.1). The results for observations of fish behaviour in the two patches are presented in Figure 7.10 in which the mean number of 30 s observations revealed higher concentration of exploring fish in P1 compared with P2 where fish were mostly holding their position within the flow. Across the two patches, behaviour showed some diurnal trends, with station holding in the area closest to the submerged wood (Figure 7.12, Figure 7.13) observed early in the morning and in the evening, while exploring behaviour was observed during the central part of the day, with an exception for an hour with high luminosity (where the patch was temporarily not in shade). For P1, fish were observed to swim from the outer zone to the right bank (close to the wood), with a low frequency of observations of resting activity (Figure 7.10A). In P2, fish were observed to maintain their position close to the wood features for most of the day with exception for the central part of the day in which exploring exceeded station holding (Figure 7.10B).

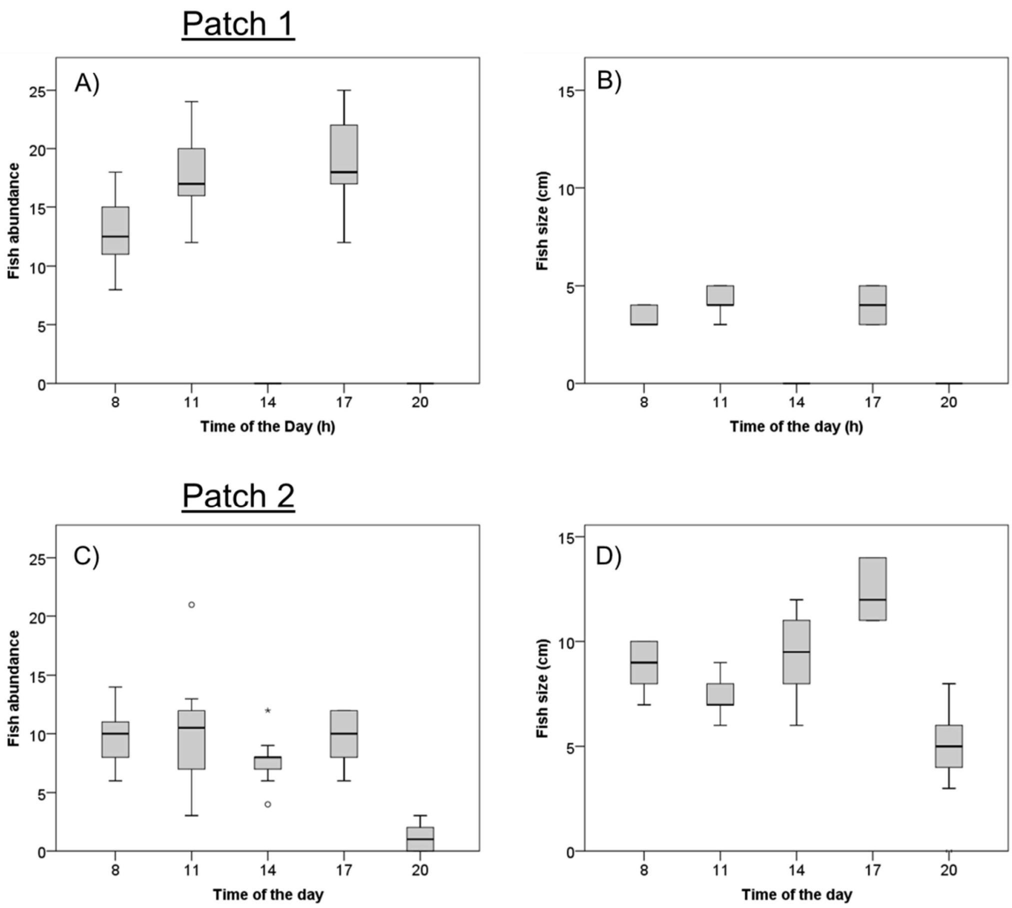

Figure 7.9 Fish abundance (A-C) and size (total body length) (B-D) across the first (A-B) and second (C-D) patches across daily hour.

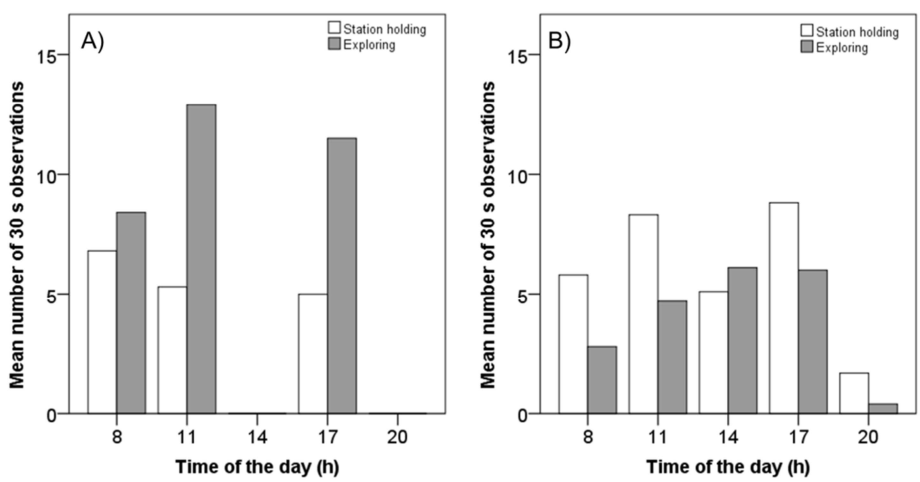

Figure 7.10 Daily fish activity across the first (A) and second (B) patches.

In both patches, the net swimming cost was empirically calculated by Equation 7.2 and Equation 7.3 for quantifying the energy spent by small (average length 4 cm) and large (average length 9 cm) fish during activities of station holding and exploring and results are presented in Table 7.4. For both patches, the directed swimming was significantly higher compared with the forced swimming with highest median values at mid-afternoon (17) in P1 and at early morning (8 and 11) in P2 (Figure 7.11). Fish spent more energy when exploring compared with station holding indicating an increase in the cost to transport the body over a distance. Larger fish spent more energy compared with smaller fish. The net swimming cost ratio revealed higher positive values for P1 at 8 am with slightly reduction during the day while similar values were observed for P2.

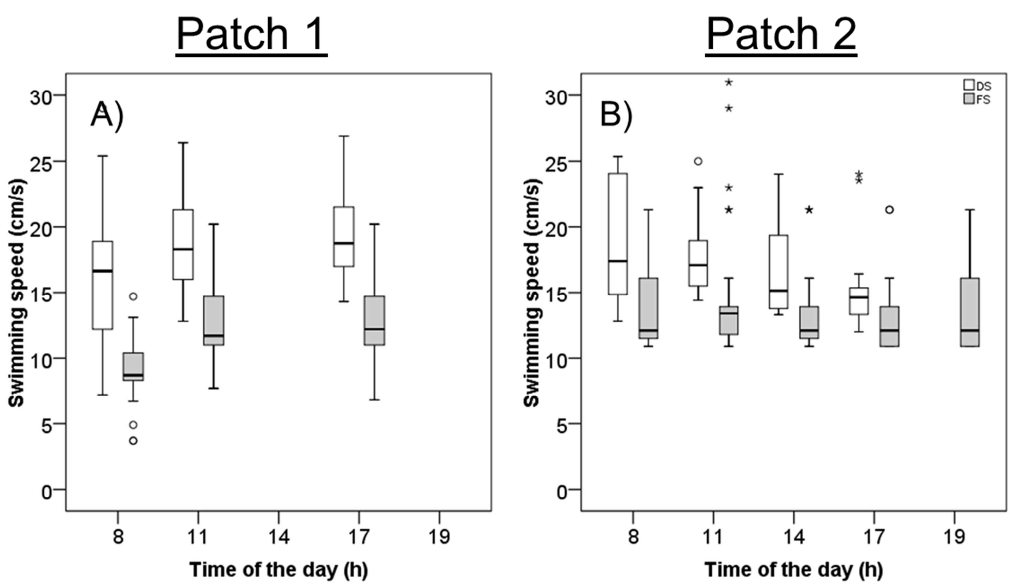

Figure 7.11 The distribution of swimming speed at the patch 1 (A) and patch (2) across time of the day for exploring activity (using Directed Swimming) and holding resting (Forced Swimming).

Table 7.3 Description of estimated body mass for *P. Phoxinus*.

Length(cm)	*Mass (g)*
3	*0.26*
5	*1.06*
7	*2.72*
9	*5.48*
11	*9.58*

Table 7.4 Parameters of forced (SF) and directed swimming (DS) (cm s^{-1}) and net swimming cost (mg O^2 h^{-1}) during the day for patches one and two. The fish body mass used in the experimental equation of net swimming cost was related to average length 4 cm for patch 1 and 9 cm for patch 2. Swimming cost ratio is the ratio between net cost DS and net cost FS.

Patch	Time	Forced Swimming (cm s^{-1})	Directed Swimming (cm s^{-1})	Net swimming cost FS (mgO^2 h^{-1})	Net swimming cost DS (mg O^2 h^{-1})	Swimming cost ratio
1	8	9.0	16.6	0.09	1.17	12.42
	11	11.4	17.9	0.13	1.28	10.12
	17	13.2	19.1	0.15	1.37	9.18
2	8	15.1	19.0	0.36	2.33	6.44
	11	15.7	19.6	0.38	2.42	6.38
	14	13.4	16.7	0.31	2.03	6.48
	17	14.1	18.4	0.33	2.26	6.79
	19	13.8	-	0.32	-	-

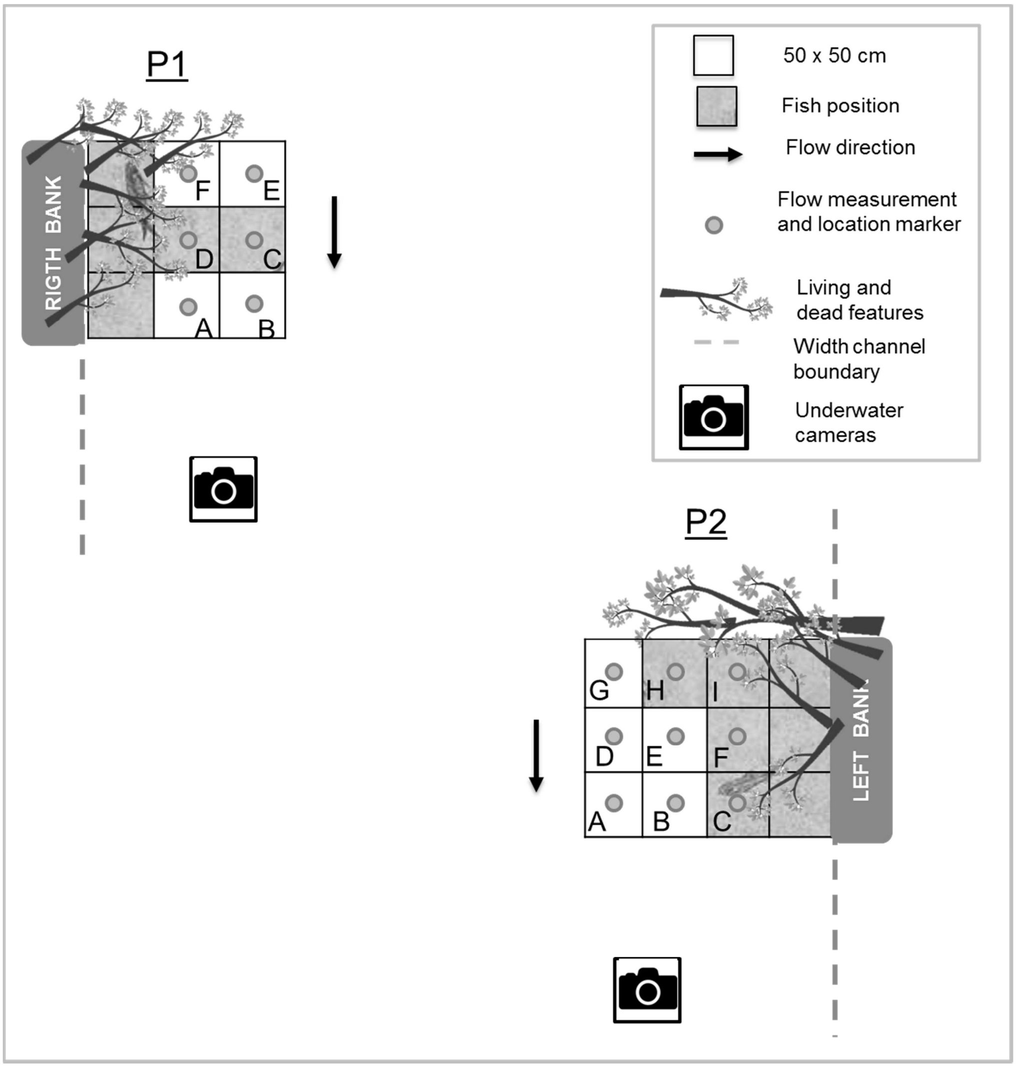

Figure 7.12 Description of the high percentage of area covered by fish during the survey across daylight. No measurements nearest the bank were densely vegetated and did not allow taking measurements.

7.3.3 Interaction between *P. phoxinus properties and turbulence* in the two patches

Table 7.5 presents the ratio of eddy length to fish length, F_L. The ratio exhibited lower values (<1) for large fish in both patches and for small fish along the vertical (w) components. For the majority of measurement points, eddy size (in all three dimensions) was considerably smaller than large fish length, the exception being one point in P2. In contrast, for small fish the eddy length (on u and/or v dimensions) to fish length ratio was close to 1 for all point in P1 and for two points in P2.

Table 7.5 Non dimensional ratios for streamwise (u), lateral (v) and vertical (w) direction defined by the eddy length for the body fish (L_F) for *P. Phoxinus*. Bold font underlines refer to the ratio around 1 that may affect the stability of fish.

Small fish F_L = 4 cm			**Large fish** F_L = 9cm			**Grid Position**	**Patch**
Ratio u	*Ratio v*	*Ratio w*	*Ratio u*	*Ratio v*	*Ratio w*		
0.63	**1.00**	0.30	0.28	0.44	0.13	A	1
1.00	0.25	0.13	0.44	0.11	0.06	B	
0.55	**0.88**	0.65	0.69	0.39	0.29	C	
1.00	1.38	0.40	0.44	0.61	0.18	D	
1.25	**0.80**	0.75	0.56	0.36	0.33	E	
1.40	0.45	0.30	0.62	0.20	0.13	F	
1.10	0.50	0.75	0.44	0.22	0.33	A	2
0.50	0.75	0.50	0.22	0.33	0.22	B	
0.65	0.51	0.38	0.74	0.50	0.38	C	
1.30	0.25	0.25	**0.86**	0.11	0.11	D	
0.52	0.62	0.25	0.22	0.33	0.11	E	
0.50	**1.00**	0.63	0.22	0.44	0.28	F	
1.25	0.38	0.25	0.56	0.17	0.11	G	
1.60	1.75	0.25	0.44	0.78	0.11	H	
0.50	0.75	0.25	0.22	0.33	0.11	I	

Figure 7.13 presents a combination of key turbulence parameters to evaluate the interactions between hydraulic habitat and fish. Fish variables were calculated as the average of abundance, size and activity across the whole day. The topography of the two patches was described by negative residuals, defining two areas of local depression with most pronounced topographic variations in P2. Fish abundance was highest in areas near the wood that were also characterized by low/medium kinetic energy. Station holding behaviour was generally observed in areas close to the wood, and exploring behaviour in areas further from the wood. The eddy length: fish length ratio indicated that the area near banks and close to the wood (blue grids) was the most suitable area for fish in terms of avoiding dislocation and reductions in swimming performance. These were the areas associated with the highest abundance of fish.

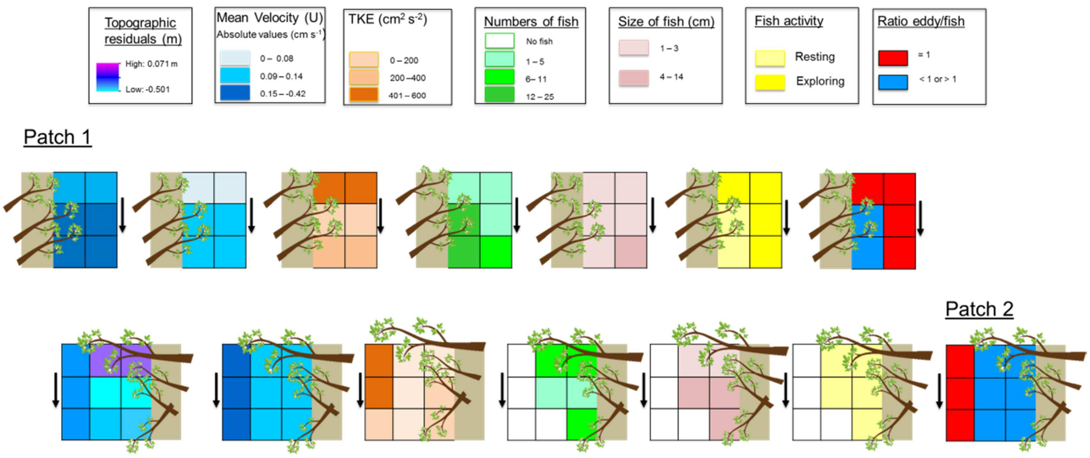

Figure 7.13 The combination of topographic, absolute mean velocity on streamwise direction (U), turbulent kinetic energy (TKE), average number of fish and their size, fish activity defined by holding position and exploring (swimming) and finally the dimensionless ratio between eddy and fish length. Values of fish preferences were considered in average for whole day.

7.4 Discussion

7.4.1 IPOS turbulence parameters around wood patches

Across the two wood-related patches, the hydraulic properties revealed differences in mean velocity in the streamwise (u) dimension but there were no statistically significant differences in key turbulent properties between the patches. Both patches were instead characterised by regions of lower and higher turbulence intensity. Two general zones were observed, reflecting the influence of wood features: a lower intensity flow region closer to the wood and a higher intensity outer flow zone with more pronounced ejections/ inrushes. Wood features diverted the water flow to the central part of the channel developing sheltered areas of lower shear stress and kinetic energy at the margins, conditions favourable for trapping fine sediment and particulate organic matter (Osei *et al.*, 2015) and generating suitable habitat for fish (Johnson *et al.*, 2003).

However, the hydraulic effects of wood features are to some extent dependent on the positioning of the wood itself. For example, Tullos and Walter (2015) investigated the benefits of re-introduction of wood for fish, focusing on the characteristics of the flow field generated by wood. They found two broad areas with both low and high velocity and turbulent kinetic energy respectively. In contrast to this study, the more turbulent area characterized by flow contraction, expansion and acceleration was observed nearer the wood features. The differences in size and position of wood related to channel dimensions will therefore determine the exact nature of hydraulic habitat produced.

7.4.2 Fish characteristics and behaviour around wood

Despite recent advances in development of automatic tracking software in laboratory experiments, manual image-based tracking was chosen to provide key information on fish related variables and behaviour at the microscale in this natural channel (Dell *et al.*, 2014). Different habitats may be used by fish for different activities (e.g. feeding, resting, avoiding predators, exploring) and habitat selection varies with the size (age) of the fish in combination with physical conditions such as flow velocity (Tiffan *et al.*, 2010).

Fish abundance revealed that the presence of fish was relatively uniform for most of the day except for a decrease in fish presence during the early morning for P1 and at sunset for P2. Fish in P1 were smaller and more frequently exhibited exploring behaviours than fish in P2. In P2, fish generally remained close to the wood feature and the majority were station holding rather than exploring. The wood represents an element of cover and concentration of fish in this area may also indicate a response to the moderation of temperature afforded by the shading which has implications for oxygen consumption (Cui and Wootton, 1988; Plath *et al.*, 2013). For P2, larger fish were observed maintaining their position in the flow and were less mobile, staying close to the wood features in the zone of lower turbulence intensity and higher predictability. Estimated net swimming costs provide insights into the crucial role of fish size in determining the ability to control energy expenditure and the cost effectiveness of fish activities. Larger fish spend more energy compared to smaller fish and therefore need to carefully manage their energy costs. Orientating their body upstream helps to minimize the energy cost (Northcutt, 1997) and exploit the current and vortices to reduce energy required for swimming (Fish, 2010). In this study, the net swimming cost ratio was up to two times higher in P1 compared to P2, indicating that the increased energy costs required for directed swimming were proportionately greater in P1. This reflects the different size of fish associated with the two patches: larger fish (P2) require more energy for forced and directed swimming, but the increased energy costs are proportionately less in comparison to smaller fish, potentially as a result of swimming efficiency (Webb *et al.*, 1984; Fish, 2010).

Fish were generally observed in the areas closer to the wood features where turbulence intensities were reduced and eddy length: fish length ratios were not close to 1 (Figure 7.13). This is consistent with previous experiments using *Iberian Barbel* (Silva *et al.*, 2011) which indicated that fish spent more time in areas with lower turbulence intensity and in areas with eddies either larger than or smaller than their body size. However, research to date has generated contrasting opinions on the influence of turbulence intensity (absolute intensity and TKE) on fish with some studies suggesting that the influence could be greater at higher flow stages and less important at low flow stages (Lacey *et al.*, 2012).

Tritico and Cotel (2010) used laboratory experiments to demonstrate how eddy size influenced the stability system of fish, reducing their body control and causing individuals to lose their swimming trajectories. The importance of a dimensionless length scale ratio, comparing fish body length and characteristic eddy length scale, has been proposed as a key influence on fish behaviour and stability (Cotel and Webb, 2015). This study suggests that fish abundance was more closely related to this parameter and other higher order flow properties (e.g. TKE) than to the mean flow velocity. This finding is significant, since it suggests that these more sophisticated IPOS-related flow parameters provide a better explanation of fish behaviour and habitat use compared to the traditional, simpler measures such as temporally averaged streamwise velocity.

CHAPTER 8: Conclusions

8.1 Introduction

The importance of physical habitat diversity for overall river health is widely recognised (Padmore, 1998; Jowett, 2003; Harvey *et al.*, 2008; Wallis *et al.*, 2012) and integrated into river assessment methods primarily through the visual identification of key geomorphic features. Chapter 2 outlined the diverse ways in which aquatic organisms interact with turbulent flow in rivers at small spatio-temporal scales. The turbulent properties of flow are of vital importance to aquatic biota, yet these are rarely quantified during routine habitat assessments or in the design of river restoration schemes. This partly reflects the complex nature of 'higher order' flow properties that require more sophisticated data collection and analysis compared to more standard hydraulic variables (e.g. temporally averaged flow velocity).

This thesis has addressed some of the key knowledge gaps associated with the relationships between geomorphology, turbulence and aquatic biota within rivers at scales that are relevant to river assessment and restoration. In particular, it has provided insights from field data that have been lacking in previous research due to the challenges associated with capturing high frequency flow properties under field conditions; explored high frequency flow properties at the reach and geomorphic unit scales used in standard habitat assessments; explored temporal variability in turbulence properties associated with an increase in flow stage and with seasonal variations in vegetation cover; and investigated direct links between turbulence properties and habitat use by fish under field conditions. Overall this has led to a number of important contributions to ecohydraulics research and these are outlined in the subsequent sections, concluding with suggestions for further research.

8.2 Conclusion

8.2.1 Characterisation of reach-scale hydraulic habitat using turbulence properties

The objectives of chapter 4 involved quantifying turbulence properties (intensity, periodicity, orientation and scale) and exploring how these differed across reaches of different gradient. This included exploring the spatial organisation of turbulent properties and relating these to the spatial organisation of bedforms and/or other characteristic roughness elements.

Multivariate statistical analysis identified key gradients in turbulence properties that reflected the ‘scale’, ‘intensity’ and ‘orientation’ categories in Lacey *et al.*’s (2012) IPOS framework (‘predictability’ variables did not meet statistical assumptions of the technique and therefore were not represented*).* This *suggests that the IPOS categories capture the principal sources of variance in turbulence properties from a statistical point of view and hence supports the use of the IPOS framework as a sensible means of categorising the diverse turbulence parameters that can be computed.* Importantly, however, relationships between the three velocity planes (e.g. for turbulence intensity) and between intensity and mean velocity, were more complex than those previously reported in the literature, reflecting sub-reach scale variability introduced by roughness elements such as macrophytes and bedforms. This *emphasises the importance of direct measurement since the nature of relationships may vary spatially according to river type.*

There were few statistically significant differences between the reaches, reflecting the spatial variability in turbulence properties within each reach. Overall, however, turbulence properties varied with reach gradient across all three categories and these differences can be interpreted to reflect fundamental differences in turbulence generation associated with key roughness elements within the three reaches. The intensity of turbulent fluctuations and size of dominant eddies increased with reach gradient, while the predictability of the flow structure decreased. The event structures differ between reaches, with greater contributions from ejections and inrushes in the low and high gradient reaches indicating the direct influence of small-scale vegetative elements and large clasts respectively in controlling sweep-like and burst-like turbulence generation events. In the intermediate gradient reach where these features were not present, the event structure was dominated by inward and outward interactions, suggesting a strong control of microscale form roughness on styles of turbulence generation. The scale of flow structures also increased with reach gradient, with eddy sizes scaling on microtopography and small vegetation elements in the lower gradient reaches, and with large boulders for the high gradient reach.

These observations were supported by geospatial analysis that demonstrated a complex spatial organisation of turbulence properties in the vegetation-dominated reach (low gradient), a more periodic spatial structure in the riffle-pool reach (intermediate gradient) and the step-pool reach (high gradient), where bedform spacing showed closer correspondence with the spatial structure of turbulence properties. These results indicates that *while the geomorphic unit scale may have potential to explain the spatial organisation of turbulence properties in some reaches, relationships are complex and may vary in space*. These ideas are explored further in the following section.

8.2.2 Hydraulic characterization of geomorphic units across different gradient rivers

The objectives of chapter 5 involved exploring the relationships between geomorphic units (GUs) and turbulence properties more explicitly. The turbulence properties of GUs were quantified, the utility of turbulence parameters in predicting GU occurrence was evaluated, and scales of variability outside of the principal GUs was explored.

Overall reach gradient had a stronger influence on the variation in turbulence properties than individual GUs, but some distinctions were noted for some of the IPOS variables. Importantly, the capacity of the IPOS categories to effectively discriminate between GUs varied depending on the combination of GUs studied. For example, no clear and consistent differences in turbulence intensity were identified between GUs, although turbulence intensity was the best predictor of GU occurrence within the low gradient reach. Eddy scale was the best predictor of GUs in the riffle-pool (intermediate gradient) and step-pool (high gradient) reaches, where eddy sizes were smaller in pools compared to respective riffles/steps. To a certain degree, *ecologically relevant turbulence parameters therefore show some distinction between GUs, indicating that visual field assessment protocols can offer some* *relatively broad insights into hydraulic habitat conditions at this spatial scale*. Predictability of the flow structure, however, varied between types of pools, with higher levels of predictability in low gradient pools compared to higher gradient pools. This emphasises that *the same broad type of GU can provide considerably different hydraulic habitat conditions, and therefore the style of that unit (reflecting broader reach-scale characteristics) should be captured as part of standard habitat assessment protocols*.

When sampling locations were objectively classified into clusters, however, derived clusters did not conform with visually assessed GUs. This suggests that *the visual approach to GUs classification does not comprehensively capture the principal scales of variability associated with turbulence properties that are of direct relevance to aquatic organisms*. Instead, statistically derived groups corresponded to sub-GU scale patches that were observed to be related to individual flow obstructions such as vegetation and boulders in the low and high gradient reaches respectively. This indicates that *the presence of roughness elements at scales smaller than GUs can have an important influence on hydraulic habitat, requiring consideration in river assessment and restoration design*.

8.2.3 Influence of changes in flow stage and aquatic vegetation cover on turbulence properties and their spatial organization

The objectives of chapter 6 involved exploring the dynamics of turbulence properties in relation to two key sources of temporal variability in rivers: hydrologically driven changes in flow stage and the seasonal growth and senescence of aquatic plants. Changes in turbulence properties associated with an increase in flow stage were explored for the high gradient (step-pool) reach, and changes associated with vegetation growth were explored for the low gradient reach. These are explored in turn below.

For changes in flow stage, multivariate statistical analysis revealed key gradients in turbulence properties that corresponded broadly with three IPOS categories across the low and higher flow stage data sets: intensity, orientation, scale (u dimension) and scale (w dimension). No clear differences were observed at the reach scale in relation to intensity and predictability variables, although wavelet analysis revealed an increase in the dominant period of coherent flow structures as well as an increase in the overall complexity of the flow structure at the higher flow stage. Turbulent events became longer in duration but this was not associated with an increase in the magnitude of contributions to the shear stress, reflecting the interaction between turbulence generating events and overall higher flow velocities which may, for instance, constrain the magnitude of ejections and sweeps. The scale of dominant eddies decreased at the higher flow stage, although eddy length: fish length ratios (based on the characteristic fish species, *Salmo trutta*) were consistently greater than, or less than the critical ratio of 1 (i.e. when eddy length = fish length), indicating minimal impacts on swimming performance from eddy size.

Overall, turbulence properties became more spatially homogenous at the higher flow stage, but with notable exceptions such as eddy scale on the u dimension. The greatest magnitude changes in scale and orientation categories were observed around individual boulders and at the transitions between GUs (pool margins). This suggests that *while the reach may become more hydraulically homogeneous overall, higher magnitude change in the size and orientation of flow structure may be concentrated around individual flow obstructions creating hotspots that may be relevant to aquatic organisms such as fish*. This supports the call in the previous section for *greater consideration of the influence of individual small-scale roughness elements on hydraulic habitat*.

For changes in vegetation cover, multivariate statistical analysis revealed the same key gradients in turbulence properties that corresponded broadly with three IPOS categories across the low cover and high cover data sets: intensity, orientation, scale (u dimension) and scale (w dimension). For the intensity parameters, the nature of change with vegetation growth differed between velocity components. Overall, intensity increased with vegetation cover for combined metrics and those relating to fluctuations in the longitudinal (u) and lateral (v) dimensions, particularly around the margins of vegetation patches, while intensity decreased on the w component. These observations indicate that *the presence of aquatic plants generates an intensification of turbulent fluctuations in longitudinal and lateral planes, while suppressing vertical motions*, consistent with previous work. For orientation parameters, predictability of the flow structure was lower and also more spatially variable at the peak vegetation period, reflecting the non-pseudo periodic motions introduced into the flow by natural movement of plant foliage. The reduction in predictability and the reduction in size of dominant eddies decreased at the higher vegetation cover also illustrates the role of aquatic plants in breaking down eddies.

These changes appear to have direct ecological relevance: when vegetation cover was low, a greater number of sample locations were characterised by eddy length: fish length ratios approximately equal to 1 (eddy length = fish length). Hence, during periods of higher vegetation cover the role of vegetation in breaking down eddies may be important in generating suitable habitat for adult and juvenile brown trout. This suggests *an additional habitat function of aquatic plants may arise from the interactions between vegetation, turbulence and fish habitat use*.

Overall, the presence of vegetation was associated with greater spatial heterogeneity in turbulence properties. This is important, since GUs tend to be considered separately from vegetation parameters in visual assessments of habitats. *The interactions between GUs and vegetation should be considered more explicitly in both river assessment and restoration design to maximise hydraulic habitat benefits*.

8.2.4 Interactions between turbulence and wood habitat features, and implications for fish habitat use

The objectives of Chapter 7 sought to explore the relationships between large wood habitat, turbulence properties and fish habitat use and swimming costs at the patch scale under field conditions. A novel combination of field survey and underwater videography was used in two patches around submerged wood pieces in the intermediate gradient (riffle-pool dominated) reach.

Both wood features studied generated two zones as a result of flow diversion around the wood: lower intensity areas around the wood pieces at the channel margins; and higher intensity areas at the transition to adjacent free flow areas. One patch was used primarily by smaller fish which exhibited a higher frequency of exploring behaviour, while the other was used primarily by larger fish for station-holding. Estimated swimming cost ratios may partly explain this habitat use: increased energy costs were associated with patch occupied by smaller fish, and smaller fish are generally more able to reduce energy costs through swimming efficiency gains. In both cases, fish were concentrated in the low intensity zones around the wood pieces and fish abundance was most closely associated with higher order flow properties such as intensity and eddy length: fish length ratio. This finding is particularly important since it provides field evidence that *more sophisticated IPOS-related flow parameters provide a better explanation of fish behaviour and habitat use compared to simpler, traditional metrics such as temporally averaged streamwise velocity.*

8.3 Management implications and future research directions

The IPOS framework parameters explored in this thesis constitute a wide-ranging portfolio of turbulence properties. These range from simpler time-averaged measures such as Turbulent Kinetic Energy and Reynolds Stresses, to time series analysis in the time and frequency domains. Increasing sophistication of turbulence descriptors is necessarily associated with increasing analytical demands, and the suite of metrics appropriate to a particular study will depend on the questions posed. It is hoped that advances in data acquisition, numerical codes and computer hardware (Tonina and Jorde, 2014) will help to facilitate more widespread application within river assessment and restoration contexts, as well as river science.

The new insights into interactions between geomorphology, hydraulics and aquatic organisms highlighted above offer some opportunities for refining habitat assessment and restoration design protocols. In particular, future work could focus on capturing the sub-geomorphic unit scale features of significance for turbulence generation and improving the field technique capable of directly estimate eddy dimension and vorticity. The availability of robust sensors that have minimal interference with the flow field can assist in this regard and ongoing developments such as the adaptation of PIV methods for widespread field use represent a potential step-change. Such methods enable direct capture of the spatio-temporally evolving characteristics of coherent flow structures as opposed to their computation from time series data at a single location. In addition to exploring the turbulence across sub-geomorphic scale features, future research needs to investigate the effect of vegetation on key hydraulic key variables throughout the growth season and also on the influence of grain size on eddy distribution at different spatial scales. For example, Taylor's frozen turbulence hypothesis, used in this thesis to estimate the eddy size, is an assumption and needs to be used with caution (Clifford *et al.,* 1996). Ultimately, further examination of the relationships between depth and grain size may help to clarify the eddy propagation.

REFERENCES

ABBE, T. B., BROOKS, A. P. & MONTGOMERY, D. R. 2003. Wood in in River Rehabilitation and Management. *American Fisheries Society Symposium*.

ABBE, T. B. & MONTGOMERY, D. R. 1996. Large woody debris jams, channel hydraulics and habitat formation in large rivers. *Regulated Rivers Research & Management,* 12**,** 201-221.

ADRIAN, R., CHRISTENSEN, K. & LIU, Z.-C. 2000. Analysis and interpretation of instantaneous turbulent velocity fields. *Experiments in Fluids,* 29**,** 275-290.

ADRIAN, R. J. 2005. Twenty years of particle image velocimetry. *Experiments in Fluids,* 39**,** 159-169.

ADRIAN, R. J. 2007. Hairpin vortex organization in wall turbulence. *Physics of Fluids,* 19**,** 041301.

ARGYROPOULOS, C. & MARKATOS, N. 2015. Recent advances on the numerical modelling of turbulent flows. *Applied Mathematical Modelling,* 39**,** 693-732.

ARNOTT, S., HILTON, J. & WEBB, B. 2009. The impact of geological control on flow accretion in lowland permeable catchments. *Hydrology Research,* 40**,** 533-543.

ASAEDA, T. & RASHID, M. 2016. Effects of turbulence motion on the growth and physiology of aquatic plants. *Limnologica-Ecology and Management of Inland Waters*.

BAGNOLD, R. 1966. An approach to the sediment transport problem from general physics. *US Geological Survey Professional Paper,* 422-I.

BAKER, K., CHADWICK, M. & HAJI SULAIMAN, Z. 2016. Eco-hydromorphic Classification for Understanding Stream Macroinvertebrate Biodiversity in Brunei Darussalam, Northern Borneo. *Zoological Studies,* 55**,** 1-26.

BARBER, I. & WRIGHT, H. A. 2001. How strong are familiarity preferences in shoaling fish? *Animal Behaviour,* 61**,** 975-979.

BELLETTI, B., RINALDI, M., BUIJSE, A., GURNELL, A. & MOSSELMAN, E. 2015a. A review of assessment methods for river hydromorphology. *Environmental Earth Sciences,* 73**,** 2079-2100.

BELLETTI, B., RINALDI, M., COMITI, F., NARDI, L., MAO, L. & BUSSETTINI, M. 2015b. The Geomorphic Units survey and classification System (GUS). Deliverable, D6.2, 2007-2013. Available at: http://www.reformrivers.eu/geomorphic-units-survey-and-classification-system-gus.

BERNHARDT, E. S., PALMER, M., ALLAN, J., ALEXANDER, G., BARNAS, K., BROOKS, S., CARR, J., CLAYTON, S., DAHM, C. & FOLLSTAD-SHAH, J. 2005. Synthesizing US river restoration efforts. *Science,* 308**,** 636-637.

BEST, J. 1993. On the interactions between turbulent flow structure, sediment transport and bedform development: some considerations from recent experimental research. *In:* CLIFFORD, N. J., FRENCH, J. R. AND

HARDISTY, J. (ed.) *Turbulence: Perspectives on Flow and Sediment Transport.* Chichester, UK: John Wiley & Sons.

BEST, J., BUFFIN-BÉLANGER, T., KIRKBRIDE, A. & REID, I. 2001. Visualization of coherent flow structures associated with particle clusters: Temporal and spatial characterization revealed using ultrasonic Doppler velocity profiling. *IAHR Conference.* Canterbury New Zealand Hydraulic Society

BETTI, L. 2001. Carta ittica del Trentino. *Servizio Faunistico, 255 pp*.

BISSON, P. A., BILBY, R. E., BRYANT, M. D., DOLLOFF, C. A., GRETTE, G. B., HOUSE, R. A., MURPHY, M. L., KOSKI, K. V. & SEDELL, J. R. 1987. Large woody debris in forested streams in the Pacific Northwest: past, present, and future. *Streamside Management: Forestry and Fishery Interactions.* .

BLANCKAERT, K., GARCIA, X. F., RICARDO, A. M., CHEN, Q. & PUSCH, M. 2013. The role of turbulence in the hydraulic environment of benthic invertebrates. *Ecohydrology,* 6**,** 700-712.

BOISCLAIR, D. & TANG, M. 1993. Empirical analysis of the influence of swimming pattern on the net energetic cost of swimming in fishes. *Journal of Fish Biology,* 42**,** 169-183.

BRADBROOK, K., BIRON, P., LANE, S., RICHARDS, K. & ROY, A. 1998. Investigation of controls on secondary circulation in a simple confluence geometry using a three‐dimensional numerical model. *Hydrological Processes,* 12**,** 1371-1396.

BRASINGTON, J., RUMSBY, B. & MCVEY, R. 2000. Monitoring and modelling morphological change in a braided gravel-bed river using high resolution GPS-based survey. *Earth Surface Processes and Landforms,* 25**,** 973-990.

BREVIS, W., GARCÍA-VILLALBA, M. & NIÑO, Y. 2014. Experimental and large eddy simulation study of the flow developed by a sequence of lateral obstacles. *Environmental Fluid Mechanics,* 14**,** 873-893.

BRIERLEY, G. J. & FRYIRS, K. A. 2013. *Geomorphology and river management: applications of the river styles framework*, John Wiley & Sons.

BROOKS, A. J., HAEUSLER, T., REINFELDS, I. & WILLIAMS, S. 2005. Hydraulic microhabitats and the distribution of macroinvertebrate assemblages in riffles. *Freshwater Biology,* 50**,** 331-344.

BUFFIN-BÉLANGER, T. & ROY, A. G. 1998. Effects of a pebble cluster on the turbulent structure of a depth-limited flow in a gravel-bed river. *Geomorphology,* 25**,** 249-267.

BUFFIN-BÉLANGER, T. & ROY, A. G. 2005. 1 min in the life of a river: selecting the optimal record length for the measurement of turbulence in fluvial boundary layers. *Geomorphology,* 68**,** 77-94.

BUFFINGTON, J. & MONTGOMERY, D. 2013. Geomorphic classification of rivers. Available at: https://www.fs.fed.us/rm/pubsother/rmrs2013buffingtonj001.pdf.

BUFFINGTON, J. M. & MONTGOMERY, D. R. 1999. A procedure for classifying textural facies in gravel-bed rivers. *Water Resource Research,* 35**,** 1903-1914.

BUNTE, K. & ABT, S. R. 2001. Sampling surface and subsurface particle-size distributions in wadable gravel-and cobble-bed streams for analyses in sediment transport, hydraulics, and streambed monitoring. Fort Collins,CO:

U.S. Department of Agriculture, Forest Service, Rocky Mountain Research Station. .

CAMERON, S., NIKORA, V., ALBAYRAK, I., MILER, O., STEWART, M. & SINISCALCHI, F. 2013. Interactions between aquatic plants and turbulent flow: a field study using stereoscopic PIV. *Journal of Fluid Mechanics,* 732**,** 345-372.

CHAMPION, P. D. & TANNER, C. C. 2000. Seasonality of macrophytes and interaction with flow in a New Zealand lowland stream. *Hydrobiologia,* 441**,** 1-12.

CHANCE, M. & CRAIG, D. 1986. Hydrodynamics and behaviour of Simuliidae larvae (Diptera). *Canadian Journal of Zoology,* 64**,** 1295-1309.

CHANSON, H. Acoustic Doppler velocimetry (ADV) in the field and in laboratory: practical experiences. International Meeting on Measurements and Hydraulics of Sewers IMMHS'08, Summer School GEMCEA/LCPC, 2008 Bouguenais, France, 19-21 August 2008. Department of Civil Engineering at the University of Queensland, 49-66.

CHATFIELD, C. 2004. *The analysis of time series: an introduction,* Boca Raton, Florida, USA, CRC press LLC.

CHIN, A. 2003. The geomorphic significance of step–pools in mountain streams. *Geomorphology,* 55**,** 125-137.

CHINESE ACADEMY OF FISHERY SCIENCE 2006. *Phoxinus phoxinus (Linnaeus, 1758). [online] at:* http://eol.org/data_objects/21013417.

CHURCH, M. 1992. Channel morphology and typology. *In:* CALOW, P. A. P., G. E. (ed.) *The rivers handbook: Hydrological and Ecological Principles. Pages 126-143.* Oxford: Blackwell.

CLIFFORD, N. & FRENCH, J. 1993a. Monitoring and modelling turbulent flows: historical and contemporary perspectives. *In:* CLIFFORD, N. J., FRENCH, J. R. AND HARDISTY, J. (ed.) *Turbulence: Perspectives on Flow and Sediment Transport.* John Wiley & Sons: 1-34.

CLIFFORD, N. & FRENCH, J. 1993b. Monitoring and modelling turbulent flows: some analytical and conceptual issues. *In:* CLIFFORD, N. J., FRENCH, J. R. AND HARDISTY, J. (ed.) *Turbulence: Perspectives on Flow and Sediment Transport.* Chichester, UK: John Wiley & Sons Ltd: 93-120.

CLIFFORD, N., ROBERT, A. & RICHARDS, K. 1992. Estimation of flow resistance in gravel bedded rivers: A physical explanation of the multiplier of roughness length. *Earth Surface Processes and Landforms,* 17**,** 111-126.

CLIFFORD, N. J., FRENCH, J. R. AND HARDISTY, J. 1993c. *Turbulence: Perspectives on Flow And Sediment Transport,* Chichester, UK, John Wiley & Sons Ltd.

CLIFFORD, N. 1996. Morphology and stage-dependent flow structure in a gravel-bed river. In: ASHWORTH, P., BENNETT, S. J., BEST, J. L. & MCLELLAND, S (ed.) Coherent flow structures in open channels. Chichester: John Wiley and Sons. Pag. 545-566.

CLIFFORD, N. J. 1997. A comparison of flow intensities in alluvial rivers: characteristics and implications for modelling flow processes. Earth Surface Processes and Landforms, 23, 109-121.

CLIFFORD, N. J., SOAR, P. J., EMERY, J. C., GURNELL, A. M. & PETTS, G. E. 2002a. Sustaining water-related ecosystems-the role of in-stream bedform design in river channel rehabilitation. Friend 2002- Regional Hydrology: Bridging the Gap Between Research and Practice (Proceedings of the Fourth International FRIEND Conference), 407-413.

CLIFFORD, N. J., SOAR, P. J., EMERY, J. C., GURNELL, A. M. & PETTS, G. E. 2002b. Numerical flow modelling for eco-hydraulic and river rehabilitation applications: a case study of the River Cole, Birmingham, UK. . In: Bousmar, D. and Zech, Y (eds.), River Flow 2002 - Proceedings of the International Conference on Fluvial Hydraulics, 4-6 September 2002, Louvain-le-Neuve, Belgium. Lisse, Swets & Zeitlinger/Balkema: 1195-1204.

CLIFFORD, N. J., SOAR, P. J., HARMAR, O. P., GURNELL, A. M., PETTS, G. E. & EMERY, J. C. 2005. Assessment of hydrodynamic simulation results for eco-hydraulic and eco-hydrological applications: A spatial semivariance approach. *Hydrological Processes,* 19**,** 3631-3648.

CLIFFORD, N. J., HARMAR, O. P., HARVEY, G. & PETTS, G. E. 2006. Physical habitat, eco-hydraulics and river design: a review and re-evaluation of some popular concepts and methods. *Aquatic Conservation: Marine and Freshwater Ecosystems,* 16**,** 389-408.

CLIFFORD, N., WRIGHT, N., HARVEY, G., GURNELL, A., HARMAR, O. & SOAR, P. 2009. Numerical modeling of river flow for ecohydraulic applications: Some experiences with velocity characterization in field and simulated data. Journal of Hydraulic Engineering, 136, 1033-1041.

COMITI, F., LUCÍA, A. & RICKENMANN, D. 2016. Large wood recruitment and transport during large floods: A review. *Geomorphology,* 269**,** 23-39.

CONSTANTINESCU, G., MIYAWAKI, S., RHOADS, B., SUKHODOLOV, A. & KIRKIL, G. 2011. Structure of turbulent flow at a river confluence with momentum and velocity ratios close to 1: Insight provided by an eddy - resolving numerical simulation. *Water Resources Research,* 47**,** W05507.

COTEL, A. & WEBB, P. Living in a turbulent world-Impacts on fish habitat choices and swimming. Integrative and comparative biology, 2015. Oxford Univ press inc journals dept, 2001 Evans RD, Cary, NC 27513 USA, 662-672.

COTEL, A. J., WEBB, P. W. & TRITICO, H. 2006. Do brown trout choose locations with reduced turbulence? *Transactions of the American Fisheries Society,* 135**,** 610-619.

CREUTIN, J., MUSTE, M., BRADLEY, A., KIM, S. & KRUGER, A. 2003. River gauging using PIV techniques: a proof of concept experiment on the Iowa River. *Journal of Hydrology,* 277**,** 182-194.

CUI, Y. & WOOTTON, R. 1988. The metabolic rate of the minnow, *Phoxinus phoxinus (L.)(Pisces: Cyprinidae*), in relation to ration, body size and temperature. *Functional ecology***,** 157-161.

DAVID, G. C., LEGLEITER, C. J., WOHL, E. & YOCHUM, S. E. 2013. Characterizing spatial variability in velocity and turbulence intensity using 3-D acoustic Doppler velocimeter data in a plane-bed reach of East St. Louis Creek, Colorado, USA. *Geomorphology,* 183**,** 28-44.

DAVIDSON, P. 2004. *Turbulence: an introduction for scientists and engineers*, Oxford University Press, USA.

DELCOURT, J., DENOËL, M., YLIEFF, M. & PONCIN, P. 2013. Video multitracking of fish behaviour: a synthesis and future perspectives. *Fish and Fisheries,* 14**,** 186-204.

DELL, A. I., BENDER, J. A., BRANSON, K., COUZIN, I. D., DE POLAVIEJA, G. G., NOLDUS, L. P., PÉREZ-ESCUDERO, A., PERONA, P., STRAW, A. D. & WIKELSKI, M. 2014. Automated image-based tracking and its application in ecology. *Trends in Ecology & Evolution,* 29**,** 417-428.

DENG, Z., GUENSCH, G. R., MCKINSTRY, C. A., MUELLER, R. P., DAUBLE, D. D. & RICHMOND, M. C. 2005. Evaluation of fish-injury mechanisms during exposure to turbulent shear flow. *Canadian Journal of Fisheries and Aquatic Sciences,* 62**,** 1513-1522.

DEVI, T. B. & KUMAR, B. 2016. Flow characteristics in an alluvial channel covered partially with submerged vegetation. *Ecological Engineering,* 94**,** 478-492.

DUC, B. M., WENKA, T. & RODI, W. 2004. Numerical modeling of bed deformation in laboratory channels. *Journal of Hydraulic Engineering,* 130**,** 894-904.

DZIUBAN, C. D. & SHIRKEY, E. C. 1974. When is a correlation matrix appropriate for factor analysis? Some decision rules. *Psychological Bulletin,* 81**,** 358-361.

EMERY, J. C., GURNELL, A. M., CLIFFORD, N. J., PETTS, G. E., MORRISSEY, I. P. & SOAR, P. J. 2003. Classifying the hydraulic performance of riffle–pool bedforms for habitat assessment and river rehabilitation design. *River Research and Applications,* 19**,** 533-549.

ENDERS, E. & BOISCLAIR, D. 2016. Effects of environmental fluctuations on fish metabolism: Atlantic salmon *Salmo salar* as a case study. *Journal of Fish Biology,* 88**,** 344-358.

ENDERS, E. C., BOISCLAIR, D. & ROY, A. G. 2003. The effect of turbulence on the cost of swimming for juvenile Atlantic salmon (*Salmo salar*). *Canadian Journal of Fisheries and Aquatic Sciences,* 60**,** 1149-1160.

ENVIRONMENT AGENCY 2010a. Rehabilitating the river Frome SSSI. Technical Report.

ENVIRONMENT AGENCY 2010b. Environment Agency Fish Pass Manual.

FARGE, M. 1992. Wavelet transforms and their applications to turbulence. *Annual Review of Fluid Mechanics,* 24**,** 395-458.

FENOGLIO, S., BOANO, F., BO, T., REVELLI, R. & RIDOLFI, L. 2013. The impacts of increasing current velocity on the drift of Simulium monticola (Diptera: Simuliidae): a laboratory approach. *Italian Journal of Zoology,* 80**,** 443-448.

FERNÁNDEZ, D. P., BARQUÍN, J. & RAVEN, P. J. 2011. A review of river habitat characterisation methods: indices vs. characterisation protocols. *Limnetica,* 30**,** 217-234.

FERNER, M. C. & WEISSBURG, M. J. 2005. Slow-moving predatory gastropods track prey odors in fast and turbulent flow. *Journal of Experimental Biology,* 208**,** 809-819.

FINNIGAN, J. 2000. Turbulence in plant canopies. *Annual Review of Fluid Mechanics,* 32**,** 519-571.

FISH, F. E. 2010. Swimming strategies for energy economy. *In:* PAOLO DOMENICI, B. G. K. (ed.) *Fish Locomotion: An Etho-ecological Perspective.* Oxford: Taylor and Francis.

FOX, J. & PATRICK, A. 2008. Large-scale eddies measured with large scale particle image velocimetry. *Flow Measurement and Instrumentation,* 19**,** 283-291.

FROESE, R. 1998. Short Communication Length-weight relationships for 18 less-studied fish species. *Journal Applied Ichthyology,* 14**,** 117-118.

FRYIRS, K. A. & BRIERLEY, G. J. 2016. Assessing the geomorphic recovery potential of rivers: forecasting future trajectories of adjustment for use in management. *Wiley Interdisciplinary Reviews: Water,* 3**,** 727-748.

GARCÍA, C. M., CANTERO, M. I., NIÑO, Y. & GARCÍA, M. H. 2005. Turbulence measurements with acoustic Doppler velocimeters. *Journal of Hydraulic Engineering,* 131**,** 1062-1073.

GAZZOLA, M., ARGENTINA, M. & MAHADEVAN, L. 2014. Scaling macroscopic aquatic locomotion. *Nature Physics,* 10**,** 758-761.

GIPPEL, C. J. 1995. Environmental hydraulics of large woody debris in streams and rivers. *Journal of Environmental Engineering,* 121**,** 388-395.

GOOVAERTS, P. 1997. *Geostatistics for Natural Resources Evaluation*, Oxford University Press

GORING, D. G. & NIKORA, V. I. 2002. Despiking acoustic Doppler velocimeter data. *Journal of Hydraulic Engineering,* 128**,** 117-126.

GRABOWSKI, R. & GURNELL, A. 2014. Hydromorphological assessment of the River Frome (UK): a lowland Northern European river. *Blamauer B, Belletti B, García De Jalón D, González del Tánago M, Grabowski RC, Gurnell AM, Habersack H, Klösch M, Marcinkowski P, Martínez-Fernández V, Nardi L, Okruszko T, Rinaldi M (2014) Catchment case studies: full applications of the hierarchical multi-scale framework. Deliverable*

GREEN, J. C. 2005. Velocity and turbulence distribution around lotic macrophytes. *Aquatic Ecology,* 39**,** 01-10.

GURNELL, A. 2014. Plants as river system engineers. *Earth Surface Processes and Landforms,* 39**,** 4-25.

GURNELL, A. & PETTS, G. 2006. Trees as riparian engineers: the Tagliamento River, Italy. *Earth Surface Processes and Landforms,* 31**,** 1558-1574.

GURNELL, A. & SWEET, R. 1998. The distribution of large woody debris accumulations and pools in relation to woodland stream management in a small, low‐gradient stream. *Earth Surface Processes and Landforms,* 23**,** 1101-1121.

GURNELL, A., TOCKNER, K., EDWARDS, P. & PETTS, G. 2005. Effects of deposited wood on biocomplexity of river corridors. *Frontiers in Ecology and the Environment,* 3**,** 377-382.

GURNELL, A., VAN OOSTERHOUT, M., DE VLIEGER, B. & GOODSON, J. 2006. Reach‐scale interactions between aquatic plants and physical habitat: River Frome, Dorset. *River Research and Applications,* 22**,** 667-680.

GURNELL, A. M., PETTS, G. E., HANNAH, D. M., SMITH, B. P., EDWARDS, P. J., KOLLMANN, J., WARD, J. V. & TOCKNER, K. 2000. Wood storage within the active zone of a large European gravel-bed river. *Geomorphology,* 34**,** 55-72.

GURNELL, A. M., PETTS, G. E., HANNAH, D. M., SMITH, B. P., EDWARDS, P. J., KOLLMANN, J., WARD, J. V. & TOCKNER, K. 2001. Riparian vegetation and island formation along the gravel-bed Fiume Tagliamento, Italy. *Earth Surface Processes and Landforms,* 26**,** 31-62.

GURNELL, A. M., RINALDI, M., BELLETTI, B., BIZZI, S., BLAMAUER, B., BRACA, G., BUIJSE, A., BUSSETTINI, M., CAMENEN, B. & COMITI, F. 2016. A multi-scale hierarchical framework for developing understanding of river behaviour to support river management. *Aquatic Sciences,* 78**,** 1-16.

HAMILTON, W. D. 1971. Geometry for the selfish herd. *Journal of Theoretical Biology,* 31**,** 295-311.

HARDY, R. J., BEST, J. L., LANE, S. N. & CARBONNEAU, P. E. 2009. Coherent flow structures in a depth-limited flow over a gravel surface: The role of near-bed turbulence and influence of Reynolds number. *Journal of Geophysical Research: Earth Surface,* 114, F01003.

HARPER, D. M., KEMP, J. L., VOGEL, B. & NEWSON, M. D. 2000. Towards the assessment of 'ecological integrity'in running waters of the United Kingdom. *Assessing the Ecological Integrity of Running Waters.* Springer.

HART, D. D., CLARK, B. D. & JASENTULIYANA, A. 1996. Fine‐scale field measurement of benthic flow environments inhabited by stream invertebrates. *Limnology and Oceanography,* 41**,** 297-308.

HART, D. D. & FINELLI, C. M. 1999. Physical-biological coupling in streams: the pervasive effects of flow on benthic organisms. *Annual Review of Ecology and Systematics,* 30**,** 363-395.

HART, P. J. 2003. Habitat use and feeding behaviour in two closely related fish species, the three‐spined and nine‐spined stickleback: An experimental analysis. *Journal of Animal Ecology,* 72**,** 777-783.

HARVEY, G. L. & CLIFFORD, N. J. 2009. Microscale hydrodynamics and coherent flow structures in rivers: implications for the characterization of physical habitat. *River Research and Applications,* 25**,** 160-180.

HARVEY, G. L., CLIFFORD, N. J. & GURNELL, A. M. 2008. Towards an ecologically meaningful classification of the flow biotope for river inventory, rehabilitation, design and appraisal purposes. *Journal of Environmental Management,* 88**,** 638-650.

HIGHAM, T. E., STEWART, W. J. & WAINWRIGHT, P. C. 2015. Turbulence, temperature, and turbidity: the ecomechanics of predator–prey interactions in fishes. *Integrative and Comparative Biology,* 55**,** 6-20.

HOCKLEY, F. A., WILSON, C., BREW, A. & CABLE, J. 2014. Fish responses to flow velocity and turbulence in relation to size, sex and parasite load. *Journal of The Royal Society Interface,* 11**,** 20130814.

HOSMER JR, D. W. & LEMESHOW, S. 2004. *Applied logistic regression*, John Wiley & Sons.

HRODEY, P. J., KALB, B. J. & SUTTON, T. M. 2008. Macroinvertebrate community response to large-woody debris additions in small warmwater streams. *Hydrobiologia,* 605**,** 193-207.

JIMÉNEZ, J. 2011. Cascades in wall-bounded turbulence. *Annual Review of Fluid Mechanics,* 44**,** 27.

JOHNSON, M., THOMAS, R., DIJKSTRA, J., PAUL, M., PENNING, W. & RICE, S. 2014. Using surrogates, including scaling issues, in laboratory flumes and basins. *In:* FROSTICK, L. E., THOMAS, R.E., JOHNSON, M.F., RICE, S.P.

& MCLELLAND, S. (ed.) *Users Guide to Ecohydraulic Modelling and Experimentation: Experience of the Ecohydraulic Research Team (PISCES) of the HYDRALAB Network.* Leiden, The Netherlands: CRC Press.

JOWETT, I. 2003. Hydraulic constraints on habitat suitability for benthic invertebrates in gravel-bed rivers. *River Research and Applications,* 19**,** 495-507.

JOWETT, I. G. 1993. A method for objectively identifying pool, run, and riffle habitats from physical measurements. *New Zealand Journal of Marine and Freshwater Research,* 27**,** 241-248.

KARRENBERG, S., KOLLMANN, J., EDWARDS, P. J., GURNELL, A. M. & PETTS, G. E. 2003. Patterns in woody vegetation along the active zone of a near-natural Alpine river. *Basic and Applied Ecology,* 4**,** 157-166.

KEMP, J. L., HARPER, D. M. & CROSA, G. A. 1999. Use of 'functional habitats' to link ecology with morphology and hydrology in river rehabilitation. *Aquatic Conservation: Marine and Freshwater Ecosystems,* 9**,** 159-178.

KEMP, J. L., HARPER, D. M. & CROSA, G. A. 2000. The habitat-scale ecohydraulics of rivers. *Ecological Engineering,* 16**,** 17-29.

KIRKBRIDE, A. & FERGUSON, R. 1995. Turbulent flow structure in a gravel-bed river: Markov chain analysis of the fluctuating velocity profile. *Earth Surface Processes Landforms,* 20**,** 721-733.

KOLMOGOROV, A. N. 1941. The local structure of turbulence in incompressible viscous fluid for very large Reynolds numbers. *Proceedings: Mathematical and Physical Science.* The Royal Society.

KONDOLF, G. M., MONTGOMERY, D. R., PIÉGAY, H. & SCHMITT, L. 2005. Geomorphic Classification of Rivers and Streams. *In:* KONDOLF, G. M. A. P., H. (ed.) *Tools in Fluvial Geomorphology.* John Wiley & Sons, Ltd.

KOTTELAT, M. & FREYHOF, J. R. 2007. *Handbook of European freshwater fishes*, Publications Kottelat.

LACEY, R., NEARY, V. S., LIAO, J. C., ENDERS, E. C. & TRITICO, H. M. 2012. The IPOS framework: linking fish swimming performance in altered flows from laboratory experiments to rivers. *River Research and Applications,* 28**,** 429-443.

LACEY, R. J. & ROY, A. G. 2008a. Fine-scale characterization of the turbulent shear layer of an instream pebble cluster. *Journal of Hydraulic Engineering,* 134**,** 925-936.

LACEY, R. J. & ROY, A. G. 2008b. The spatial characterization of turbulence around large roughness elements in a gravel-bed river. *Geomorphology,* 102**,** 542-553.

LAMARRE, H. & ROY, A. G. 2005. Reach scale variability of turbulent flow characteristics in a gravel-bed river. *Geomorphology,* 68**,** 95-113.

LANE, S., BIRON, P., BRADBROOK, K., BUTLER, J., CHANDLER, J., CROWELL, M., MCLELLAND, S., RICHARDS, K. & ROY, A. 1998. Three-dimensional measurement of river channel flow processes using acoustic Doppler velocimetry. *Earth Surface Processes and Landforms,* 23**,** 1247-1267.

LANE, S., BRADBROOK, K., RICHARDS, K., BIRON, P. & ROY, A. 1999. The application of computational fluid dynamics to natural river channels: three-dimensional versus two-dimensional approaches. *Geomorphology,* 29**,** 1-20.

LATULIPPE, C., LAPOINTE, M. F. & TALBOT, T. 2001. Visual characterization technique for gravel‐cobble river bed surface sediments; validation and environmental applications Contribution to the programme of CIRSA(Centre Interuniversitaire de Recherche sur le Saumon Atlantique). *Earth Surface Processes and Landforms,* 26**,** 307-318.

LEEDER, M. 1983. On the dynamics of sediment suspension by residual Reynolds stresses - confirmation of Bagnold's theory. *Sedimentology,* 30**,** 485-491.

LEGENDRE, P. & LEGENDRE, L. F. 2012. *Numerical ecology,* Amsterdam, The Netherlands, Elsevier.

LEGLEITER, C. J., PHELPS, T. L. & WOHL, E. E. 2007. Geostatistical analysis of the effects of stage and roughness on reach-scale spatial patterns of velocity and turbulence intensity. *Geomorphology,* 83**,** 322-345.

LI, Y., WANG, Y., ANIM, D. O., TANG, C., DU, W., NI, L., YU, Z. & ACHARYA, K. 2014. Flow characteristics in different densities of submerged flexible vegetation from an open-channel flume study of artificial plants. *Geomorphology,* 204**,** 314-324.

LIAO, J. C. 2007. A review of fish swimming mechanics and behaviour in altered flows. *Philosophical Transactions of the Royal Society B: Biological Sciences,* 362**,** 1973-1993.

LIAO, J. C., BEAL, D. N., LAUDER, G. V. & TRIANTAFYLLOU, M. S. 2003. Fish exploiting vortices decrease muscle activity. *Science,* 302**,** 1566-1569.

LIAO, J. C. & COTEL, A. 2013. Effects of Turbulence on Fish Swimming in Aquaculture. *In:* PALSTRA, A. P. & PLANAS, J. V. (eds.) *Swimming Physiology of Fish: Towards Using Exercise to Farm a Fit Fish in Sustainable Aquaculture.* Berlin, Heidelberg: Springer Berlin Heidelberg.

LIMERINOS, J. T. 1970. Determination of the Manning coefficient from measured bed roughness in natural channels. Washington: Department of Water Resources.

LISLE, T. E. 1995. Effects of coarse woody debris and its removal on a channel affected by the 1980 eruption of Mount St. Helens, Washington. *Water Resources Research,* 31**,** 1797-1808.

LOGAN, P. & BROOKER, M. 1983. The macroinvertebrate faunas of riffles and pools. *Water Research,* 17**,** 263-270.

LU, S. & WILLMARTH, W. 1973. Measurements of the structure of the Reynolds stress in a turbulent boundary layer. *Journal of Fluid Mechanics,* 60**,** 481-511.

LUPANDIN, A. 2005. Effect of flow turbulence on swimming speed of fish. *Biology Bulletin,* 32**,** 461-466.

MACVICAR, B. & ROY, A. 2007a. Hydrodynamics of a forced riffle pool in a gravel bed river: 1. Mean velocity and turbulence intensity. *Water Resources Research,* 43.

MACVICAR, B. & ROY, A. 2007b. Hydrodynamics of a forced riffle pool in a gravel bed river: 2. Scale and structure of coherent turbulent events. *Water Resources Research,* 43.

MADDOCK, I. 1999. The importance of physical habitat assessment for evaluating river health. *Freshwater Biology,* 41**,** 373-391.

MADSEN, J. D., CHAMBERS, P. A., JAMES, W. F., KOCH, E. W. & WESTLAKE, D. F. 2001. The interaction between water movement, sediment dynamics and submersed macrophytes. *Hydrobiologia,* 444**,** 71-84.

MAIA, A., SHELTZER, A. P. & TYTELL, E. D. 2015. Streamwise vortices destabilize swimming bluegill sunfish (*Lepomis macrochirus*). *Journal of Experimental Biology,* 218**,** 786-792.

MANNERS, R. B., DOYLE, M. & SMALL, M. 2007. Structure and hydraulics of natural woody debris jams. *Water Resources Research,* 43**,** W06432.

MARJORIBANKS, T. I., HARDY, R. J., LANE, S. N. & PARSONS, D. R. 2016. Does the canopy mixing layer model apply to highly flexible aquatic vegetation? Insights from numerical modelling. *Environmental Fluid Mechanics,* 16**,** 1-25.

MARQUIS, G. A. & ROY, A. G. 2011. Bridging the gap between turbulence and larger scales of flow motions in rivers. *Earth Surface Processes and Landforms,* 36**,** 563-568.

MCLELLAND, S. J. & NICHOLAS, A. P. 2000. A new method for evaluating errors in high frequency ADV measurements. *Hydrological Processes,* 14**,** 351-366.

MEIRE, D., KONDZIOLKA, J. & NEPF, H. Patches in a side-by-side configuration: a description of the flow and deposition fields. Informatics, Networking and Intelligent Computing: Proceedings of the 2014 International Conference on Informatics, Networking and Intelligent Computing (INIC 2014), 16-17 November 2014, Shenzhen, China, 2015. CRC Press, 401.

MILLS, C. A. & ELORANTA, A. The biology of *Phoxinus phoxinus (L.)* and other littoral zone fishes in Lake Konnevesi, central Finland. Annales Zoologici Fennici, 1985. JSTOR, 1-12.

MILNE, J. & SEAR, D. 1997. Modelling river channel topography using GIS. *International Journal of Geographical Information Science,* 11**,** 499-519.

MIRANDA, R., OSCOZ, J., LEUNDA, P. & ESCALA, M. 2006. Weight–length relationships of cyprinid fishes of the Iberian Peninsula. *Journal of Applied Ichthyology,* 22**,** 297-298.

MONTGOMERY, D. R. & BUFFINGTON, J. M. 1997. Channel-reach morphology in mountain drainage basins. *Geological Society of America Bulletin,* 109**,** 596-611.

MONTGOMERY, D. R., COLLINS, B. D., BUFFINGTON, J. M. & ABBE, T. B. 2003. Geomorphic Effects of Wood in River. *American Fisheries Society Symposium*.

MORRIS, D. G., FLAVIN, R. & MOORE, R. 1990. A digital terrain model for hydrology. *4th International Symposium on Spatial Data Handling.* Zurich.

MORRIS, M., MOHAMMADI, M. H., DAY, S., HONDZO, M. & SOTIROPOULOS, F. 2015. Prediction of Glossosoma biomass spatial distribution in Valley Creek by field measurements and a three ‐ dimensional turbulent open ‐ channel flow model. *Water Resources Research,* 51**,** 1457-1471.

MÜLLER, N. 1996. River dynamics and floodplain vegetation and their alterations due to human impact. *Large Rivers,* 9**,** 477-512.

MUÑOZ-MAS, R., MARTINEZ-CAPEL, F., ALCARAZ-HERNÁNDEZ, J. D. & MOUTON, A. 2015. Can multilayer perceptron ensembles model the ecological niche of freshwater fish species? *Ecological Modelling,* 309**,** 72-81.

NADEN, P., RAMESHWARAN, P., MOUNTFORD, O. & ROBERTSON, C. 2006. The influence of macrophyte growth, typical of eutrophic conditions, on river flow velocities and turbulence production. *Hydrological Processes,* 20**,** 3915-3938.

NAKAGAWA, H. & NEZU, I. 1977. Prediction of the contributions to the Reynolds stress from bursting events in open-channel flows. *Journal of Fluid Mechanics,* 80**,** 99-128.

NEPF, H. 1999. Drag, turbulence, and diffusion in flow through emergent vegetation. *Water Resources Research,* 35**,** 479-489.

NEPF, H. & VIVONI, E. 2000. Flow structure in depth-limited, vegetated flow. *Journal of Geophysical Research: Oceans,* 105**,** 28547-28557.

NEPF, H. M. 2012. Hydrodynamics of vegetated channels. *Journal of Hydraulic Research,* 50**,** 262-279.

NEWSON, M. & NEWSON, C. 2000. Geomorphology, ecology and river channel habitat: mesoscale approaches to basin-scale challenges. *Progress in Physical Geography,* 24**,** 195-217.

NEZU, I. & NAKAGAWA, H. 1995. Turbulence measurements in unsteady free-surface flows. *Flow Measurement and Instrumentation,* 6**,** 49-59.

NIKORA, V. 2010. Hydrodynamics of aquatic ecosystems: an interface between ecology, biomechanics and environmental fluid mechanics. *River Research and Applications,* 26**,** 367-384.

NIKORA, V., ABERLE, J., BIGGS, B., JOWETT, I. & SYKES, J. 2003. Effects of fish size, time ‐ to ‐ fatigue and turbulence on swimming performance: a case study of Galaxias maculatus. *Journal of Fish Biology,* 63**,** 1365-1382.

NORTEK, A. 1998. ADV operation manual. *Vollen, Norway*.

NORTHCUTT, R. G. 1997. Animal behaviour: swimming against the current. *Nature,* 389**,** 915-916.

NYSTROM, E. A., OBERG, K. A. & REHMANN, C. R. Measurement of turbulence with acoustic Doppler current profilers-Sources of error and laboratory results. Hydraulic Measurements and Experimental Methods, 2002 Estes Park, Colorado, 28 July-1 August 2002. 1-10.

ODEH, M., NOREIKA, J., HARO, A., MAYNARD, A., CASTRO-SANTOS, T. & CADA, G. 2002. Evaluation of the effects of turbulence on the behavior of migratory fish. Report prepared for U.S. Department of Energy, Bonneville Power Administration, & Division of Fish and Wildlife, DOE/BP-00000022-1.

ÖMER, K. 2011. Distribution of turbulence statistics in open-channel flow. *International Journal of the Physical Science,* 6**,** 3426-3436.

OPENDATA, T. 2014. OpenData Trentino. [online] at http://dati.trentino.it/dataset?tags=idrografia.

ORTIZ, A. C., ASHTON, A. & NEPF, H. 2013. Mean and turbulent velocity fields near rigid and flexible plants and the implications for deposition. *Journal of Geophysical Research: Earth Surface,* 118**,** 2585-2599.

OSCOZ, J., CAMPOS, F. & ESCALA, M. 2005. Weight–length relationships of some fish species of the Iberian Peninsula. *Journal of Applied Ichthyology,* 21**,** 73-74.

OSEI, N. A., GURNELL, A. M. & HARVEY, G. L. 2015. The role of large wood in retaining fine sediment, organic matter and plant propagules in a small, single-thread forest river. *Geomorphology,* 235**,** 77-87.

PADMORE, C. 1998. The role of physical biotopes in determining the conservation status and flow requirements of British rivers. *Aquatic Ecosystem Health & Management,* 1**,** 25-35.

PADMORE, C., NEWSON, M. & CHARLTON, M. 1998. Instream habitat in gravel bed rivers: identification and characterisation of biotopes. *In:* KLINGEMAN, P. C., BESCHTA, R. L., KOMAR, P. D. AND BRADLEY, J. B., (ed.) *Gravel bed rivers in the environment.*: Highlands Ranch, CO: Water Resources Publications, 345-364.

PADMORE, C. L. 1997. *Physical biotopes in representative river channels: identification, hydraulic characterisation and application.* Newcastle University.

PAN, Y., FOLLETT, E., CHAMECKI, M. & NEPF, H. 2014. Strong and weak, unsteady reconfiguration and its impact on turbulence structure within plant canopies. *Physics of Fluids,* 26**,** 105102.

PAPANICOLAOU, A. N., ELHAKEEM, M. & HILLDALE, R. 2007. Secondary current effects on cohesive river bank erosion. *Water Resources Research,* 43**,** W12418.

PARDO, I., ALVAREZ, M., CASAS, J., MORENO, J., VIVAS, S., BONADA, N., ALBA-TERCEDOR, J., JAIMEZ-CUELLAR, P., MOYA, G. & PRAT, N. 2002. The habitat of the Mediterranean rivers. Design of the habitat diversity index. *Limnetica,* 21**,** 115-133.

PEAKE, S. J. 2008. Swimming performance and behaviour of fish species endemic to Newfoundland and Labrador: A literature review for the purpose of establishing design and water velocity criteria for fishways and culverts. St. John's, NL, Canada: Fisheries and Oceans Canada, 2843, 1-52.

PERKS, J. 2017. Filming freshwater fish (presentation). In: Institute of Fisheries Management Greater London and SE Branch Meeting, 1st February 2017, Kings College London, London, 2017.

PILOTTO, F., BERTONCIN, A., HARVEY, G. L., WHARTON, G. & PUSCH, M. T. 2014. Diversification of stream invertebrate communities by large wood. *Freshwater Biology,* 59**,** 2571-2583.

PITCHER, T. J. 1986. Functions of shoaling behaviour in teleosts. *In:* PITCHER, T. J. (ed.) *The behaviour of teleost fishes.* Springer.

PLATH, M., SARBU, A., ERKOC, K., BIERBACH, D., JOURDAN, J. & SCHLEUCHER, E. 2013. Energetic costs of group-living? A reversed “group effect” in shoaling minnows (*Phoxinus phoxinus*). *Bulletin of Fish Biology Volume,* 14**,** 1-10.

POKRAJAC, D., CAMPBELL, L. J., NIKORA, V., MANES, C. & MCEWAN, I. 2007. Quadrant analysis of persistent spatial velocity perturbations over square-bar roughness. *Experiments in Fluids,* 42**,** 413-423.

POPE, N., WIDDOWS, J. & BRINSLEY, M. 2006. Estimation of bed shear stress using the turbulent kinetic energy approach: a comparison of annular flume and field data. *Continental Shelf Research,* 26**,** 959-970.

POPE, S. B. 2000. *Turbulent flows,* Cambridge, UK, Cambridge University Press.

PRZYBILLA, A., KUNZE, S., RUDERT, A., BLECKMANN, H. & BRÜCKER, C. 2010. Entraining in trout: a behavioural and hydrodynamic analysis. *Journal of Experimental Biology,* 213**,** 2976-2986.

QUINN, J., HICKEY, C. & LINKLATER, W. 1996. Hydraulic influences on periphyton and benthic macroinvertebrates: simulating the effects of upstream bed roughness. *Freshwater Biology,* 35**,** 301-309.

RAUPACH, M. R., FINNIGAN, J. & BRUNET, Y. 1996. Coherent eddies and turbulence in vegetation canopies: the mixing-layer analogy. *Boundary-Layer Meteorology 25th Anniversary Volume, 1970–1995.* Springer.

RAVEN, P., HOLMES, N., DAWSON, F. & EVERARD, M. 1998. Quality assessment using River Habitat Survey data. *Aquatic Conservation: Marine and Freshwater Ecosystems,* 8**,** 477–499.

RHOADS, B. L. & SUKHODOLOV, A. N. 2004. Spatial and temporal structure of shear layer turbulence at a stream confluence. *Water Resources Research,* 40**,** W06304.

RICE, S. P., BUFFIN-BELANGER, T., LANCASTER, J. & REID, I. 2008. Movements of a macroinvertebrate species across a gravel-bed substrate: effects of local hydraulics and micro-topography under increasing discharge. *In:* HABERSACK, H., PIEGAY, H. AND RINALDI M. (ed.) *Gravel-bed rivers VI: from process understanding to river restoration.* Amsterdam, The Netherlands: London : Elsevier Science, pp. 637-660.

RICHARDS, K. S. Stochastic processes in one-dimensional series: an introduction. 1979. Geo Abstracts, University of East Anglia.

RIFFLART, R., CARREL, G., LE COARER, Y. & FONTEZ, B. N. T. 2009. Spatio‐temporal patterns of fish assemblages in a large regulated alluvial river. *Freshwater Biology,* 54**,** 1544-1559.

RINALDI, M., BELLETTI, B., VAN DE BUND, W., BERTOLDI, W., GURNELL, A., BUIJSE, T. & MOSSELMAN, E. 2013a. Review on eco-hydromorphological methods. *Deliverable D1.1, 2007-2013. Available at: http://www.reformrivers.eu/deliverables/d1-1.*

RINALDI, M., GURNELL, A., DEL TÁNAGO, M. G., BUSSETTINI, M. & HENDRIKS, D. 2016. Classification of river morphology and hydrology to support management and restoration. *Aquatic Sciences,* 78**,** 17-33.

RINALDI, M., SURIAN, N., COMITI, F. & BUSSETTINI, M. 2013b. A method for the assessment and analysis of the hydromorphological condition of Italian streams: the Morphological Quality Index (MQI). *Geomorphology,* 180**,** 96-108.

RINALDI, M., SURIAN, N., COMITI, F. & BUSSETTINI, M. 2015. A methodological framework for hydromorphological assessment, analysis and monitoring (IDRAIM) aimed at promoting integrated river management. *Geomorphology,* 251**,** 122-136.

ROBINSON, C. A., THOM, T. J. & LUCAS, M. C. 2000. Ranging behaviour of a large freshwater invertebrate, the white‐clawed crayfish Austropotamobius pallipes. *Freshwater Biology,* 44**,** 509-521.

ROBINSON, S. K. 1991. *Coherent motions in the turbulent boundary layer. Annual Review of Fluid Mechanics,* 23**,** 601-639.

RODI, W., CONSTANTINESCU, G. & STOESSER, T. 2013. *Large-eddy simulation in hydraulics,* London, UK, Crc Press.

ROY, A. G., BUFFIN-BELANGER, T. & DELAND, S. 1996. Scales of turbulent coherent flow structures in a gravel-bed river. *In:* ASHWORTH, P., BENNETT, S. J., BEST, J. L. & MCLELLAND, S (ed.) *Coherent Flow Structures in Open Channels.* Chichester, UK: John Wiley & Sons Ltd, 147-164.

ROY, A. G., BUFFIN-BELANGER, T., LAMARRE, H. & KIRKBRIDE, A. D. 2004. Size, shape and dynamics of large-scale turbulent flow structures in a gravel-bed river. *Journal of Fluid Mechanics,* 500**,** 1-27.

ROY, M., ROY, A. & LEGENDRE, P. 2010. The relations between 'standard'fluvial habitat variables and turbulent flow at multiple scales in morphological units of a gravel-bed river. *River Research and Applications,* 26**,** 439-455.

RRC 2013. Felling and placing trees for habitat and flow diversity. *Manual of River Restoration Techniques ed. Silsoe: River Restoration Centre,* 3**,** 1-12.

RUSELLO, P. J., LOHRMANN, A., SIEGEL, E. & MADDUX, T. 2006. Improvements in acoustic Doppler velocimetery. *7th International Conferrence on Hydroscience and Engineering (ICHE-2006), Sep 10 –Sep 13, Philadelphia, USA.*

SAND ‐ JENSEN, K. & PEDERSEN, O. 1999. Velocity gradients and turbulence around macrophyte stands in streams. *Freshwater Biology,* 42**,** 315-328.

SCHNEIDER, K. N. & WINEMILLER, K. O. 2008. Structural complexity of woody debris patches influences fish and macroinvertebrate species richness in a temperate floodplain-river system. *Hydrobiologia,* 610**,** 235-244.

SHAW, E. 1978. Schooling fishes: the school, a truly egalitarian form of organization in which all members of the group are alike in influence, offers substantial benefits to its participants. *American Scientist,* 66**,** 166-175.

SILVA, A. T., KATOPODIS, C., SANTOS, J. M., FERREIRA, M. T. & PINHEIRO, A. N. 2012. Cyprinid swimming behaviour in response to turbulent flow. *Ecological Engineering,* 44**,** 314-328.

SILVA, A. T., SANTOS, J. M., FERREIRA, M. T., PINHEIRO, A. N. & KATOPODIS, C. 2011. Effects of water velocity and turbulence on the behaviour of Iberian barbel (*Luciobarbus bocagei*, Steindachner 1864) in an experimental pool-type fishway. *River Research and Applications,* 27**,** 360-373.

SMITH, D. L. & BRANNON, E. L. 2007. Influence of cover on mean column hydraulic characteristics in small pool riffle morphology streams. *River Research and Applications,* 23**,** 125-139.

SMITH, D. L., BRANNON, E. L. & ODEH, M. 2005. Response of juvenile rainbow trout to turbulence produced by prismatoidal shapes. *Transactions of the American Fisheries Society,* 134**,** 741-753.

SMITH, D. L., GOODWIN, R. A. & NESTLER, J. M. 2014. Relating turbulence and fish habitat: a new approach for management and research. *Reviews in Fisheries Science & Aquaculture,* 22**,** 123-130.

SMITH, R., SIDLE, R. C., PORTER, P. & NOEL, J. 1993. Effects of experimental removal of woody debris on the channel morphology of a forest, gravel-bed stream. *Journal of Hydrology,* 152**,** 153-178.

SOLUK, D. A. & CRAIG, D. A. 1988. Vortex feeding from pits in the sand: A unique method of suspension feeding used by a stream invertebrate. *Limnology and Oceanography,* 33**,** 638-645.

SOLUK, D. A. & CRAIG, D. A. 1990. Digging with a vortex: flow manipulation facilitates prey capture by a predatory stream mayfly. *Limnology and Oceanography,* 35**,** 1201-1206.

SOULSBY, R. 1980. Selecting record length and digitization rate for near-bed turbulence measurements. *Journal of Physical Oceanography,* 10**,** 208-219.

SPAMPINATO, C., GIORDANO, D., DI SALVO, R., CHEN-BURGER, Y.-H. J., FISHER, R. B. & NADARAJAN, G. Automatic fish classification for underwater species behavior understanding. Proceedings of the first ACM international workshop on Analysis and retrieval of tracked events and motion in imagery streams, 2010. ACM, 45-50.

STANDEN, E. & LAUDER, G. 2007. Hydrodynamic function of dorsal and anal fins in brook trout (Salvelinus fontinalis). *Journal of Experimental Biology,* 210**,** 325-339.

STATZNER, B., GORE, J. A. & RESH, V. H. 1988. Hydraulic stream ecology: observed patterns and potential applications. *Journal of the North American Benthological Society***,** 307-360.

STEWART, R. L. & FOX, J. F. 2015. Role of macroturbulence to sustain turbulent energy in decelerating flows over a gravel bed. *Geomorphology,* 248**,** 147-160.

SUKHODOLOV, A. N. & SUKHODOLOVA, T. A. 2014. Shallow wake behind exposed wood-induced bar in a gravel-bed river. *Environmental Fluid Mechanics,* 14**,** 1071-1083.

SULAIMAN, M., SINNAKAUDAN, S. & SHUKOR, M. 2013. Near bed turbulence measurement with acoustic doppler velocimeter (ADV). *KSCE Journal of Civil Engineering,* 17**,** 1515-1528.

SVENDSEN, J. C., SKOV, J., BILDSOE, M. & STEFFENSEN, J. F. 2003. Intra-school positional preference and reduced tail beat frequency in trailing positions in schooling roach under experimental conditions. *Journal of Fish Biology,* 62**,** 834-846.

TAYLOR, G. I. The spectrum of turbulence. Proceedings of the Royal Society of London A: Mathematical, Physical and Engineering Sciences, London, 18 February 1938 1938. The Royal Society, 476-490.

THOMAS, R. E., JOHNSON, M. F., FROSTICK, L. E., PARSONS, D. R., BOUMA, T. J., DIJKSTRA, J. T., EIFF, O., GOBERT, S., HENRY, P.-Y. & KEMP, P. 2014. Physical modelling of water, fauna and flora: knowledge gaps, avenues for future research and infrastructural needs. *Journal of Hydraulic Research,* 52**,** 311-325.

THOMPSON, D. M. 2007. The characteristics of turbulence in a shear zone downstream of a channel constriction in a coarse-grained forced pool. *Geomorphology,* 83**,** 199-214.

THOMPSON, D. M., NELSON, J. M. & WOHL, E. E. 1998. Interactions between pool geometry and hydraulics. *Water Resources Research,* 34**,** 3673-3681.

THOMSON, J., CLARK, B., FINGERUT, J. & HART, D. 2004. Local modification of benthic flow environments by suspension-feeding stream insects. *Oecologia,* 140**,** 533-542.

THOMSON, J., TAYLOR, M., FRYIRS, K. & BRIERLEY, G. 2001. A geomorphological framework for river characterization and habitat assessment. *Aquatic Conservation: Marine and Freshwater Ecosystems,* 11**,** 373-389.

TIFFAN, K. F., HASKELL, C. A. & KOCK, T. J. 2010. Quantifying the behavioral response of spawning chum salmon to elevated discharges from Bonneville Dam, Columbia river, USA. *River Research and Applications,* 26**,** 87-101.

TOCKNER, K., WARD, J. V., ARSCOTT, D. B., EDWARDS, P. J., KOLLMANN, J., GURNELL, A. M., PETTS, G. E. & MAIOLINI, B. 2003. The Tagliamento River: a model ecosystem of European importance. *Aquatic Sciences,* 65**,** 239-253.

TONETTO, A. F., CARDOSO-LEITE, R., NOVAES, M. C. & GUILLERMO-FERREIRA, R. 2015. The relationship between macroalgal morphological complexity and hydraulic conditions in stream habitats. *Hydrobiologia,* 747**,** 33-41.

TONETTO, A. F., CARDOSO‐LEITE, R., PERES, C. K., BISPO, P. D. C. & BRANCO, C. C. Z. 2014. The effects of habitat complexity and hydraulic conditions on the establishment of benthic stream macroalgae. *Freshwater Biology,* 59**,** 1687-1694.

TONINA, D. & JORDE, K. 2013. Hydraulic Modelling Approaches for Ecohydraulic Studies: 3D, 2D, 1D and Non Numerical Models. *In:* MADDOCK I, H. A., KEMP P AND WOOD P (ed.) *Ecohydraulics: An Integrated Approach.* Chichester, UK: John Wiley & Sons, Ltd.

TORRENCE, C. & COMPO, G. P. 1998. A practical guide to wavelet analysis. *Bulletin of the American Meteorological society,* 79**,** 61-78.

TRITICO, H. & COTEL, A. 2010. The effects of turbulent eddies on the stability and critical swimming speed of creek chub (*Semotilus atromaculatus*). *The Journal of Experimental Biology,* 213**,** 2284-2293.

TRITICO, H., COTEL, A. & CLARKE, J. 2007. Development, testing and demonstration of a portable submersible miniature particle imaging velocimetry device. *Measurement Science and Technology,* 18**,** 2555.

TRITICO, H. M. & HOTCHKISS, R. H. 2005. Unobstructed and obstructed turbulent flow in gravel bed rivers. *Journal of Hydraulic Engineering,* 131**,** 635-645.

TULLOS, D. & WALTER, C. 2015. Fish use of turbulence around wood in winter: physical experiments on hydraulic variability and habitat selection by juvenile coho salmon, Oncorhynchus kisutch. Environmental Biology of Fishes, 98, 1339-1353.

VAUGHAN, I. P. & ORMEROD, S. J. 2010. Linking ecological and hydromorphological data: approaches, challenges and future prospects for riverine science. Aquatic Conservation: Marine and Freshwater Ecosystems, 20, S125-S130.

VEZZA, P., PARASIEWICZ, P., CALLES, O., SPAIRANI, M. & COMOGLIO, C. 2014. Modelling habitat requirements of bullhead (*Cottus gobio*) in Alpine streams. *Aquatic Sciences,* 76**,** 1-15.

VOGEL, S. 1994. *Life in moving fluids: the physical biology of flow,* Chichester, UK, Princeton University Press.

VOULGARIS, G. & TROWBRIDGE, J. H. 1998. Evaluation of the acoustic Doppler velocimeter (ADV) for turbulence measurements. *Journal of Atmospheric and Oceanic Technology,* 15**,** 272-289.

WALLERSTEIN, N. P., ALONSO, C. V., BENNETT, S. J. & THORNE, C. R. 2002. Surface wave forces acting on submerged logs. *Journal of Hydraulic Engineering,* 128**,** 349-353.

WALLIS, C., MADDOCK, I., VISSER, F. & ACREMAN, M. 2012. A framework for evaluating the spatial configuration and temporal dynamics of hydraulic patches. *River Research and Applications,* 28**,** 585-593.

WARD, A. J. & KRAUSE, J. 2001. Body length assortative shoaling in the European minnow, Phoxinus phoxinus. *Animal Behaviour,* 62**,** 617-621.

WARD, J. & TOCKNER, K. 2001. Biodiversity: towards a unifying theme for river ecology. *Freshwater Biology,* 46**,** 807-820.

WARD, J. V., TOCKNER, K., EDWARDS, P. J., KOLLMANN, J., BRETSCHKO, G., GURNELL, A. M., PETTS, G. E. & ROSSARO, B. 1999. A reference river system for the Alps: The'Fiume Tagliamento'. *Regulated Rivers Research & Management,* 15**,** 63-75.

WEBB, P. & COTEL, A. 2010a. Turbulence: does vorticity affect the structure and shape of body and fin propulsors? *Integrative and Comparative Biology,* 50**,** 1155-1166.

WEBB, P., COTEL, A. & MEADOWS, L. 2010b. Waves and eddies: effects on fish behavior and habitat distribution. *Fish Locomotion: an Eco-ethological Perspective. Science Publishers, Enfield***,** 1-39.

WEBB, P., KOSTECKI, P. & STEVENS, E. D. 1984. The effect of size and swimming speed on locomotor kinematics of rainbow trout. *Journal of Experimental Biology,* 109**,** 77-95.

WEBB, P. W. & COTEL, A. J. 2011. Assessing possible effects of fish-culture systems on fish swimming: the role of stability in turbulent flows. *Fish Physiology and Biochemistry,* 37**,** 297-305.

WELTON, J., BEAUMONT, W. & LADLE, M. 1999. Timing of migration and changes in age structure of Atlantic salmon, Salmo salar L., in the River Frome, a Dorset chalk stream, over a 24 ‐ year period. *Fisheries Management and Ecology,* 6**,** 437-458.

WHARTON, G., COTTON, J. A., WOTTON, R. S., BASS, J. A., HEPPELL, C. M., TRIMMER, M., SANDERS, I. A. & WARREN, L. L. 2006. Macrophytes and suspension-feeding invertebrates modify flows and fine sediments in the Frome and Piddle catchments, Dorset (UK). *Journal of Hydrology,* 330**,** 171-184.

WILCOX, A. C. & WOHL, E. E. 2007. Field measurements of three-dimensional hydraulics in a step-pool channel. *Geomorphology,* 83**,** 215-231.

WILCOX, A. C., WOHL, E. E., COMITI, F. & MAO, L. 2011. Hydraulics, morphology, and energy dissipation in an alpine step ‐ pool channel. *Water Resources Research,* 47**,** W07514.

WILKES, M. 2014. *The Hydrodynamics of River Ecosystems: Towards an Objective and Ecologically Relevant Classification of Mesohabitats.* University of Worcester.

WILKES, M., MADDOCK, I., VISSER, F. & ACREMAN, M. 2012. Hydrodynamic Variability in the Physical Biotopes of a Trout Stream. *9th International Symposium on Ecohydraulics.* Vienna, Austria.

WILKES, M. A., MADDOCK, I., VISSER, F. & ACREMAN, M. C. 2013. Incorporating hydrodynamics into ecohydraulics: the role of turbulence in the swimming performance and habitat selection of stream-dwelling fish. *In:* MADDOCK, I., HARBYM A., KEMP, P. AND WOOD, P. (ed.) *Ecohydraulics: An Integrated Approach.* Chichester, UK: John Wiley & Sons, Ltd, 9-30.

WILSON, C., STOESSER, T., BATES, P. & PINZEN, A. B. 2003. Open channel flow through different forms of submerged flexible vegetation. *Journal of Hydraulic Engineering,* 129**,** 847-853.

WOHL, E. E. & THOMPSON, D. M. 2000. Velocity characteristics along a small step–pool channel. *Earth Surface Processes and Landforms,* 25**,** 353-367.

WU, W., RODI, W. & WENKA, T. 2000. 3D numerical modeling of flow and sediment transport in open channels. *Journal of Hydraulic Engineering,* 126**,** 4-15.

YUE, W., MENEVEAU, C., PARLANGE, M. B., ZHU, W., VAN HOUT, R. & KATZ, J. 2007. A comparative quadrant analysis of turbulence in a plant canopy. *Water Resources Research,* 43**,** W05422.

ZIKA, U. & PETER, A. 2002. The introduction of woody debris into a channelized stream: effect on trout populations and habitat. *River Research and Applications,* 18**,** 355-366.

ZONG, L. & NEPF, H. 2010. Flow and deposition in and around a finite patch of vegetation. Geomorphology, 116, 363-372.

ZOLEZZI, G., SIVIGLIA, A., TOFFOLON, M. & MAIOLINI, B. 2011. Thermopeaking in Alpine streams: event characterization and time scales. *Ecohydrology,* 4**,** 564-576.

Appendix I

Semivariograms of kurtosis (A,B,C), integral time scale (D, E, F) along all the three components, the magnitude (G, H, I) and cumulative duration (L, M, N) of flow events across the low, medium and high gradient reaches.